FINAL REPORT

Molecular Biomarkers for Detecting, Monitoring and Quantifying Reductive Microbial Processes

SERDP Project ER-1588

July 2013

Alfred Spormann
Stanford University

Lewis Semprini
Oregon State University

SERDP
DOD ▪ EPA ▪ DOE

REPORT DOCUMENTATION PAGE

Form Approved
OMB No. 0704-0188

1. REPORT DATE *(DD-MM-YYYY)*	2. REPORT TYPE	3. DATES COVERED *(From - To)*
05-09-2013	Final	Jul 2007- Sep 2013

4. TITLE AND SUBTITLE

Molecular Biomarkers for Detecting, Monitoring

And Quantifying Reductive Microbial Processes

5a. CONTRACT NUMBER
ER-1588

5b. GRANT NUMBER

5c. PROGRAM ELEMENT NUMBER

6. AUTHOR(S)
Spormann, Alfred, M

Semprini, L

5d. PROJECT NUMBER

5e. TASK NUMBER

5f. WORK UNIT NUMBER

7. PERFORMING ORGANIZATION NAME(S) AND ADDRESS(ES)

Leland Stanford Junior University, 3160 Poster Drive, Ste. 100, Palo Alto, CA 94304

Office of Sponsored Programs
308 Kerr Administration Building
Corvallis, OR 97331-214

8. PERFORMING ORGANIZATION REPORT NUMBER

9. SPONSORING / MONITORING AGENCY NAME(S) AND ADDRESS(ES)
USACE, HUMPHREYS ENGR CTR SPT
:CEHEC-CT,
7701 Telegraph Drive
Alexandria, VA 22315-J000

10. SPONSOR/MONITOR'S ACRONYM(S)

11. SPONSOR/MONITOR'S REPORT NUMBER(S)

12. DISTRIBUTION / AVAILABILITY STATEMENT

13. SUPPLEMENTARY NOTES

14. ABSTRACT

15. SUBJECT TERMS

16. SECURITY CLASSIFICATION OF:			17. LIMITATION OF ABSTRACT	18. NUMBER OF PAGES	19a. NAME OF RESPONSIBLE PERSON
a. REPORT	b. ABSTRACT	c. THIS PAGE			Alfred M. Spormann
UU	UU			162	19b. TELEPHONE NUMBER *(include area code)* 650-723-3668

Standard Form 298 (Rev. 8-98)
Prescribed by ANSI Std. Z39.18

Table of Content

List of Tables

List of Figures

List of Acronyms, Keywords and Acknowledgments

acronym	name
BDF	Backward Differentiation Formula
BLAST	Basic Local Alignment Search Tool
BPF	Bright Probe Fraction
BSLDS	bright-segment length dependent score
BvcA	Strain BAV 1 putative vinyl chloride reductase
CAH	Chlorinated aliphatic hydrocarbon
cDCE	*cis*-dichloroethene
cDNA	Complementary Deoxyribonucleic Acid
CSTR	Continuous Stirred Tank
DGGE	Denaturing-Gradient Gel Electrophoresis
DMSO	Dimethyl-sulfoxide
DNA	Deoxyribonucleic Acid
DOD	U.S Department of Defense
DOE	U.S Department of Energy
EDTA	ethylenediaminetetraacetic acid
eeq/mol	Electron equivalent per mol
EPA	Environmental Protection Agency
ETH	Ethene
EV	Evanite
FGENESB	Finding Genes in Microbial Genomes
GC	Gas Chromatograph
hydB	Hydrogenase subunit B gene
IMG/ER	Integrated Microbial genome
IMG/M	Integrated Microbial Genome and Microbionome Database
MDA	Mulitple Displacement Amplification
MO BIO	Molecular Biology kit
mRNA	Messenger Ribonucleic Acid
NCBI	National center for Bioinformatics
NEB	New England Biolabs
oQ	epoxyqueuosine
ORF	Open Reading Frame
PABA	p-aminobenzoic acid
PCE	Tetrachloroethene
PceA	Perchloroethene reductase
PI	Principal Investigator
qPCR	Quantitative Polymerase Chain Reaction
RAST	Rapid Annotation using Subsystem Technology
RdhA	Reductive Dehalogenase, active cobalamin-containing subunit
RdhB	Reductive Dehalogenase, membrane-bound subunit
RGD	Reductive Gas Detector
rRNA	Ribosomal Ribonucleic Acid
SPRI	Solid Phase Reversible Immobilization
TCD	Thermal Conductivity Detector
TCE	Trichloroethene
TceA	Trichloroethene reductase
UTP	Uridine triphosphate

UV/VIS	UV Visible Spectrometer
VC	Vinyl Chloride
VcrA	Vinyl chloride reductase
VS	Dehalococcoides maccartyi strain Victoria Stanford

1 ABSTRACT

Chlorinated solvents, such as PCE, TCE, and chlorobenzenes, are the most prevalent groundwater contaminants at DOD and DOE sites. Anaerobic bioremediation treatment technologies are most promising for cost effective removal of these contaminants at a large scale. With natural attenuation, the most important need by practitioners is information about the natural rates of biodegradation, which is very difficult to obtain because of the very slow rate of the process. With engineered bioremediation rates tend to be much faster, but often when applied, the process does not work as planned, which may be due to a variety of problems, such as lack of suitable organisms, strong competition for substrate by other organisms, lack of appropriate nutrients, insufficient supply of electron donor (reductant), inhibitory conditions, etc. Thus, biomarkers are needed to help assess critical biological parameters at problem sites such as whether or not (i) the key microorganisms are present, (ii) the key genes are present, and (iii) the key genes are active (induced). The rate of hydrogen release as well as knowledge of competing hydrogen-consuming reactions are critical for the practitioner to know to guide successful remediation efforts. Thus, monitoring presence, abundance and expression status of diverse hydrogenase as well as reductive dehalogenase genes should provide semi-quantitative markers to predict in situ rates of reductive dehalogenation.

Objectives

The research conducted had the following specific objectives:

1. To develop and test quantitative molecular biomarkers for the hydrogen-producing and hydrogen-consuming microbial population present in groundwater and sediment material;
2. To correlate the quantitative data obtained by molecular biomarkers with experimentally determined transformation rates, and to test and refine a mathematical model with these data.

Technical Approach

We developed a novel and broad-ranging approach to the characterization of complex microbial communities by analyzing the abundance and expression of key functional genes using a tiling DNA microarray. A test hybridization showed that the detection limit for the microbial community system was found to be between ~1% and ~10% of the total microbial community. This molecular tool is useful for monitoring the presence, shift in abundance, as well as expression status of hydrogenase as well as reductive dehalogenase genes, and to semi-quantitatively predict H_2 flux in complex microbial communities. This tool also allowed us to observe shifts in populations of dehalogenating microorganisms, as well as evolution of novel lineages.

Results

Simulation of the anaerobic dehalogenation of TCE in a continuous stirred tank reactor (CSTR) experiment under excess and limited electron donor addition was carried out. Formate and TCE were fed to 2-L and 5-L CSTRs containing the Evanite culture (EV). To simulate the results of the two experiments, a non-steady-state model was developed, that coupled thermodynamic and kinetic models described in Project 2 to include CSTR flow conditions. Our model includes inhibition kinetics for the dehalogenation reactions as described by Yu and Semprini (2004), and

permits the growth of homoacetogens and dehalogenators as competing hydrogen (H_2) consuming processes. Three microbial communities were simulated in the CSTR, dechlorinators that transform TCE to cDCE, dechlorinators that transform cDCE to ethene and homoacetogens. H_2 is assumed to be in equilibrium with formate. The system of model equations was solved numerically using COMSOL 3.5a. VC dehalogenation kinetics was determined in batch experiments using cells harvested from the CSTR. The model simulated well the steady-state and transient performance of the CSTR when excess and limiting electron donor were added. The batch-determined kinetic parameters did a good job of capturing the observed CAHs, H_2, acetate and biomass concentration in both the CSTR and in separate batch experiments. VC dehalogenation was rate limited when electron donor was in excess and stoichiometry limited when electron donor was not in excess. Simulations required a H_2 threshold for homoacetogens of 40 nM to match CSTR observations, which is lower than reported in the literature. The agreement of the model with the experimental results gives us confidence in the kinetic parameters being used and our ability to simulate these complex processes that include the competition for H_2.

Benefits

This tool has demonstrated for the first time the proof of concept of using semi-quantitative monitoring of key genes and their expression. This and in conjunction with selecting more efficient electron donor, such as formate, can make bioremediation of chloroethene-contaminated sites more efficient and less expensive.

2 OBJECTIVE

The research conducted had the following specific objectives:

1. To develop and test quantitative molecular biomarkers for the hydrogen-producing and hydrogen-consuming microbial population present in groundwater and sediment material;
2. To correlate the quantitative data obtained by molecular biomarkers with experimentally determined transformation rates, and to test and refine a mathematical model with these data.

3 BACKGROUND

Halogenated aliphatic compounds are widespread contaminants and constitute a serious threat to groundwater quality in industrialized countries (McCarty, 1993). Trichloroethene (TCE) is among the most abundant groundwater contaminant requiring remediation (EPA, 1993). Under anaerobic conditions, TCE can be reduced to nontoxic ethene (McCarty, 1993). Bioremediation of organohalide contaminants is carried out by a diverse set of organohalide-respiring anaerobic bacteria, with each strain capable of dehalogenating a different set of organohalide compounds. Several halorespiring organisms dechlorinate TCE to cDCE (Holliger et al., 1998; Scholz-

Muramatsu et al., 1995; He et al., 2003), but for bioremediation to be successful, complete dechlorination to ethene must be achieved. To date, only *Dehalococcoides* strains have been isolated that are capable of halorespiration of DCEs to ethene, while using H_2 as their electron donor (He et al., 2003; Sung et al., 2006; Cupples et al., 2004). The removal of each individual halide from the carbon backbone is typically carried out in a stepwise manner, with different strains removing halides from different parts of the molecule. For example, the only species capable of reducing carcinogenic vinyl chloride (VC) to harmless ethene is *Dehalococcoides mccartyi*, but the reduction of tetrachloroethene (PCE) to VC is carried out by strains incapable of metabolically reducing VC to ethene. This means that a community of multiple *D. mccartyi* strains is necessary for the complete dechlorination of PCE. Continuous successful reductive dehalogenation can thus depend on the composition of the microbial community that carries it out. Microbial community composition changes in three ways: strains can increase or decrease in abundance, new strains can enter an environment, and speciation events can occur where a mutation causes a single strain to split into two independent populations. Such changes are driven by a combination of externally imposed changes in the physical-chemical environment and stochastic phenomena. One goal was to observe changes in the community composition of reductively dechlorinating bacteria in the most stable environment possible, the laboratory chemostat. After obtaining a baseline understanding of the microbial community shifts under very stable conditions, we introduced changes in the chemical composition of the influent in certain chemostats and observed subsequent changes in the community of reductively dehalogenating bacteria. In doing this we had three goals: (a) to trial a novel tiling-microarray-based method to accurately track changes in reductively dehalogenating bacterial community composition, (b) to learn what factors might threaten the effectiveness of such communities, and (c) to gain a more broad ecological understanding of how community composition of a specific functional guild of microorganisms can vary during long-term stable operation.

Several DNA-based methods have been developed for the inventory of different reductively dehalogenating bacteria in a mixed microbial community. Such approaches can be broadly placed into two categories: phylogenetic tools and reductive dehalogenase-based tools. Phylogenetic tools typically target the diversity of 16S ribosomal RNA genes (Taş et al. 2009; Futamata et al. 2009) or highly conserved protein-encoding genes [Berggren et al. 2013] using clone libraries or denaturing-gradient gel electrophoresis (DGGE). This exploits the fact that *D. mccartyi* strains and other organohalide-respiring bacteria are somewhat phylogenetically distinct, having been placed in three major phylogenetic subgroups (Pinellas, Cornell, Victoria) (Hendrickson et al. 2002). However, phylogenetic tools are insufficient for differentiating certain physiologically distinct reductively dehalogenating strains. For example, *D. mccartyi* strain GT shares 100% 16S rRNA sequence identity with strains CBDB1 and FL2, but is capable of reducing a different set of organohalide compounds (Sung et al. 2006). The genomic basis of this metabolic diversity is in the genes encoding reductive dehalogenases, the enzymes responsible for reductive dehalogenation. Reductive dehalogenases consist of two subunits, an active cobalamin-containing subunit (RdhA) and a membrane-bound subunit (RdhB). Different *rdhA* genes are specific to the dehalogenation of different organohalide substrates. For example, PCE reduction is mediated by PceA (Suyama et al. 2002), trichloroethene (TCE) reduction by TceA (Magnuson et al. 2000), and VC reduction by VcrA (Müller et al. 2004) or BvcA (Krajmalnik-Brown et al. 2004). Genomes of different reductively dehalogenating bacteria show that each strain possesses a distinctive set of *rdhA*, and that differences in respirable organohalide substrates are determined by these different sets of genes

(McMurdie et al. 2009). Methods to monitor changes in the community composition of reductively dehalogenating bacteria based on *rdhA* have been developed based on quantitative PCR, clone libraries (Futamata et al. 2009), and DNA microarrays (Taş et al. 2009; Dugat-Bony et al. 2012; 2011). However, until now only the qPCR method has been used to link specific *rdhA* with each other and with a specific bacterial population, and that was limited to two *rdhA* with known substrate specificity.

A continuous stirred tank reactor (CSTR) was used to study bacterial metabolism, physiology and population dynamics of this process. CSTRs are used to study microbial processes under pseudo-steady-state and transient conditions (Nielsen et al., 2003). In addition, CSTRs have been used to grow cells of batch anaerobic reductive dechlorination tests (Fennell and Gossett, 1998; Yang and McCarty, 1998; and Cupples et al. 2004). Yang and McCarty (1998) grew a PCE-dehalogenating culture in a 4-L CSTR. The cells were harvested and used to determine the threshold H_2 concentration in batch systems, using benzoate as a producing H_2 electron donor. They found that a 25% reduction in the benzoate concentration in the feed to the CSTR, resulted in a slight increase in the VC effluent concentration with a constant PCE influent. No attempt was made to model the results of this CSTR study. Cupples et al. (2004) used the harvested cells harvested from a CSTR to investigate the effect of H_2 concentration on cDCE and VC dechlorination. CSTRs provide a good means of studying the effect of perturbations in electron donor supply on population performance. Hydrogen concentrations can be maintained at low and pseudo-steady-state levels and chlorinated ethene levels can also be maintained at constant concentrations. The biomass concentration can also be maintained at pseudo-steady-state levels.

Numerous models have been formulated to simulate the results of dehalogination experiments in batch systems (Fennell and Gossett, 1998; Haston and McCarty, 1998; Cupples et al., 2004; Yu and Semprini, 2004). Several models have been developed for continuous-flow systems, such as transport in porous media (Clapp et al., 2004, Clement et al., 2004) using simplified kinetic models. However, to our knowledge the simulation of anaerobic reductive dehalogenation under CSTR growth conditions with detailed kinetics coupled with thermodynamic constants has not been performed.
In this study, we explored the effects of formate addition on TCE transformation in CSTR experiments with the Evanite (EV) dehalogenating culture. Anaerobic reductive dehalogenation in the CSTR was simulated for pseudo-steady-state and transient conditions. In addition, the thermodynamics of H_2 production and acetate formation were evaluated.

A comprehensive numerical model for a CSTR fed formate and TCE was used. Thermodynamic and kinetic equations were coupled with CSTR transport equations. The kinetics of dehalogenation, thermodynamically controlled acetate formation, the use of H_2 as the electron donor was coupled to the growth of the key microbial populations. The model was used to simulate the impact of reducing the electron donor concentration on TCE transformation and acetate formation in the CSTR.

4 MATERIALS AND METHODS

The research conducted was based on two interconnected projects:

- PROJECT 1
A tiling DNA microarray approach for the analysis of hydrogenases and reductive dehalogenases in reductively dehalogenating microbial communities

Performers: Ian P.G. Marshall and Alfred M. Spormann

- PROJECT 2
Understanding population dynamics of complex reductively dehalogenating communities as a function of electron donor type and availability as well as competing electron acceptor

Performers: Mohammed F. Azizian, Dusty Berggren, and Lewis Semprini

4.1 Materials and Methods for Project 1

4.1.1 Methods Related to Tiling DNA Microarrays

4.1.1.1 Obtaining Gene Sequences

Genes for three different types of microarrays were obtained. Specific DNA microarray designs are referred to as 'Chips' to avoid confusion between general discussion of the tiling functional gene DNA microarray approach and specific DNA microarray designs.

Hydrogenase Genes
To ensure that the most complete set of hydrogenase genes was employed for each experiment described in this study, the microarray design was revised four times in the three-year span of the reported experiments to reflect changes in up-to-date genomic and metagenomic databases. Furthermore, this enabled the microarray to be amended with non-hydrogenase genes relevant to the different study systems when space on the array allowed.

Hydrogenase gene sequences for the Test Microarray were obtained using BLAST on the NCBI non-redundant database (Altschul et al. 1990) with gene sequences listed for [NiFe]-hydrogenase large subunits and [FeFe]-hydrogenase sequences as query sequences. Resulting hydrogenase genes and genes similar to hydrogenases were clustered to 97% using CD-HIT (Li and Godzik 2006), and the longest sequence for each cluster was selected as the representative sequence for use on the array. Overlapping 60-mer probes for each gene were designed to 2× coverage. To investigate the effect of mismatched probes, several mismatches were introduced for a probe

encoding the *hydB* gene from *Shewanella oneidensis* MR-1 (IMG 637345681). 19 probes with a series of single mismatches (98% sequence identity with the true sequence) in different positions at either end of the probe sequence were included, and an 11 nucleotide (82% sequence identity with the true sequence) mismatch section from the center of the probe was also included, with 9 different random mismatch sequences on 9 different probes.

All amino acid and nucleic acid sequences for the Hydrogenase Chip versions 1, 2, 3, and 4 were retrieved from the Integrated Microbial Genomes and Microbiomes database (IMG/M) versions 2.5, 2.8, 2.9, and 3.3 respectively (Markowitz et al. 2012). The amino acid sequences were screened for hydrogenases based on PROSITE sequence signatures for all [NiFe]- and [FeFe]-hydrogenase groups previously determined (Vignais and Billoud 2007) using ScanProsite (Gattiker, Gasteiger, and Bairoch 2002). Non-hydrogenase gene sequences were removed from the resulting gene set based on annotation, and genes were clustered to 97% nucleic acid sequence identity using CD-HIT.

Additional Genes Used on each Hydrogenase Chip Design
In addition to the hydrogenase genes selected in the manner described above, other genes were included on each array design:

For Hydrogenase Chip version one, 199 genes involved in formate metabolism were retrieved from IMG/M by searching for annotations of genes encoding pyruvate formate lyase, formate hydrogen lyase, and formate dehydrogenase. These genes were added to the design after all retrieved hydrogenase genes were included and space for more probes remained.

For Hydrogenase Chip version two, 57 reductive dehalogenase (*rdhA*) genes were retrieved from the NCBI non-redundant nucleotide database to fill space after all hydrogenase genes were included.

For Hydrogenase Chip version 3, additional gene sequences were obtained from three sources: by retrieving all annotated hydrogenase and reductive dehalogenase gene sequences from all "*Dehalococcoides*" genomes in IMG version 2.9 (these were then not subjected to CD-HIT clustering), by retrieving hydrogenase sequences from published clone libraries (Boyd, Spear, and Peters 2009; Xing, Ren, and Rittmann 2008), and from the uptake [NiFe]-hydrogenase sequence from the genome of *Microcoleus chthonoplastes* PCC 7420. The reductive dehalogenase gene sequences were derived from all *Dehalococcoides* genomes in IMG version 2.9.

Reductive Dehalogenase Genes
RdhA amino acid sequences were collected based on a search for relevant gene annotations in the NCBI protein database and Integrated Microbial Genomes and Metagenomes database. In order to exclude misannotated epoxyqueuosine (oQ) reductase genes from the final array design (a recent publication has suggested that reductive dehalogenases and oQ reductases are homologous (Miles et al. 2011)) a phylogenetic tree was constructed from an alignment of 280 RdhA sequences and 5 known oQ reductases. This showed that oQ reductases across diverse groups of microorganisms formed a monophyletic clade only distantly related to annotated reductive dehalogenase genes (Data not shown).

A custom Python script was used to download the total 889 nucleotide sequences encoding the RdhA amino acid sequences retrieved from the NCBI nucleotide database and IMG/M. To ensure multiple copies of highly identical or duplicate nucleic acid sequences did not unnecessarily take up space on the microarray, CD-HIT was used to cluster sequences at 97% nucleic acid sequence identity in order to choose a representative sequence for each cluster of high identity. This resulted in a final number of 294 *rdhA* genes for the Reductive Dehalogenase Chip.

4.1.1.2 Array Design Approach

All DNA microarrays were designed by taking the complete set of gene sequences intended to be monitored by the array, then determining the maximum coverage of those genes on an Agilent 4x44K (4 arrays per glass slide each containing 44,000 60-mer oligonucleotide spots) DNA microarray. For the reductive dehalogenase chip the 8x15K array format was used (8 arrays per glass slide each containing 15,000 60-mer oligonucleotide spots). This method maximized the number of probes used to target each gene of interest. See Table 1 for details of all arrays used during the experiments presented in this dissertation.

Microarray Name	Number of Genes	Coverage	Mean Probes per Gene	Design Date [month-year]	Array Format
Test Microarray	845	2.00X	47.29	Oct-07	4x44K
Hydrogenase Chip version 1	936	2.00X	46.19	Jul-08	4x44K
Hydrogenase Chip version 2	998	2.00X	43.24	Jul-09	4x44K
Hydrogenase Chip version 3	1324	1.67X	32.93	Nov-09	4x44K
Hydrogenase Chip version 4	2275	1.00X	19.25	Feb-11	4x44K
Thiovulum Chip	2218	1.00X	19.6	May-11	4x44K
Reductive Dehalogenase Chip	294	2.00X	47.20	Aug-11	8x15K

Table 1 – Overview of tiling DNA microarray designs applied in this dissertation.

4.1.1.3 DNA/RNA extraction

Pure Culture DNA Extraction

DNA for the Test Microarray hybridization was extracted using the DNeasy Blood and Tissue Kit (Qiagen, Hamburg, Germany) according to the manufacturer's instructions for bacterial genomic DNA extraction and purification, then quantified using the Qubit Fluorometer and broad-range double-stranded DNA quantification kit (Invitrogen, San Diego, CA, USA). 1.5µg of genomic DNA from each of *Escherichia coli*, *Bacillus subtilis*, *Shewanella oneidensis* MR-1, *Pseudomonas aeruginosa*, and *Shewanella sediminis* HAW-EB3 was mixed for subsequent labeling and hybridization. The same DNA extraction protocol was used to obtain DNA for the sensitivity analysis hybridization of DNA from *Escherichia coli*, *Shewanella oneidensis* MR-1, *Azotobacter vinelandii*, and *Methanococcus maripaludis*.

Reductively Dehalogenating Soil Column DNA Extraction
Genomic DNA was extracted from Bio-Sep adsorbent beads removed from the microbial sampling ports using the Ultraclean Soil DNA Isolation Kit according to the manufacturer's instructions (MO BIO Laboratories, Carlsbad, CA).

Reductively Dehalogenating Batch Cultures and Chemostats
Liquid batch and chemostat cultures were transferred to 50 mL Falcon tubes, then centrifuged for 30 minutes at 9000 rpm and 4°C. Supernatant was decanted, and the pellets were stored at -80°C until analysis. Frozen cell pellets were subjected to the RNA/DNA co-isolation described below.

Standard DNA/RNA Co-Isolation Procedure
Cell material was immersed in 1 mL of a lysis solution consisting of 10 mM EDTA, 50 mM Tris-HCl, 4 M guanidine thiocyanate, 2% sodium dodecyl sulfate, and 130 mM β-mercaptoethanol in a 2 mL tube containing ~0.1g acid-washed glass beads 150-212 μm in diameter (Sigma-Aldrich, St. Louis, MO, USA). Tubes were vortexed at 4ºC at maximum speed for five minutes, then 1 mL of pH 4.5 acid-phenol:chloroform:isoamyl alcohol in the ratio 125:24:1 (Ambion, Austin, TX, USA) was added. The solution was briefly vortexed, incubated at room temperature for five minutes, then centrifuged at 16,000 g (Eppendorf, Hamburg, Germany) for five minutes. The aqueous phase was removed and mixed with 40 μL of RNase-free 3 M sodium acetate (Ambion) and 1.7 mL of -20ºC 100% ethanol. The mixture was incubated at -20ºC for one hour, centrifuged at 16,000 g, 4ºC for 30 minutes. The liquid phase was decanted leaving a nucleic acid pellet that was air-dried for ten minutes then re-suspended in 200 μL of nuclease-free water. 100 μL of this solution was stored at -20ºC for DNA analysis. 10 μL TURBO DNase buffer and 2μL (4 units) TURBO DNase (Ambion) were added to the remaining 100 μL, then incubated at 37ºC for 30 minutes. An additional 2 μL (4 units) of DNase was added then incubated for a further 30 minutes. 120 μL of the acid-phenol:chloroform:IAA solution were added, then the mixture was vortexed briefly, incubated at room temperature for one minutes, then centrifuged at 16,000 g for two minutes. The aqueous phase was removed and mixed with 10 μL 3 M sodium acetate solution and 300 μL ethanol, incubated at -20ºC for 30 minutes, then centrifuged at 4ºC, 16,000 g for 30 minutes. The liquid was decanted, RNA solution re-suspended in 50 μL nuclease-free water. RNA and DNA were quantified in the solution using the Qubit fluorometer and broad-range double-stranded DNA and broad-range RNA Quant-it quantification kits (Invitrogen).

4.1.1.4 MDA and DNA labeling

Multiple Displacement Amplification
For most DNA hybridized to microarrays in this study the starting quantity of DNA was insufficient. It was therefore first subjected to amplification by multiple displacement amplification (MDA) using the REPLI-g Mini Kit (Qiagen) according to the manufacturer's instructions using 5 μL (approximately 5-10 ng) of starting DNA in solution.

DNA Labeling
DNA was mixed with random hexamers (Invitrogen) at a final concentration of 250 ng/μL in 39 μL of water, then incubated at 95ºC for 10 minutes. The mixture was placed on ice for 30 seconds,

then 5 µL of NEBuffer 2 (New England Biolabs (NEB), Ipswich, MA, USA), 2 µL of a dNTP labeling mix (5 mM dATP, cCTP, dGTP, dTTP (Invitrogen), 1.67 mM amino-allyl labeled dUTP (Fermentas, Vilnius, Lithuania), and 4 µL of Klenow Fragment (3´→5´ exo–) at 5000 units/mL (NEB). This Klenow reaction mixture was incubated for 16 hours at 37ºC, then stopped by the addition of 5 µL 0.5 M EDTA. The amino-allyl labeled DNA (aa-DNA) was purified using the QIAquick PCR Purification Kit (Qiagen) with a custom-made phosphate wash buffer in place of the Qiagen-supplied buffer PE (50 mM KPO_4, 80% ethanol, pH 8.5) then dried at 45ºC in a SpeedVac (Thermo Scientific, Waltham, MA, USA). A Cy3 mono-reactive dye pack (GE Healthcare Biosciences, Piscataway, NJ, USA) was re-suspended in 13 µL Dimethyl-sulfoxide (DMSO). aa-DNA was re-suspended in 10 µL nuclease-free water, 0.5 µL 1 M sodium bicarbonate solution and 3 µL of dissolved Cy3 dye, then incubated in the dark at room temperature for 60 minutes. Cy3-labeled DNA was again purified using the QIAquick PCR Purification Kit. Labeled DNA was quantified and Cy3 incorporation determined using a Nanodrop (Thermo Scientific).

4.1.1.5 Test PCR Amplicon Hybridization

The test PCR amplicon was generated using a PCR volume of 50 µL containing 5 µL of 10X PCR buffer and 0.2 µL Taq polymerase from the Taq PCR Core Kit (Qiagen, Hamburg, Germany), 0.5 µM of forward primer SO_hydA_F (5'-AACGACAACTTATCAACC-3'), 0.5 µM of reverse primer SO_hydA_R (5'-AATGTTACCCAGCCA-3'), 2 µL of the dNTP labeling mix described, and 1 µL of genomic DNA from *Shewanella oneidensis* MR-1. This amino-allyl labeled amplicon was labeled with Cy3 dye.

4.1.1.6 Whole Community RNA Amplification

The RNA amplification and labeling protocol was based on the Whole-Community RNA Amplification protocol previously published (Gao et al. 2007). cDNA synthesis was performed with the Superscript III First-Strand synthesis kit (Invitrogen) following the manufacturer's instructions, with the following modifications: 7 µL of dissolved RNA (containing at least 500 ng RNA) was used as starting material, and the primer added was 2 µL 0.5 µg/µL T7N6S primer (5'-AATTGTAATACGACTCACTATAGGGNNNNNN-3'), and the reverse transcription was performed overnight (18 hours) at 50ºC. The second strand cDNA was synthesized by adding 1 µL of Klenow Fragment (New England Biolabs), 1 µL 50 ng/µL random hexamer solution (Invitrogen) to the cDNA first strand synthesis solution then incubated for two hours at 37ºC. The resulting cDNA was purified using the QIAquick PCR Purification Kit, quantified using the Qubit fluorometer and Quant-it broad-range double-stranded DNA kit, then dried down in a SpeedVac. This cDNA was used as a template for amino-allyl labeled RNA using the MEGAscript T7 Kit (Ambion) according to the manufacturer's instructions, with the following modification: the 2 µL UTP solution was replaced with 3 µL of a 50 mM 3:1 amino-allyl UTP : UTP solution mixture (Ambion). The resulting amino-allyl labeled cRNA was purified using the RNeasy Mini Kit (Qiagen) and eluted in 30 µL nuclease-free water. A Cy3 mono-reactive dye pack (GE Healthcare) was re-suspended in 13 µL DMSO. 1.5 µL 1 M sodium bicarbonate adjusted to pH 9.3 and 3 µL reactive Cy3 in DMSO were mixed with the amino-allyl-labeled cRNA then incubated in the dark at room temperature for 60 minutes. The resulting Cy3-labeled cRNA was purified using the RNeasy Mini Kit. Cy3 dye incorporation and cRNA quantity were determined using a Nanodrop. Cy3-labeled cRNA was

fragmented using fragmentation buffer from the Gene Expression Hybridization Kit according to the manufacturer's instructions (Agilent Technologies, Santa Clara, CA, USA).

4.1.1.7 Microarray Hybridization, Washing and Scanning

Labeled DNA or RNA was hybridized to the DNA microarray at 65ºC for 17 hours according to the manufacturer's protocol for one-color gene expression analysis (Agilent). The hybridized microarray was scanned using a Genepix 4000B Microarray Scanner (Molecular Devices, Sunnyvale, CA, USA) and median probe intensity value used for further analysis.

4.1.1.8 Microarray Data Analysis

DNA Microarrays were analyzed using Feature Extraction software version 9.5.3 and included protocol GE1-v5_95_Feb07 (Agilent). Numeric spot intensity data was processed using the R package TilePlot version 1.2.1 developed as part of this study for analysis of functional gene tiling microarrays. This package has been deposited to the Comprehensive R Archive Network (CRAN – http://cran.r-project.org/). The bright probe cutoff used in TilePlot was three times the median intensity of all spots on the array unless otherwise stated, with spots brighter than this cutoff defined as bright and spots dimmer than this cutoff defined as dim. The bright probe fraction (BPF) for each gene was defined as the number of bright probes for the gene divided by the total number of gene probes. For each gene on the array, a bright-segment length dependent score (BSLDS) was calculated based on the length of each contiguous section of the gene with bright probes (or "bright segment length"). The sum of squares of all bright segment lengths for a given gene was said to be the BSLDS. The BSLDS is a method of differentiating results not just based on the fraction of bright probes, but rather the length of contiguous bright segments.

For multiple array comparisons, median intensities for each probe on the array were fed into the tileplot.double function, with each sample loess-normalized to a common reference sample in a similar fashion to conventional microarray analysis (Smyth and Speed 2003). For experiments where no quantitative comparison between arrays was performed, the tileplot.single() function (no normalization or multiple array comparison) was used.

Quantitative shifts in gene or transcript abundance between samples were determined by calculating ln(A/B) for each probe targeting a given gene, where A is the probe intensity from one sample and B from another, then finding the median of these numbers. This median value is referred to as the log intensity ratio. A log intensity ratio > 0 signifies a greater abundance in sample A, and a result below 0 signifies greater abundance in sample B. Since the set of ln(A/B) for a given gene generally fails tests of normality, statistics to determine significant changes in gene or transcript abundance based on an assumption that a distribution is normal could not be applied. Instead, the median absolute deviation was used as an estimate of variability in the measurement, and the binomial test (R function binom.test()) was applied to test the null hypothesis that the genes are in equal abundance (50% of probes with ln(A/B) > 0). Genes were considered of significantly different abundances in the two samples if the binomial test resulted in a null hypothesis probability of less than 0.01.

4.1.2 Other Molecular Microbial Ecological Methods

4.1.2.1 Clone Libraries

General Clone Library Method

All clone libraries were constructed using the TOPO TA Cloning Kit using the pCR2.1-TOPO cloning vector (Invitrogen). Generally speaking, the protocol provided by the manufacturer was followed, with the following clarifications of certain steps:

Ligation and cloning were carried out on the same day as the polymerase chain reaction (PCR) to retain the overhanging adenosines necessary for successful ligation. PCR products were cleaned up using the Wizard SV PCR Clean-up Kit (Promega, Madison, WI, USA). 4 µL of eluted PCR amplicon solution were used in the ligation reaction. To maximize the number of useful clones, the ligation reaction was carried out for 30 minutes and the pre-transformation incubation on ice of competent cells and plasmid was carried out for 30 minutes. Cells were plated on LB agar plates with 50 mg/L kanamycin and 80 mg/L X-gal. Colonies were picked with sterile pipette tips and transferred to 96-well plates containing 200 µL of LB medium with the same kanamycin and X-gal concentrations as the agar plates. 96-well liquid cultures were grown overnight and then shipped either to Sequetech in Mountain View, CA for rolling-cycle amplification of the plasmid and subsequent Sanger sequencing, or to Beckman Coulter Genomics in Danvers, MA for Solid Phase Reversible Immobilization (SPRI) plasmid extraction followed by Sanger sequencing.

Bacterial 16S rRNA Gene Clone Libraries

PCR amplification of a ~1400bp fragment of the bacterial 16S rRNA gene for clone libraries was carried out in a manner similar to that which was previously described (Behrens et al. 2008). Amplicons were obtained through PCR using primers GM3F (5'- AGAGTTTGATCMTGGC-3') (Muyzer, de Waal, and Uitterlinden 1993) and UNI1392R (5'- ACGGGCGGTGTGTRC-3') (Lane et al. 1985). Amplifications were carried out in 50 µL volumes containing 25 µL DreamTaq Green PCR Master Mix (Fermentas), 0.5 µM of each primer, 1 µL of DNA template, and the remainder as nuclease-free water (Invitrogen). The reaction proceeded with an initial denaturation step at 95ºC for 10 minutes, followed by 30 cycles with a 1-minute denaturation step at 95ºC, a 1-minute annealing step at 48ºC, and a 1-minute extension step at 72ºC. The reaction was completed with a 10-minute final extension step at 72ºC. PCR amplifications were performed in a PTC-200 gradient cycler (MJ Research, Inc., Watertown, MA). After single-read Sanger sequences for each clone were obtained, 16S rRNA gene clone libraries were analyzed using the classifier function of the Ribosomal Database Project (Wang et al. 2007).

Dissimilatory Sulfite Reductase Gene Clone Libraries

A 400bp fragment of *dsrA* was PCR-amplified using forward primer Dsr-1F-GC (5'- ACSCACTGGAAGCACG-3') and reverse primer Dsr-DGGE-Rev (5'- CGGTGMAGYTCRTCCTG-3') as previously described (Leloup et al. 2009). PCR was performed in 50 µL reactions containing 25 µL 2X DreamTaq Green PCR Master Mix (Fermentas), 0.2 µM of each primer, and 1 µL of DNA in solution. Thermal cycling conditions were: 10 minutes at 95°C for initial denaturation; 35 cycles of 40 s at 94°C, 40 s at 55°C, 1 min at 72°C and a final extension for 10 min at 72°C. Gel extraction of the fragment with the expected amplicon size of approximately 400 bp was performed using the Wizard SV Gel and PCR Clean-up System according to the manufacturer's instructions (Promega).

dsrA sequences obtained through Sanger sequencing were analyzed by clustering nucleic acid sequences at 97% using CD-HIT (Li and Godzik 2006). A representative sequence for each cluster was used as a query sequence in a BLAST search (Altschul et al. 1990) against the NCBI non-redundant protein database to obtain closest relative sequences. Clone library nucleotide sequences and relatives were then aligned using Geneious (Biomatters, Auckland, New Zealand) with the MUSCLE program (Edgar 2004) and placed in a phylogenetic tree using the PHYML maximum-likelihood tree-building program (Guindon and Gascuel 2003).

Desulfovibrio hynA-1 *Clone Libraries*

Primers DMR-15600_F-717 (5'-MAARAACCCSCAYMCCCAG-3') and DMR-15600_R-1720 (5'-GACRTGYACRSMRCAG-3') targeting the *hynA-1* gene in *Desulfovibrio* sp. were designed based on *hynA-1* sequences from *Desulfovibrio* sp. related to *Desulfovibrio magneticus* (IMG identifiers 637123154, 637783027, 639819476, 643139751, 643538766, 643581839, 644801811, 644840066, and 645564504). These primers were used at a concentration of 500 nM each to PCR-amplify *hynA-1* from DNA sample S in 50 µL reactions with 25 µL 2X DreamTaq Green Master Mix, cycled with an initial 95ºC denaturation step for 3min, followed by 45 cycles with 30s at 95ºC, 30s at 48ºC, 30s at 72ºC, then a final 72ºC extension step of 10 min. Gel extraction of the fragment with the expected amplicon size of approximately 1000 bp was performed using the Wizard SV Gel and PCR Clean-up System according to manufacturer's instructions (Promega). *hynA-1* sequences were computationally analyzed using the same protocol as *dsrA* sequences (see above).

Dehalococcoides *[NiFe] Hydrogenase Large Subunit (*hupL*) Clone Libraries*

Primers HupL_F (5'- ATGCAGAAGATAGTAATTGAYC-3') and HupL_R (5'-GCCAATCTTRAGTTCCATMR-3') for amplification of a 1246 bp fragment of the *hupL* gene from *Dehalococcoides* sp. used in the plasmid standard was designed based on sequence alignments of *hupL* from *Dehalococcoides* sp. genomes of strains 195, BAV-1, CBDB1, and VS (IMG gene object identifiers 637119679, 646445988, 637702682, and 640529159). Primers were used at a concentration of 0.5 µM each to PCR-amplify *hupL* in 50 µL reactions with 25 µL 2X DreamTaq Green Master Mix, cycled with an initial 95ºC denaturation step for 3 min, followed by 45 cycles with 30 s at 95ºC, 30 s at 55ºC, 30 s at 72ºC, then a final 72ºC extension step of 10 min. *hupL* sequences were computationally analyzed using the same protocol as *dsrA* sequences with the following modification: that CD-HIT clustering was performed at 99.5% rather than 97%.

Accession Numbers

Dehalococcoides hupL and sulfate-reducing bacteria *dsrA,* and *Desulfovibrio hynA-1* sequences were submitted to Genbank. *hupL* sequences were assigned accession numbers JX012186-JX012220, *dsrA* sequences were assigned accession numbers HQ399561- HQ399563 and JX012221-JX012223, *hynA-1* sequences were assigned accession numbers HQ399559 and HQ399560.

Quantification of specific genes

Bacterial 16S rRNA Gene

Bacterial 16S rRNA genes were quantified by qPCR amplification using primers Eub341F (5'-CCTACGGGAGGCAGCAG-3') and Eub534R (5'-ATTACCGCGGCTGCTGGC-3'). Plasmids containing 16S rRNA gene fragments from various bacteria were used as quantification standards. The choice of standard plasmid was typically influenced by other 16S rRNA genes being quantified in the

same sample, so that quantification of total bacteria and the phylotype of interest could be performed with the same set of standard dilutions.

Dehalococcoides 16S rRNA Gene

Dehalococcoides 16S rRNA genes were quantified by qPCR amplification using primers Dehalo505F (5'-GGCGTAAAGTGAGCGTAG-3') and Dehalo686R (5'-GACAACCTAGAAAACCGC-3') (Behrens et al. 2008). The standard used was either a 1.4 kb fragment of *Dehalococcoides* 16S rRNA gene obtained as part of community analysis of the reductive dechlorinating soil column inoculated with the Point Mugu culture (Azizian et al. 2010) or the pCR2.1_rdh16S plasmid containing fragment of the *Dehalococcoides* 16S gene and several reductive dehalogenase genes constructed as part of an earlier study (Behrens et al. 2008). The plasmid was digested using the PciI restriction enzyme for 3-5 hours prior to use.

Dehalococcoides Reductive Dehalogenase Genes

Genes encoding *Dehalococcoides* vinyl chloride reductase (*vcrA* and *bvcA*), trichloroethene reductase (*tceA*), and tetrachloroethene reductase (*pceA*) were quantified as previously described (Behrens et al. 2008) using the pCR2.1_rdh16S plasmid as a standard as described above.

Dehalococcoides hupL *Gene*

Abundance and expression of the *Dehalococcoides hupL* ([NiFe] Hydrogenase Large Subunit) were measured by qPCR amplification using primers developed as part of this study based on a multiple sequence alignment of *hupL* genes from *Dehalococcoides ethenogenes* 195 and *Dehalococcoides* sp. VS, CBDB1, GT, and BAV1. Primers are HupL_Fq_56 (5'- AAGCCACCGTAGACGGCG-3') and HupL_Rq_190 (5'- AGTGCCGTGRGAGGTGGG-3') and yield a 134bp amplicon. The standard used was a plasmid containing a 1246 bp fragment of the *Dehalococcoides hupL* gene created as described in section 5.1.1.2.1. The plasmid was digested using the PciI restriction enzyme for 3-5 hours prior to use.

Desulfitobacterium *16S rRNA Gene*

Primers for measurement of *Desulfitobacterium* 16S rRNA gene abundance were Dsb406F (5'-GTACGACGAAGGCCTTCGGGT-3') and Dsb619R (5'- CCCAGGGTTGAGCCCTAGGT-3') (Smits et al. 2004). The standard used was a 1.4kb fragment of a *Desulfitobacterium* 16S rRNA gene obtained as part of community analysis of the reductive dechlorinating soil column inoculated with the Point Mugu culture (Azizian et al. 2010).

Desulfovibrio *Dissimilatory Sulfite Reductase (*dsrA*) Gene*

To quantify *Desulfovibrio* sp. a qPCR primer set targeting *dsrA* genes present in the Point Mugu culture was used. These primers were first tested *in silico* against the *dsrA* gene fragments sequences obtained from clone libraries representing the day 543 and day 1172 time points in the PM2L chemostat. Forward primer DSV_dsrA_Fq (5'-TCCTGGGTGTCGTAGCAG-3') and reverse primer DSV_dsrA_Rq (5'-CCTGACCAACATGCACGG-3') were shown using Geneious to target 85 of the 91 obtained sequences and 90/91 sequences with one mismatch allowed. A plasmid from the clone library generated from the PM2L chemostat was used as a standard.

Geobacteraceae *16S rRNA Gene*
Primers for measurement of *Geobacteraceae* 16S rRNA gene abundance were GEO_577F (5'-GCGTGTAGGCGGTTTSTTAA-3') and GEO_822R (5'-TACCCGCRACACCTAGTACT-3') (Azizian et al. 2010). The standard used was a 1.4kb fragment of a Geobacter 16S rRNA gene obtained as part of community analysis of the reductive dechlorinating soil column inoculated with the Point Mugu culture (Azizian et al. 2010).

4.2 Materials and Methods for Project 2:

4.2.1 Model Development of Continuous-Stirred Tank Reactor Using EV Culture

The model is based on the processes presented in Figure 1.

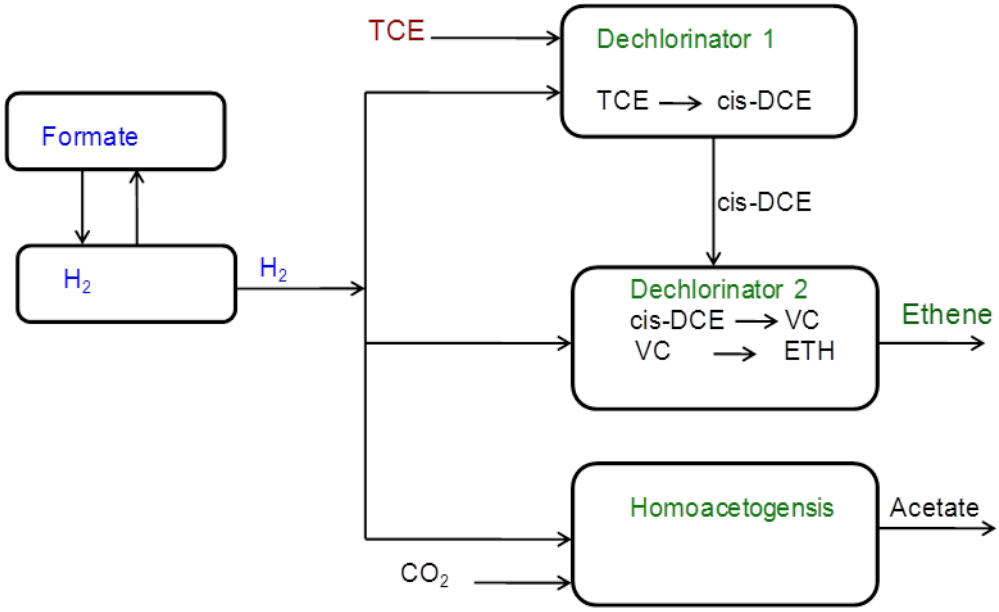

Figure 1. Conceptual model of electron donor and electron acceptor, formate is assumed in equilibrium with H_2 and acetate was not considered as an electron donor in the dechlorination process.

The model accounts for H_2 production by formate dissociation, where formate is in equilibrium with H_2 and the ratio of formate to H_2 is 121 (Fennell and Gossett, 1998). Three microbial communities were simulated in the model, two dehalogination cultures and homoacetogens. Previous enrichment culture studies have indicated that two different dechlorinator populations are often involved in the complete transformation of PCE to ethene (Rosner et al., 1997; Flynn et al., 2000). Therefore, two microbial populations were assumed in the model to be responsible for complete dechlorination of TCE to ethene: TCE dechlorinators (X_{d1}) and cDCE/VC dechlorinators (X_{d2}). A third H_2-utilizing, homoacetogenesis ($X_{homoacet}$) population, was also included in the model

to simulate competition for H_2 between these organisms and dechlorinating populations(Bagley, 1998).

Previous studies (Yu and Semprini, 2004; Behrens et al., 2008) showed the absence of methanogenes in the EV culture, which is consistent with the lack of methane formation observed in the CSTR. The model developed here coupled the thermodynamic and kinetic models previously described by Fennell and Gossett (1998). The biokinetic equations for CAHs dechlorination used in the model were described by double-Monod-type expressions as presented in Cupples et al. (2004). The dual Monod expressions were used to represent both electron donor (H_2) and electron acceptor (CAHs) availability. Inhibition kinetics for the dechloriation reactions were also included where parent products inhibited daughter products (Yu and Semprini, 2004; Yu et al., 2005. The electron donor (H_2) concentration term includes a H_2 threshold as presented in Cupples et al. (2004) and is given in Equations 5.1 to 5.4. Homoacetogens were included as a competing process for H_2 consumption. The set of equations are coupled to those required to simulate the input/output and accumulation terms for a CSTR. The system of equations was solved numerically using COMSOL 3.5a applying the Chemical Engineering Module.

The resulting numerical model was verified by comparing its results to previously published results of Fennell and Gossett (1998). The model was also found to conserve mass and electron balance when applied to CSTR.

The following assumptions were considered in developing the CSTR model:

- Microorganisms follow the same intrinsic growth kinetics as in batch reactors;
- Ideal mixing conditions exist in the CSTR;
- Liquid volume in the CSTR reactor is constant;
- The pH was constant due to the high buffer capacity applied;
- Two dechlorinator microbial communities were responsible for TCE dechlorination to ethene: TCE reducers, for TCE transformation to cDCE and *Dehalococcoidis* spp for cDCE degradation to ethene via VC
- Initial biomass inocula consists of 70 % of the dechlorinators are *Dehalococcoidos* spp;
- Competitive inhibition of parent chlorinated ethenes and daughter (Yu et al., 2005) with inhibition constants represented by the K_s value (Yu and Semprini., 2004);
- H_2 is the only electron donor used for reductive dehalogenation;
- Competition for H_2 exists between the dehalogenators and homoacetogens;
- The contribution of acetate as an electron donor to the dehalogenation process is assumed to be negligible;
- H_2 is assumed to be in equilibrium with formate at a ratio of 121 moles of formate to H_2;
- An additional constraint to the acetate formation reaction is provided by thermodynamic consideration (ΔG_{rxn} of acetate formation must be less than $\Delta G_{critical}$).

4.2.2 Modeling of CAH Transformation

The anaerobic reductive dechlorination of CAHs in the CSTR was simulated using dual Monod-type kinetics with competitive inhibition presented by Cupples et al. (2004) and Yu et al. (2005).

The Monod kinetic expressions for chlorinated solvent degradation and with H_2 as the electron donor are expressed by the following equations:

$$R^{PCE} = \left(\frac{K_{\max\_PCE}\ X_{d1}\ [PCE]}{K_{S\_PCE} + [PCE]} \right) \left(\frac{[H_2] - [H_{2,th}]}{K_{s,H_2} + ([H_2] - [H_{2,th}])} \right) \quad (5.1)$$

$$R^{TCE} = \left(\frac{K_{\max\_TCE}\ X_{d1}\ [TCE]}{K_{S\_TCE}\left(1 + \frac{[PCE]}{K_{CI\_PCE}}\right) + [TCE]} \right) \left(\frac{[H_2] - [H_{2,th}]}{K_{s,H_2} + ([H_2] - [H_{2,th}])} \right) \quad (5.2)$$

$$R^{VC} = \left(\frac{K_{\max\_VC}\ X_{d2}\ [VC]}{K_{S\_VC}\left(1 + \frac{[TCE]}{K_{CI\_TCE}} + \frac{[cDCE]}{K_{CI\_cDCE}}\right) + [VC]} \right) \left(\frac{[H_2] - [H_{2,th}]}{K_{s,H_2} + ([H_2] - [H_{2,th}])} \right) \quad (5.3)$$

$$R^{VC} = \left(\frac{K_{\max\_VC}\ X_{d2}\ [VC]}{K_{S\_VC}\left(1 + \frac{[TCE]}{K_{CI\_TCE}} + \frac{[cDCE]}{K_{CI\_cDCE}}\right) + [VC]} \right) \left(\frac{[H_2] - [H_{2,th}]}{K_{s,H_2} + ([H_2] - [H_{2,th}])} \right) \quad (5.4)$$

where R^{PCE}, R^{TCE}, R^{cDCE}, and R^{VC} are the rates of PCE, TCE, cDCE, VC dechlorination (mol/L-d); [PCE], [TCE], [cDCE] , and [VC] are the aqueous phase concentrations of the contaminant species (mol/L); $K_{max,PCE,}$ $K_{max,TCE,}$ $K_{max,cDCE,}$ $K_{max,VC,}$ are the maximum dechlorination rates of PCE, TCE, cDCE and VC, respectively (mol /L); X_{d1} is the biomass of dechlorinators of PCE into cDCE through TCE (mg/L); X_{d2} is the biomass of dechlorinatores of cDCE into ethene through VC (mg/L); K_{C_PCE}, K_{C_TCE}, K_{C_cDCE}, are the inhibition constants of each chlorinated ethene, (mol/L), which were set equal to their respective half-velocity coefficients (K_S) as previously reported (Yu, 2003); C_{H_2} is the hydrogen concentration (mol/L); $C^*_{H_2}$ is the hydrogen threshold concentration (mol/L); and K_{s,H_2} is the half-saturation coefficient for H_2 used by dechlorinators (mol/L).

The equations for each step in the dehalogenation process for a CSTR configuration are presented in equations 5.5-5.8.

$$V\frac{dC_{TCE}}{dt} = QC_{TCEin} - QC_{TCE} - \frac{K_{\max,TCE}X_{d1}C_{TCE}}{K_{S,TCE}+C_{TCE}}\left(\frac{C_{H_2}-C_{H_2,th,TCE}}{K_{s,H_2}+(C_{H_2}-C_{H_2,th,TCE})}\right)V \tag{5.5}$$

$$V\frac{dC_{DCE}}{dt} = QC_{DCEin} - QC_{DCE} + \frac{K_{\max,TCE}X_{d1}C_{TCE}}{K_{S,TCE}+C_{TCE}}\left(\frac{C_{H_2}-C_{H_2,th,TCE}}{K_{s,H_2}+(C_{H_2}-C_{H_2,th,TCE})}\right)V$$
$$-\frac{K_{\max,DCE}X_{d2}C_{DCE}}{K_{S,DCE}(1+\frac{C_{TCE}}{K_{C_{TCE}}})+C_{DCE}}\left(\frac{C_{H_2}-C_{H_2,th,DCE}}{K_{s,H_2}+(C_{H_2}-C_{H_2,th,DCE})}\right)V \tag{5.6}$$

$$V\frac{dC_{VC}}{dt} = QC_{VCin} - QC_{VC} + \frac{K_{\max,DCE}X_{d2}C_{DCE}}{K_{S,DCE}(1+\frac{C_{TCE}}{K_{C_{DCE}}})+C_{DCE}}\left(\frac{C_{H_2}-C_{H_2,th,DCE}}{K_{s,H_2}+(C_{H_2}-C_{H_2,th,DCE})}\right)V \tag{5.7}$$
$$-\frac{K_{\max,VC}X_{d2}C_{VC}}{K_{S,VC}(1+\frac{C_{TCE}}{K_{C_{TCE}}}+\frac{C_{DCE}}{K_{C_{DCE}}})+C_{VC}}\left(\frac{C_{H_2}-C_{H_2,th,VC}}{K_{s,H_2}+(C_{H_2}-C_{H_2,th,VC})}\right)V$$

(5.8)

$$V\frac{dC_{ETH}}{dt} = QC_{ETH,in} - QC_{ETH} + \left\{\frac{K_{\max,VC}X_{d2}C_{VC}}{K_{S,VC}(1+\frac{C_{TCE}}{K_{C_{TCE}}}+\frac{C_{DCE}}{K_{C_{DCE}}})+C_{VC}}\left(\frac{C_{H_2}-C_{H_2,th,VC}}{K_{s,H_2}+(C_{H_2}-C_{H_2,th,VC})}\right)\right\}V$$

where Q is the volumetric flow rate (L/day), and V is the reactor volume (L), and *TCE*, cDCE, *VC* and Eth is the effluent; CAHs concentrations (mmol/L); K_{max} is the maximum specific utilization rate (µmol/mg protein/day); X is the biomass concentration (mg protein/L); and K_S is the half-velocity coefficient (µmol/L); $K_{c,TCE}$ and $K_{c,cDCE}$, is the competitive inhibition coefficient of *TCE* and *cDCE* on dechlorination of the lesser chlorinated compounds respectively (µmol/L).

4.2.3 Modeling of formate and H2.

Formate was used as an electron donor with formate dissociating to produce H_2. Formate in the aqueous phase is assumed to be in equilibrium with aqueous H_2. The ratio of formate$_{(aq)}$ to $H_{2(aq)}$ is 121 (Fennell, 1998) as presented in Equations (5.9) and (5.10), where equilibrium is represented as a ratio of forward to reverse rates of reaction:

$$K_{eq} = \frac{[H_2]}{[Formate]} = \frac{1}{121} = \frac{k_f}{k_r} \tag{5.9}$$

$$V\frac{dC_{for}}{dt} = QC_{for,in} - QC_{for} - k_f C_{for} + k_r C_{H_2} \tag{5.10}$$

H_2 production and consumption is simulated using Equation 5.11:

$$V\frac{dC_{H2}}{dt} = QC_{H2,in} - QC_{H2} + \{k_f C_{for}\}V - \begin{Bmatrix} R_{TCE} + R_{cDCE} + R_{VC} \\ k_r C_{H_2} + \dfrac{dC_{Acet_{H_2}}}{dt} \end{Bmatrix} V \tag{5.11}$$

where $dC_{Acet,H2}/dt$ is the rate of acetate formation using H_2 for homoacetogenesis; Q is the volumetric flow rate (L/day), V is the reactor volume (L), and C_{for} is the CSTR formate concentration in (mM); C_{H2} is the CSTR H_2 concentration (nM); k_f is the forward rate constant of dissociation of formate (day^{-1}); k_r is the reversible rate constant of formate formation; R_{TCE} is the rate of TCE dehalogenation; R_{cDCE} is the rate of cDCE dehalogenation; R_{VC} is the rate of VC dehalogenation; k_f is the first order constant (d^{-1}); and k_r is the reverse equilibrium constant (d^{-1}). The k_f and k_r for formate dissociation are high enough for equilibrium to be reached. The R_c terms are provided below:

4.2.4 Modeling of Acetate Production

The CSTR model incorporates the thermodynamically based equations for simulating acetate formation (Fennell and Gossett, 1998). Acetate production and consumption is governed by both thermodynamics as well as kinetics (Equation 5.12). The rate of acetate formation in the CSTRs given by:

$$V\frac{dC_{acet}}{dt} = QC_{acet,in} - QC_{acet} + \left\{\frac{1}{4}\frac{dAcet_{,H_2}}{dt} + \frac{dX_{acet}}{dt}\right\}V - \frac{dX_{growth}}{dt}V \quad (5.12)$$

where $\frac{dC_{Acet,H_2}}{dt}$ is the rate of acetate production by acetogenesis; $\frac{dX_{acet}}{dt}$ is the rate of acetate production from decaying cells; $\frac{dX_{growth}}{dt}$ is the rate of acetate utilization for cell synthesis.

4.2.5 Biomass Modeling

The growth of microorganisms in the CSTR requires the input of a carbon source (substrate), electron donor (energy), and electron acceptor. Acetate is assumed the carbon source, while H_2 is the energy source. The growth of each biomass population is a function of cell yield, electron acceptor and first order microbial decay. Based on the conceptual model of donor and acceptor utilization (Figure 1) three microbial populations were included for potential growth in the CSTR; one grows on TCE, another (*Dehalococcoides*) that grows as a result of the dehalogenation of cDCE to ethene and the third, homoacetogens, that grow as a result of producing acetate from H_2. The following equations (Equation 5.13-5.15) describe the biomass growth and decay for the three populations:

$$V\frac{dX_{d1}}{dt} = QX_{d1in} - QX_{d1} + (Y_{d1}(R_{TCE}) - k_{d1}X_{d1})V \quad (5.13)$$

$$V\frac{dX_{d2}}{dt} = QX_{d_{2in}} - QX_{d2} + (Y_{d2}(R_{cDCE} + R_{VC}) - k_{d2}X_{d2})V \quad (5.14)$$

$$V\frac{dX_{Homoacet}}{dt} = QX_{Homoacet,_{in}} - QX_{Homoacet} + \begin{pmatrix} Y_{Homoacet}(\frac{dC_{Acet\_H2}}{dt}) \\ -k_{d,Homoacet}X_{Homoacet} \end{pmatrix}V \quad (5.15)$$

Where Y is the biomass yield (mg of protein/μ mole of substrate); k_d is the first-order endogenous decay (d^{-1}); X is the biomass concentration (mg protein/L).

4.2.6 EV Culture enrichment and growth and CSTR operation

The EV anaerobic mixed culture used in the CSTR study was isolated from subsurface samples from the Evanite site in Corvallis, Oregon (EV). Details of the enrichment process are provided by Yu et al. (2003). Previous studies (Yu et al., 2005; Azizian et al., 2008; Sabalowsky, 2008; Sabalowsky et Semprini, 2010; Behrens et al., 2008) showed that EV culture had *Dehalococcoides*-like microorganisms with the ability of complete reductive dehalogenate PCE to ethene. This EV enriched culture was used to inoculate the CSTR.

The EV culture was grown in a basal growth medium, containing Na_2S to maintain anaerobic conditions and buffer to maintain constant pH. The formulation of the medium is presented in

Appendix A. The experiment was conducted in two independent bench-scale CSTRs (Berggren, 2011). The hydraulic volumes of reactors A and reactor B were 5.6 and 2.3 liters, respectively. Both reactors were fed formate at a concentration of 45 mM, TCE at a concentration of 10 mM and were operated at room temperature (20° C). Under these conditions formate was fed in excess of the amount to completely dehalogenate TCE to ethene. The feed was added to each reactor using peristaltic pump at a rate of 100 mL/day for reactor A and 50 mL/day for reactor B resulting in a hydraulic residence time of 55 days and 46 days for reactors A and B, respectively.

The bioreactors were first filled with media and a cell suspension. The input stream was then used to feed the reactors with fresh media, while an output stream is used to withdraw the cells and liquid media simultaneously from the CSTR. The CSTR was maintained as all liquid volume chemostat.

Over the course of the experiment, the influent formate and TCE were continuously measured along with effluent TCE and transformation products, formate, H_2, acetate and biomass. Details of the chemostat operation are provided by Berggren (2011). The 2-L and 5-L CSTRs operating conditions are presented in Table 2.

Table 2 - Physical, chemical and Hydraulic input parameters for the 5-L and 2-L CSTRs

Parameter	Unit	5-L CSTR value	2-L CSTR value
Reactor volume	L	5.66	2.35
Influent flow	ml/day	100	50
Hydraulic and cell residence time	day	56.6	45.7
Influent TCE saturation concentration	mM	10.2	10.2
Formate as the substrate	mM	45	45
Influent acetate concentration	mM	0.0	0.0
Influent biomass (protein concentration)	mg/L	0.0	0.0

The 5-L CSTR was operated as a control and feed conditions were held constant. The 2-L CSTR had transient feed conditions. The 2-L CSTR was operated for more than 600 days. During the first phase (120-180 days) the influent formate and TCE concentration were 45 mM and 10 mM respectively. During the second phase (180-620 days) formate was reduced to 25 mM while TCE was maintained at 10 mM.

4.2.7 Kinetics of EV culture

The 2-L and 5-L CSTRs growing EV culture were operated for more than 600 days. Therefore, there are two sources of VC kinetic parameters: (i) using the previously batch determined EV kinetic parameters by Yu and Semprini (2004); (ii) VC kinetic parameters determined in batch experiments using cells harvested from the 5-L and 2-L CSTR.

4.2.8 Previously determined EV kinetic parameters

Yu and Semprini (2004) determined the kinetic parameters of EV culture in batch kinetic reactors (Table 3).

Table 3 - EV culture kinetic parameters determined in batch experiments by Yu and Semprini (2004) and the modified kinetic parameters based on microbial distribution in the model formulation.

	EV culture Kinetics (Yu and Semprini, 2004)					
	K_{max} (μ mole/mg protein/d)	K_s (μM)	Y mg protein / μ mol of substrate	K_d (d^{-1})	$K_{s\text{-}H2}$[#] utilization (nM)	H_2 Threshold (nM)
TCE	125	1.8	0.006	0.024	7	0.35[1]
cis-DCE	13.8	1.76	0.006	0.024	7	0.35[2]
VC	8.1	62.6	0.006	0.024	7[2]	1.0[1,2,3,4, #]
Acetogenesis	25.3	19.4	0.034	0.04	7	40

Competitive inhibition coefficients were set equal to their respective half-velocity coefficients (K_S) as previously reported (Yu, 2003).
The yield of dechlorinators is 0.006 mg protein/μmol substrate.
The cells decay coefficient is 0.024 d^{-1}.
$K_{s\text{-}H2}$ utilization is 7 nM
[#] Cupples et al., 2004.
[1] Loffler et al., 1996; [2] Cupples et al., 2003; [3] Breznak, 1994.; [4] Cord-Ruwisch et al., 1988; [5] This study

These kinetics were based on a total protein concentration. However, in our simulations, the dehalogenation population were divided in two populations, the kinetic parameters were modified based on population distribution (42% *Dehalococcoides*, 28 % TCE reducers and 30% acetogens and other reducers). The modified kinetic parameters for EV culture are presented in Table 4, column A.

Table 4 - VC dechlorination kinetic parameters determined in batch experiments using cells harvested from the 5-L CSTR and 2-L CSTR at different time points

Model Parameter	Unit	Value			
		A	B (5L CSTR)	C (2L CSTR)	D (2L CSTR)
K_{max_VC}	µmol/mg protein/d	17.0	26.0	7.8	16.0
K_{s_VC}	µ mol/L	62.6	12.0	14.0	10.0
Y_{dech1}	mg protein/µmol of substrate	0.006	0.0043	0.0043	0.0043
$Y_{dech\ 2}$	mg protein/µmol of substrate	0.006	0.0031	0.0031	0.0031
$K_{d\_dech\ 1}$	(d^{-1})	0.024	0.045	0.045	0.045
$K_{d\_dech\ 2}$	(d^{-1})	0.024	0.051	0.055	0.055
utilization in VC dechlorination	nM	7.0	7.0	7.0	7.0

A : Modified Yu and Semprini (2004) kinetics.
B : Kinetic parameters determined in batch experiment using cells harvested from the 5-L CSTR at steady-state with excess formate condition, on day 190, with adjusted yield and decay.
C : Kinetic parameters determined in batch experiment using cells harvested from the 2-L CSTR on day 520, at point 2 as shown in Figure 34.
D : Kinetic parameters determined in batch experiment using cells harvested from the 2-L CSTR on day 600, at point 3 as shown in Figure 34, with adjusted yield and decay.

This microbial distribution was based on preliminary simulations of the steady-state biomass distribution in the simulated 2-L and 5-L CSTR and based on using molecular methods, *Dehalococcoides* 16S rRNA gene copy number determined by *q PCR* where the culture measured to be 73% dehalogenators (Behrens et al., 2008), during the period Yu and Semprini measured the EV kinetic parameters. The kinetic parameters for the EV culture are approximately 10 times faster for TCE dechlorination than VC dechlorination. The competitive inhibition coefficient of higher chlorinated compounds on dechlorination of the lesser chlorinated compounds (µM) was modeled as equivalent to the half-velocity coefficients for that CAH (Yu and Semprini, 2004; Yu et al., 2005).

4.2.9 VC Kinetic Parameters Determined Using Cells Harvested From the CSTRs Batch Experiments Using Cells Harvested From the 5-L CSTR.

To simulate the CSTR using EV culture and formate under excess electron donor, VC batch kinetic tests were carried out using cells harvested from the 5-L CSTR at steady-state operation. While the CSTR was running at steady-state, cells were harvested on day 190 from the 5-L CSTR and used in batch reactor experiments to evaluate VC dehalogenation rates. The K_{max} and K_s for VC dehalogenation from the 5-L CSTR are presented in Table 4, column B on a total protein concentration basis. The initial measured total biomass concentration was 30 mg protein/L. The culture from the CSTR was inoculated to a 156 ml reactor with 75 ml liquid and 81 ml headspace. The H_2 concentration was non-limiting through the experiment. VC was spiked in the reactor resulting in an initial aqueous concentration of 160 μM.

The multi-equilibrium method of Yu and Semprini (2004) was used to determine K_{max} and K_s values. Non-linear fitting was used to determine the kinetic parameters for VC. A summary of kinetic parameters determined is presented in Table 4, column B. $K_{max\text{-}VC}$ dechlorination was of 26 μmol/mg protein/d) and $K_{s\text{-}VC}$ of 12 μM. The $K_{max\text{-}VC}$ is higher and $K_{s\text{-}VC}$ is lower than values determined by Yu and Semprini (2004). The determined VC kinetic parameters in batch experiments using cells harvested from the 5-L CSTR showed a higher VC transformation rate than reported by Yu and Semprini (2004). This could be due to apparent shifts in culture performance under chemostat growth conditions.

4.2.10 Modeling Approach and Verification

A literature review was performed to determine "average" values for the model kinetic parameters, the yield coefficient and the endogenous decay coefficient (Table 4). Modified CAHs transformation K_{max} and K_s values determined by Yu and Semprini (2004) for PM culture are presented in Table 4. Maximum utilization (K_{max}) rate was determined (Yu and Semprini, 2004) based on total protein concentration.

The developed model was constructed and implemented in the commercial finite element code COMSOL Multiphysics 3.5a (www.comsol.com). To solve the systems of ordinary differential equations with initial values, the transient Chemical Engineering Module was used. The time step for calculation was adjusted to yield the relative tolerance smaller than 1×10^{-5}, which specifies the largest acceptable solver error, relative to the size of each state during each time step. Fennell and Gossett (1998) reported that a small time step was required to avoid numerical instability for the calculation of H_2 concentration. A time step of 100 seconds was used to avoid numerical instability for the calculation of H_2 concentration. Output was overlaid on experimental data to examine closeness of fit.

The COMSOL numerical solution of the set of reaction equations 5.1 - 5.14 was coupled with the CSTR model. Equations were verified through mass balance and electron balance. Furthermore, the numerical model was verified by comparison with solutions obtained using Stella_ software for batch reactor kinetics as in Yu and Semprini (2004) and simulations reported by Fennell and Gossett (1998) which were programmed with the same kinetic expressions. Excellent agreement was obtained between the COMSOL and Stella_ software simulations (Model Validation).

5 RESULTS AND DISCUSSION

5.1 Results and Discussion for Project 1:

5.1.1 Testing and Validation of the Tiling DNA Microarray Approach

The tiling DNA microarray approach is an attempt to solve a problem that had become evident in the use of DNA microarrays for monitoring gene abundance and expression in mixed microbial communities. DNA microarrays are also susceptible to false negative results, as target genes of interest must be sufficiently identical to probe sequences in order to correctly hybridize. The intention of using the tiling DNA microarray approach was to overcome this false positive problem. Using many probes per gene and requiring a large majority of those probes to show a strong hybridization signal was intended as a means of avoiding false positives. The intention of the validation experiments described in this chapter was:

- to confirm the insensitivity of the tiling DNA microarray approach to false positive gene detection,
- to determine the detection limit of the method to identify situations in which low-abundance target gene will produce false negative results,
- and to determine the minimum required target gene sequence identity to avoid false negative results due to probe sequences that differ too greatly from the probe sequence to effectively hybridize and produce a fluorescence signal.

5.1.1.1 PCR-Product Test Hybridization

One experiment performed during the early phase of DNA microarray testing was the labeling and hybridization of a single PCR product to the Test Microarray. The *hydA* gene (locus tag SO_3920) from *Shewanella oneidensis* MR-1 was amplified, labeled, and hybridized. This amplicon was 1225bp in length, and thus consisted of almost the complete 1233bp of the SO_3920 open reading frame (ORF). The Bright Probe Fraction (BPF) values for all genes on the array were calculated and ordered from highest to lowest (Figure 2).

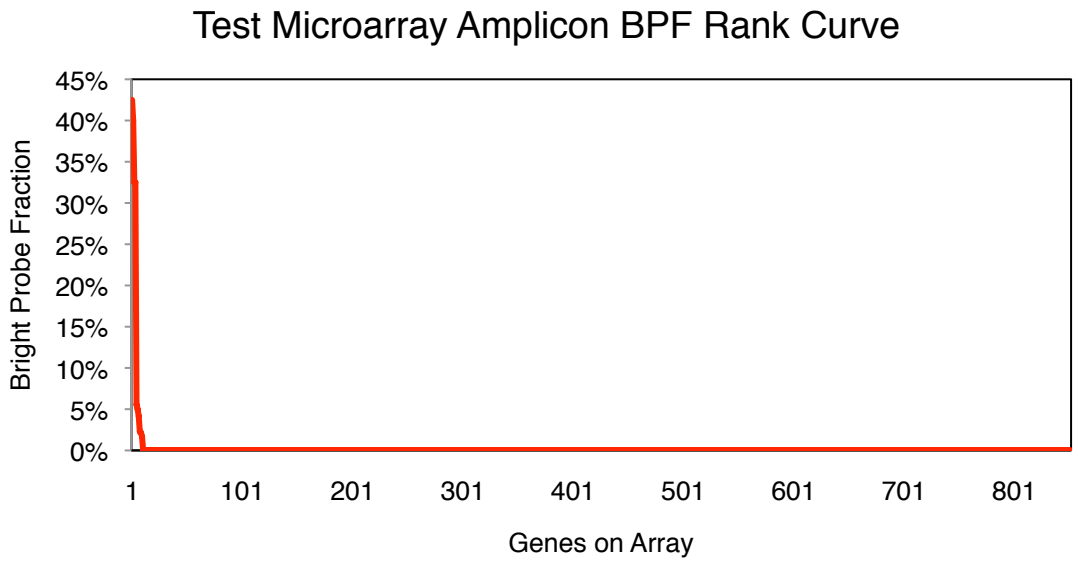

Figure 2 – BPF Values for all probes on the Test DNA Microarray hybridized with PCR-amplified *Shewanella oneidensis* MR-1 *hydA*.

The genes with the top ten BPF values are listed in Table 5.

Gene Product Annotation	BPF
[FeFe] Hydrogenase HydA (SO_3920), *Shewanella oneidensis* MR-1	42.5%
[FeFe] Hydrogenase HydA (SO_3920), *Shewanella oneidensis* MR-1, reverse complement	40.0%
[FeFe] Hydrogenase HydA (Shewmr4_3250), *Shewanella oneidensis* MR-4	32.5%
[FeFe] Hydrogenase HydA (SO_3920), *Shewanella oneidensis* MR-1 (array duplicate)	32.5%
[FeFe] Hydrogenase from Termite Gut Metagenome, IMG/M ID 2005608198	5.6%
[FeFe] Hydrogenase from Termite Gut Metagenome, IMG/M ID 2005622586	5.0%
[FeFe] Hydrogenase from Termite Gut Metagenome, IMG/M ID 2005599188	4.2%
[FeFe] Hydrogenase Dde_0474, *Desulfovibrio alaskensis* G20	2.3%
[FeFe] Hydrogenase from Termite Gut Metagenome, IMG/M ID 2005575053	2.2%
[FeFe] Hydrogenase Dvul_1384, *Desulfovibrio vulgaris* DP4	1.7%

Table 5 - Genes with top ten BPF values for the *Shewanella oneidensis hydA* PCR amplicon test hybridization.

As predicted, the probes targeting the hybridized *hydA* gene yielded the highest BPF (Table 5). Since the PCR product is double stranded, it is no surprise that the probes targeted both the gene itself and the reverse complement of the gene. However, these BPF values were surprisingly low, ranging from 32.5-42.5% of the gene when the PCR amplicon consists of almost 100% of the gene. Closer examination of the fluorescence intensity of the individual probes for these genes explained these surprisingly low BPF values (Figure 3).

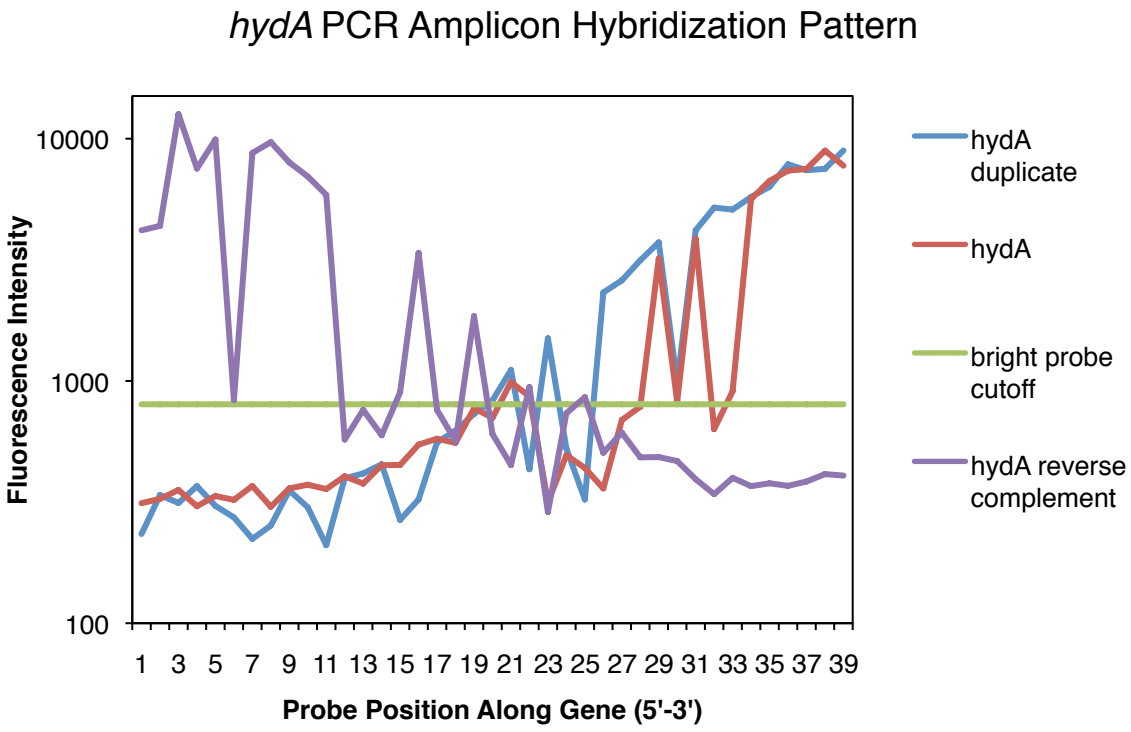

Figure 3 – Hybridization Patterns for the PCR amplicon hybridization (probe fluorescence intensities ordered from the 5' to the 3' end of each gene)

For both duplicates of the probes targeting the *hydA* gene, there is a clear trend in fluorescence intensity from the 5' to the 3' end of the gene. The fact that this trend is reversed for the reverse complement probes suggest that this is a result of steric hindrance to binding of the amplicon DNA to the probe DNA, with probes oriented with their 5' ends attached to the glass slide surface meaning that less DNA extending beyond that 5' end will increase the potential hybridization efficiency. As this was not an effect observed using bulk DNA hybridization (section 5.1.2.2) this was most likely an artifact of hybridizing complete and intact amplicons greater than 1 kilobase in length. Under these conditions more than half of the amplicon was not available for hybridization to the array. Since hybridization of a complete unfragmented PCR amplicon is an unusual circumstance and not how this array method was intended for use, these unexpectedly low BPF values were not thought to present a problem when evaluating mixed microbial communities. Some other microarray methods where amplicons are hybridized to the microarray typically employ a fragmentation step prior to hybridization to avoid this problem (DeSantis et al. 2007).

5.1.1.2 Genome Test Hybridizations

The goal of using the tiling DNA microarray approach was to avoid false positive gene identifications against an unknown and complex genomic background. In order to test whether or not this goal was achieved, two test hybridization experiments were performed: the first with genomic DNA from a single microorganism, and the second with a mixture of genomic DNA from five different microorganisms.

5.1.1.2.1 Single Genome Hybridization

The first step in evaluating the tiling DNA microarray approach with regard to its potential for cross hybridization was to test how the microarray would perform with DNA hybridized from the simplest possible microbial community: a single microbial species. Genomic DNA from *Shewanella oneidensis* MR-1 was labeled and hybridized to the Test Microarray. The BPF Rank Curve for this hybridization is shown in Figure 4. The BPF rank curve demonstrates a clear separation between those genes present in the *Shewanella oneidensis* MR-1 genome whose detection is expected, and those genes not present in the *Shewanella oneidensis* genome. This shows that for the simplest possible genomic background of a single microorganism, the tiling DNA microarray approach does not produce false positive gene identification results.

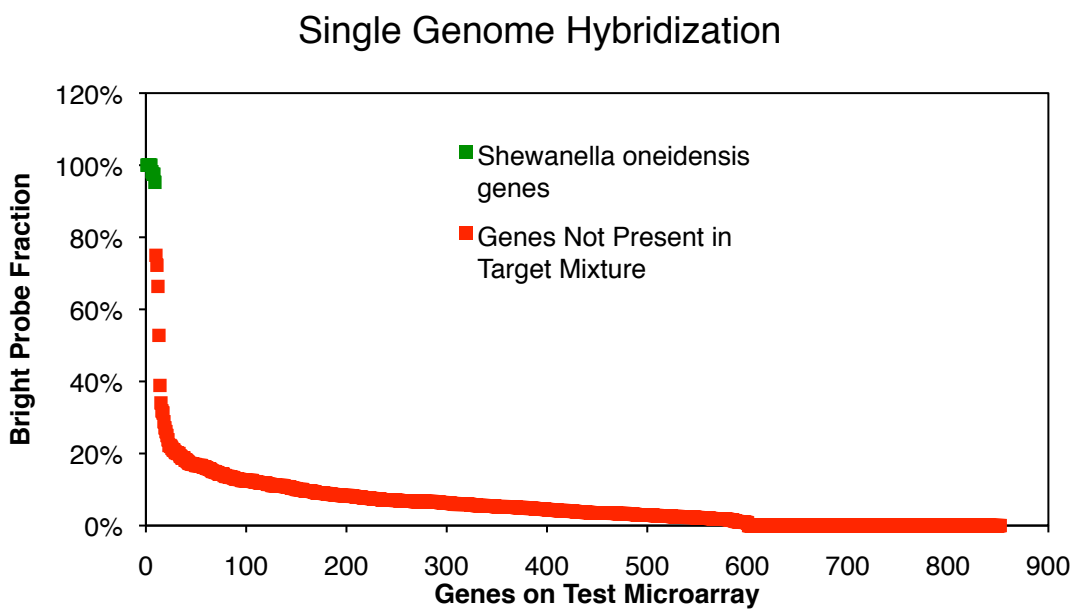

Figure 4 – BPF Rank Curve for *Shewanella oneidensis* MR-1 genomic DNA hybridized to the Test Microarray

Also performed as part of this single genome hybridization experiment was a test of hybridization efficiency to mismatch probes. One probe from the *Shewanella oneidensis hydB* gene (SO_3921) was placed on the array in 28 additional instances, each with a different kind of mismatch. 19 of these additional instances included single nucleotide changes at different locations, and 9 of these instances involved the substitution of 11 nucleotides from the center of the probe sequence. The results of these mismatch hybridizations are presented in Table 6. Single nucleotide changes (98% identity) did not significantly reduce the fluorescence intensity relative to the perfect-match probes. Continuous mismatch sections of 11 nucleotides (82% identity) did significantly reduce fluorescence intensity, suggesting that this tiling DNA microarray approach is insensitive to small differences in identity between the probe and target sequences, but there is an identity threshold (>82%) below which significant a significant fluorescence signal should not be expected.

Probe ID	Probe Sequence	Spot Intensity	Identity
MR1HA01	ATGAACAAGAAAAAACACCTATTTGCCGAGGACAGTTTCTTTCTGTCACGCCGTAAATTT	100%	100%
MR1HMM01	CTGAACAAGAAAAAACACCTATTTGCCGAGGACAGTTTCTTTCTGTCACGCCGTAAATTT	89%	98%
MR1HMM02	ACGAACAAGAAAAAACACCTATTTGCCGAGGACAGTTTCTTTCTGTCACGCCGTAAATTT	91%	98%
MR1HMM03	ATCAACAAGAAAAAACACCTATTTGCCGAGGACAGTTTCTTTCTGTCACGCCGTAAATTT	78%	98%
MR1HMM04	ATGCACAAGAAAAAACACCTATTTGCCGAGGACAGTTTCTTTCTGTCACGCCGTAAATTT	82%	98%
MR1HMM05	ATGACCAAGAAAAAACACCTATTTGCCGAGGACAGTTTCTTTCTGTCACGCCGTAAATTT	79%	98%
MR1HMM06	ATGAATAAGAAAAAACACCTATTTGCCGAGGACAGTTTCTTTCTGTCACGCCGTAAATTT	73%	98%
MR1HMM07	ATGAACCAGAAAAAACACCTATTTGCCGAGGACAGTTTCTTTCTGTCACGCCGTAAATTT	80%	98%
MR1HMM08	ATGAACACGAAAAAACACCTATTTGCCGAGGACAGTTTCTTTCTGTCACGCCGTAAATTT	73%	98%
MR1HMM09	ATGAACAACAAAAAACACCTATTTGCCGAGGACAGTTTCTTTCTGTCACGCCGTAAATTT	81%	98%
MR1HMM10	ATGAACAAGAAAAAACACCTATTTGCCGAGGACAGTTTCTTTCTGTCACGCCGTAAATTC	106%	98%
MR1HMM11	ATGAACAAGAAAAAACACCTATTTGCCGAGGACAGTTTCTTTCTGTCACGCCGTAAATCT	99%	98%
MR1HMM12	ATGAACAAGAAAAAACACCTATTTGCCGAGGACAGTTTCTTTCTGTCACGCCGTAAACTT	122%	98%
MR1HMM13	ATGAACAAGAAAAAACACCTATTTGCCGAGGACAGTTTCTTTCTGTCACGCCGTAACTTT	110%	98%
MR1HMM14	ATGAACAAGAAAAAACACCTATTTGCCGAGGACAGTTTCTTTCTGTCACGCCGTACATTT	80%	98%
MR1HMM15	ATGAACAAGAAAAAACACCTATTTGCCGAGGACAGTTTCTTTCTGTCACGCCGTCAATTT	77%	98%
MR1HMM16	ATGAACAAGAAAAAACACCTATTTGCCGAGGACAGTTTCTTTCTGTCACGCCGCAAATTT	94%	98%
MR1HMM17	ATGAACAAGAAAAAACACCTATTTGCCGAGGACAGTTTCTTTCTGTCACGCCCTAAATTT	84%	98%
MR1HMM18	ATGAACAAGAAAAAACACCTATTTGCCGAGGACAGTTTCTTTCTGTCACGCTGTAAATTT	83%	98%
MR1HMM19	ATGAACAAGAAAAAACACCTATTTGCCGAGGACAGTTTCTTTCTGTCACGTCGTAAATTT	88%	98%
MR1HMM20	ATGAACAAGAAAAAACACCTATTTATATATATATATTTCTTTCTGTCACGTCGTAAATTT	0%	82%
MR1HMM21	ATGAACAAGAAAAAACACCTATTTGCGCGCGCGCGTTTCTTTCTGTCACGTCGTAAATTT	7%	82%
MR1HMM22	ATGAACAAGAAAAAACACCTATTTAGAGAGAGAGATTTCTTTCTGTCACGTCGTAAATTT	4%	82%
MR1HMM23	ATGAACAAGAAAAAACACCTATTTTTTTTTTTTTTTCTTTCTGTCACGTCGTAAATTT	1%	82%
MR1HMM24	ATGAACAAGAAAAAACACCTATTTAAAAAAAAAAATTTCTTTCTGTCACGTCGTAAATTT	1%	82%
MR1HMM25	ATGAACAAGAAAAAACACCTATTTGGGGGGGGGGGTTTCTTTCTGTCACGTCGTAAATTT	6%	82%
MR1HMM26	ATGAACAAGAAAAAACACCTATTTCCCCCCCCCCCTTTCTTTCTGTCACGTCGTAAATTT	2%	82%
MR1HMM27	ATGAACAAGAAAAAACACCTATTTACACACACACATTTCTTTCTGTCACGTCGTAAATTT	1%	82%
MR1HMM28	ATGAACAAGAAAAAACACCTATTTGTGTGTGTGTGTTTCTTTCTGTCACGTCGTAAATTT	5%	82%

Table 6 - Relative changes in hybridization intensity caused by mismatch probes on the Test Microarray.

The true sequence (MR1HA01) is listed first, mismatch probes have mismatch nucleotides labeled red, then fluorescence intensity and sequence identity relative to MR1HA01 listed.

This mismatch probe test is by no means a complete evaluation of the mismatch binding between target DNA and probes, but was rather intended as a broad evaluation of the best-case (single nucleotide mismatch) and worst-case (long continuous stretch of mismatches in the center of the probe) mismatch scenarios.

5.1.1.2.2 Five Genome Mixture Hybridization

In order to determine the sensitivity of the tiling DNA microarray technique to false positives, we hybridized a mixture of genomic DNA from five different bacteria to the Test Microarray (the γ-proteobacteria *Escherichia coli*, *Shewanella oneidensis*, *Shewanella sediminis*, *Pseudomonas aeruginosa*, and the Gram-positive *Bacillus subtilis*). These genomes were selected to represent both closely and distantly related microorganisms. The fact that these genomes were sequenced meant that the true set of genes present in this sample was known ahead of time, and that this dataset could therefore be used to understand the behavior of the tiling DNA microarray method when used in microbial communities where the genomic content is unknown.

The first parameter for evaluation of tiling DNA microarrays that had to be determined was the fluorescence intensity above which a probe could be said to be a positive hybridization or "bright", and below which fluorescence could be attributed to background noise or cross-hybridization of non-target DNA or RNA. One would expect that an acceptable fluorescence intensity cutoff would increase with increasing microbial community richness, as a greater diversity of genomic DNA present increases the probability of cross hybridization. This could be observed by comparing the single-genome hybridization to the five genome hybridization. While the mass of DNA hybridized in the five genome hybridization was five times larger than that hybridized for the single-genome experiment, the median probe intensity for all probes on the array was 17.2 times greater. If this increasing probe fluorescence were purely a consequence of increasing DNA quantity, one would expect the fluorescence intensity to roughly scale linearly as we observed in other experiments. However, it seems that there is also a qualitative effect as a consequence of a mixture of genomes being hybridized rather than just a single genome. This suggests that increasing community diversity does indeed increase the frequency of cross-hybridization and thus the fluorescence intensity cutoff for distinguishing "bright" probes from "dark" probes should be a function of the median probe intensity to account for different degrees of diversity in different microbial communities.

The goal in determining the optimal bright probe cutoff intensity was to have a value as low as possible without allowing false positive detection of genes that were not present in the five genome hybridization mixture. Cutoff values calculated by multiplying the median intensity value for all probes on the array by either two or three yielded bright probe fraction (BPF) values of 100% for the 49 genes on the Test Microarray from the genomes of *Bacillus subtilis*, various strains of *Escherichia coli*, and *Shewanella oneidensis*. On the other hand, a cutoff multiplier of 1× yielded false positive gene identifications (BPF 100%) with genes not contained in the five genome hybridization mixture. Since requiring all positively identified genes in a microbial community to have a 100% success rate in the hybridization of target DNA to their probes was considered too stringent, we sought out a cutoff multiplier value that would allow true positive

gene detection down to a BPF of 90%. In this way, if several probes failed due to spatial inconsistencies in the microarray production or hybridization then this would not prevent the positive identification of genes. At the 2× median cutoff, 10 genes showed a BPF greater than or equal to 90% but below 100%. False positive genes included representatives of the genera *Salmonella*, *Anaeromyxobacter*, *Geobacter*, *Streptomyces*, *Magnetospirillum*, *Azoarcus*, and *Novosphingobium*. At the 3× median cutoff, four genes showed a BPF greater than or equal to 90% but below 100%. All four of these false positive genes were from two genomes of strains within the species *Salmonella enterica*. *S. enterica* is closely related to *E. coli*, with these genes being 88-89% identical to *E. coli* genes in the five genome hybridization mixture (Figure 5). False identification of *S. enterica* genes with the hybridization of *E. coli* genomic DNA seemed an acceptable false positive, as most microorganisms as closely related as *S. enterica* and *E. coli* typically share significant physiological similarities.

These results show that by applying a bright probe fluorescence intensity cutoff of 3× the median value for all genes on the array, genes known to be present in a microbial community can be accurately and unambiguously detected in a moderately complex microbial community using the tiling DNA microarray approach.

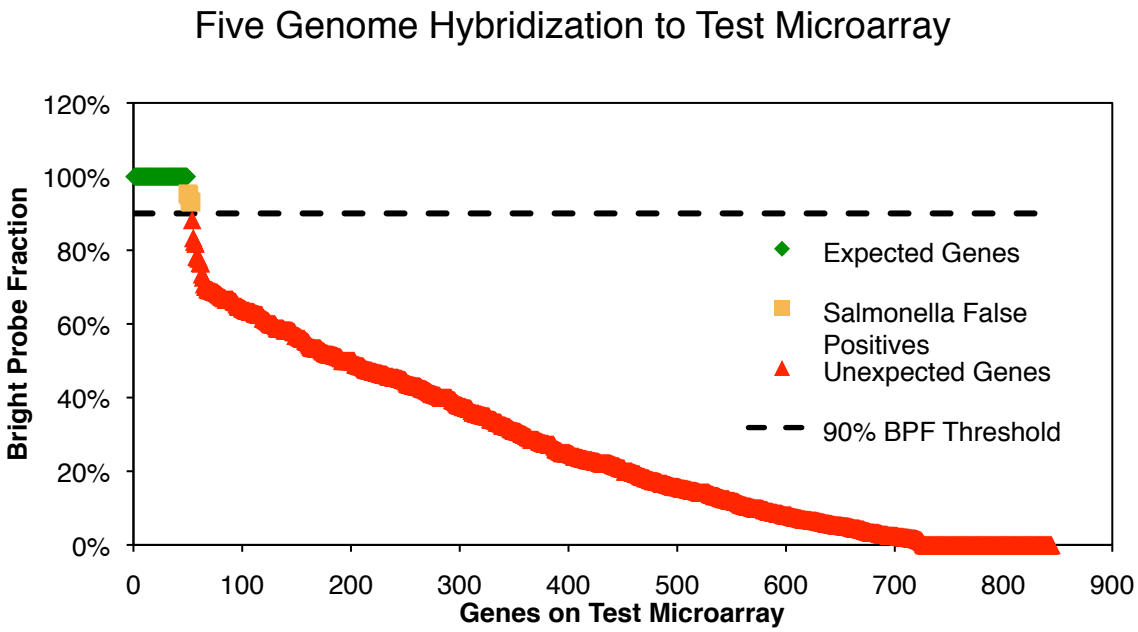

Figure 5 – BPF Rank Curve for a mixture of five genomes hybridized to the Test Microarray.

Expected genes are those genes found in the genomes used for the hybridization, unexpected genes are all other genes on the array.

Through the labeling and hybridization of a defined genomic DNA mixture, we have shown that the tiling approach is generally free of false positive gene detection. A BPF > 90% was demonstrated as a robust measure of positive gene identification. The Test Microarray did reveal

an exception to this robustness where target genes share sequence identity with probe sequences at some threshold above 82% identity but below 88%. This is an acceptable false positive threshold for applications in metabolic molecular microbial ecology, where the goal is to define major physiological groups. Most relevant physiologically distinct groups of microorganisms are differentiated by greater than 18% nucleotide sequence difference. Moreover, this 82-88% identity window is within the 80-95% identity window where genetic discontinuities that differentiate many discrete ecologically discernable populations of microbes occur (Caro-Quintero and Konstantinidis 2012). This makes the tiling DNA microarray ideal for identifying major discrete groups of individuals carrying out a given function in an ecosystem for situations where a highly resolved picture of the diversity within those discrete groups is unnecessary.

Due to the complexity involved in constructing a realistically complex yet defined mixture of RNA, the risk of false positive gene identification during RNA hybridization was not assessed as it was for DNA. However, since even with a 2× cutoff multiplier the microbial mat RNA hybridization yielded only a two-gene subset of the 31 genes identified in the microbial mat DNA hybridization, we saw no reason to believe that the RNA hybridization method would be more prone to false positives than the DNA method.

5.1.1.3 MDA Sensitivity Analysis

To determine the lowest possible quantity of DNA necessary for the identification of a gene, genomic DNA samples from *Escherichia coli*, *Shewanella oneidensis* MR-1, *Azotobacter vinelandii*, and *Methanococcus maripaludis* were mixed together in quantities ranging from 0.1ng to 100ng, then subjected to MDA and hybridized to the Hydrogenase Chip version 3. This experiment was carried out with the assistance of Shirley Galbiati, a high school intern who spent some time in the Spormann Lab. We found that the lowest abundance at which a gene was confidently detected with a BPF > 90% was in the range between 1ng and 10ng of genomic DNA, or between 0.9% and 9% of the total DNA added to the MDA reaction (Table 7).

IMG Gene ID	Gene Product	Genome	BPF	DNA used (ng)	% of total DNA used
637015833	[NiFe] Hydrogenase	*Escherichia coli* K-12 MG1655	24%	0.1	0.09%
637016062	[NiFe] Hydrogenase	*Escherichia coli* K-12 MG1655	33%	0.1	0.09%
637343964	[NiFe] Hydrogenase	*Shewanella oneidensis* MR-1	7%	1	0.90%
637345680	[FeFe] Hydrogenase	*Shewanella oneidensis* MR-1	35%	1	0.90%
638196014	[NiFe] Hydrogenase	*Methanococcus maripaludis* S2	100%	10	9.00%
638196017	[NiFe] Hydrogenase	*Methanococcus maripaludis* S2	100%	10	9.00%
638196352	[NiFe] Hydrogenase	*Methanococcus maripaludis* S2	100%	10	9.00%
638196588	[NiFe] Hydrogenase	*Methanococcus maripaludis* S2	100%	10	9.00%
638196668	[NiFe] Hydrogenase	*Methanococcus maripaludis* S2	100%	10	9.00%
638196913	[NiFe] Hydrogenase	*Methanococcus maripaludis* S2	100%	10	9.00%
643803361	[NiFe] Hydrogenase	*Azotobacter vinelandii* DJ	100%	100	90.01%
643807887	[NiFe] Hydrogenase	*Azotobacter vinelandii* DJ	100%	100	90.01%

Table 7 - Results of a sensitivity analysis performed with a mixture of four different genomic DNA samples at different concentrations. This sample mixture was amplified by MDA and hybridized to Hydrogenase Chip version 3.

This result suggests that in a community of microbes with similar-sized genomes, the detection limit for detecting genes from a given microorganism is somewhere between 0.9% and 9% of the community.

5.1.1.4 Sequence Identity – Bright Probe Fraction relationship

Mismatch probe fluorescence intensities described in section 5.1.2.2.1 gave some limited insight into the expected fluorescence intensities of target DNA partially hybridized to a probe where the sequence does not perfectly match the probe sequence. However, since the tiling DNA microarray approach is based on the fluorescence intensity of many probes targeting an entire gene, it makes more sense to evaluate the hybridization efficiency of non-identical sequences on the scale of an entire gene rather than a single probe. To perform this evaluation we hybridized genomic DNA from *Dehaloccoides* sp. VS to the Reductive Dehalogenase Chip. There are 43 reductive dehalogenase (*rdhA*) genes from sources other than the VS genome with relatively high identity (74.8% - 96.8%) to genes in the VS genome. 12 of these are from the genomes of *Dehalococcoides* sp. GT, 9 from *Dehalococcoides ethenogenes* 195, 9 from *Dehalococcoides* sp. BAV1, 3 from *Dehalococcoides* sp. CBDB1, 2 from *Dehalococcoides* sp. MB, 7 from various *rdhA* clone libraries, and one from the metagenome of the *Dehalococcoides*-containing KB-1 enrichment culture. The BPF for each of these is shown plotted against its sequence identity to its closest relative in the VS genome in Figure 6.

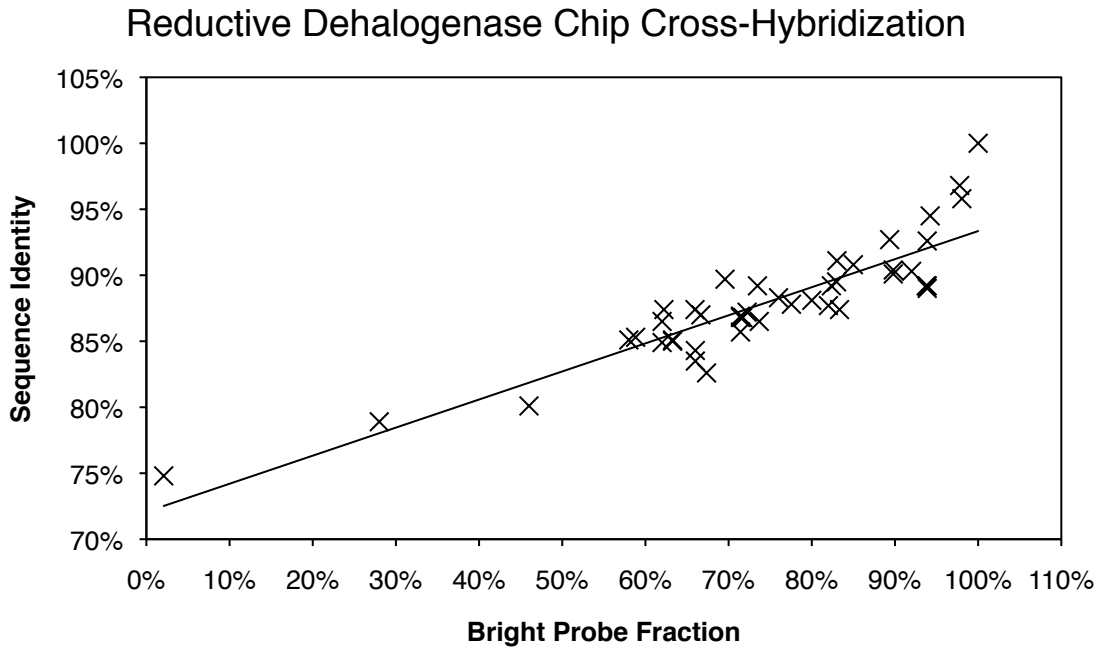

Figure 6 – Sequence identity and BPF for 43 *rdhA* genes highly identical to *rdhA* genes in the VS genome. BPF values come from a hybridization of genomic DNA from *Dehalococcoides* sp. VS hybridized to the Reductive Dehalogenase Chip.

The regression calculated showed a linear correlation between BPF and sequence identity for these *rdhA* genes ($R^2 = 0.79$), although this relationship appears to become nonlinear in the 90-100% sequence identity range (Figure 6). This shows that target gene sequences that are not perfectly identical to the probe sequence on the array will still hybridize to the microarray, although the number of probes above the bright probe cutoff will increase with increasing identity. This finding does not mean that target genes with moderate identity (80-90%) to probe sequences can still be reliably detected in mixed microbial communities, as non-target genes can cause cross hybridization that may generate BPF values in this range.

5.1.2 The Hydrogenase Chip

The Hydrogenase Chip was developed in order to identify H_2-producing and H_2-consuming microbes in anaerobic microbial communities by measuring the abundance and expression of hydrogenase genes from a diverse set of different microorganisms. Four different designs of the Hydrogenase Chip were used during the course of these experiments; these are outlined in the complete list of DNA Microarray design iterations in Table 1. This section describes the different environments and questions to which the Hydrogenase Chip was applied and describes the extent to which the goal of mapping interspecies H_2 transfer was realized.

5.1.2.1 Reductively Dehalogenating Soil Columns

One of the applications planned for the Hydrogenase Chip was to observe competition for H_2 between different physiological groups of microbes during bioremediation, where H_2 is a key

electron donor. Respiration of organohalides is most often linked to the oxidation of H_2. Competing microbial H_2 oxidation linked to the reduction of non-organohalide electron acceptors like sulfate, iron (III), and carbon dioxide can negatively impact upon the efficiency of bioremediation (Yang and McCarty 1998). An anoxic reductive dechlorinating soil column, pictured in Figure 7, operated by Dr. Mohammad F. Azizian at Oregon State University was used as a test scenario for the Hydrogenase Chip to monitor H_2 competition amongst different physiological groups during reductive dechlorination. The operation of this column was fully described in a previous publication (Azizian et al. 2010). This column was inoculated with the "Point Mugu" culture, a microbial culture enriched from chloroethene-contaminated sediment and having gone through ten years of batch cultivation as previously described (Yu, Dolan, and Semprini 2005).

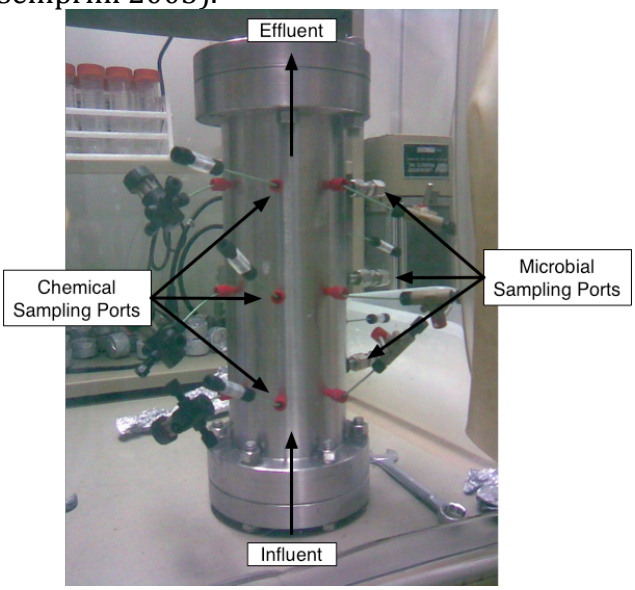

Figure 7 - Reductively dehalogenating soil-packed column operated at Oregon State University. The column is pictured here in an anaerobic glove box prior to disassembly at the end of the experiment. The column is 30 cm in height with an internal diameter of 7.5 cm. See Azizian et al. 2010 for a full

5.1.2.1.1 Analysis of the Soil Column Microbial Community by 16S rRNA Gene Clone Library and qPCR

Initial characterization of the microbial community in the soil column was carried out using 16S rRNA gene clone libraries and quantitative PCR. Bio-Sep® beads from the mesh inserts were removed from the microbial sampling ports situated closest to the influent at three time points during three different column operations. The three samples were representative for steady-state operating conditions with 1.0 – 4.0 mM formate, 0.68 – 1.0 mM lactate, and 0.58 mM propionate on operation days 727, 887, and 1050 respectively. After sampling, the removed beads were replaced with new ones before putting the mesh inserts back into the microbial sampling ports. For each time point, 16S rRNA gene clone libraries were constructed, 384 clones were screened by PCR, and clones that appeared not to contain *Dehalococcoides* 16S rRNA genes were sequenced. Of the 864 total clones screened, 650 produced amplicons indicating the presence of both a full-length insert and *Dehalococcoides* sequence, 124 clones contained full-length non-*Dehalococcoides*, and 90 clones lacked an insert. In addition to the 124 non-*Dehalococcoides* clones sequenced, 20 *Dehalococcoides* clones were sequenced to confirm the accuracy of the PCR screening assay. Of the 144 clones submitted for sequencing, 124 had sequence quality high enough for assembly of a full-length sequence. Of those 124, 43 were identified as putative chimeras (spurious gene sequences

derived from more than one DNA template during PCR), leaving 81 total sequences to analyze. 11 clone sequences were found to be affiliated with the *Dehalococcoides.* These clones were expected to be *Dehalococcoides*-affiliated based on PCR pre-screening. The phylogenetic affiliations of the remaining 70 clone sequences are shown in Figure 7. The 16S rRNA gene sequences from this study have been submitted to Genbank and assigned accession numbers GU139261 to GU139307 (lactate), GU139308 to GU139320 (propionate), and GU139321 to GU139341 (formate).

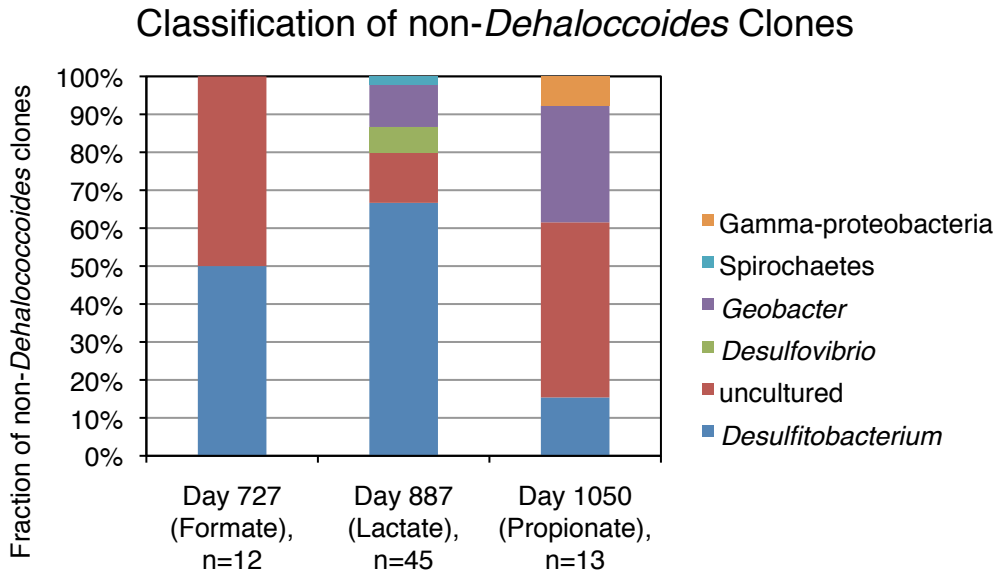

Figure 8 – Microbial community composition of the non-*Dehalococcoides* fraction of the reductive dechlorinating soil column community.

For each time point, 16S rRNA gene copy numbers for *Dehalococcoides*, *Geobacter*, *Desulfitobacterium*, and *Spirochaetes* were quantified. To infer changes in microorganism abundance relative to *Dehalococcoides*, 16S rRNA gene copy numbers of the three non-*Dehalococcoides* phylotypes were divided by *Dehalococcoides* 16S rRNA gene copy numbers (Figure 9). In general, the relative abundance of 16S rRNA gene copy numbers of phylotypes other than *Dehalococcoides* was highest with lactate as electron donor, second-highest with propionate, and lowest with formate.

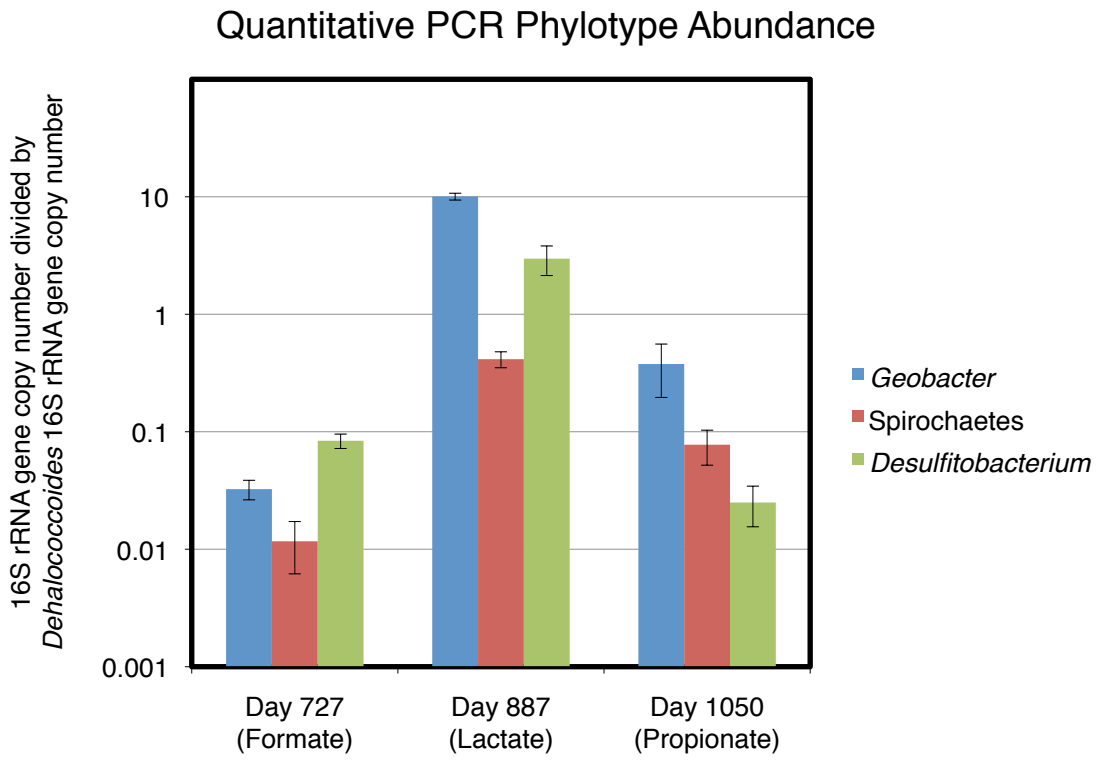

Figure 9 – Quantitative PCR measurement of phylotype abundance in the reductive dechlorinating soil column at three different time points.

5.1.2.1.2 Characterization of the Soil Column Microbial Community by Hydrogenase Chip Analysis

DNA samples from three time points each sampled at a different condition of column operation were then analyzed using the Hydrogenase Chip. Each time point represented the steady state of a different amendment of electron donor to the soil column, with formate in March 2008, lactate in July 2008, and propionate in January 2009. The soil column was operated over a time period of 1050 days. Time points representing lactate and formate amendment were analyzed using version 1 of the Hydrogenase Chip, and version 2 was used for the time point representing propionate amendment. This ensured that the sample was evaluated using the most up-to-date set of hydrogenase gene sequences according to genomic and metagenomic databases. For comparative analyses of hydrogenase genes present in multiple samples, only the subset of 20,957 probes (targeting 458 genes) common to both Hydrogenase Chip versions were analyzed (Supplemental Table S2).

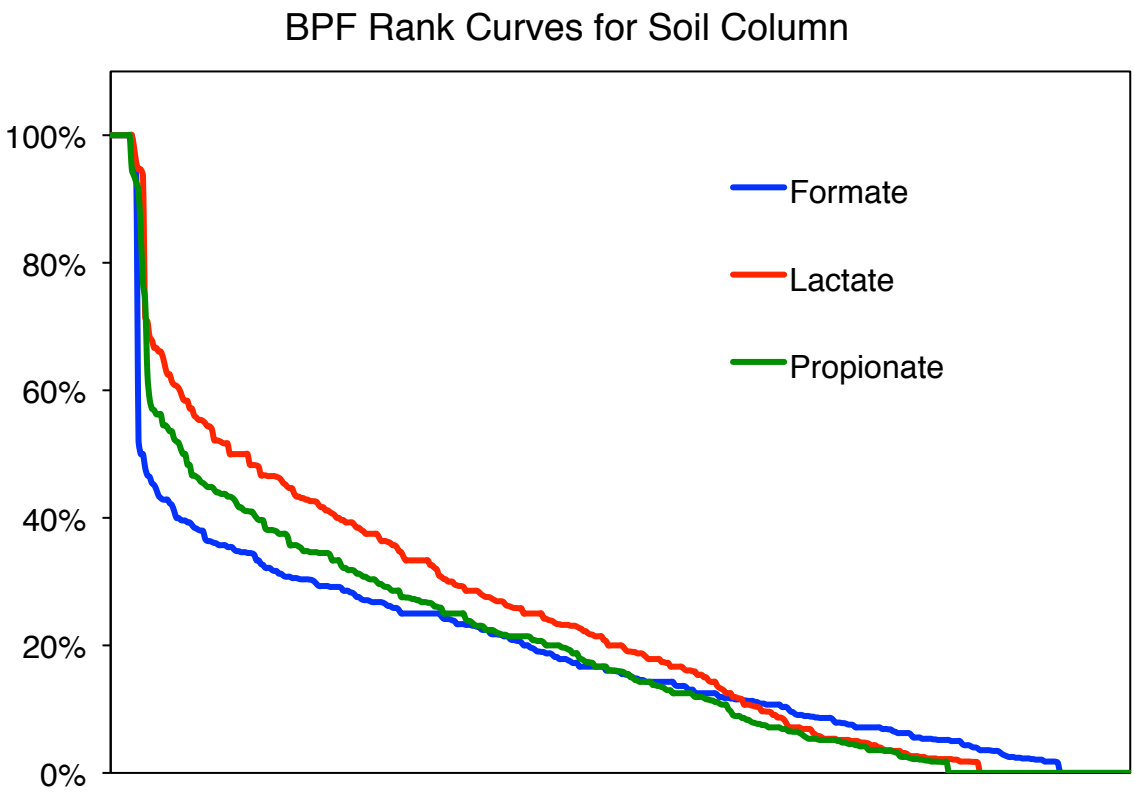

Figure 10 – BPF rank curves for DNA hybridized to the Hydrogenase Chip from the three reductively dechlorinating soil column samples.

IMG Identifier	Gene	Genome	Bright Probe Fraction		
			Formate	Lactate	Propionate
637119715	*hymC* [Fe] hydrogenase	*Dehalococcoides ethenogenes* 195	100.0%	100.0%	100.0%
637119679	*hupL* [NiFe] hydrogenase	*Dehalococcoides ethenogenes* 195	100.0%	100.0%	100.0%
637120180	*vhuA* [NiFe] hydrogenase	*Dehalococcoides ethenogenes* 195	100.0%	100.0%	100.0%
637120431	*echE* [NiFe] hydrogenase	*Dehalococcoides ethenogenes* 195	100.0%	100.0%	100.0%
637702717	*hymC* [Fe] hydrogenase	*Dehalococcoides* sp. CBDB1	100.0%	100.0%	100.0%
637702682	*hupL* [NiFe] hydrogenase	*Dehalococcoides* sp. CBDB1	100.0%	100.0%	100.0%
637703076	*vhuA* [NiFe] hydrogenase	*Dehalococcoides* sp. CBDB1	100.0%	100.0%	100.0%
637703307	*echE* [NiFe] hydrogenase	*Dehalococcoides* sp. CBDB1	100.0%	100.0%	100.0%
641416413	*vhuA* [NiFe] hydrogenase	*Dehalococcoides* sp. VS	96.4%	94.6%	94.6%
641416378	*hymC* [Fe] hydrogenase	*Dehalococcoides* sp. VS	100.0%	98.1%	100.0%
641416218	*hupL* [NiFe] hydrogenase	*Dehalococcoides* sp. VS	93.6%	93.6%	93.6%
637914488	[NiFe] hydrogenase	*Desulfitobacterium hafniense* Y51	100.0%	100.0%	92.6%
637780610	[NiFe] hydrogenase	*Geobacter metallireducens* GS-15	43.5%	95.7%	91.3%
637127109	[NiFe] hydrogenase	*Geobacter sulfurreducens* PCA	50.0%	100.0%	84.8%

Table 8 – Hydrogenase genes with BPF > 90% in the reductively dechlorinating soil column.

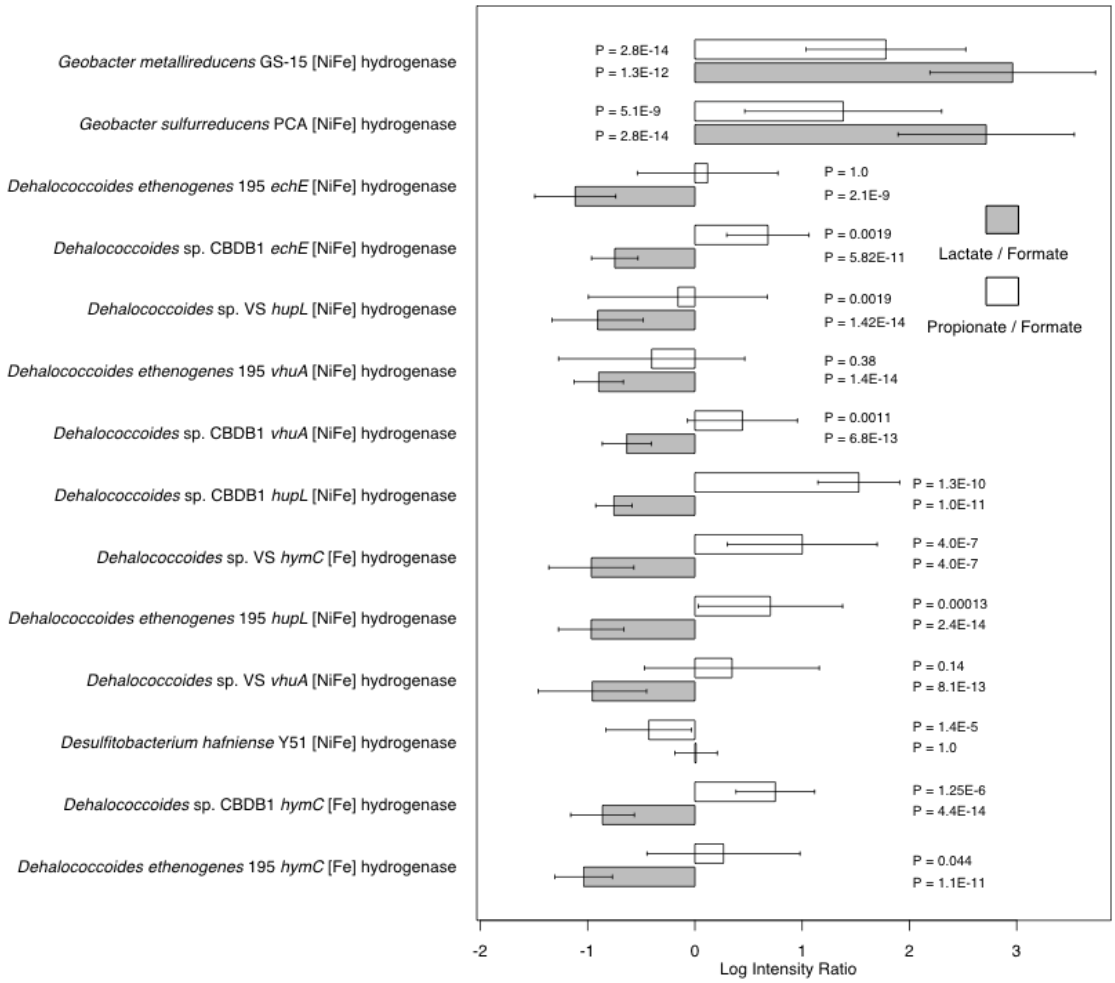

Figure 11 – Median log intensity ratios for all genes with BPF > 90% from the reductively dechlorinating soil column. Values show the natural logarithm of the median of all probe fluorescence intensity ratios for each gene. P-values show the probability that the abundance of the gene in both samples is the same based on the binomial test with the null hypothesis being that 50% of probes for a given gene show greater abundance in one sample and 50% of probes for a given gene show that the gene is more abundant in the other sample.

Of the 458 genes represented by probes common to both microarray designs, 14 genes show hybridizations with a bright probe fraction (BPF) > 90% in at least one of the three samples (Table 8, Supplemental Table S2). Log intensity ratios for all samples are shown in Figure 11 For the detected *Dehalococcoides sp.* hydrogenase genes, some showed significant differences between probe intensities for the propionate and formate amendments. In general, genes from the *Dehalococcoides* strain CBDB1 genome were enriched in the propionate amendment, genes from the genome of *Dehalococcoides ethenogenes* strain 195 showed no significant difference between the two treatments, and some *Dehalococcoides* strain VS genes showed enrichment while others did not. Although there is bound to be significant cross-hybridization between all *Dehalococcoides* sp. strains due to > 90% sequence identity, the consistent abundance difference for hydrogenase genes of strains 195 and CBDB1 compellingly suggest differences in *Dehalococcoides* population

structure between the time points representative of formate and propionate amendment. The lactate time point showed generally diminished probe intensities for all *Dehalococcoides* hydrogenase genes, consistent with a diminished fraction of electrons contributing towards reductive dehalogenation with lactate as electron donor. Chemical measurements of the column effluent showed that propionate and formate resulted in 10% and 14% of electron equivalents contributing to chloroethene reduction, respectively, while only 6.5% of electron equivalents contributed to chloroethene reduction under lactate oxidizing conditions (Azizian et al. 2010). There was a significant increase in the intensity of *Geobacter* hydrogenase genes in samples from the lactate- and propionate-amended time points relative to the formate-amended time point. This is consistent with an increase in the fraction of electrons partitioned to Fe(III) reduction in this system during propionate or lactate amendment. Measurement of soluble Fe(II) in the column effluent accounted for 2.0% and 1.6% of electron equivalents under propionate- and lactate-oxidizing conditions, respectively, while accounting for 1.1% of electron equivalents under formate-oxidizing conditions (Azizian et al. 2010). Since the majority of Fe(II) was likely bound in the solid phase and thus would not have entered the effluent, these figures should be interpreted in relative terms. The detected *Desulfitobacterium hafniense* [NiFe] hydrogenase showed significantly reduced probe intensities under propionate amendment relative to formate, but no significant difference between lactate and formate amendments. This is consistent with the fact that to date no pure culture isolate of *Desulfitobacterium* sp. has been shown to use propionate as an electron donor substrate, in contrast to formate and lactate (Christiansen and Ahring 1996; Finneran et al. 2002; Sanford et al. 1996; Utkin, Woese, and Wiegel 1994).

Notably, no H_2-producing fermenting microorganisms were detected with the Hydrogenase Chip in any of the samples analyzed from the soil column. However, *Geobacter* sp. detected in the lactate- and propionate-amended soil column may be fermenting these substrates to H_2 and acetate in this environment, as *Geobacter* isolates have been shown to syntrophically produce hydrogen during fermentation of organic compounds in the past (Cord-Ruwisch, Lovley, and Schink 1998). *Desulfovibrio* species have also been shown to produce H_2 syntrophically (McInerney and Bryant 1981), and although *Desulfovibrio* was not detected using the Hydrogenase Chip it was detected in the 16S rRNA gene clone library (Figure 8).

These analyses also showed that gene richness trends between different treatments were reflected by species richness trends as observed within 16S rRNA gene clone libraries shown in section 5.1.3.1.1. A ranking in hydrogenase gene richness in the order lactate > propionate > formate was revealed by the array in terms of the relative positions of BPF rank curves (Figure 10) and numbers of genes with a BPF > 90% (14 genes for lactate > 13 genes for propionate > 12 genes for formate, see Figure 11). Notably, all hydrogenase genes identified using the Hydrogenase Chip belonged to genera were also identified in the 16S rRNA gene clone libraries.

We also detected genes not common to both microarray designs. Of the 481 hydrogenase and formate metabolism genes unique to the Hydrogenase Chip version 1 used to analyze the formate and lactate time points, 27 genes had BPF values >90% (Supplemental Table S3). Nineteen of these genes were from *Desulfitobacterium* sp. genomes, five from *Dehalococcoides* sp. genomes, and three from *Geobacter sp.* genomes. Of the 540 hydrogenase and reductive dehalogenase genes unique to the Hydrogenase Chip version 2 used for the propionate time point, 19 had BPF values

>90% (Supplemental Table S4). These were hydrogenase and reductive dehalogenase genes exclusively from *Dehalococcoides* sp. and *Desulfitobacterium* sp.

5.1.2.2 Reductively Dehalogenating Chemostats

To more accurately characterize the community of hydrogen producing and consuming microorganisms in reductively dehalogenating systems, we decided to determine the hydrogenase genes that were not only present as DNA, but also transcribed. Thus, for evaluating the performance of the Hydrogenase Chip for detecting gene expression, we used undefined reductively dehalogenating mixed cultures in chemostat and batch reactor experiments. This is because preliminary data showed that abundant high-quality RNA could not be extracted from the Biosep beads used to sample the soil column (data not shown). Two separate experiments were performed: monitoring of an anoxic reductive dechlorination chemostat and three anoxic batch reactions in 2010, called here "RNA Experiment One", and the monitoring the same dechlorinating chemostat and another three batch reactions from a similar experiment in 2011, called "RNA Experiment Two". The samples analyzed originated from chemostats and batch cultures operated by Mohammad Azizian and Dusty Berggren at Oregon State University. Complete details on the operation of these reactors can be found in a previous publication (Marshall et al. 2012) and Dusty Berggren's MS thesis (Berggren 2011; Berggren et al 2013). The long-term anoxic chemostat used for these experiments was originally inoculated with the Point Mugu culture (described in section 5.1.3.1) amended with 4.3 mM lactate and 1.15 mM tetrachloroethene (PCE). It is referred to here as the "Point Mugu 5L" or "PM5L" reactor.

5.1.2.2.1 Reductive Dechlorination RNA Experiment One

Batch cultures in RNA Experiment One (50mL cultures in 125mL glass bottles) were derived from the PM5L chemostat and then maintained for 44 days with H_2 and one of three electron acceptor mixtures hypothesized to correlate with different hydrogenase gene expression patterns. Batch sample P was amended with 15 µmol PCE only, sample S with 16 µmol sulfate only, and sample SP with both 16 µmol sulfate and 15 µmol PCE. On day 44, every bottle was incubated with both PCE and sulfate for one day before being harvested for molecular analysis in order to simulate three different moderately complex microbial ecosystems undergoing simultaneous sulfate and PCE reduction, each optimized for different rates of both sulfate and PCE reduction (Figure 12).

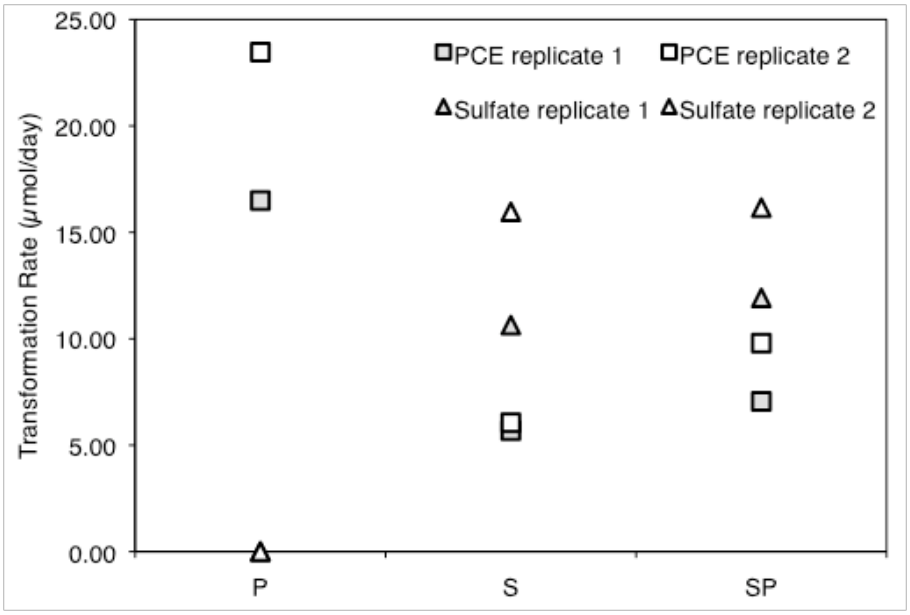

Figure 12 - Transformation rates of PCE and sulfate under different batch conditions. Two replicates were performed for each sample (S, SP, P). These measurements were made by Mohammad Azizian and Dusty Berggren at Oregon State University.

To examine the hydrogenase genes expressed under these three conditions, we first used our DNA microarray to identify the hydrogenase genes present in the ancestral chemostat and acclimated batch cultures. Of the 1324 hydrogenase genes printed on the array, 36 yielded BPF > 90% in at least one of the samples (Figure 13, Table 9). Thirty-five of these were from *Dehalococcoides* sp., and one from *Desulfitobacterium hafniense*.

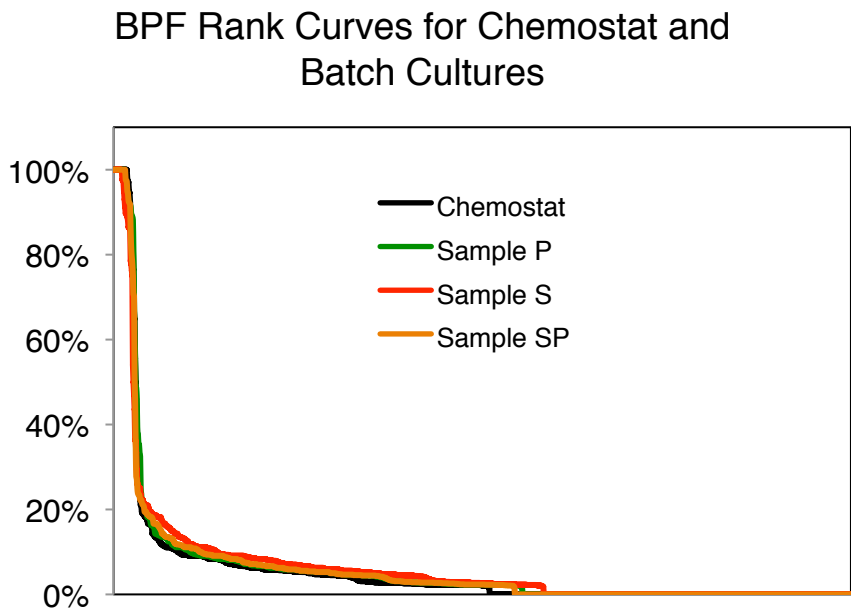

Figure 13 - BPF rank curve for RNA extracted from reductive dechlorinating PM5L chemostat and batch cultures P, S, and SP hybridized to the Hydrogenase Chip version 4.

IMG Identifier	Gene	Genome	Chemostat	Sample P	Sample S	Sample SP
641416413	*vhuA* [NiFe] hydrogenase	*Dehalococcoides* sp. VS	**97.67%**	**95.35%**	**93.02%**	**97.67%**
637703076	*vhuA* [NiFe] hydrogenase	*Dehalococcoides* sp. CBDB1	**100.00%**	**100.00%**	**100.00%**	**100.00%**
640529491	*vhuA* [NiFe] hydrogenase	*Dehalococcoides* sp. BAV1	**100.00%**	**100.00%**	**100.00%**	**100.00%**
637120180	*vhuA* [NiFe] hydrogenase	*Dehalococcoides ethenogenes* 195	**97.22%**	**100.00%**	86.11%	**100.00%**
637119649	*tceA* reductive dehalogenase	*Dehalococcoides ethenogenes* 195	**100.00%**	**100.00%**	**97.62%**	**100.00%**
640529763	reductive dehalogenase	*Dehalococcoides* sp. BAV1	**100.00%**	**100.00%**	**100.00%**	**100.00%**
637703991	reductive dehalogenase	*Dehalococcoides* sp. CBDB1	**100.00%**	**100.00%**	**100.00%**	**100.00%**
637703817	reductive dehalogenase	*Dehalococcoides* sp. CBDB1	**100.00%**	**97.30%**	**97.30%**	**97.30%**
637703819	reductive dehalogenase	*Dehalococcoides* sp. CBDB1	**100.00%**	**94.59%**	86.49%	70.27%
641416188	*vcrA* reductive dehalogenase	*Dehalococcoides* sp. VS	**94.87%**	**97.44%**	**94.87%**	**97.44%**
637703976	reductive dehalogenase	*Dehalococcoides* sp. CBDB1	**100.00%**	**100.00%**	**100.00%**	**100.00%**
637119747	reductive dehalogenase	*Dehalococcoides ethenogenes* 195	**100.00%**	35.29%	**91.18%**	79.41%
637702732	reductive dehalogenase	*Dehalococcoides* sp. CBDB1	**100.00%**	**91.18%**	**100.00%**	**100.00%**
640529076	reductive dehalogenase	*Dehalococcoides* sp. BAV1	**100.00%**	88.24%	**100.00%**	**100.00%**
637703982	reductive dehalogenase	*Dehalococcoides* sp. CBDB1	**94.59%**	**94.59%**	86.49%	**94.59%**
641416427	reductive dehalogenase	*Dehalococcoides* sp. VS	**97.06%**	38.24%	88.24%	70.59%
641416021	reductive dehalogenase	*Dehalococcoides* sp. VS	**92.31%**	**92.31%**	89.74%	**94.87%**
641416006	reductive dehalogenase	*Dehalococcoides* sp. VS	86.11%	**91.67%**	75.00%	75.00%
637121103	reductive dehalogenase	*Dehalococcoides ethenogenes* 195	81.58%	89.47%	76.32%	**92.11%**
637119740	reductive dehalogenase	*Dehalococcoides ethenogenes* 195	36.84%	**97.37%**	18.42%	**100.00%**
637120490	*nuoD* oxidoreductase	*Dehalococcoides ethenogenes* 195	**100.00%**	**100.00%**	89.29%	**100.00%**
637703333	*nuoD* oxidoreductase	*Dehalococcoides* sp. CBDB1	**100.00%**	**100.00%**	**100.00%**	**100.00%**
640529727	*nuoD* oxidoreductase	*Dehalococcoides* sp. BAV1	**100.00%**	**100.00%**	**100.00%**	**100.00%**
641415883	*nuoD* oxidoreductase	*Dehalococcoides* sp. VS	89.29%	89.29%	78.57%	**92.86%**
637119715	*hymC* [Fe] hydrogenase	*Dehalococcoides ethenogenes* 195	**100.00%**	**100.00%**	**100.00%**	**100.00%**
637702717	*hymC* [Fe] hydrogenase	*Dehalococcoides* sp. CBDB1	**100.00%**	**100.00%**	**100.00%**	**100.00%**
640529126	*hymC* [Fe] hydrogenase	*Dehalococcoides* sp. BAV1	**100.00%**	**100.00%**	**100.00%**	**100.00%**
641416378	*hymC* [Fe] hydrogenase	*Dehalococcoides* sp. VS	**100.00%**	**100.00%**	**97.50%**	**100.00%**

637119679	*hupL* [NiFe] hydrogenase	*Dehalococcoides ethenogenes* 195	**100.00%**	**100.00%**	**100.00%**	**100.00%**
637702682	*hupL* [NiFe] hydrogenase	*Dehalococcoides* sp. CBDB1	**100.00%**	**100.00%**	**100.00%**	**100.00%**
640529159	*hupL* [NiFe] hydrogenase	*Dehalococcoides* sp. BAV1	**100.00%**	**100.00%**	**100.00%**	**100.00%**
641416218	*hupL* [NiFe] hydrogenase	*Dehalococcoides* sp. VS	88.89%	**91.67%**	86.11%	**91.67%**
637703307	*echE* [NiFe] hydrogenase	*Dehalococcoides* sp. CBDB1	**100.00%**	**100.00%**	77.78%	81.48%
640529701	*echE* [NiFe] hydrogenase	*Dehalococcoides* sp. BAV1	**100.00%**	**100.00%**	88.89%	77.78%
637120431	*echE* [NiFe] hydrogenase	*Dehalococcoides ethenogenes* 195	55.56%	**96.30%**	25.93%	**100.00%**
643563191	[NiFe] hydrogenase	*Desulfitobacterium hafniense* DCB-2	**100.00%**	5.13%	89.74%	**92.31%**

Table 9 - Genes with BPF > 90% from the RNA Experiment One chemostat and batch reductive dechlorinating RNA samples.

We then examined the quantitative capacity of the tiling DNA microarray approach by measuring the relative abundances of *Dehalococcoides hupL* in the acclimated batch cultures using both the Hydrogenase Chip and reverse-transcriptase quantitative PCR (RT-qPCR). As expected, when examining the rates of electron acceptor consumption, sample P had become acclimated to high PCE reduction rates and low sulfate reduction rates, sample S to low PCE reduction rates and high sulfate reduction rates, and sample SP to both sulfate and PCE reduction (Figure 14). We then investigated whether the observed rates correlated with shifts in abundance of *Dehalococcoides hupL* hydrogenase mRNA using the Hydrogenase Chip version 3. As Figure 14A shows, trends in *Dehalococcoides hupL* median probe intensity followed trends in PCE transformation rate. This is consistent with earlier work showing *hupL* transcript abundance correlates with PCE respiration rates in *Dehalococcoides* (Rahm and Richardson 2008). To independently assess *hupL* mRNA abundance to determine the accuracy of the Hydrogenase Chip, RT-qPCR targeting this gene was performed. As Figure 14B shows, shifts in mRNA abundance observed using the Hydrogenase Chip correlated with qPCR quantification of the abundance of *Dehalococcoides hupL* hydrogenase. The high median absolute deviation for sample SP was likely caused by cross-hybridization from a *Dehalococcoides* type more closely related to strain 195, as the median probe intensity strain 195 *hupL* increased significantly in sample SP relative to samples S and P. Apart from this aberration, the Hydrogenase Chip quantification appeared to correlate linearly with reverse transcriptase quantitative PCR measurements from the same samples.

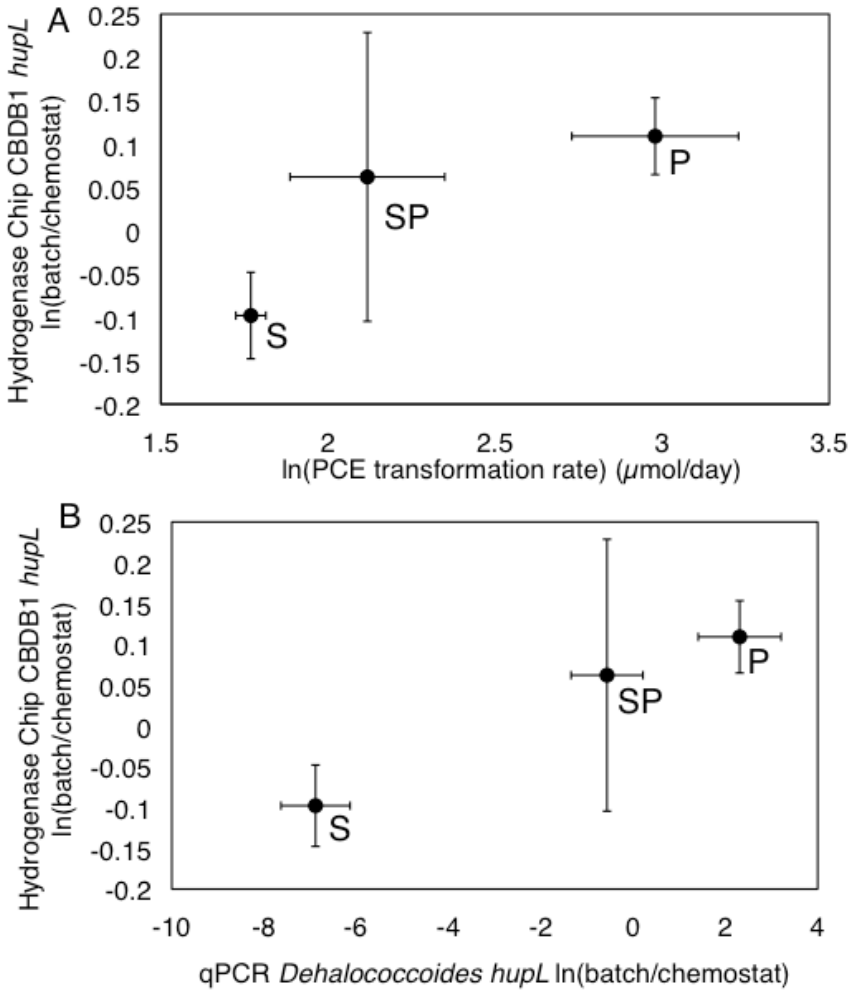

Figure 14. *hupL* expression level as indicator for *Dehalococcoides* dehalogenation activity in batch cultures in RNA Experiment One.

Log intensity ratios of *Dehalococcoides hupL* with RNA hybridized to the Hydrogenase Chip version 3 compared to mean PCE transformation rates (A) and RT-qPCR (B). Gene abundance measurements show the natural logarithm of batch copy number (qPCR) or median probe intensity (Hydrogenase Chip) divided by the corresponding measurement in the chemostat sample. PCE transformation rates in (A) were used without normalizing to chemostat rates, but the natural logarithm is shown for consistency with microarray and qPCR data. Vertical error bars show median absolute deviation from the array, horizontal error bars show standard deviation from three qPCR replicates or from PCE degradation rates measured in two replicates for each batch culture.

The apparent absence of hydrogenase genes from known sulfate-reducers was noteworthy, considering the observation of active sulfate reduction in the derived batch cultures under H_2-

oxidizing conditions. This could be subsequently explained by a *dsrA* clone library of sample S and hydrogenase sequencing to determine sulfate-reducer members of the community. We found that all *dsrA* sequences appeared to be derived from *Desulfovibrio* sp. relatives (Figure 15). This led us to sequence the *Desulfovibrio hynA-1* hydrogenase gene from sample S to find it was only 67% identical to the hydrogenase gene on the array with which it shares the highest identity (well below the identity threshold at which one could expect cross-hybridization). This explains the apparent absence of hydrogenase genes from sulfate reducers.

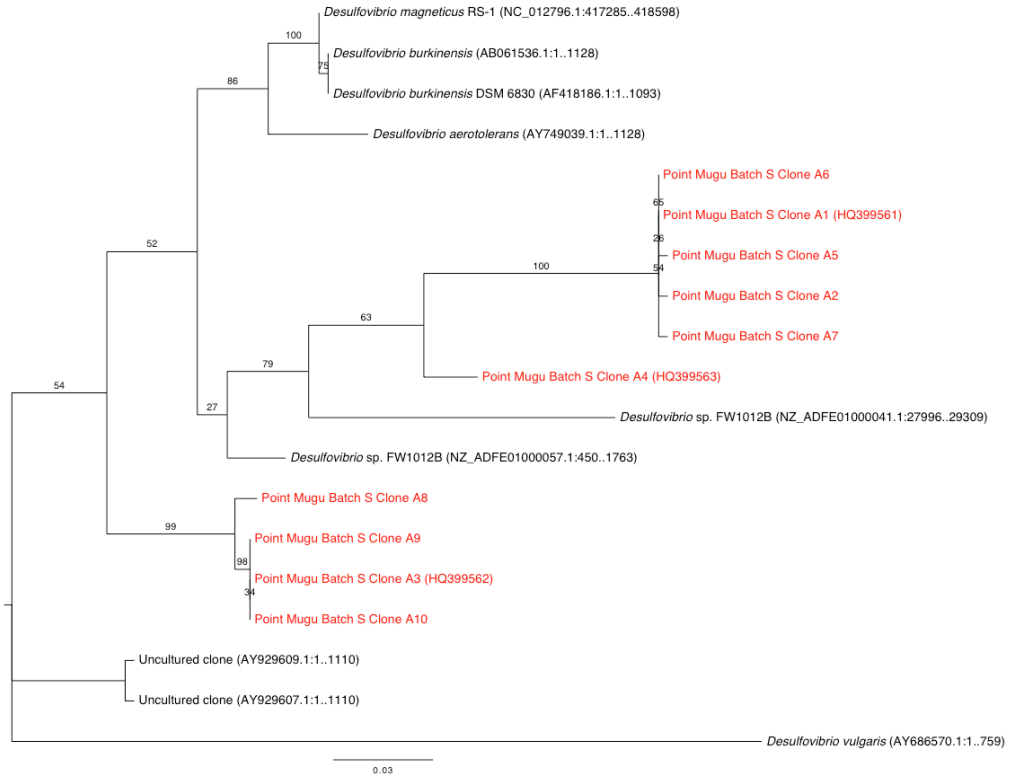

Figure 15. - Phylogenetic tree based on *dsrA* sequences collected as part of RNA Experiment One from batch culture S and nearest neighbors collected from the NCBI nr database using BLAST. PHYML tree bootstrapped 100 times. Branch labels show bootstrap support percentage.

5.1.2.2.2 Reductive Dechlorination RNA Experiment Two

An opportunity to test a newer version of the Hydrogenase Chip (version 4) presented itself in 2011 when a similar experiment to RNA Experiment One was carried out by Dusty Berggren (RNA Experiment Two). The intention of this experiment was to distinguish whether the observed shift in the *Dehalococcoides* population was due to competition for H_2 by sulfate reducing microbes in the Point Mugu culture, or to toxicity of the end product of sulfate reduction, H_2S. The main purpose of extracting RNA from these samples and hybridizing that RNA to the Hydrogenase Chip version 4 was to determine whether the additional *Desulfovibrio* hydrogenase genes present on the microarray would enable detection of the *Desulfovibrio* hydrogenase gene linked to H_2 oxidation coupled to sulfate reduction. While in RNA Experiment One there was no hydrogenase

gene targeted by Hydrogenase Chip version 3 sufficiently identical to the *Desulfovibrio* hydrogenase gene found in the Point Mugu culture, version 4 of the Hydrogenase Chip included probes from a gene sequence that should have been sufficiently identical to the *Desulfovibrio hynA*-1 gene found in the Point Mugu culture to enable detection. This was *hynA*-1 from *Desulfovibrio fructosovorans* (IMG gene ID 648711125), which is 90.0% similar to the *hynA*-1 sequenced from the Point Mugu culture.

As in RNA Experiment One, three batch reactions were started using material from the PM5L chemostat. One reactor was amended solely with 15 µmol PCE, another with 15 µmol PCE and 16 µmol sulfate, and another with 15 µmol PCE and 4.6 µmol sodium sulfide. The reactors were incubated for 47 days. RNA was then extracted from the cultures and from the PM5L chemostat (from a t=0 sample at the same time as material for the batch reactors) before being analyzed using Hydrogenase Chip version 4. Upon first analysis of this microarray data no *Desulfovibrio* genes were detected, with only seven *Dehalococcoides* genes detected (data not shown). We hypothesized that 3' RNA degradation may have reduced the fluorescence intensity for probes targeting the 3' end of the transcript, and thus restricted the analysis to the first 10 probes from the 5' end of the gene and used 2× median as the bright probe cutoff rather than the typical 3× median. The BPF rank curves for this modified analysis are shown in Figure 16.

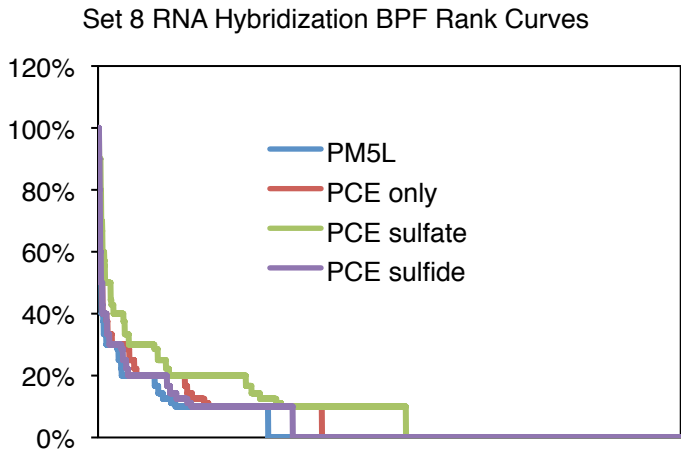

Figure 16 – BPF rank curves for PM5L and RNA Experiment Two reductive dechlorinating batch reaction

A BPF threshold of 80% was used to capture those genes with BPF values of 80%, 90%, and 100% (90% was considered too stringent for a 10-probe-per-gene analysis). Genes with BPF > 80% are listed in Table 10. Three *Desulfovibrio* genes were detected in RNA Experiment Two. Moreover, these transcripts were at their most abundant under sulfate-reducing conditions (Figure 17). There was also a general shift in abundance of transcripts related to *Dehalococcoides*, with relatives of *Dehalococcoides* sp. CBDB1 dominant in the chemostat and relatives of *Dehalococcoides ethenogenes* 195 dominant in the batch cultures, especially in those amended with sulfate or sulfide. This shift in *Dehalococcoides* population structure was confirmed by generating *Dehalococcoides hupL* clone libraries from DNA extracted from the RNA Experiment Two batch and chemostat samples (Figure 18).

IMG/M ID	Gene Product	Genome/Metagenome	PM5L	PCE only	PCE /sulfate	PCE /sulfide
637119679	[Ni/Fe] Hydrogenase, HupL subunit	*Dehalococcoides ethenogenes* 195	**100%**	**90%**	**90%**	**100%**
637119715	[FeFe] Hydrogenase, HymC subunit	*Dehalococcoides ethenogenes* 195	**80%**	40%	**90%**	**90%**
637120180	[NiFe] Hydrogenase, VhuA subunit	*Dehalococcoides ethenogenes* 195	60%	60%	**100%**	**80%**
637120431	[NiFe] Hydrogenase, EchE subunit	*Dehalococcoides ethenogenes* 195	20%	20%	**90%**	**90%**
637702682	[NiFe] Hydrogenase, HupL subunit	*Dehalococcoides* sp. CBDB1	**100%**	**100%**	**100%**	**100%**
637702717	[FeFe] Hydrogenase, HymC subunit	*Dehalococcoides* sp. CBDB1	**90%**	**80%**	**80%**	60%
637703076	[NiFe] Hydrogenase, VhuA subunit	*Dehalococcoides* sp. CBDB1	**80%**	70%	60%	50%
637703307	[NiFe] Hydrogenase, EchE subunit	*Dehalococcoides* sp. CBDB1	30%	**90%**	60%	40%
646445988	[NiFe] Hydrogenase, HupL subunit	*Dehalococcoides* sp. VS	**90%**	70%	70%	60%
2013891653	[NiFe] Hydrogenase, EchE subunit	Aquatic dechlorinating community (KB-1) (Sample 10166)	30%	**90%**	60%	40%
2014742389	[NiFe] Hydrogenase, EchE subunit	ANAS dechlorinating bioreactor (Sample 196)	10%	30%	**90%**	70%
2014774044	[NiFe] Hydrogenase, EchE subunit	ANAS dechlorinating bioreactor (Sample 196)	10%	30%	**100%**	**100%**
2014776768	[FeFe] Hydrogenase, HymC subunit	ANAS dechlorinating bioreactor (Sample 196)	33%	33%	**100%**	**100%**
644800488	[FeFe] Hydrogenase	*Desulfovibrio magneticus* RS-1	20%	20%	**90%**	20%
647340228	[FeFe] Hydrogenase	*Desulfovibrio* sp. FW1012B	20%	40%	**90%**	20%
648711125	[NiFe] Hydrogenase Large Subunit	*Desulfovibrio fructosovorans* JJ	30%	20%	**80%**	20%

Table 10 - Genes with BPF > 90% from the RNA Experiment Two chemostat and batch reductive dechlorinating RNA samples.

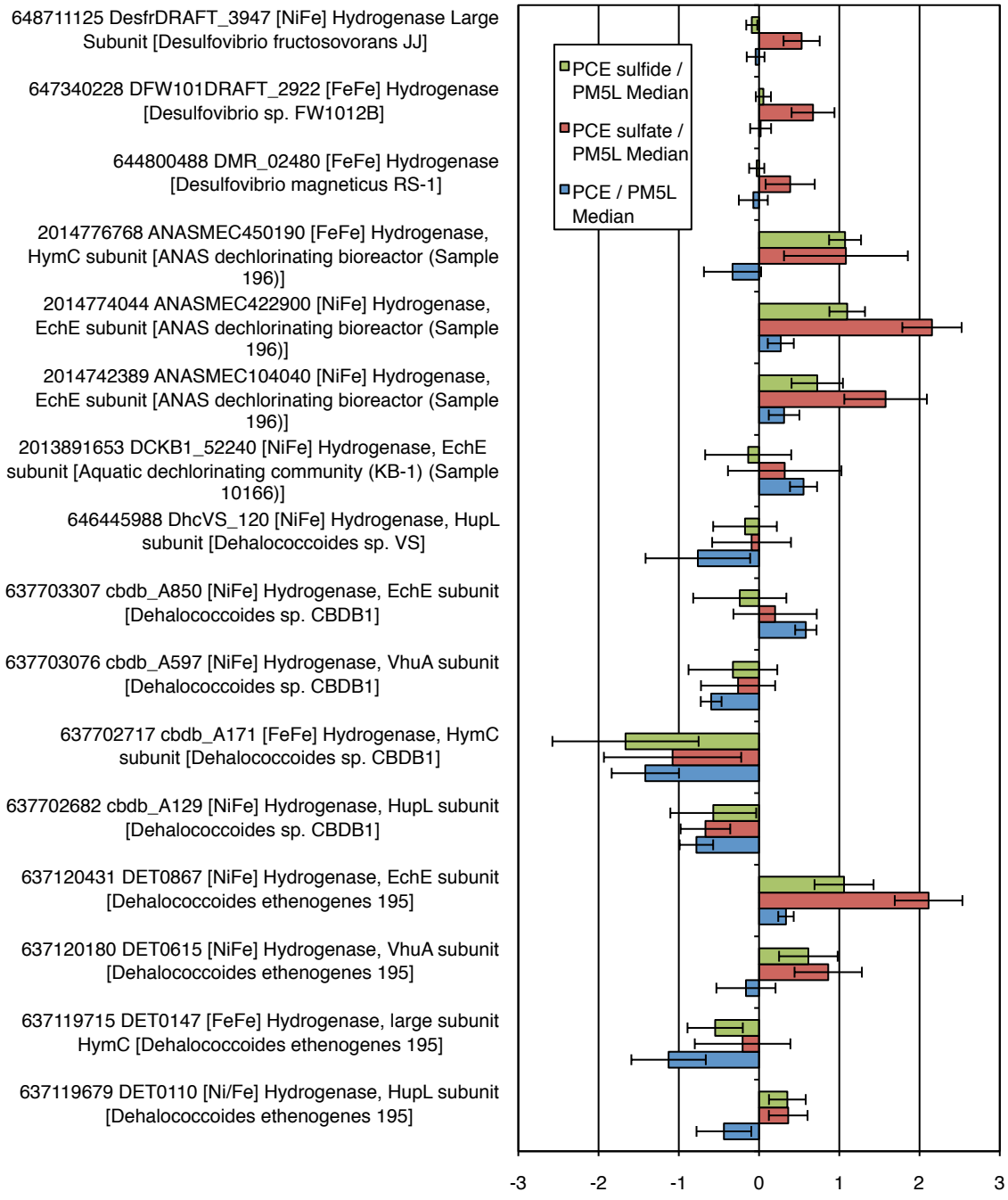

Figure 17 - Median log intensity ratios for all genes with BPF > 90% from batch reactors in RNA Experiment Two. Values show the natural logarithm of the median of all probe fluorescence intensity ratios for each gene.

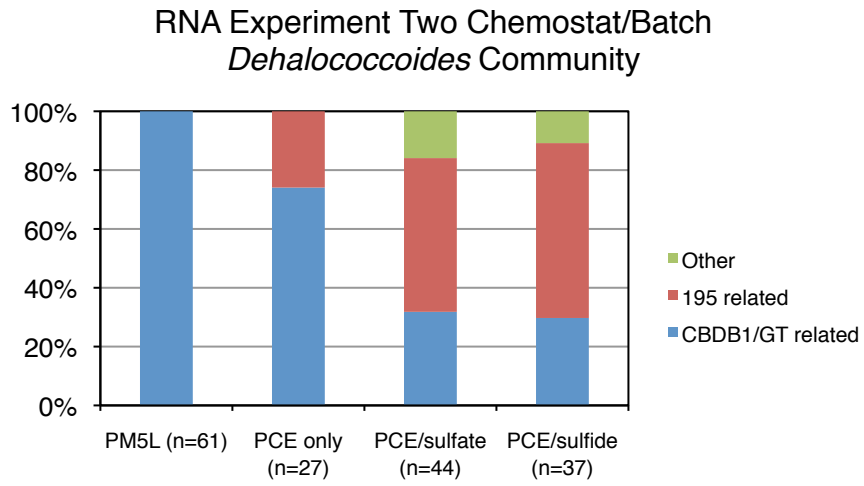

Figure 18 - Characterization of *Dehalococcoides* sp. community composition in the PM5L chemostat and batch cultures derived from it based on *Dehalococcoides hupL* clone libraries.

Hybridizing RNA from the RNA Experiment Two chemostat and batch cultures to the Hydrogenase Chip version 4 demonstrated that the expected *Desulfovibrio hynA*-1 gene was expressed under sulfate-reducing conditions and provided some interesting hints of the effect of sulfate-reducing microbes or the direct addition of sulfide to *Dehalococcoides* community composition.

5.1.3 The Reductive Dehalogenase Chip

Following our experiments with the Hydrogenase Chip that showed hydrogenase genes can be successfully detected and quantified when target hydrogenase genes are of sufficient abundance and identity to probe sequences on the microarray, we decided to apply the tiling DNA microarray technique to genes encoding reductive dehalogenases. The goal was to develop a tool to track communities of organohalide-respiring microorganisms in natural environments and experimental microcosms through monitoring reductive dehalogenase gene presence and abundance.

5.1.3.1 The Effect of Sulfide on Dehalococcoides Community Composition

During the long-term operation of chloroethene-reducing chemostats in the laboratory of Dr. Lewis Semprini at Oregon State University certain changes in the reactors' capacity for chloroethene reduction became apparent over time. The first reactor was a 2 L chemostat inoculated with the Point Mugu reductive dechlorinating culture, dubbed the 'PM2L' chemostat. This chemostat was operated with lactate as electron donor and PCE as electron acceptor. After 500 days' operation of the PM2L chemostat its effluent was used as the starting material for a chemostat operated under identical conditions with a 5L capacity, dubbed the 'PM5L' chemostat. PM2L and PM5L chemostats are pictured in Figure 19.

Figure 19 – PM2L (left) and PM5L (right) chemostats pictured in January 2009. Chemostats are typically covered in aluminum foil to inhibit growth of phototrophic microorganisms – the foil was removed for these photographs.

In an attempt to encourage competition for H_2 between organochlorine-respiring and sulfate-reducing microorganisms as a simulation of a PCE-contaminated, sulfate-containing aquifer undergoing bioremediation, the PM2L influent was amended with 1 mM concentration sodium sulfate as of 733 days of operation. Soon after this, vinyl chloride (VC) reduction, the final step in the complete dechlorination of PCE to ethene, began to slow down and eventually stop completely (Figure 20). It was hypothesized that a change in the composition of the reductive dechlorinating microbial community might be responsible for this change in vinyl-chloride reducing activity. In particular a change in the composition of the *Dehalococcoides* community was thought to have occurred, since *Dehalococcoides* is the only known vinyl-chloride respiring microorganism discovered to date (Taş et al. 2010). We set out to determine the basis of this hypothesized microbial community shift using molecular biological tools to analyze the microbial community composition at different time points throughout the transition of the chemostat from being free of sulfate to sulfate-reducing.

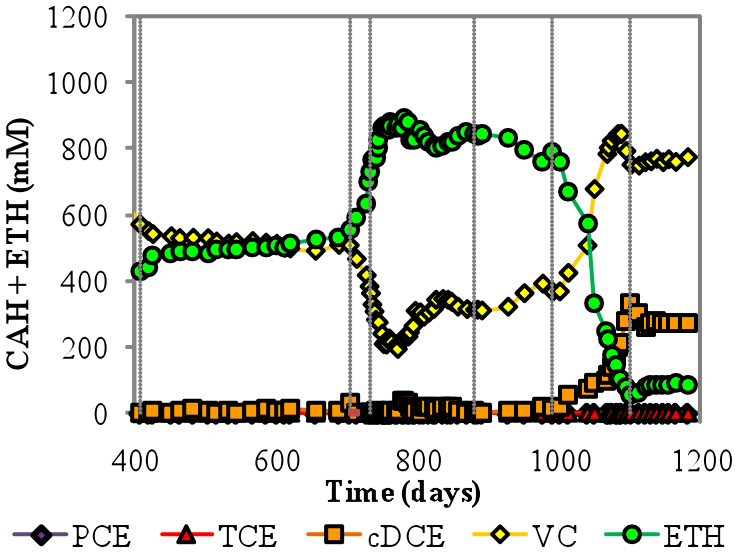

Figure 20 – Reductive dechlorination performance of the PM2L chemostat over time. This data and figure were provided by Lewis Semprini, Mohammad Azizian, and Dusty Berggren of Oregon State University.

5.1.3.1.1 PM2L Chemostat Characterization with Clone Library

The shift in the overall composition of the microbial community found within the PM2L chemostat was first assessed using qPCR. From the 16S rRNA gene clone library and Hydrogenase Chip analyses performed on the soil column (section 5.1.3.1) we hypothesized that the main organohalide-respiring portion of the Point Mugu culture microbial community comprised species of the genera *Dehalococcoides* and *Desulfitobacterium*. Moreover, from *dsrA* clone libraries constructed based on DNA extracted from the PM2L chemostat it appeared that two *Desulfovibrio* phylotypes were responsible for much of the sulfate-reducing capacity of the Point Mugu culture, with the *Desulfovibrio* community shifting from a population "Cluster 0" types at day 543 to a population of "Cluster 1" types at day 1172 (Figure 21).

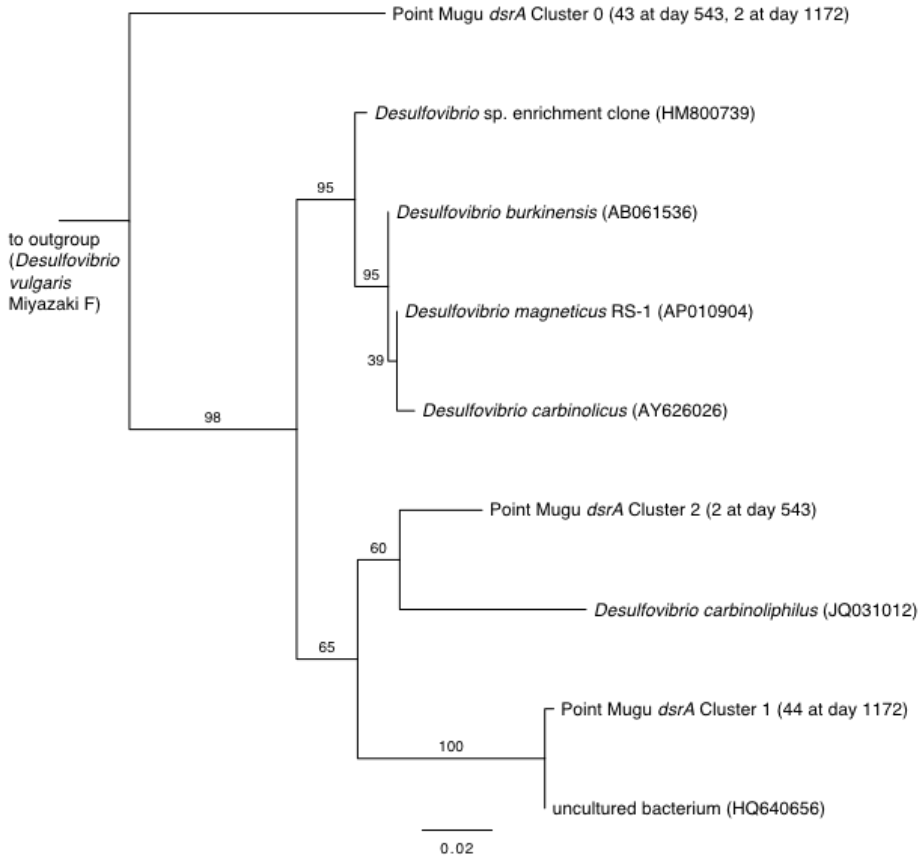

Figure 21– Phylogenetic tree reconstructed from *dsrA* nucleotide sequences in the PM2L chemostat. Sequences collected in this study are representative sequences from 97% nucleotide sequence clusters generated with CD-HIT. Numbers of sequences in each cluster at each time point are given in parentheses. Close relatives from Genbank have accession numbers in parentheses. Maximum likelihood tree with 100× bootstrap. Bootstrap percentages are shown at branching points.

We therefore used qPCR assays that targeted these specific genera to obtain a broad picture of the shifts in PM2L chemostat microbial community over time (Figure 22). This data demonstrated that the targeted genera accounted for the majority of the bacterial community at all time points assessed.

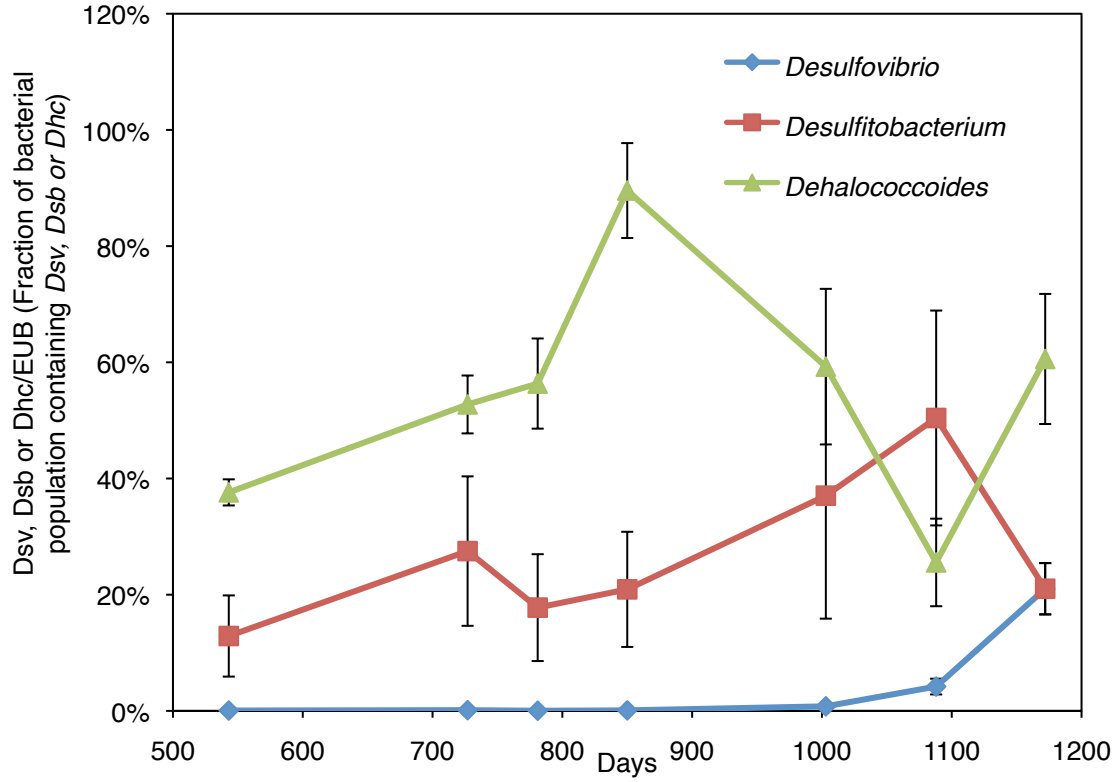

Figure 22 – Relative abundance shifts of *Desulfovibrio*, *Desulfitobacterium*, and *Dehalococcoides* in the PM2L chemostat. *Dehalococcoides* and *Desulfitobacterium* abundances were assessed on the basis of 16S rRNA gene copy numbers; *Desulfovibrio* was based on *dsrA*.

The general trend in the PM2L chemostat appeared to be a gradual increase in the abundance of sulfate-reducers of the *Desulfovibrio* type following the addition of sulfate to the chemostat influent, a general decrease in the abundance of *Dehalococcoides* and a general increase in the abundance of *Desulfitobacterium*. It makes sense that *Desulfitobacterium* would be better adapted to sulfidogenic conditions, since as a sulfite-reducer *Desulfitobacterium* would produce hydrogen sulfide itself (Villemur et al. 2006). Moreover, increased *Desulfitobacterium* abundance would partially explain the incomplete VC reduction, as no *Desulfitobacterium* capable of VC reduction has been isolated to date.

However, at the last time point analyzed in Figure 20 (1200 days) VC reduction had completely stopped in the PM2L reactor in spite of the resurgence in *Dehalococcoides* abundance. This makes it unlikely that the increase in *Desulfitobacterium* abundance and a decrease in *Dehalococcoides* abundance *per se* is an adequate explanation of the slowdown in VC reduction following the onset of sulfidogenic conditions. Based on the results of sulfide and sulfate introduced into batch

cultures, in particular the shifts in *Dehalococcoides* community composition evident in Figure 18 and Figure 17, it was hypothesized that a change in the composition of the *Dehalococcoides* community with respect to different *Dehalococcoides* types was responsible for the slow down in VC reduction, rather than a change in total *Dehalococcoides* abundance. The capacity to metabolically reduce VC to ethene is one of the differentiating characteristics of the different *Dehalococcoides* isolates (McMurdie et al. 2009). To test this hypothesis *Dehalococcoides hupL* clone libraries from a series of time points throughout the operation of the PM2L chemostat were constructed. *hupL* clones were assigned to different groups based on maximum likelihood grouping of 99.5% sequence identity clusters (Figure 23).

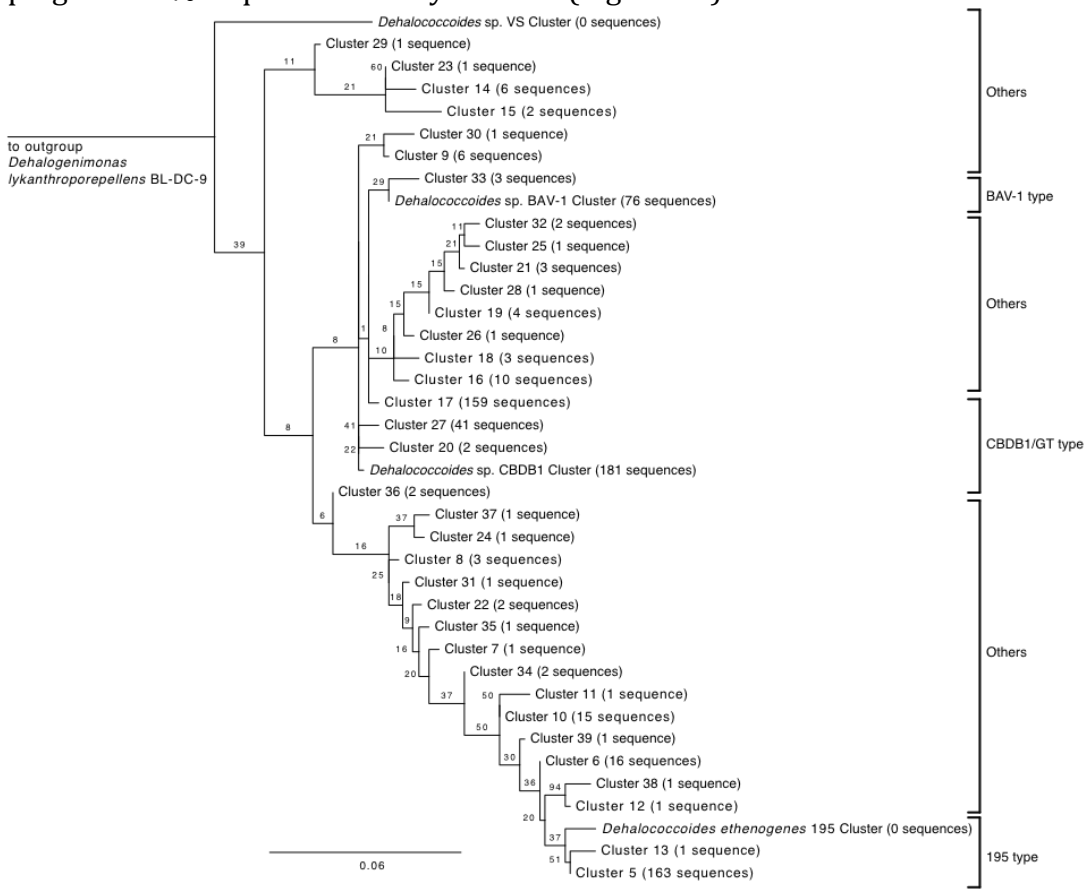

Figure 23 – All *Dehalococcoides hupL* sequences generated as part of this dissertation clustered to 99.5% using CD-HIT and representative sequences used to construct a maximum likelihood tree with 100× bootstrap. Bootstrap percentages are shown at branching points.

The changes in abundance of clones that occupied these different clusters over time are plotted in Figure 24. There was a clear trend from a *Dehalococcoides* community dominated by relatives of strains BAV1 and CBDB1/GT to a community free of strain BAV1 relatives, dominated by strain 195 relatives, and with a diminished fraction of strain CBDB1/GT relatives. This is similar to the phenomenon observed when sulfide and sulfate were introduced to Point Mugu batch cultures not previously exposed to sulfide or sulfate. In these cultures a switch in *Dehalococcoides* community composition from domination by CBDB1/GT relatives to 195 relatives occurred to a greater extent

in batch cultures exposed to sulfide either directly or through the activity of sulfate-reducing bacteria than in control cultures without sulfide or sulfate. It appeared that the Point Mugu culture contain multiple populations of *Dehalococcoides*, some of which are more negatively impacted by the presence of sulfide than others.

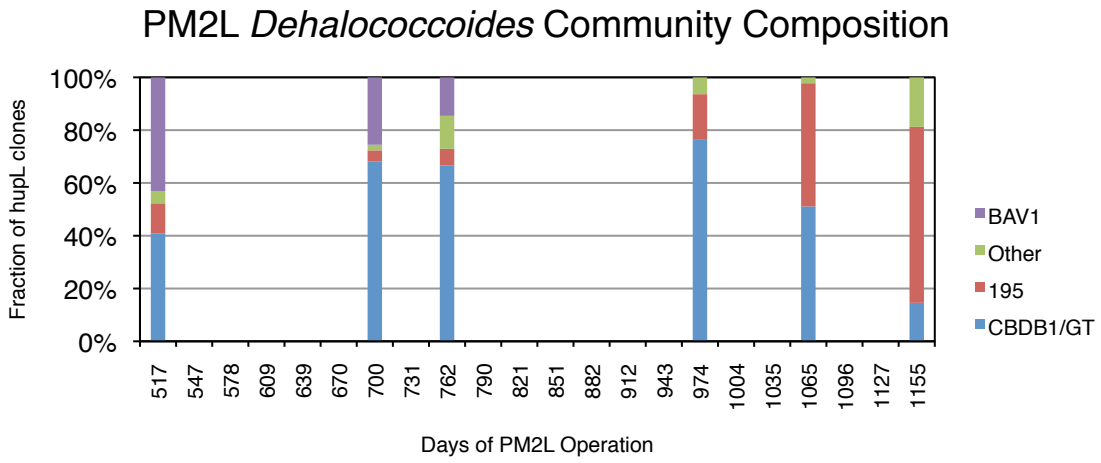

Figure 24 –*Dehalococcoides* community composition in the PM2L chemostat as assessed by *hupL* clone libraries. The numbers of clones sequenced for each time point are (from left to right): 44, 47, 48, 47, 45, 48.

5.1.3.2 Characterization of the PM2L Chemostat with the Rdh tiled DNA microarray

One shortcoming of a *hupL*-based analysis of the *Dehalococcoides* community composition in the PM2L chemostat is that it is based only on the phylogenetic identity of the bacteria, and not on the content of their genomes. Different strains of *Dehalococcoides* can be considered phylogenetically identical based on conserved markers such as *hupL* while containing different sets of reductive dehalogenase genes and thus different ranges of organohalide substrate respiration potential. For example, while the *hupL* sequences of *Dehalococcoides* strains CBDB1 and GT are 99.8% identical (within reported Sanger sequencing error rates (Hoff 2009) and thus practically indistinguishable), only strain GT is capable of respiring vinyl chloride (Sung et al. 2006). Reductive dehalogenase genes have been identified in so-called "high plasticity regions" of *Dehalococcoides* genomes and are thought to be subject to a higher rate of lateral gene transfer than the rest of the genome (McMurdie et al. 2009). For this reason we decided to assess the *Dehalococcoides* community composition of the PM2L chemostat based on *rdhA* gene content in addition to *hupL* clone library analysis. The Reductive Dehalogenase Chip was designed to assess *rdhA* gene content and abundance and thus was a well-placed tool to address this question.

DNA extracted from five different PM2L time points was amplified, fluorescently labeled and hybridized to the Reductive Dehalogenase Chip. Sixty *rdhA* genes were found to have a BPF of greater than 90% (Table 12). One notable aspect of these 60 *rdhA* genes is that there is no complete set from any given *Dehalococcoides* isolate genome or metagenome, suggesting that no *Dehalococcoides* strain in the PM2L chemostat fully resembles an existing isolate or representative of a sequenced community. Abundance values for genes encoding the two known vinyl-chloride

reducing reductive dehalogenases are depicted in Figure 25. As expected, these show an overall decline in abundance over the course of PM2L operation that coincides with the slow down of VC reduction rates.

Accession (NCBI or IMG/M)	Source	rdhA	7-29-09	1-X-10	3-24-10	1-6-11	4-19-11
AAW39605.1	*Dehalococcoides ethenogenes* 195.		**100%**	**100%**	**100%**	**100%**	**100%**
CAI83191.1	*Dehalococcoides* sp. CBDB1.		**100%**	**100%**	**100%**	**100%**	**100%**
AAT64888.1	*Dehalococcoides* sp. BAV1.	*bvcA*	**100%**	**100%**	20%	88%	27%
AAW40589.1	*Dehalococcoides ethenogenes* 195.		**100%**	**100%**	**100%**	**100%**	**100%**
ABQ16695.1	*Dehalococcoides* sp. BAV1.		**100%**	**100%**	**100%**	20%	80%
ABQ16712.1	*Dehalococcoides* sp. BAV1.		**100%**	**100%**	**98%**	24%	65%
AAW39214.1	*Dehalococcoides ethenogenes* 195.		**100%**	**98%**	88%	**100%**	**100%**
ABQ16703.1	*Dehalococcoides* sp. BAV1.		**100%**	**100%**	**100%**	14%	56%
ADC74651.1	*Dehalococcoides* sp. GT.		**100%**	**100%**	**100%**	**100%**	82%
ADC74655.1	*Dehalococcoides* sp. GT.		**100%**	**100%**	**100%**	**100%**	78%
ADC74658.1	*Dehalococcoides* sp. GT.		**100%**	**100%**	**100%**	**100%**	78%
ADC74676.1	*Dehalococcoides* sp. GT.		**100%**	**100%**	**100%**	**100%**	**100%**
ADC74708.1	*Dehalococcoides* sp. GT.		**100%**	**100%**	**100%**	**100%**	**100%**
BAG72167.1	uncultured bacterium.		**100%**	**100%**	**100%**	**100%**	**100%**
AAR24312.1	*Dehalococcoides* sp. CBDB1.		**100%**	**100%**	**100%**	**96%**	**98%**
AAW39229.1	*Dehalococcoides ethenogenes* 195.		**100%**	**98%**	**94%**	**100%**	**100%**
ABA64547.1	*Dehalococcoides* sp. KB1.		**100%**	**100%**	**100%**	**100%**	**100%**
ADC74548.1	*Dehalococcoides* sp. GT.		**100%**	**100%**	**98%**	**100%**	**98%**
ADC74550.1	*Dehalococcoides* sp. GT.		**100%**	**100%**	**100%**	**100%**	**100%**
ADC74627.1	*Dehalococcoides* sp. GT.		**100%**	**100%**	**94%**	**96%**	67%
ADC74673.1	*Dehalococcoides* sp. GT.		**100%**	**100%**	**100%**	**100%**	**100%**
ADC74702.1	*Dehalococcoides* sp. GT.		**100%**	**100%**	**100%**	**100%**	**100%**
AAT48556.1	*Dehalococcoides* sp. BAV1.		**100%**	**100%**	**100%**	**100%**	**100%**
ABA64539.1	*Dehalococcoides* sp. KB1.		**100%**	**98%**	**100%**	**96%**	**98%**
ABQ16710.1	*Dehalococcoides* sp. BAV1.		**100%**	**98%**	81%	6%	44%
ADC74693.1	*Dehalococcoides* sp. GT.		**100%**	**100%**	**100%**	**100%**	**96%**
AAT48548.1	*Dehalococcoides* sp. BAV1.		**100%**	**100%**	**100%**	**100%**	**100%**
CAI83531.1	*Dehalococcoides* sp. CBDB1.		**100%**	**100%**	**100%**	**98%**	**98%**
AAW40575.1	*Dehalococcoides ethenogenes* 195.		**100%**	**100%**	**100%**	**100%**	**100%**
ABQ16764.1	*Dehalococcoides* sp. BAV1.		**100%**	**100%**	**100%**	**100%**	**100%**
ACZ61341.1	*Dehalococcoides* sp. VS.		**100%**	**100%**	**98%**	**100%**	**100%**
BAG55976.1	uncultured bacterium.		**100%**	**100%**	**100%**	**100%**	**100%**
ADR80140.1	uncultured *Dehalococcoides* sp..		**100%**	**100%**	**100%**	**100%**	**100%**
ABB89703.1	*Dehalococcoides* sp. FMC-TCE.	*tceA*	**98%**	**91%**	44%	**100%**	**95%**
AAQ94119.1	bacterium VS.	*vcrA*	**98%**	**98%**	65%	13%	33%
ACZ62463.1	*Dehalococcoides* sp. VS.		**98%**	**100%**	82%	**96%**	57%
ACZ62419.1	*Dehalococcoides* sp. VS.		**98%**	**90%**	65%	10%	29%
ACZ62529.1	*Dehalococcoides* sp. VS.		**98%**	**96%**	**92%**	90%	90%

2013897169	Aquatic dechlorinating community (KB-1)		**98%**	**98%**	**96%**	10%	37%
AAT48554.1	*Dehalococcoides* sp. BAV1.		**98%**	**98%**	**96%**	89%	**91%**
CAI83570.1	*Dehalococcoides* sp. CBDB1.		**96%**	**100%**	**98%**	**96%**	58%
ADR00316.1	*Dehalococcoides* sp. enrichment culture SL2	*tceA*	**96%**	**92%**	42%	**100%**	**96%**
BAI70451.1	uncultured bacterium.		**96%**	**98%**	**96%**	**96%**	**91%**
CAI83563.1	*Dehalococcoides* sp. CBDB1.		**96%**	**100%**	76%	**96%**	17%
ADR80137.1	uncultured *Dehalococcoides* sp..		**94%**	**94%**	89%	89%	83%
ACZ62459.1	*Dehalococcoides* sp. VS.		**94%**	**94%**	87%	89%	87%
ACZ62415.1	*Dehalococcoides* sp. VS.		**94%**	**96%**	84%	86%	88%
CAI83566.1	*Dehalococcoides* sp. CBDB1.		**94%**	**100%**	83%	**94%**	35%
ADC74662.1	*Dehalococcoides* sp. GT.		**92%**	**96%**	90%	88%	76%
ACZ62498.1	*Dehalococcoides* sp. VS.		**92%**	**96%**	86%	86%	84%
BAJ06127.1	uncultured *Dehalococcoides* sp..	*tceA*	**91%**	73%	18%	**91%**	**91%**
ACZ62535.1	*Dehalococcoides* sp. VS.		**90%**	88%	81%	88%	83%
2013897488	Aquatic dechlorinating community (KB-1)		88%	76%	66%	**92%**	**92%**
BAF34982.1	uncultured *Dehalococcoides* sp..	*tceA*	83%	74%	44%	**93%**	81%
BAE82944.1	*Desulfitobacterium hafniense* Y51.	*cprA*	61%	**100%**	**100%**	64%	**100%**
ACH47983.1	*Desulfitobacterium* sp. enrichment culture clone C1.	*pceA*	17%	**100%**	**100%**	17%	**100%**
ACH87596.1	*Dehalobacter* sp. WL.		11%	**97%**	**100%**	11%	**100%**
BAF57046.1	*Desulfitobacterium* sp. CR1.	*pceA*	9%	**93%**	**96%**	11%	**96%**
AAO60101.1	*Desulfitobacterium* sp. PCE-S.	*pceA*	5%	**95%**	**96%**	4%	**98%**
ACH87594.1	*Dehalobacter* sp. WL.		4%	**93%**	**95%**	5%	**95%**

Table 11 – BPF values for *rdhA* genes identified in the PM2L chemostat using the Reductive Dehalogenase Chip at five different time points. *rdhA* genes considered present (BPF>90%) have their BPF values in bold text. Genbank (NCBI) accession numbers begin with letters, IMG/M accession numbers begin with numbers.

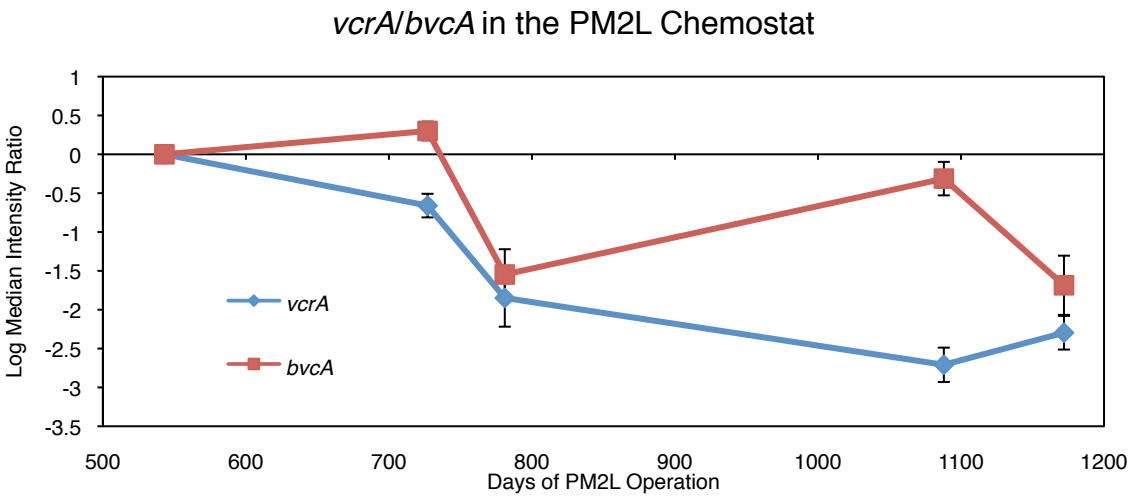

Figure 25 - Median log intensity ratios for *vcrA* and *bvcA* in the PM2L chemostat. Values show the natural logarithm of the median of all probe fluorescence intensity ratios for each gene, with each time point divided by the 543 day time point.

Analyzing the abundance of *vcrA* and *bvcA* alone provide an impression of the abundance shifts for those strains of *Dehalococcoides* carrying *vcrA*, but it does not reveal whether a single *Dehalococcoides* type carries each of these genes or whether a group of *Dehalococcoides* types carry *vcrA* or *bvcA*. However, the data reveal that *vcrA* and *bvcA* are not genetically linked. To shed light on the question of Dehalococcoides population structure we decided to examine the abundance changes for all the detected reductive dehalogenase genes over time. Those genes that all belong to a single genome would be expected to be tightly linked and go through identical changes in abundance that would manifest themselves as similar changes in log median probe intensity ratios. In order to differentiate between the effect of a single gene cross-hybridizing to several highly identical sets of target probes and true clusters of genes varying in a synchronized manner due to presence in the same genome, the nucleotide sequences of all 60 identified *rdhA* genes were subjected to clustering at 85% identity using CD-HIT. This yielded a set of 38 *rdhA* clusters with a minimal probability of between-cluster cross hybridization. The *rdhA* gene with the highest median probe fluorescence intensity at any of the time points analyzed was selected as the representative gene for that cluster.

To find these clusters of genes belonging to the same genome, the Euclidean distance between each gene pair was established based on the four-dimensional set of log median intensity ratios for each gene. These distances were subjected to hierarchical clustering and arranged into four clusters: three *Dehalococcoides* clusters and one *Desulfitobacterium* cluster, with three being the number of *Dehalococcoides* clusters hypothesized based on the *hupL* clone library data (Figure 24). The clustering dendrogram and inferred clusters are depicted in Figure 26.

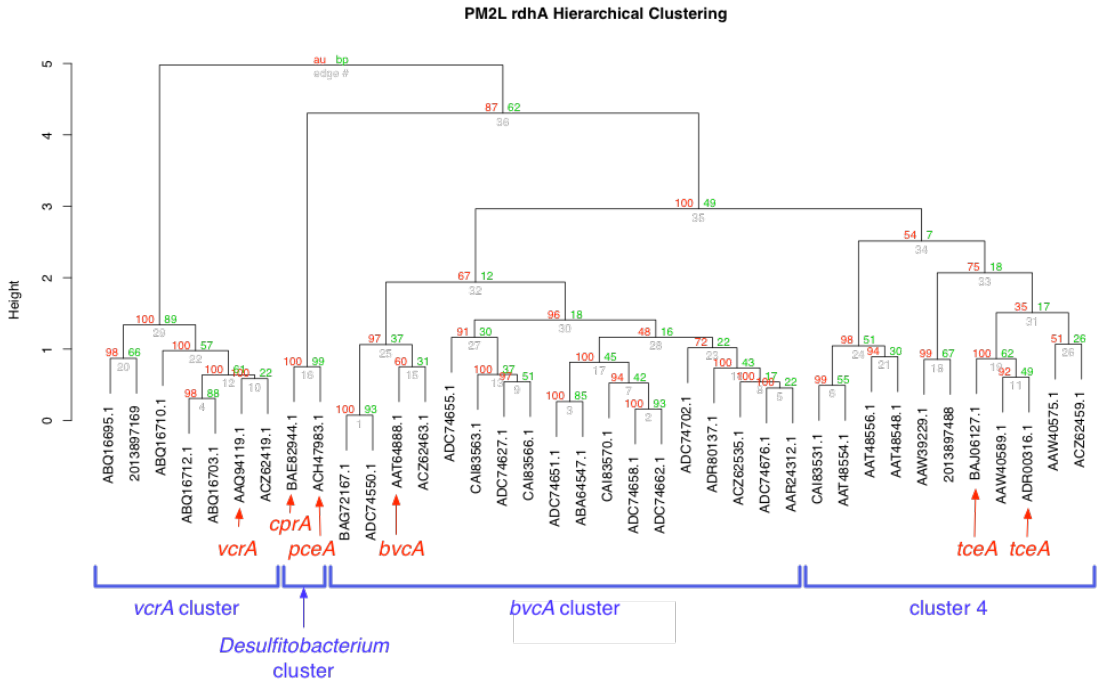

Figure 26 – Hierarchical clustering of reductive dehalogenase DNA microarray data from the PM2L chemostat. Numbers is red show "Approximate Unbiased" % probabilities of that cluster, numbers in green show bootstrap probabilities.

Relative changes in abundance for each of those four clusters are depicted in Figure 27. It is impossible to say based on this data whether each cluster represents a genetically identical population of cells or a population of multiple genotypes each carrying some of the *rdhA* genes from that particular cluster. However, it appears to show that at least three different *Dehalococcoides* genotypes are present, with the *vcrA* cluster in constant decline over the course of the experiment, the *bvcA* cluster increasing slightly and dominating the *Dehalococcoides* community from day 600 to sometime between days 800 and 1100 before eventually declining, and cluster 4 steadily increasing from approximately day 800 to become dominant before day 1100. This is consistent with the observation that VC reduction slowed down from day 700 to 1100 (while the *bvcA* cluster dominated) before stopping entirely from around day 1100 (when the cluster 4, which lacks both *vcrA* and *bvcA*, became dominant). It appears that the introduction of sulfate into the chemostat and the onset of sulfate reduction happened simultaneously to a decline in VC-respiring *Dehalococcoides* community. This demonstrates the usefulness of the Reductive Dehalogenase Chip as a tool for simultaneously monitoring changes in *Dehalococcoides* community composition and in the functional capacity of that community to reduce different organohalide compounds.

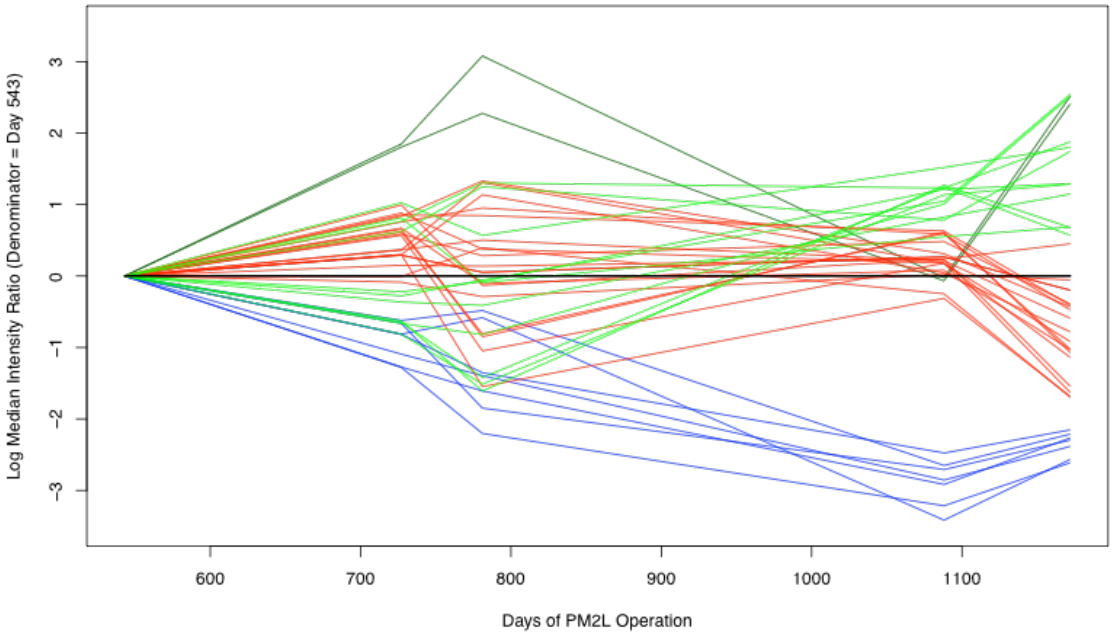

Figure 27 – Log median intensity shifts for *rdhA* gene clusters: *vcrA* cluster (blue), *bvcA* cluster (red), *Desulfitobacterium* cluster (dark green), cluster 4 (light green). Values show the natural logarithm of the median of all probe fluorescence intensity ratios for each gene cluster, with each time point divided by the **543 day time point.**

5.2 Results for Project 2

5.2.1 5-L Experimental Results

The 5-L CSTR was operated to investigate the EV culture performance under excess electron donor. The CAH monitoring data during the time period from day 100-300 are presented in Figure 28. The 5-L CSTR was operated with influent concentrations of 45 mM formate and 10 mM TCE. The CSTR monitoring data, including the CAHs concentrations, hydrogen concentrations, and the acetate concentration produced from day 100 to 300 are presented in Figure 3. The CSTR reached a pseudo steady-state around 100 days of operation. TCE transformed to VC and ethene through cDCE, with minor concentrations of TCE and cDCE observed. The steady-state VC concentration was 0.9 mM while ethene was 9.1 mM. The steady-state H_2 concentration was around 42 nM. Acetate was produced and achieved a steady-state concentration of 3.75 mM. The approximate steady-state biomass was 31 mg/L on a protein basis. Experimental results showed that acetate was produced by homoacetogens at this low H_2 tension, suggesting that H_2 threshold for acetate

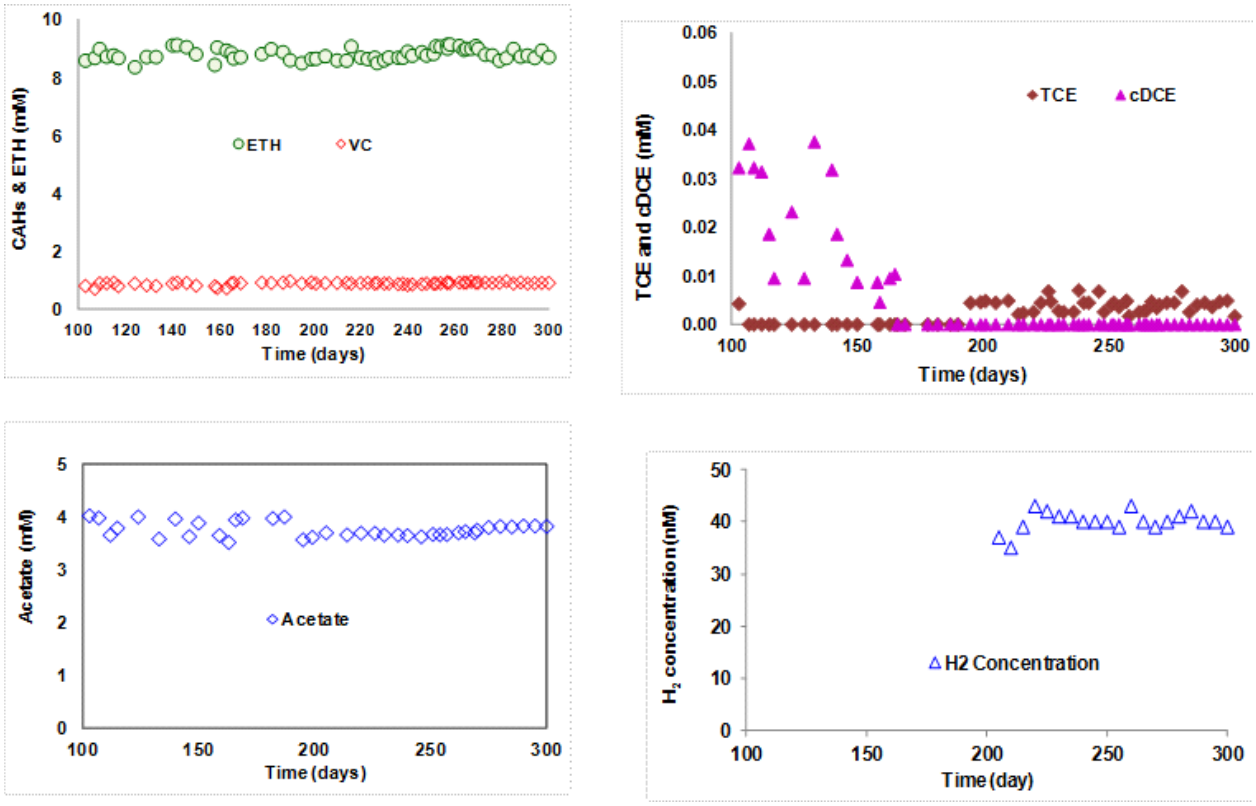

Figure 28 - Experimental results of 5-L CSTR, results of CAHs, acetate and H_2 during the time period of 100-300 days of operation.

production ($H_{2\text{-Acet}}$) is around 40 nM in the CSTR. This threshold is in contrast to values reported in the literature (higher than 350 nM) (Löffler et al., 1999; Breznak, 1994; Luijten et al., 2004).

5.2.2 Simulations of the 5-L CSTR

We started our simulations by using the previously determined EV kinetic parameters from batch experiments (Yu and Semprini, 2004), then using modified Yu and Semprini (2004) kinetic parameters based on population composition, and finally by using the VC kinetic parameters determined in batch experiments using cells harvested from the 5-L CSTR when formate was in excess. Based on 5-L CSTR simulations, the kinetic parameters which provide a good match to the observed results and reflects the performance of the 5-L CSTR will be used to simulate the 2-L CSTR performance.

5.2.3 Case 1:Using Yu and Semprini (2004) Kinetic Parameters

The first simulation attempt used the EV kinetic parameters determined in batch experiments by Yu and Semprini (2004). Simulations were performed using the input parameters (Table 2) and applying the EV kinetic parameters (Table 3) along with K_{s_H2} utilization of 7 nM (Cupples et al., 2004). Simulation results of the transient period during the first 100 days of CSTR operation captured the transformation of TCE, trace levels of cDCE built up (1.5×10^{-4} mM), build up of VC

and ethene to steady-state levels (results of first 100 days not shown). Figure 29 shows the comparison of experimental data with model simulations for CAHs, acetate, H_2, and microbial concentrations after steady-state operation was achieved. The model captured the CAHs trends, TCE transformed to VC and ethene with the formation and transformation of cDCE as an intermediate. VC reached a steady-state value of 0.2 mM while the observed VC was 1 mM. The simulation showed a pseudo steady-state of 1.5×10^{-4} mM for TCE and cDCE. High VC transformation rate was predicted. The simulated ethene was 9.8 mM while the observed ethene is 9.0 mM. The simulated H_2 and acetate values were in agreement with experimental results. However, the simulated biomass (60 mg/L protein) was three times higher than measured from the CSTR (31 mg/L protein). Applying the previously derived kinetic parameters that are based on total protein concentration did a good job capturing the overall response observed in the CSTR reactor, however, the predicted biomass concentration was very high. The simulated results indicate that the biomass yield in the CSTR may be lower and the biomass decay coefficient ($K_{d,dech}$) was potentially higher than reported by Yu and Semprini (2004). Simulations using EV kinetics parameters determined by Yu and Semprini (2004) showed a higher VC transformation rate and biomass yield.

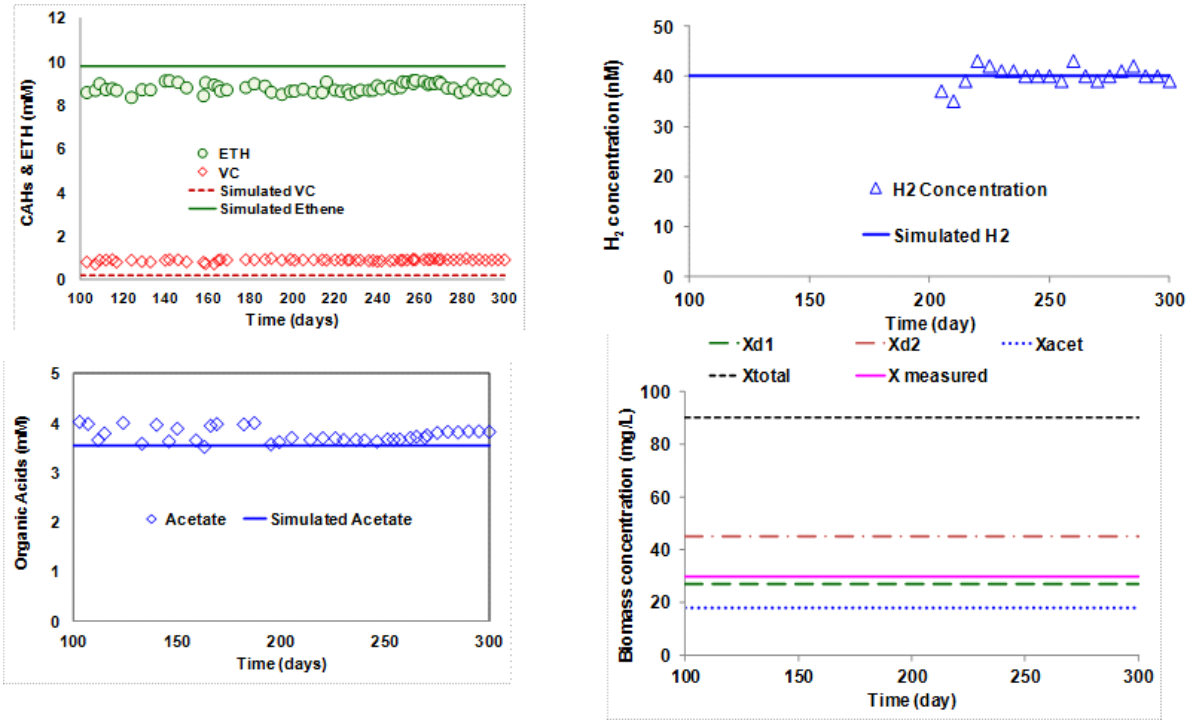

Figure 29 - Experimental and simulated results of 5-L CSTR using Yu and Semprini (2004), kinetics (Table 3). $K_{s\text{-}H2}$ utilization of 7 nM.

5.2.4 Case 2: Modified Yu and Semprini (2004) kinetic parameters

Modification of the kinetic parameters determined by Yu and Semprini (2004) was done based on two populations being responsible for the complete dechlorination of TCE to ethene, the population distribution (45% *Dehalococcoides*, 25% TCE reducers and 30% acetogens). This distribution is based on Behrens et al. (2008) which shows that around 75% of microbial population was *Dehalococcoides* in the EV culture during the time the kinetic parameters were measured. Kinetic parameters were also adjusted based on trial and error in simulation of batch experiments of CAHs with cultures harvested from the CSTR (results are not presented). The modified parameters are presented in Table 4, column A. Simulation results using modified Yu and Semprini (2004) kinetic parameters shows a higher VC transformation extent (VC concentration 0.04 mM) and ethene concentration 9.6 mM) and a biomass concentration higher than measured. Simulated biomass was 42 mg/L compared to 30 mg/L that was measured (Figure 30).

To get the biomass concentration within the range of observed biomass, the yield and decay coefficients were adjusted for each population based on literature values (Maymó-Gatell et al., 1997; Holliger et al., 1998; Holliger et al., 1993; Fennell and Gossett, 1998; Clapp et al., 2004). Simulation results showed a better match to the experimental results with the adjusted parameters (Figure 30). The yield and decay of dechlorinators were heuristically adjusted to provide a good match to the observed CAHs, acetate, H_2 and biomass distribution. The yield was reduced from 0.006 to 0.0043 mg protein/μmol of substrate. Cell decay coefficients for each population were set to be in the range of 0.05-0.06 d^{-1}, the decay coefficient was increased from 0.024 d^{-1} to 0.05 d^{-1}. This decay value seems to be high for anaerobic cultures, however, Cupples et al. (2004) used 0.09 d^{-1} in their simulations of anaerobic culture. The total simulated biomass was 42 mg/L while the measured was 31 mg/L. Low yield and high decay coefficient of X_{d1} and X_{d2} showed a decrease in the transformation rate of VC, while the simulated total biomass (42 mg/L) was higher than observed (31 mg/L). Attempts to get a good match of the total biomass by lowering the biomass yield (Y_{d2}) resulted in a low transformation rate for VC than observed in the 5-L CSTR (VC of 4 mM and ethene of 6 mM). Simulation results showed it was difficult to get biomass and CAHs in agreement with the experimental results, using the modified Yu and Semprini's kinetic parameters.

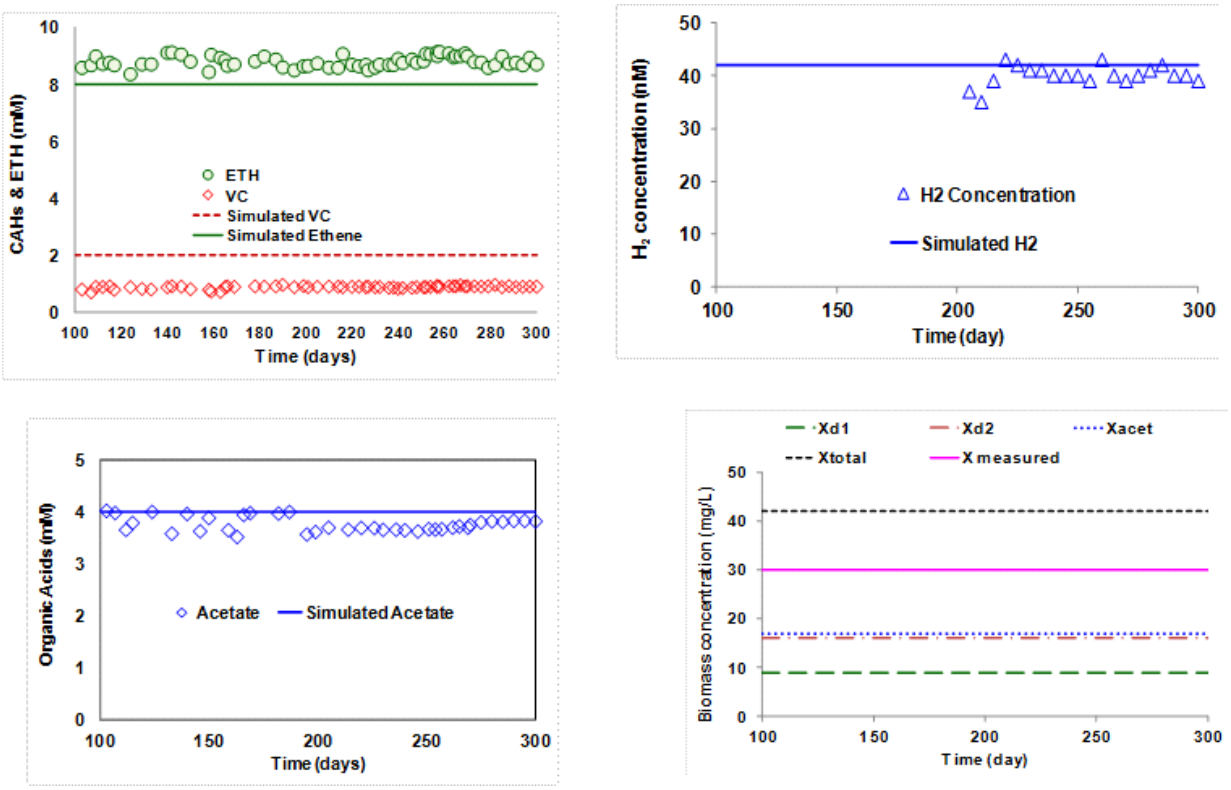

Figure 30 - Experimental and simulated results of the 5L CSTR using Modified Yu Kinetics with y =0.0043 kinetics batch determined kinetics as in Table 4, column A, $K_{s\text{-}H2}$ utilization of 7 nM.

5.2.5 Case 3: Using Kinetics determined in batch experiments.

Previous simulations predicted a higher biomass concentration than measured in the CSTR. The third case of simulation was using the VC kinetic parameters determined in batch experiments with cells harvested from the 5-L CSTR (Table 4, column B). The biomass yield and decay coefficients determined by Yu and Semprini were initially used. A $K_{s\text{-}H2}$ for H_2 utilization of 7 nM for dehalogenators was used in simulating the CSTR, based on values reported by Cupples et al. (2004). Simulations using input parameters given in Table 2, and VC kinetics determined in batch experiments (Table 4, column B) resulted in a high dehalogenation rate, with VC and ethene concentrations of 0.2 and 9.8 mM, respectively. A high value of biomass concentration of 60 mg/L was predicted, while the observed value was 30 mg/L. Also a low H_2 concentration of 42 nM was observed. The biomass yield and decay coefficients were adjusted to produce comparable amount of biomass as measured in the CSTR effluent. Heuristical adjustments were carried out for the yield and decay coefficients. A yield value of 0.0031 mg protein/μmol of substrate and the decay coefficient of 0.045 and 0.055 d^{-1} for X_{d1} and X_{d2}, respectively were used. The adjusted coefficients resulted in a better match of the VC, ethene, H_2 and biomass concentrations. Figure 31 shows the comparison of experimental data with model simulations for CAHs, acetate, H_2, and microbial concentrations. The model captured the CAHs trends, TCE transformed to VC and ethene with the formation and transformation of cDCE as an intermediate. The VC and ethene concentrations were comparable to the experimental results, with a steady-state value of 0.9 mM and 9.1 mM for VC and ethene, respectively. The simulated acetate was of 3.75 mM, using a calibrated acetogenesis threshold of 40 nM. This threshold gives a good match of acetate production. Predicted total biomass was 34 mg/L which is in agreement with the measured value. Also, comparable simulated H_2 concentrations to the measured values were obtained (Figure 31).

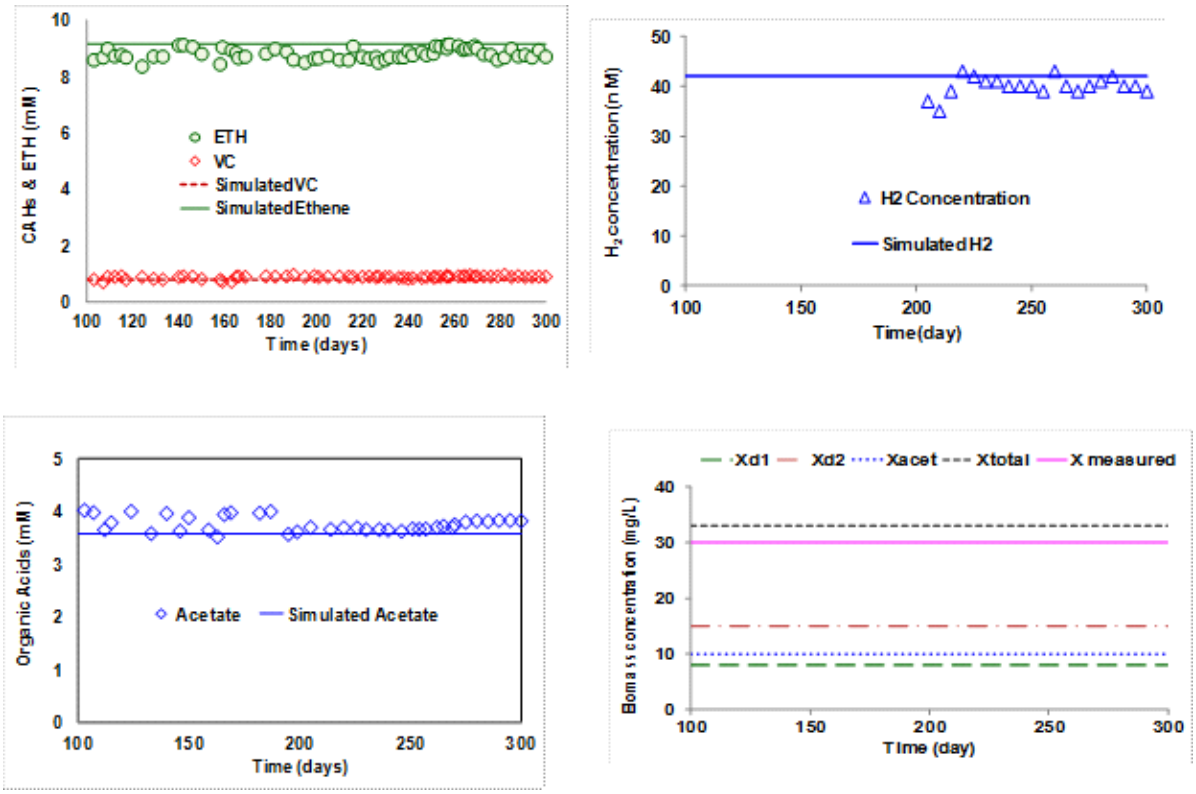

Figure 31 - Experimental and simulated results of the 5-L CSTR using VC kinetics determined in batch experiments using cells harvested from the 5-L CSTRas presented in Table 4, column B, where K_{max_VC} = 26 µmol/mg protein/d, $K_{s\text{-}VC}$ =12 µM and $K_{s\text{-}H2}$ for VC dechlorination =7 nM, Y_{d1} of 0.0042 and Y_{d2} of 0.0031, K_d of 0.051 d^{-1}.

Based on the previous simulations using VC kinetic parameters determined using cells harvested from the CSTR, it appears that the K_{max} of VC (26 μ mol/mg protein/d) was in the range determined by Yu and Semprini (2004), while K_s of 12 μmol/L was lower than the value of 62 μmol/L by Yu and Semprini (2004). The yield of 0.0031 was lower than the value used by Yu and Semprini (2004) a of 0.006 mg protein/μmol of substrate. The decay coefficient was 0.045 and 0.055 d^{-1} for X_{d1} and X_{d2}, higher than the value used by Yu and Semprini (2004) of 0.024 d^{-1} (Table 3). Overall, simulations using the kinetics determined with cells harvested from the 5-L CSTR showed a good match to the measured VC and ethene concentrations and also the measured biomass concentration.

5.2.6 Mass Balance and Electron Balance

Mass balances of the influent and effluent steady-state CAHs over the simulated phase (100–300 days) were carried out for both experimental and simulated results. Mass calculations were done by multiplying the measured effluent concentrations by the fluid flow rate and integrating over time. The CAHs and ethene recovered in the effluent of experiment and simulation accounted for 99.0% and 99.4% of the injected TCE, respectively, providing a good mass balance.

An electron balance on the influent formate and the reducing equivalents based on products formed was determined for between days 100-300 (Table 12). The formate electron reducing equivalents were associated with the following: acetate formation (32%), biomass synthesis (3%) and dehalogenation (65%). A comparable electron balance of simulated results to the experiment results was obtained. The difference between simulated electron reducing equivalents of the influent and effluent was less than 0.5%.

Table 12 - Electron balance of 5-L CSTR between day 100-300

		Effluent	
Influent			
Formate me$^-$eq		Simulated %	Experiment %
1395.5	H_2	1×10^{-4}	1×10^{-4}
	Formate	1.4×10^{-2}	1.5×10^{-2}
	Acetate	32.3	33.8
	TCE to cis-DCE	1.8×10^{-2}	1.7×10^{-2}
	TCE to VC	3.5	3.9
	TCE to ethene	59.3	57.9
	Net cells growth and decay	4.8	4.4
Total me-eq 1395.5	me-eq out	100	100

5.2.7 Comparison between experimental and simulated biomass results (5-L CSTR)

Table 13 presents the simulated steady-state biomass distribution in the 5-L CSTR.

Table 13 - The simulated microbial community distribution in the 5-L CSTR when formate was in excess (100-300 days).

	Simulated biomass distribution		Measured biomass
Microbial community	Protein Concentration (mg/L)	% of total biomass	Protein Concentration (mg/L)
TCE dechlorinators	9	26	N/A
Dehalococcoides	13.5	40	N/A
Acetogens	11.5	34	N/A
Total biomass simulated	34		31

N/A: not measured in the CSTR, only the total protein concentration was measured.

The measured protein was 31 mg/L, while the simulated value was 34mg/L. The simulated results show that the dechlorinators represent 66% of the total microbial population, (26% of biomass was TCE dechlorinators, 40% *Dehalococcoides*) while 34% were homoacetogens.

Microbial data, *Dehalococcoides* 16S rRNA gene copy number normalized to all bacterial 16S rRNA gene copy numbers determined by qPCR in the 5-L CSTRs are shown in Figure 32 (Behrens et al., 2008). The qPCR results showed that the dechlorinators represented 74% of microbial population in the 5-L CSTR when formate was in excess, while simulated biomass results showed the total CAHs reducers form 66% of the total population in the 5-L CSTR. The simulated biomass distribution agrees reasonably well with the molecular results (Figure 32) (Behrens et al., 2008).

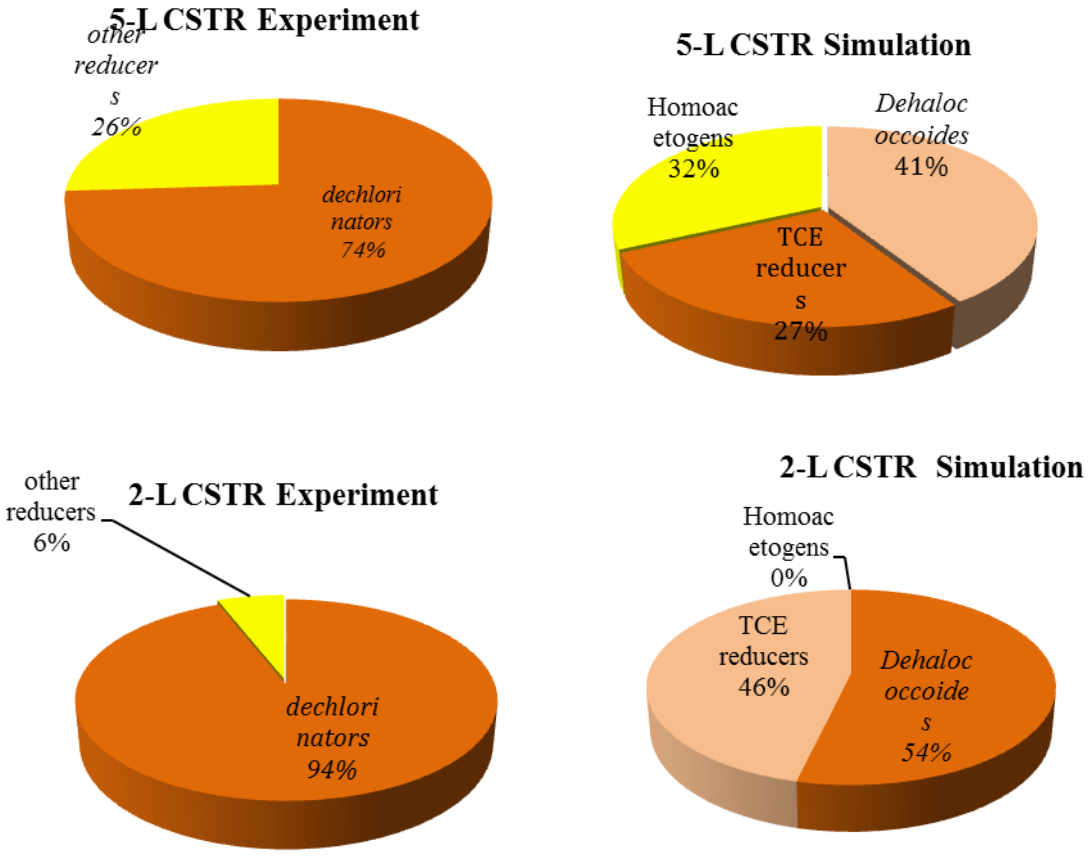

Figure 32 Experimental and simulated results of microbial community composition in the 5-L and the 2-L CSTRs.

5.2.8 Simulation of Control Batch Experiment.

The Evanite culture was taken into the batch reactor from the CSTR effluent, spiked with excess hydrogen, as an electron donor and VC as an electron acceptor. The results of the experiment are shown in Figure 33. The simulation was performed using the kinetics for VC transformation used for the CSTR simulation. The initial biomass concentration was 31 mg protein /L in the CSTR. The reactor volume was 156 mL with 25 mL liquid phase and 131 mL head space. 25 µmol of VC was spiked to the reactor, while added H_2 was in excess. Acetate formation from H_2 and bicarbonate was simulated with the inclusion of the thermodynamic influence on acetate formation and the rate of hydrogen utilized. The H_2 threshold of acetate formation was assumed to be 40 nM.

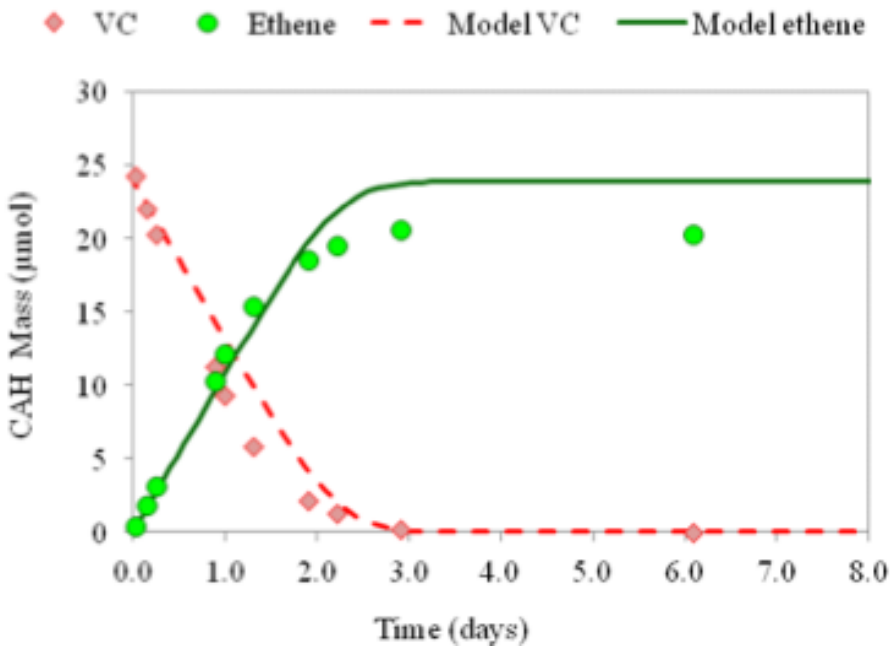

Figure 33 A Experimental and simulated results of VC transformation in batch experiment using cells harvested from the 5-L CSTR. K_{max} of VC = 26.0 µmol/mg protein-d and K_s = 12µmol/L. Initial biomass was 30 mg/L.

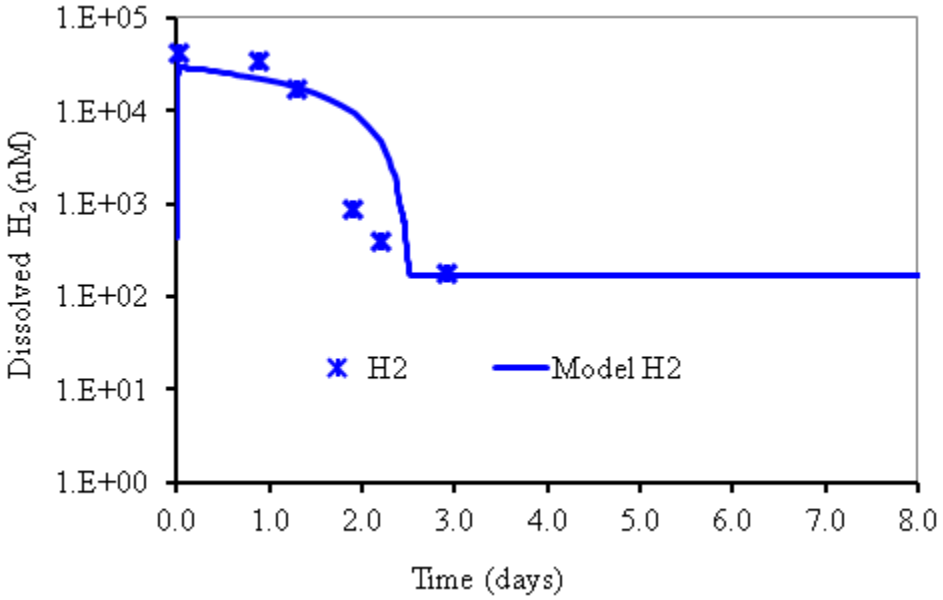

Figure 33 B: Experimental and simulated results of H_2 in batch experiment using cells harvested from the 5-L CSTR. K_{max} of VC = 26.0 µmol/mg protein-d and K_s = 12 µmol/L.

Figure 33 - Experimental and simulated results of VC transformation and H_2 in batch experiment using cells harvested from the 5-L CSTR

The model predicted a comparable rate of H_2 consumption as the experiment, then shows steady-state levels as the formation rate of acetate gradually decreased. The predicted H_2 concentration that persists in the batch reactor (170 nM) was in good agreement with the experiment (166 nM). The experimental and simulation results indicated steady-state H_2 concentration higher than the threshold of acetate formation, which likely due to the thermodynamic limitation as the acetate formation limits the consumption of H_2. Experimental and simulated results show that the predicted biomass concentrations and the modified kinetic parameters used in simulating the 5-L CSTR performance did a good job simulating the results of the batch experiments.

5.2.9 2-L CSTR Laboratory Experimental Results

The second 2-L CSTR was operated to investigate the EV culture performance under excess and limited electron donor conditions. Figures 34A and B shows the experimental results of the 2-L CSTR during the time period from 120 - 640 days. Initially, the CSTR was operated with the same influent concentration as the 5-L CSTR, 45 mM and 10 mM formate and TCE, respectively. The TCE was transformed to 9.0 mM ethene and 1.0 mM VC during the period of 100- 180 days. Acetate, H_2 and biomass protein were 3.75, 42 nM and 30 mg/L, respectively. On day 180, formate was reduced from 45 mM to 25 mM and the transient response was observed. TCE transformation decreased to 5.4 mM ethene and 4.6 mM VC, cDCE increased from 0.006 mM to 0.2 mM. The H_2 concentration gradually decreased from 42 nM to 3 nM, and acetate gradually decreased to below 0.1 mM (Figure 34C). The decrease in acetate occurred over a period of about two residence times, while VC, ethene and H_2 equilibrated more rapidly to the lower concentrations. The biomass concentration decreased from 31 mg/L to a steady-state value of 15.5 mg/L. Note, when the 2-L CSTR was running with excess formate, no biomass measurement was taken. Therefore, the experimental results of the 5-L CSTR will be used to represent the 2-L CSTR between days 120-180.

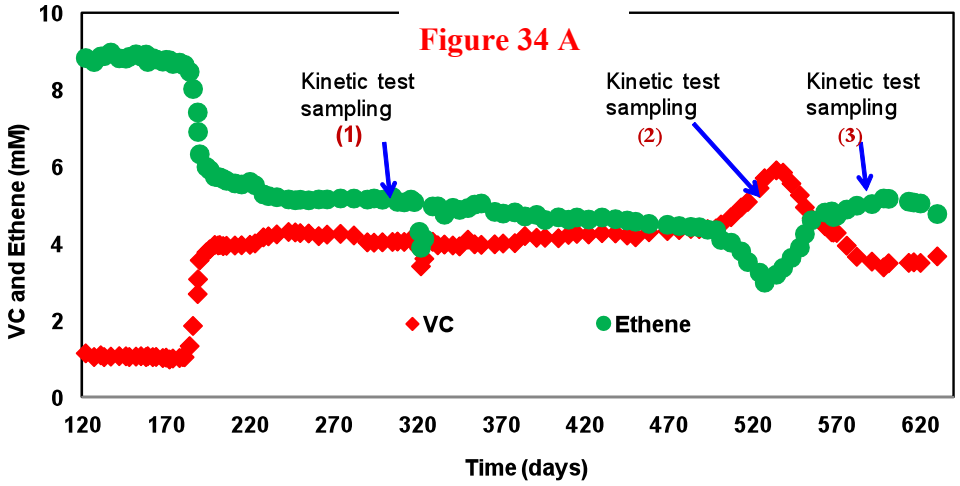
Figure 34 A
Kinetic test sampling (1)
Kinetic test sampling (2)
Kinetic test sampling (3)
VC
Ethene
VC and Ethene (mM)
Time (days)

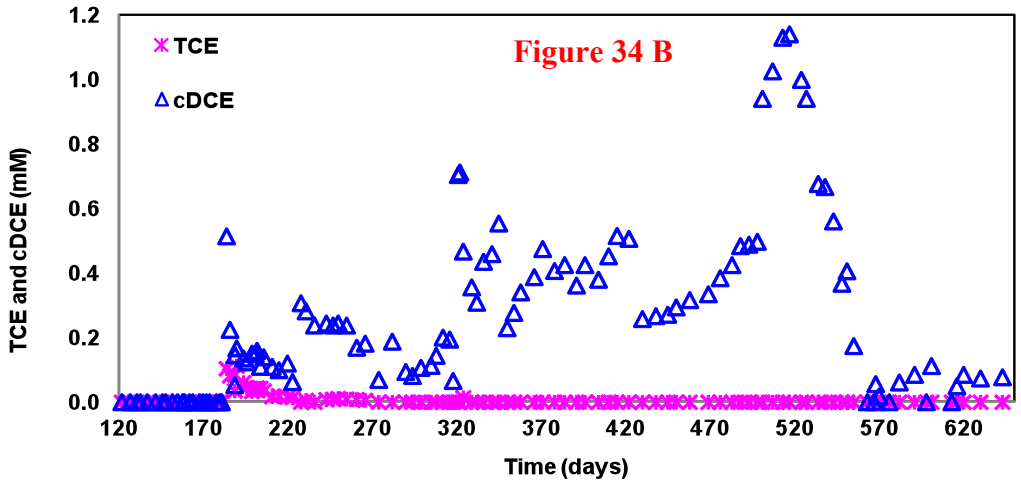
Figure 34 B
TCE
cDCE
TCE and cDCE (mM)
Time (days)

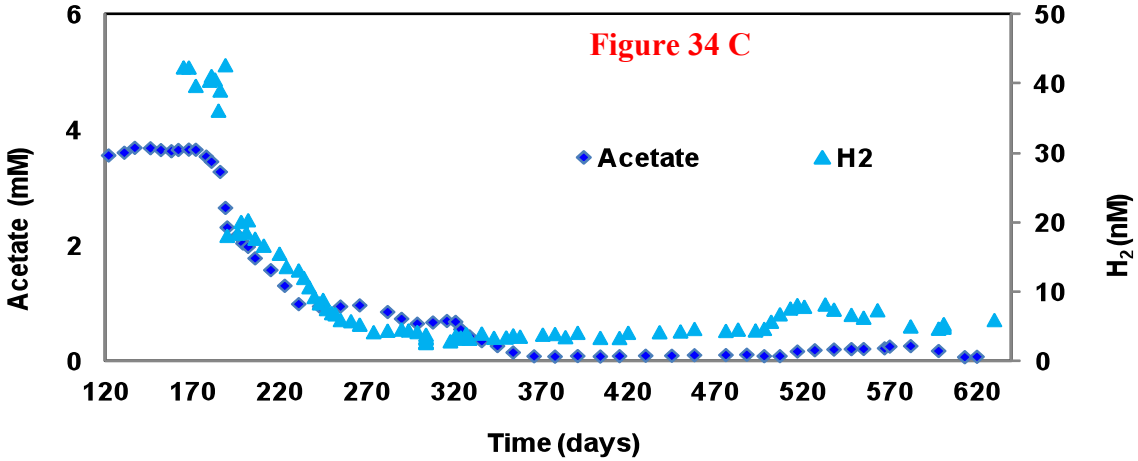
Figure 34 C
Acetate
H2
Acetate (mM)
H2 (nM)
Time (days)

Figure 34 – Experimental results of cultures in the 2-L CSTR

(A) Experimental results of VC and ethene in the 2-L CSTR using EV culture (Azizian, personal communication). The arrows indicate the time points when cells were harvested and used in batch kinetic experiments. Batch experiments were carried out by Dusty Berggren. (B): Experimental results of TCE and cDCE. (C): Experimental results for acetate and H_2.

5.2.10 Simulations of the 2-L CSTR Experimental Results Using the VC Kinetics Used in Simulating the 5-L CSTR

The VC kinetic parameters determined in batch experiments with cells harvested from the 5-L CSTR, and the biomass yield and decay coefficients that heuristically determined to get the match of the 5-L CSTR performance (Table 4, Column B were used to simulate the 2-L CSTR. Simulation results are shown in Figure 35. The simulated results matched the experimental results well during the initial pseudo-steady-state condition when formate was being fed at 45 mM (120 to 180 days). TCE is transformed to about mM ethene and 1 VC (Figure 35). The model also simulated well the steady-state hydrogen level and the amount of acetate formation as a result of formate being added in excess.

The simulation captured the response after the formate was reduced to 25 mM around day 180. The simulation also shows the result of reducing the electron donor on the transformation of TCE extent. The model shows the increase in VC concentration and decrease in ethene to a pseudo steady-state of 5.6 mM ethene and 4.4 mM VC. Due to the long hydraulic and cell residence time of 50 days the CSTR took about 100 days to achieve steady-state operating conditions. However, the experimental results showed a faster decrease in ethene and increase in VC to pseudo steady-state conditions. The model also captured the increase in cDCE after formate was reduced. The simulated H_2 concentration was around 7 nM, while the measured value decreased to below 5 nM. The model also simulated the gradual decrease and eventual washout of acetate from the CSTR.

Three microbial communities were simulated in the CSTR, dechlorinators that transform TCE to cDCE, dechlorinators that transform cDCE to ethene, and homoacetogens. Simulation results match the experimental results well during the period of 100-180 days for VC, H_2 and acetate concentrations. The simulated biomass of 34 mg/L was within the range of measured biomass of 31 mg/L in the 5-L chemostat. Changes in biomass concentrations based on protein concentration are shown in Figure 35.

When the formate concentration was lowered the total simulated biomass decreased to 17 mg/L, which is in agreement with measured biomass of 15.5 mg/L. TCE dehalogenators (X_{d1}) retained a constant concentration of 7 mg/L, X_{d2} decreased from 17 mg/L to 10 mg/L, while homoacetogens were washed out of the CSTR.

The loss in acetate production results from the H_2 concentration decreasing below the assumed acetate hydrogen of threshold concentration (40 nM) (Figure 34C). The acetate hydrogen threshold concentration is much lower than reported in the literature of homoacetogenesis (300-500 nM). This lower hydrogen threshold was required for agreement between the simulated and experimental results. The VC kinetic parameters determined with cells harvested from the 5-L

CSTR (Table 4, Column B) did a good job simulating the 5-L CSTR and the 2-L CSTR when formate was in excess and limited, suggesting that these parameters are reflecting the EV culture performance in CSTR systems. However, using a value of 7 nM for $K_{s\text{-}H2}$, the predicted H_2 concentration after formate was lowered (7 nM) was higher than the experimental H_2 concentration (3 nM) indicating that the $K_{s\text{-}H2}$ for the VC dehalogenation is less than what reported in the literature of 7 nM (Cupples et al., 2004). Overall, the ability of the model to capture the performance of the CSTR, when formate was in excess and then limited increased our confidence in the model. The agreement of the model with the experimental results gives us confidence in the kinetic parameters being used and our ability to simulate these complex processes that include the competition for H_2.

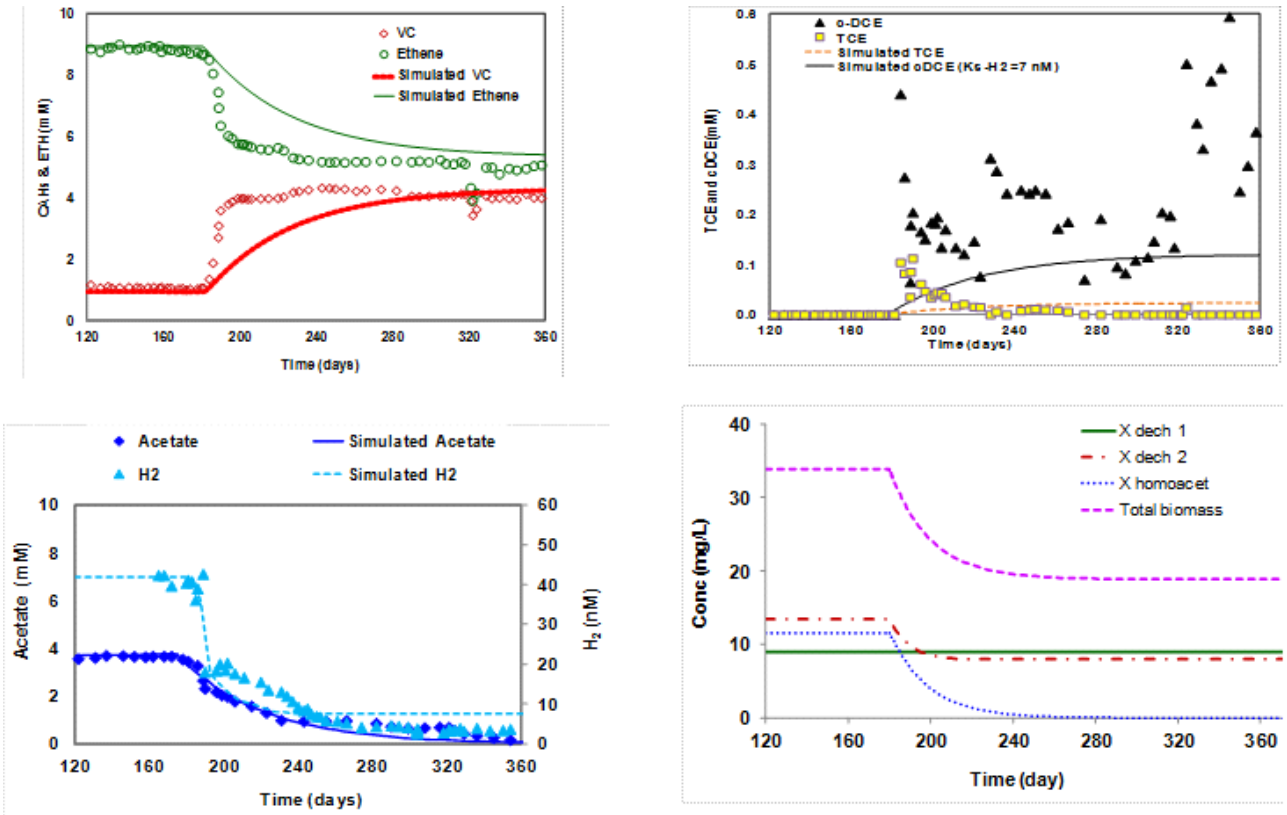

Figure 35 - Experimental and simulated results of the 2-L CSTR using VC kinetics determined in batch experiment using cells harvested from the 5-L CSTR (Table 4, column B) and $K_{s\text{-}H2}$ utilization of 7 nM), acetate H_2 threshold of 40 nM.

5.2.11 Sensitivity Analysis on the K_{s_H2} Utilization of VC

The previous simulations used a $K_{s\text{-}H2}$ value of 7 nM. A sensitivity analysis was carried out to investigate the effect of $K_{s\text{-}H2}$ value on the transformation of VC. This analysis was performed using the VC kinetic parameters determined in batch experiments with cells harvested from 5-L CSTR (Table 4, Column B), and by varying the $K_{s\text{-}H2}$ utilization for VC from 3 nM to 15 nM. Simulation results presented in Figure 36 showed that when formate was in excess, VC and ethene concentrations were sensitive to the change in $K_{s\text{-}H2}$ value, while when formate was limited less change in the CAHs was predicted (Figure 36 A and B). The results are consistent with VC dehalogenation being rate limited when formate was in excess and more stoichiometry limited when formate was limited. However, on a percentage basis, the change in H_2 concentration was less when formate was in excess than when it was limited.

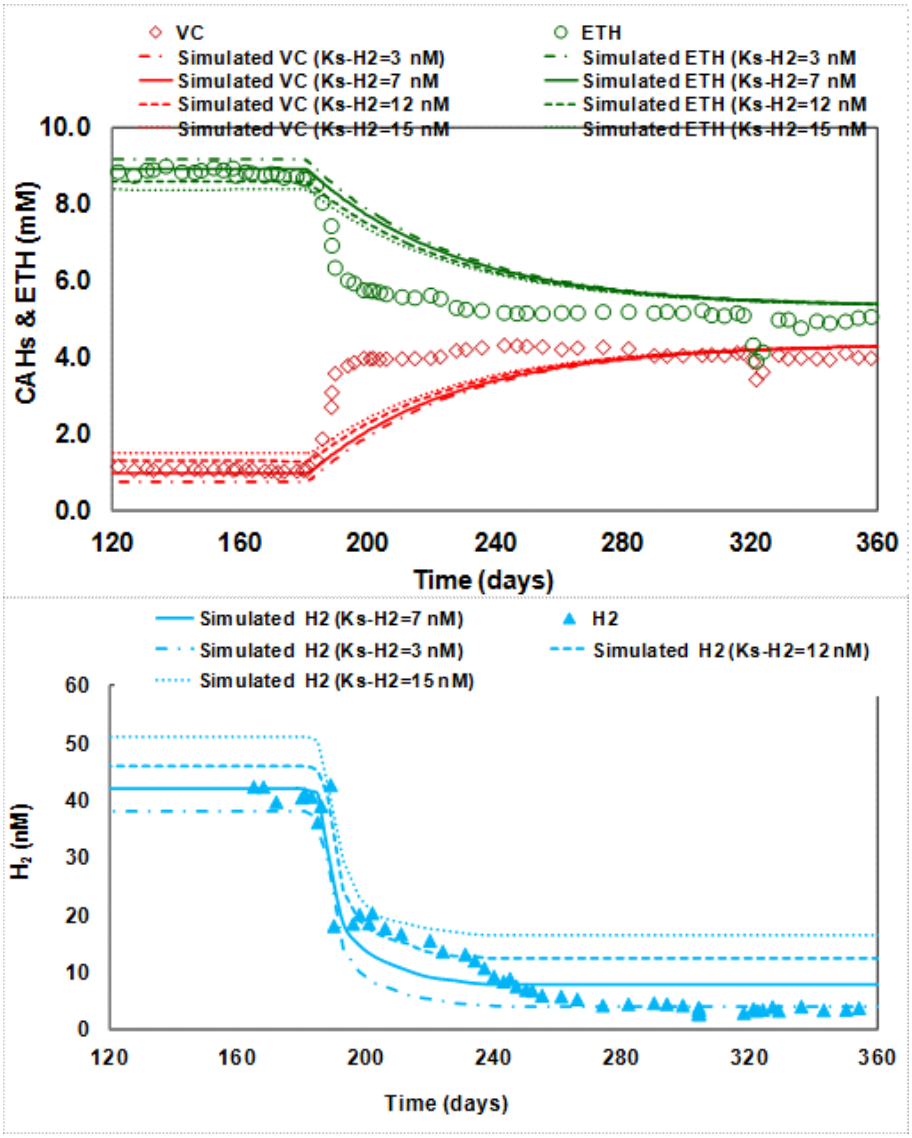

Figure 36 - Sensitivity analysis on the Ks-H2 utilization of VC in the 2-L CSTR, when formate was in excess and after cutting the formate to 25 mM. The Kmax of VC was 26 µmol/mg protein-d, Ks-VC = 12 µM and kept constant throughout the sensitivity analysis. A: for experimental and simulated VC and ethene, and B: for experimental and simulated H_2.

Simulation results using $K_{s\text{-}H2}$ of 3 provided the best overall match to the experimental results. Figure 37 shows simulation results using the same conditions as mentioned above but with $K_{s\text{-}H2}$ utilization for VC of 3 nM.

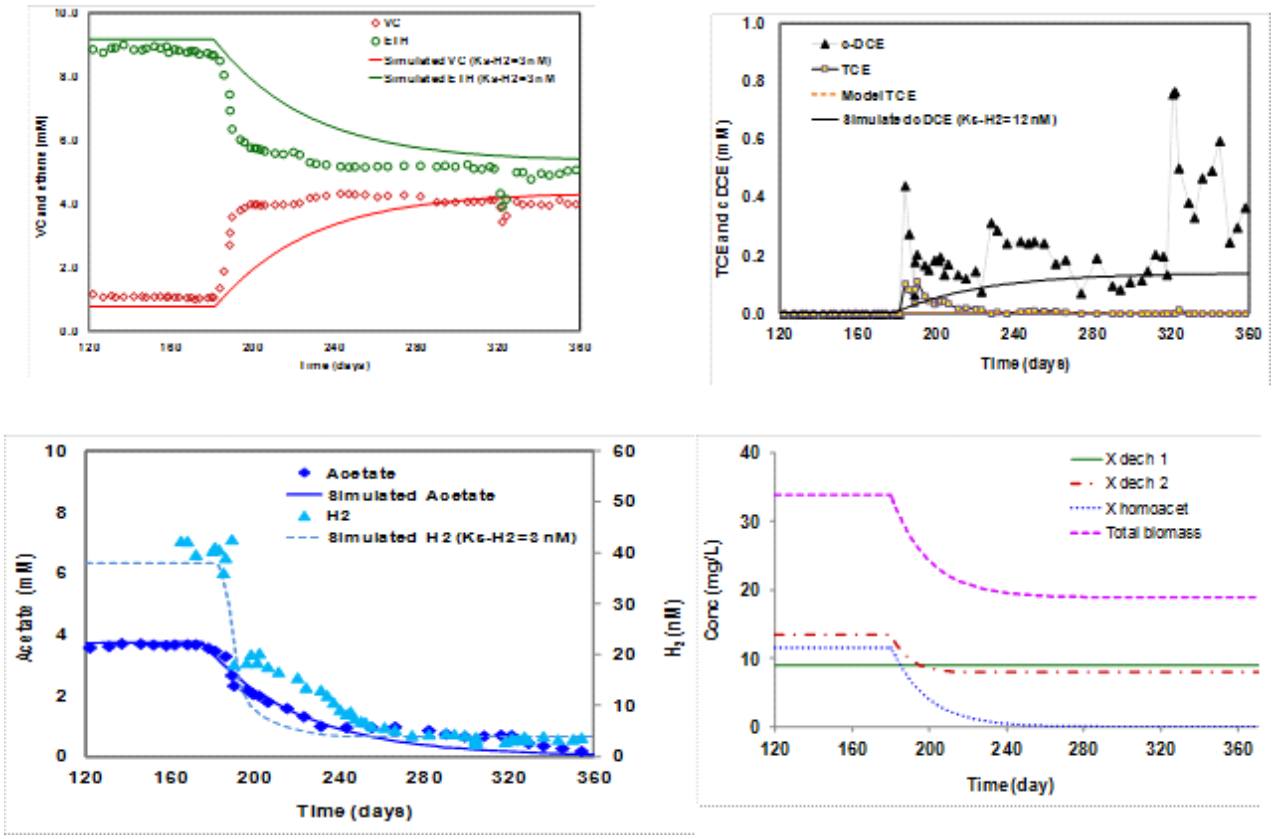

Figure 37 - Experimental and simulated results for the 2-L CSTR using a $K_{s\text{-}H2}$ utilization of 3 nM and VC kinetics determined in batch experiment using kinetic parameters determined from the 5-L calibration (Figure 13), presented in Table 4, column B.

The model slightly under estimate the H_2 tension during the period (120-180 days), but provided an good match to the H_2 tension after 180 days when formate was limited. Simulation results in Figures 36 and 37 supported the choice of 3 nM for the $K_{s\text{-}H2}$ in the 2-L CSTR.

Additional simulations were performed to get a better match of the CAHs, the H_2 tension and the rapid increase in VC and decrease in ethene concentrations that occurred after format was reduced. A possibility that a shift in the population for the VC transformation to ethene occurring after formate was decreased was investigated. A simulation was performed assuming that there are two populations responsible for the VC transformation. Initially, when formate was in excess (day 120-180), the first VC population (X_{VC1}) had a $K_{s\text{-}H2}$ of 30 nM represents 80% of the population while the second VC population (X_{VC2}) with $K_{s\text{-}H2}$ of 3 nM represents 20%. Both X_{VC1} and X_{VC2} use the same transformation kinetic parameters. The simulations determined whether the X_{VC2} population dominated after formate was reduced.

The simulations and experimental results are presented in Figure 38.

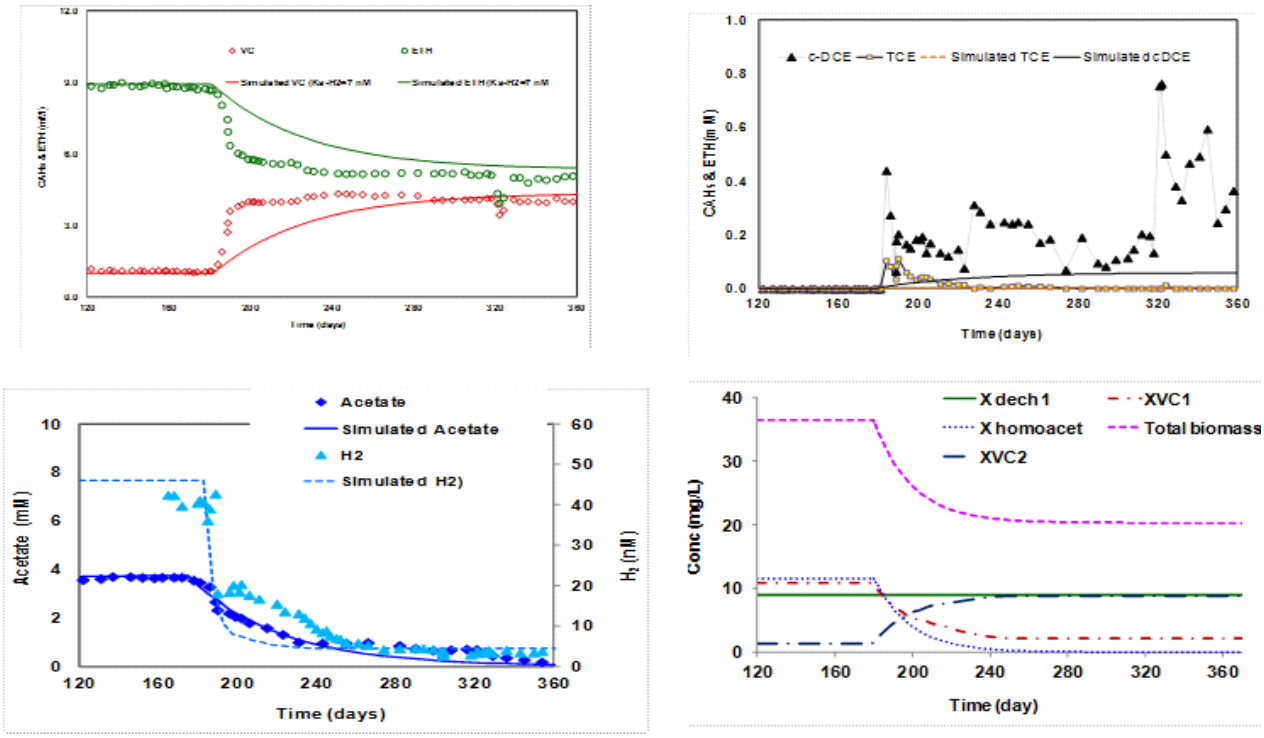

Figure 38 - Experimental and simulated results of the 2-L CSTR using VC kinetics determined in batch experiment using cells harvested from the 5-L CSTR (Table 4, column B). In this simulation two VC dehalogenating microbial population were assumed one with $K_{s\text{-}H2}$ of 15 nm and the other with 3 nM.

Simulated biomass showed a gradual decrease of X_{VC1} after formate was reduced along with an increase in X_{VC2}. The simulated CAHs better captured the transient change and showed an improvement in matching the rapid increase in VC and decrease in ethene. The predicted H_2 concentration was higher than observed when formate was in excess, and was in agreement with the experimental results when formate was limited. Still, the fact that rapid changes in VC and ethane, which occurred when formate was lowered did not completely match simulation results supported the possibility that a shift in population occurred after formate was lowered. Molecular analysis along with the transient change would give a better understanding of the population performance.

5.2.12 Sensitivity analysis on $K_{max\text{-}VC}$ dehalogenation in the 2-L CSTR

Additional analysis was carried out to the sensitivity of the $K_{max\text{-}VC}$. A range of $K_{max,VC}$ parameters (16-26 μmol/mg protein-d) were used to simulate the performance of the CSTR from day 100-360, $K_{s\text{-}H2}$ was 7 nM. The results of the sensitivity analysis to $K_{max\text{-}VC}$ are presented in Table 14.

Table 14 - Sensitivity analysis to the $K_{max\text{-}VC}$ when formate was excess and limited, assuming $K_{s\text{-}H2}$ utilization of 7 nM.

	Excess formate (45 mM) (day 120-180)				Limited formate (25 mM) (day 180-360)			
$K_{max\text{-}VC}$ μ mol/mg protein d	cDCE mM	VC mM	Ethene mM	H_2 (nM)	cDCE mM	VC mM	Ethene mM	H_2 (nM)
16	0.018	1.95	8.03	53	0.08	4.52	5.40	17
18	0.017	1.46	8.52	50	0.12	4.45	5.43	15
21	0.016	1.12	8.86	48	0.18	4.33	5.49	12
26	0.015	0.94	9.05	42	0.27	4.16	5.57	8
Experiment	0.005	1.08	8.95	42	0.20	4.25	5.17	3

The results indicate that the VC and ethene effluent concentrations showed greater sensitivity to change in $K_{max\text{-}VC}$ when formate was in excess. In the first phase (100-180 days) changing $K_{max\text{-}VC}$ from 16 to 26 resulted in about a 50% change in VC concentration, while the change in the VC concentration in the second phase (180-360 days) was about 5 %. These results help show that the VC dechlorination was rate limited in the first phase and more substrate limited in the second phase. Sensitivity analysis showed less change in the H_2 tension when formate was in excess than when it was limited. A 20% decrease in H_2 concentration (from 53 to 42 nM) was predicted with the increase in $K_{max\text{-}VC}$ when formate was in excess, while the H_2 concentration decreased by a

factor of 2 (from 17 to 8 nM) when formate was limited. The H_2 tension results showed that the change in H_2 concentration was less sensitive when formate was in excess than when it was limited during the VC dehalogenation step. The availability of H_2 when formate was in excess resulted in less H_2 concentration changes compared to when formate was limited. Both the analysis of $K_{s\text{-}H2}$ utilization for VC and the $K_{max\text{-}VC}$ in the last two sections indicated that the VC transformation was rate limited when formate was in excess and H_2 limited when formate was limited.

5.2.13 Mass and Electron Balance

Mass balance calculations were performed for the CAHs in the effluent of the 2-L CSTR. The model conserves a good mass balance during the simulation. Comparisons between simulated influent and effluent electron balances for the 2-L CSTR are presented in Table 15. For the first phase (120-180 days) there was good agreement between influent and effluent electron equivalents associated with the following: acetate formation (32%), cell synthesis (4%) and for dechlorination of TCE to VC and ethene (60%). Results were very comparable with those obtained in the 5-L CSTR operating under simulation fed conditions. Table 15 also presents the electron balance of the second phase (180-360 days) of the 2-L CSTR operation. After reducing the influent formate concentration, acetogenesis was washed out of the CSTR. TCE dehalogenation consumed 96% of the electron equivalents. Under formate limited conditions very efficient electron transfer was associated with dehalogenation reactions of the 2-L CSTR.

Table 15 – Simulated and experimental electron balances for 2-L CSTR at 45 mM and 25 mM formate

Electron balance of 2-L CSTR between day 0 - 360

Between day 120 - 180			Between day 180 - 360	
Influent formate = 279.07 meq^-			Influent formate = 450 meq^-	
	Effluent		Effluent	
	Simulated %	Experiment %	Simulated %	Experiment %
H_2	4.3×10^{-5}	1.9×10^{-5}	2×10^{-6}	2.11×10^{-6}
Formate	5.1×10^{-3}	0	2.4×10^{-4}	3.4×10^{-4}
Acetate	31.8	32.4	0.82	1.8
TCE to cDCE	0.1	0.08	0.4	0.5
TCE to VC	3.8	4.62	28.7	29.3
TCE to ethene	60.4	59	67.48	66.0
Net cells growth and decay	3.9	4	2.5	2.4

5.2.14 Simulations after day 400

CSTR results in Figure 34 show VC increases and ethene decreases after day 420 in the 2-L CSTR. This deviation from steady-state lasts until day 520 where concentrations reached a peak and then started recovering to the previous steady state. The increase in VC and decrease in ethene went along with a slight increase in both TCE and cDCE, as well as an increase in acetate and H_2 concentrations (Figure 34). On day 520, batch kinetic tests on VC transformation were carried out by Dusty Berggren using cells harvested from the CSTR. Results showed a decrease in the value of $K_{max\text{-}VC}$. The measured kinetic values are presented in Table 4, column C. Moreover, the kinetic parameters determined for cells harvested from the CSTR on day 520 were used to simulate a batch experiment using cells from the CSTR at that time (Figure 39).

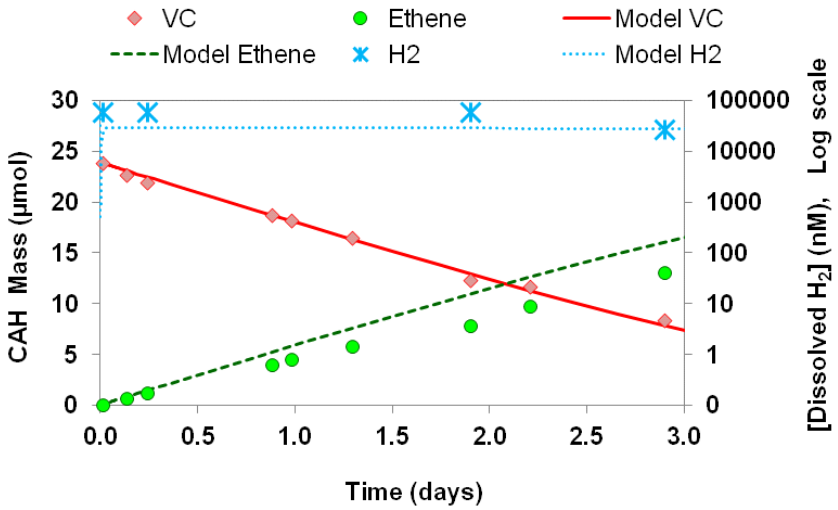

Figure 39 A: Experimental and simulated VC and ethene kinetic batch test using cells harvested from the 2-L CSTR at point 2 in Figure 34. The biomass of dehalogenators and acetogens used were determined for the CSTR simulations.

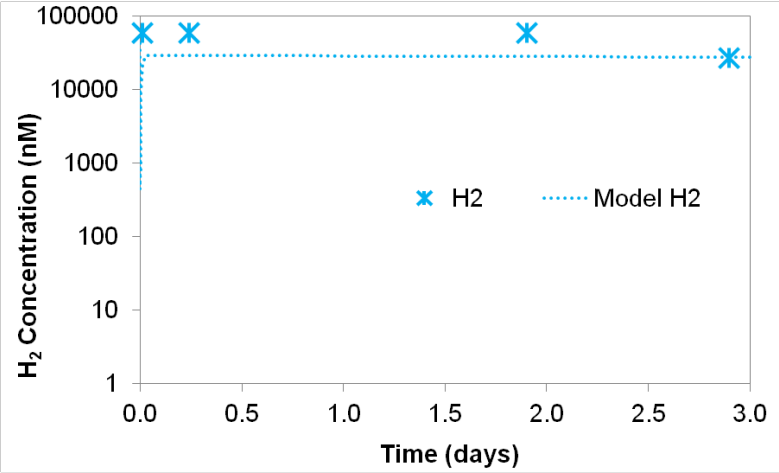

Figure 39 B: Experimental and simulated results for H_2 in a batch experiment using harvested from the 2-L CSTR at point 2 in Figure 34 an initial value of homoacetogens was 0.5 mg/L.

Figure 39 - Experimental and simulated VC and ethene kinetic batch test using cells harvested at point 2 in Figure 34.

The experiment was carried out with excess H_2. A good match of the experimental and simulated results was achieved. Kinetic tests at on day 520 and the simulation of the batch experiment support the decrease in VC transformation rate.

Two hypotheses were tested to try to explain this performance of the CSTR. The first was that lack of acetate as a carbon source for cell growth caused by the lack of acetate production. The reduction in VC dechlorination rate was followed by a slight increase in the H_2 concentration, possibly supported homoacetogenesis to produce the needed acetate for cell growth. This hypothesis was tested through simulations and did not support experimental observations (results are not presented). The second hypothesis was that while taking samples and changing the feed syringes, some oxygen leaked into the CSTR. The effect of oxygen on *Dehalococcoides* viability was explored in a recent studies of Amos et al. (2008). They found that the strains catalyzing the VC to ethene dechlorination step are very susceptible to oxygen inhibition.

On day 610 of the 2-L CSTR operation, another batch kinetic test using cells harvested from the 2-L CSTR was carried out by Dusty Berggren. VC kinetics determined on day 610 are presented in Table 4, column D. VC kinetics indicated a recovery in the VC dechlorination rate as the VC decreased and ethene increased to the previous steady-state level. Using the determined $K_{max\text{-}VC}$ of 16 µmol/mg protein/d in simulating the 2-L CSTR after day 610 showed a consistent trend with the experimental results (Figure 40). VC and ethene reached steady-state values of 4.7 mM and 5.3 mM, respectively. The simulated biomass over the transient periods observed in the 2-L CSTR (Figure 40) was consistent with the measured values. During the time period of 420 -610 days, measured and simulated biomass declined to 10.5 mg/L and 12 mg/L, respectively. After day 610 a gradual increase in measured and simulated biomass was observed to values of 14 and 15 mg/L, respectively.

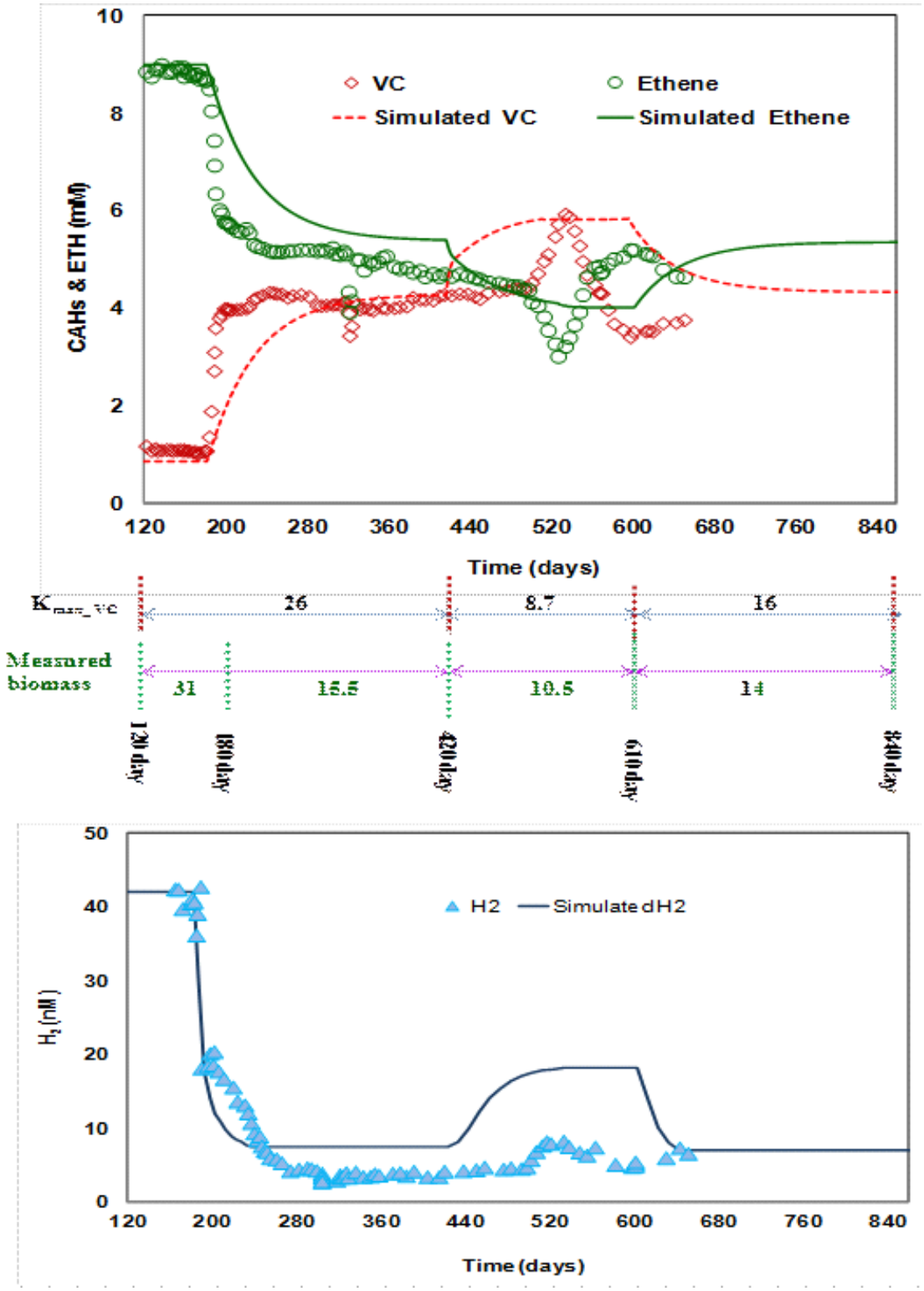

Figure 40 - Simulations using the transient change in VC and ethene concentrations. VC kinetic parameters determined using cells harvested from the CSTR at different time points as indicated in Figure 34 were used in the simulation. The second figure shows the H_2 tension as a response to the change in VC dechlorination rate.

The model captured the general trend of H_2 tension. The predicted H_2 concentration was in agreement with the measured H_2 in the 2-L CSTR (Figure 40). A gradually increase in H_2 concentration to 10 nM after day 520 was consistent with low VC transformation rate. When VC transformation recovered to a higher rate after day 600, the predicted H_2 concentration decreased to 3 nM similar to the H_2 tension before day 400. Using a value of 3 nM for the $K_{s\text{-}H2}$, the predicted H_2 concentration (3 nM) matched the observed H_2 concentration after the formate was reduced and after day 400, suggesting that the $K_{s\text{-}H2}$ is around 3 nM. Overall, simulations using the hypothesis of a perturbation in $K_{max\text{-}VC}$ did a good job predicting the transient change in VC and ethene concentrations after day 400.

5.2.15 Simulation of the transient change

Figure 34 shows that after the formate reduction to 25 mM on day 180, a rapid decrease in ethene and increase in VC concentrations occurred. However, simulations of the CSTR, showed a more gradual increase and decrease in VC and ethene that do not match the rapid transient change observed in the experiment. An investigation of this response was carried out, hypothesizing that after the formate was reduced, along with the change in H_2 tension in the 2-L CSTR, VC transformation ability stalled for about 15 days while the rest of dehalogenators remained active, and on day 195 the VC dehalogenators recovered and became active. This could be due to some oxygen leakage that occurred during the transient change. To test this possibility we performed a simulation where the VC dechlorinators were not active for 15 days after formate was decreased (180-195 days). Figure 41 shows the more rapid VC build up and ethene decrease in the CSTR. After day 195 of CSTR operation the all dechlorinators were active. The simulated VC and ethene mimicked the rapid transient change observed in the experiment during the period (180-195 days) as presented in Figure 41. Simulations captured the rapid increase of VC and decrease of ethene during the (180-195 days) and the gradual concentration change after that.

H_2 tensions initially were around 42 nM (day 120-180), followed by a rapid decrease to 28 nM between day 180 -195 when $K_{max\text{-}VC}$ was assumed zero. After day 195 a build-up of H_2 concentration to 30 nM was followed by a gradual decrease that matched the observed gradual decrease. It then reached a pseudo-steady state of 3 nM after 230 days of operation. By assuming a stall of VC dechlorination between day 180 -195, the model captured the VC and ethene history and also the H_2 tension, mainly the gradual decrease in H_2 concentration after formate was reduced to 25 mM.

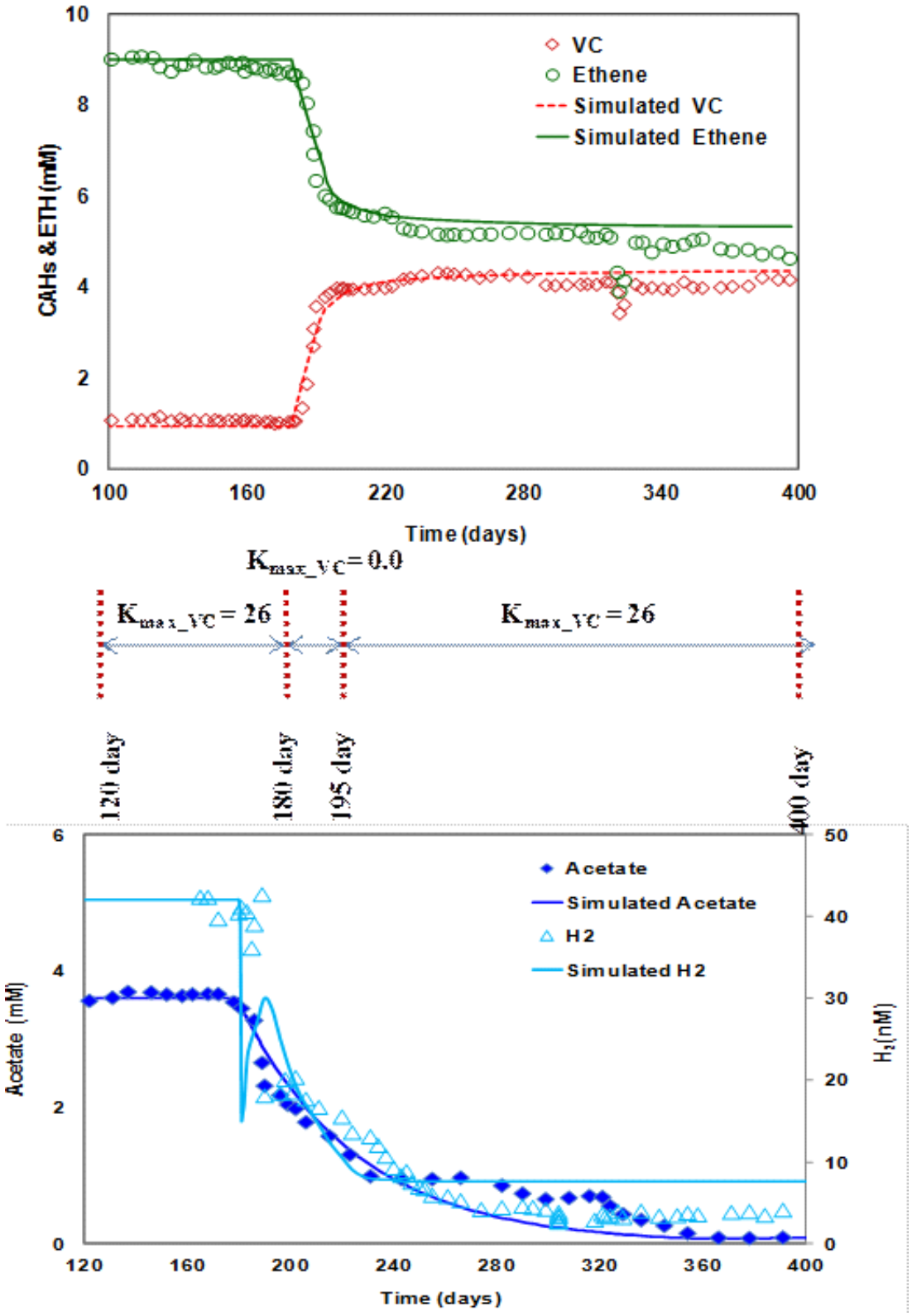

Figure 41 - 2-L CSTR simulations assuming VC dehalogenation stall for 15 days after the formate reduction followed by a recovery to explain the rapid decrease of ethene and increase of VC.

5.2.16 Comparison Between Experimental and Simulated Biomass Results

Table 16 presents the simulated steady-state biomass distribution in the 2-L CSTR using kinetics determined with cells harvested from the 5-L CSTR.

Table 16 - Simulated microbial community distribution in the 2-L CSTR when formate was in excess (45 mM) and when formate was limited (25 M).

	Influent formate concentration 45 mg/L (120-180 days)		Influent formate concentration 25 mg/L (180-360 days)	
Microbial community	Protein Concentration (mg/L)	% of total biomass	Protein Concentration (mg/L)	% of total biomass
TCE dechlorinators	9	26	9.0	52
Dehalococcoides	13.5	40	8.0	48
Acetogens	11.5	34	0.0	0.0
Total biomass simulated	34	100	17.0	100
Measured biomass	30		15.5	

The measured protein was 31 mg/L while the simulated is 34 mg/L. Simulated results had a similar distribution as that obtained in the 5-L CSTR. After reducing the formate concentration (180-360 days) the biomass percentage changed (Table 16). TCE reducers (X_{d1}) formed 52% of the biomass and *Dehalococcoides* (X_{d2}) formed 44% of the biomass. As a result of the homoacetogenesis decreasing and being washed out of the 2-L CSTR, dehalogenators were the main population when formate was limited.

Comparisons between simulated and experimental biomass results in the 2-L CSTR are illustrated in Figure 32. The *Dehalococcoides* 16S rRNA gene copy number normalized to all bacterial 16S rRNA gene copy numbers were determined by qPCR and are shown in Figure 32. The qPCR results (Ian Marshall, Stanford University. Personnel Communication) showed that the dechlorinators represented 94% in the 2-L CSTR when formate was limited. The simulated biomass distribution agrees reasonably well with the molecular results (Figure 41).

5.2.17 Discussion

The model that was developed for simulating the anaerobic reductive dechlorination of TCE in a CSTR did a reasonable job predicting both steady-state and the transient behavior that occurred in response to a changes in electron donor addition. The model predicted the steady-state CAHs

concentrations, when the electron donor was added both in excess and when it was limiting. A good job in simulating the CAHs transformation was achieved by including two microbial populations for complete reductive dehalogenation of TCE to ethene (Behrens et al., 2008; Newell et al., 2000; Major et al., 2002; Ellis et al., 2000; Adamson et al., 2003). Successful modeling of the CAH transformation was achieved using dual-Monod kinetics, competitive inhibition and using H_2 thresholds (Rittmann and McCarty, 2001; Yu and Semprini, 2004; Cupples et al., 2004; Clapp et al., 2004).

The kinetic parameters for VC transformation determined in batch experiments using cells harvested from the CSTR were within the range of kinetics determined by Yu and Semprini (2004). Dechlorinators harvested from the CSTR showed a slightly higher VC transformation rate than those determined by Yu and Semprini (2004). This increase is possibly due growth of this mixed culture under CSTR conditions compared to the original batch conditions.

The 5-L CSTR monitoring data and the simulations are shown in Figures 29, 30 and 31. Different simulation scenarios were applied using kinetic parameters determined in batch experiment (Yu and Semprini, 2004), and using VC kinetics determined in batch experiment using cells harvested from the 5-L CSTR. Simulations using the VC dehalogenation kinetic parameters determined in the batch experiments did a good job matching the experimental results (Figure 31). The simulation results indicated a higher VC dehalogenation rate in the CSTR than determined in batch experiments (Yu and Semprini, 2004), and a lower yield and higher decay coefficient than determined in batch experiments (Yu and Semprini, 2004), in order to fit the measured biomass in the CSTR

The H_2 and acetate monitoring data showed that acetate was produced the CSTR when H_2 concentration was around 40 nM. This required a H_2 threshold for acetate production ($H_2^*_{,acet}$) of 40 nM, which is one order of magnitude lower than reported in the literature for batch experiments (Löffler et al., 1999; Luijten et al., 2004; Schink, 1997). Simulation results supported this low $H_2^*_{,acet}$ threshold as well. The simulations of the 5-L and 2-L CSTRs using kinetic parameters determined in batch tests with cells harvested from the CSTR, did a reasonable job capturing the general trends observed in the CSTRs.

The experimental results showed a pseudo steady-state concentration of H_2 of 42 nM in both 5-L and 2-L CSTRs, when formate in excess. A value of $K_{s\text{-}H2}$ utilization for VC (7 nM) was used to capture the high H_2 tensions. However, when formate was limited in the 2-L CSTR (Figure 34), the steady-state H_2 concentration was around 3 nM. The lowest $K_{s\text{-}H2}$ utilization for VC reported in the literature of 7 nM was from batch experiments (Cupples et al., 2004), was initially used in the CSTR simulations. This $K_{s\text{-}H2}$ for VC of 7 nM did not capture well the observed CSTR H_2 concentration history. The sensitivity analysis to the $K_{s\text{-}H2}$ for VC utilizers showed that a better fit was obtained with a $K_{s\text{-}H2}$ of VC utilizers of around 3 nM (Figure 37). This low H_2 concentration would indicate the selection for dehalogenating microorganisms that compete better when H_2 is limiting.

Dechlorination rates have been shown to follow dual Monod-type kinetics with a dependence on H_2 concentration (Ballapragada et al., 1997; Cupples et al., 2004). A half-velocity coefficient for H_2 utilization used in the simulation of 3 nM (Figure 37) was applied when formate was in excess and limiting. The simulation showed a match to the H_2 concentration when both formate was in excess and when it was limited. However, the transient change in CAH concentration and H_2 did not fit as well. The lack of fit to the transient change possibly suggests a shift in the dehalogenation microbial community occurred after formate was reduced and the potential there were two dehalogenators responsible for VC dehalogenation. We evaluated the possibility for the first VC

dehalogenator having a $K_{s\text{-}H2}$ of 30 nM, which was dominant when formate was in excess and the second dehalogenator having a $K_{s\text{-}H2}$ of 3 nM, which became dominant when formate was reduced. A possibility of a shift in the VC dehalogenating population was investigated (Figure 38). Simulations did a good job capturing the H_2 concentration when formate was in excess and limited. The simulation results are presented in Figure 38. However, the simulations, while providing a better to the transient response still did not completely fit the data. It possible that when formate was limited and H_2 concentration was around 3 nM the second VC dehalogenator with $K_{s\text{-}H2}$ of 3 nM was the major dehalogenator. More detailed studies of the of reductase genes of mixed populations containing multiple *Dehalococcoides* strains are required to demonstrate how mixed populations could shift in response to electron donor concentration. A more complete sensitivity analysis with the two population model should also be performed.

Electron balances performed on the 2- L CSTR over the 360 days of operation indicated that approximately 65% and 95% of the electron equivalents were eventually used for dechlorination reactions when formate was in excess and limited, respectively. This is in general agreement with the microbial community distribution predicted in the 2-L CSTR (Tables 13 and 16).

A series of step-wise transitions were carried out in the 2-L CSTR where the formate concentration was lowered. When the formate concentration was lowered to 25 mM to promote an electron donor limitation, TCE was transformed at steady-state to 54% ethene, 45% VC, and 1% c-DCE. The hydrogen concentrations decreased from 40 nM to 3 nM and acetate washed out of the CSTR. Several transient changes in VC dehalogenation were observed in the 2-L CSTR after formate was reduced. In addition, after day 400, a gradual increase in VC and decrease in ethene concentrations were observed followed by a sharp transient change and recovery between days 480 and 600. VC kinetic parameters determined in batch experiments with cells harvested from the 2-L CSTR at points 2 and 3, as shown in Figure 34 A, are presented in Table 4, column C and D, which show and decrease and then increase in the $K_{max\text{-}VC.}$ There are several factors that could hinder the PCE and TCE dehalogenation extent to ethene (Loffler and Edwards, 2006; Amos et al., 2007; and 2008; Robinson et al., 2009), such as, inadequate electron donor supply (Yang and McCarty, 2002; Loffler and Edwards, 2006; Aulenta et al., 2006, 2007) insufficient contact time (Da Silva et al., 2006), absence of suitable consortia of dehalogenating bacteria (Loffler and Edwards, 2006; Amos et al., 2007). One possibility to explain the decrease and increase in $K_{max\text{-}VC}$ was a leak of oxygen or a temporal shift in the microbial population in response to the different electron donor concentrations (Loffler and Edwards, 2006; Amos et al., 2007). Simulations of the 2-L CSTR were performed using the VC kinetic parameters for each time stage, as presented in Table 4. Simulation results captured the series of transient changes in the VC transformation extent over the 650 days of the CSTR operation (Figure 40).

While the steady-state response well captured by the model, the transient was not (Figure 37). Several factors could have resulted in this rapid transient change in VC and ethene concentrations. A change in redox conditions resulted from the decrease in formate is a possibility. Another is oxygen leaks into the system, or after reducing the formate feed concentration, the H_2 concentration decreased below the H_2 threshold for homoacetogens, the homoacetogens were washed out of the CSTR and the mixed culture shifted to mainly a dehalogenating population. A simulation was performed with no VC dehalogenation happened for 15 days after formate was reduced followed by a recovery in activity. Using this scenario provided a good match to the observed VC and ethene results (Figure 41).

Using kinetic parameters determined in batch experiments with cells harvested from the CSTR did good job simulating the dehalogenation processes. The model was able to predict the

impact of lowering the electron donor sources on the dehalogenation extent and capturing the transient changes happened. This is important in estimating the treatment extent and the population dynamics, as well as in determining rate limiting factors, such as insufficient organisms, or insufficient electron donors. While the ability to predict dehalogenation rates is important, incomplete dehalogenation, understanding and predicting shift and decrease in population activity can be equally important.

6 Conclusions and Implications for Future Research/Implementation

6.1 A DNA microarray as a useful monitoring tool to semi-quantitatively predict H_2 flux in different populations of microbes involved complex reductive dehalogenation.

6.1.1 The Tiling DNA microarray approach

We developed a novel and broad-ranging approach to the characterization of complex microbial communities by analyzing the abundance and expression of key functional genes. A test hybridization showed that the detection limit for the microbial community system was found to be between ~1% and ~10% of the total microbial community. This design favors the avoidance of false positive gene identification in samples of DNA or RNA extracted from complex microbial communities. We implemented this method using hydrogenase genes to investigate anaerobic reductively dehalogenating microbial communities where H_2 is an important intermediate (the Hydrogenase Chip), and reductive dehalogenase genes to characterize ecosystems containing organohalide-respiring microorganisms (the Reductive Dehalogenase Chip).

6.1.2 Monitoring strain and population level shifts of dehalogenatros in response to shifts in electron donor amendment

DNA samples from three different time points of a previously described reductive dechlorinating soil column were analyzed using the Hydrogenase Chip. Each time point represented the steady state of a different electron donor amendment to the soil column, with formate in March 2008, lactate in July 2008, and propionate in January 2009. The soil column operated over 1050 days, spanning two versions of the Hydrogenase Chip. Median relative probe intensities comparing formate to lactate and formate to propionate are shown in Figure 42. For the detected *Dehalococcoides sp.* hydrogenase genes, some showed significant differences between probe

intensities for the propionate and formate amendments. In general, genes from the *Dehalococcoides* strain CBDB1 genome were enriched in the propionate amendment, genes from the genome of *Dehalococcoides ethenogenes* strain 195 showed no significant difference between the two treatments, and some *Dehalococcoides* strain VS genes showed enrichment while others did not. The consistent abundance difference for hydrogenase genes of strains 195 and CBDB1 compellingly suggests differences in *Dehalococcoides* community structure between the formate- and propionate-amended time points. The lactate time point showed generally diminished probe intensities for all *Dehalococcoides* hydrogenase genes, consistent with diminished fraction of electrons contributing towards reductive dehalogenation with lactate as electron donor. There was a significant increase in the intensity of *Geobacter* hydrogenase genes in samples from the lactate- and propionate-amended time points relative to the formate-amended time point. This is consistent with an increase in the fraction of electrons partitioned to Fe(III) reduction in this system during propionate or lactate amendment. The detected *Desulfitobacterium hafniense* [NiFe] hydrogenase showed significantly reduced probe intensities under propionate amendment relative to formate, but no significant difference between lactate and formate amendments.

Figure 42 - Median log probe intensity shift for the lactate compared to formate and propionate compared to formate.

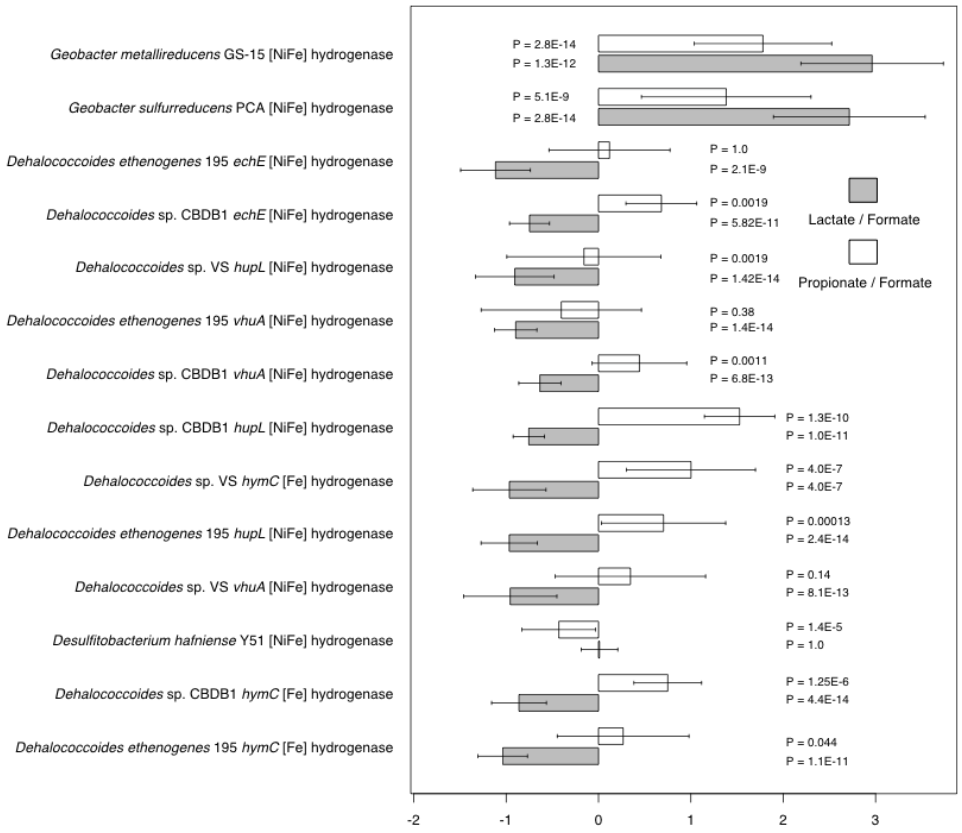

Positive values (to the right) signify greater abundance in lactate or propionate, negative values (to the left) signify greater abundance in formate relative to either propionate or lactate. Error bars show median absolute deviation, p values show the probability that the two compared samples are equal to one another according to the binomial test.

6.1.3 The tiled DNA array as useful tool for semi-quantitatively predicting H_2 flux in complex dehalogenating communities.

We investigated whether the observed rates correlated with shifts in abundance of *Dehalococcoides hupL* hydrogenase mRNA using the Hydrogenase Chip. As Figure 43a shows, trends in *Dehalococcoides hupL* median probe intensity followed trends in PCE transformation rate. To independently assess *hupL* mRNA abundance to determine the accuracy of the Hydrogenase Chip, RT-qPCR targeting this gene was performed. As Figure 43 shows, shifts in mRNA abundance observed using the Hydrogenase Chip correlated with qPCR quantification of the abundance of *Dehalococcoides hupL* hydrogenase. The high median absolute deviation for sample SP was likely caused by cross-hybridization from a *Dehalococcoides* type more closely related to strain 195, as the median probe intensity strain 195 *hupL* increased significantly in sample SP relative to samples S and P. Apart from this aberration, the Hydrogenase Chip quantification appeared to correlate linearly with reverse transcriptase quantitative PCR measurements from the same samples.

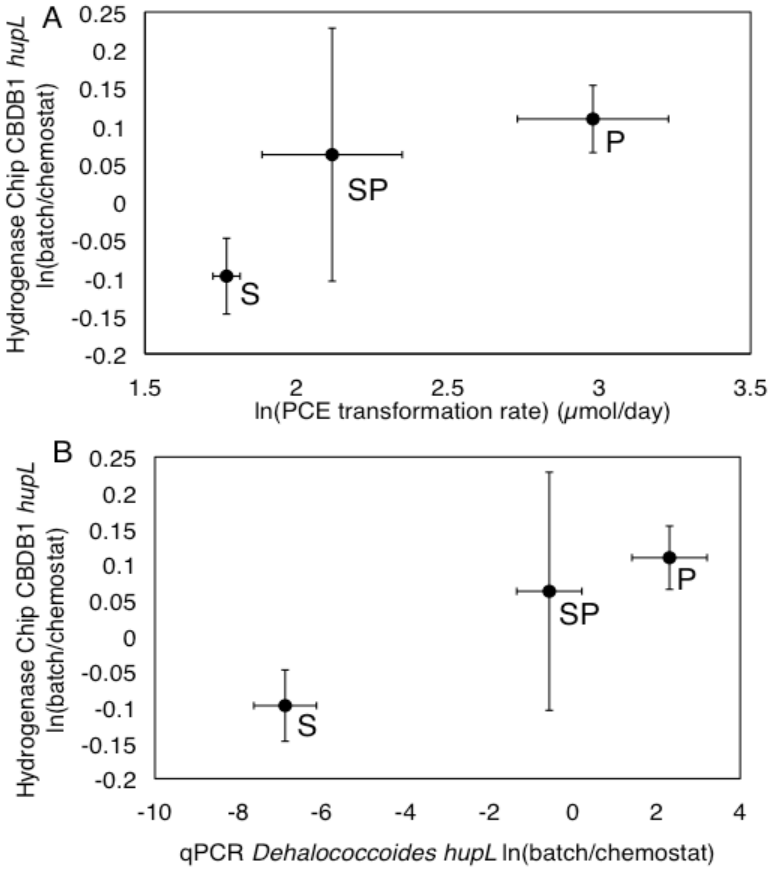

Figure 43 - *Dehalococcoides hupL* transcript quantification with RNA hybridized to the Hydrogenase Chip version 3 compared to mean PCE transformation rates (A) and RT-qPCR (B).

Gene abundance measurements show the natural logarithm of batch (S, SP, P) copy number (qPCR) or median probe intensity (Hydrogenase Chip) divided by the corresponding measurement in the chemostat sample. PCE transformation rates in (A) were used without normalizing to chemostat rates, but the natural logarithm is shown for consistency with microarray and qPCR data. Vertical error bars show median absolute deviation from the array, horizontal error bars show standard deviation from three qPCR replicates or from PCE degradation rates measured in two replicates for each batch culture.

6.1.4 Observing shifts in dehalogenator populations as well as evolution of novel lineages

Relative changes in co-clustered abundance of reductive dehalogenase genes (*rdhA*) for each of four clusters of *Dehalococcoides* strains are depicted in Figure 44. The data show that at least three different *Dehalococcoides* genotypes are present, with the *vcrA* cluster in constant decline over the course of the experiment, the *bvcA* cluster increasing slightly and dominating the *Dehalococcoides* community from day 600 to sometime between days 800 and 1100 before eventually declining, and cluster 4 steadily increasing from approximately day 800 to become dominant before day 1100. This is consistent with the observation that VC reduction slowed down from day 700 to 1100 (while the *bvcA* cluster dominated) before stopping entirely from around day 1100 (when the cluster 4, which lacks both *vcrA* and *bvcA*, became dominant). It appears that the introduction of sulfate into the chemostat and the onset of sulfate reduction happened simultaneously to a decline in VC-respiring *Dehalococcoides* community. This demonstrates the usefulness of the Reductive Dehalogenase Chip as a tool for simultaneously monitoring changes in *Dehalococcoides* population composition and in the functional capacity of that community to reduce different organohalide compounds.

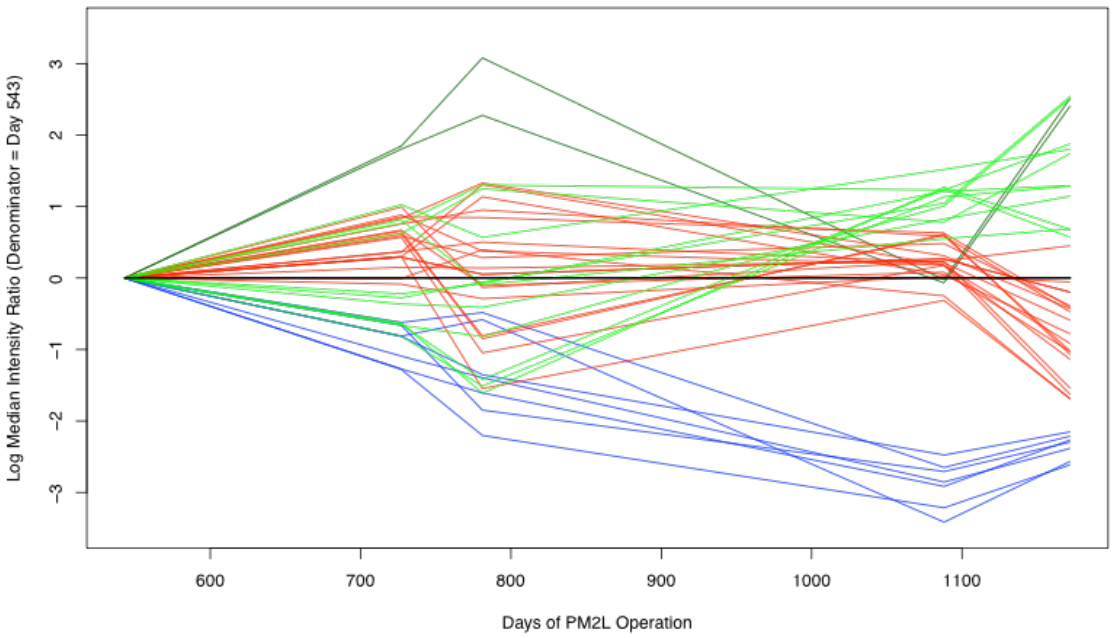

Figure 44 – Log median intensity shifts for *rdhA* gene clusters defined in Figure 27: *vcrA* cluster (blue), *bvcA* cluster (red), *Desulfitobacterium* cluster (dark green), cluster 4 (light green).

Values show the natural logarithm of the median of all probe fluorescence intensity ratios for each gene cluster, with each time point divided by the 543 day time point.

6.2 Understanding population dynamics of complex reductively dehalogenating communities as a function of electron donor type and availability as well as competing electron acceptor

Our studies about dehalogenating community dynamics in conjunction with the molecular tools we developed have important implications for choice and administration of electron donor as well as competing electron accepting processes in reductively dehalogenating communities.

6.2.1 Electron donor availability and type of electron donor.

Simulation of the anaerobic dehalogenation of TCE in a continuous stirred tank reactor (CSTR) experiment **under excess and limited electron donor addition** was carried out. Formate and TCE were fed to 2-L and 5-L CSTRs containing the Evanite culture (EV). To simulate the results of the two experiments, a non-steady-state model was developed, that coupled thermodynamic and kinetic models described in Project 2 to include CSTR flow conditions. Our model includes inhibition kinetics for the dehalogenation reactions as described by Yu and Semprini (2004), and permits the growth of homoacetogens and dehalogenators as competing hydrogen (H_2) consuming processes. Three microbial communities were simulated in the CSTR, dechlorinators

that transform TCE to cDCE, dechlorinators that transform cDCE to ethene and homoacetogens. H_2 is assumed to be in equilibrium with formate. The system of model equations was solved numerically using COMSOL 3.5a. VC dehalogenation kinetics was determined in batch experiments using cells harvested from the CSTR. The model simulated well the steady-state and transient performance of the CSTR when excess and limiting electron donor were added. The batch-determined kinetic parameters did a good job of capturing the observed CAHs, H_2, acetate and biomass concentration in both the CSTR and in separate batch experiments. VC dehalogenation was rate limited when electron donor was in excess and stoichiometry limited when electron donor was not in excess. Simulations required a H_2 threshold for homoacetogens of 40 nM to match CSTR observations, which is lower than reported in the literature. The agreement of the model with the experimental results gives us confidence in the kinetic parameters being used and our ability to simulate these complex processes that include the competition for H_2.

6.2.2 Competing electron acceptor

Interference of reductive PCE dehalogenation with a competing electron acceptor sulfate was assessed in chemostat experiments with the Point Mugu culture that was operated with 4.3 mM lactate and 1.12 mM PCE before perturbation by introduction of 1 mM sulfate. After feeding sulfate for 300 days the performance of the PM-2L chemostat rapidly declined with the complete reduction of sulfate and production of approximately 600 uM sulfide. At pseudo-steady-state PCE was transformed 67%, 25%, and 8%, to VC, c-DCE, and ethene, respectively. The batch kinetic tests with cells harvest from the chemostat indicated VC reduction was most affected, with rates deceasing by a factor of 50. This decline in performance was accompanied by an enrichment of 195-like *Dehalococcoides* strains as CBDB1/GT-like strains decreased. The shift in the composition of the *Dehalococcoides* population is credited for the decline in VC dechlorination capabilities of the PM culture, and this shift appears to be associated with long-term exposure of sulfide.

6.2.3 Formate as electron donor

Formate dehydrogenation is a rapid process by which hydrogen is formed with no hydrogen-rich intermediate products. Formate represents a potentially valuable electron donor source for field operations. The non-steady-state model successfully simulated the results of the CSTR experiments. Good matches to the experimental CSTR results were achieved applying the VC kinetic parameters determined in batch experiments using cells harvested from the CSTR. Specific conclusions that can be drawn as follows:

- Simulations matching the CSTR experimental performance were achieved using VC kinetics determined in batch experiments with cells harvested from the CSTR.
- By adjusting the yield and decay coefficients from those d by Yu and Semprini (2004) for EV culture, resulted in reasonable matches to the experimental biomass concentration.
- Experimental results showed acetate was formed when the H_2 concentration was around 42 nM. By assuming a H_2 threshold of 40 nM for acetate formation, a good match to acetate production was achieved. However, published studies have reported one order of magnitude higher acetate threshold values.
- Simulation results captured the steady-state change n CAHs, acetate, and H_2 after formate was reduced to 25 mM.
- Excess formate resulted in high H_2 tension (42 nM) and fostered the growth of homoacetogens that produced acetate. However, limited formate resulted in a low H_2 tension (3 nM) and homoacetogens and acetate washout of the CSTR.

- Sensitivity analysis on the VC dechlorination in the 2-L CSTR indicated that the VC dechlorination process was more rate-limited when electron donor was in excess and was more stoichiometry limited when formate was lowered.
- Sensitivity analysis indicated a $K_{s\text{-}H2}$ value for the VC step that was around 3 nM. This is lower than the published value of 7 nM.
- The ability to do a reasonable job simulating the experimental results in a CSTR gives us more confidence in simulating these complex processes that include the competition for H_2 under conditions of continuous growth in a 1-D aquifer column

References

Adamson, D.T.; McDade, J. M.; Hughes, J. B., 2003. Inoculation of DNAPL source zone to initiate reductive dechlorination of PCE. Environ. Sci. Technol., 37: 2525-2533.

Altschul, S F, W Gish, W Miller, E W Myers, and D J Lipman. 1990. "Basic Local Alignment Search Tool." *Journal of Molecular Biology* 215 (3) (October 5): 403–410. doi:10.1006/jmbi.1990.9999.

Amos, B.K., Suchomel, E.J., Pennell, K.D., Loffler, F.E., 2008. Microbial activity and distribution during enhanced contaminant dissolution from a NAPL source zone. Water Res., 42: 2963–74.

Aulenta, F., Gossett, J., Petrangeli Papini, M., Rossetti, S. and Majone, M., 2005. Comparative study of methanol, butyrate, and H_2as electron donors for long-term dechlorination of tetrachloroethene in mixed anerobic cultures. Biotechnol. Bioeng., 91:743–753.

Aulenta, F., Gossett, J.M., Papini, M.P., Rossetti, S., Majone, M., 2005. Comparative study of methanol, butyrate, and hydrogen as electron donors for long-term dechlorination of tetrachloroethene in mixed anaerobic cultures. Biotechnol. Bioeng., 91:743–53.

Aulenta, F., Majone, M., Tandoi, V., 2006. Enhanced anaerobic bioremediation of chlorinated solvents: Environmental factors influencing microbial activity and their relevance under field conditions. J. Chem. Technol. Biotechnol., 81:1463–74.

Aulenta, F., Pera, A., Rossetti, S., Papini, M.P., Majone, M., 2007. Relevance of side reactions in anaerobic reductive dechlorinationmicrocosms amended with different electron donors.Water Res., 41:27–38.

Azizian, M., (unpublished). Anaerobic Reductive Dehalogenation of TCE in Continuous-Stirred Tank Reactor Using EV Culture. Oregon State University, Corvallis, Oregon.

Azizian, Mohammad F, Ian P G Marshall, Sebastian Behrens, Alfred M Spormann, and Lewis Semprini. 2010. "Comparison of Lactate, Formate, and Propionate as Hydrogen Donors for the Reductive Dehalogenation of Trichloroethene in a Continuous-Flow Column." *Journal of Contaminant Hydrology* 113 (1-4) (April 1): 77–92. doi:10.1016/j.jconhyd.2010.02.004.

Bagley, D.M. 1998. Systematic approach for modeling tetrachloroethene biodegradation. J. Environ. Eng., 124: 1076–1086.

Bagley, D.M., Gossett, J.M., 1990. Tetrachloroethene Transformation to Trichloroethene and cis-1,2-Dichloroethene by Sulfate-Reducing Enrichment Cultures. Appl. Environ. Microbiol., 56: 2511-2516.

Ballapragada, B., Stensel, D., Puhakka, J. and Ferguson, J., 1997. Effect of H_2 on reductive dechlorination of chlorinated ethenes. Environ. Sci. Technol. 31:1728–1734.

Beeman, R.E., Howell, J.E., Shoemaker, S.H., Salazar, E.A., Buttram, J. R., 1994. A Field Evaluation of in situ Microbial Reductive Dehalogenation by the Biotransformation of Chlorinated Ethenes. In Hinchee, R. E., L. Semprini, and S. K. Ong (Ed.), Bioremediation of Chlorinated and Polycyclic Aromatic Hydrocarbon Compounds (pp. 14-27). Ann Arbor, MI: Lewis Publishers.

Behrens, S., Azizian, M.F., McMurdie, P.J., Sabalowsky, A., Dolan, M.E. Semprini, L., Spormann, A. M., 2008. Monitoring Abundance and Expression of "*Dehalococcoides*" Species Chloroethene-Reductive Dehalogenases in a Tetrachloroethene-Dechlorinating Flow Column, Appl. Envir. Microbiol. 74: 5695-5703.

Berggren, D.R., 2011. Kinetic and Molecular Effects of Sulfate Reduction on a Dechlorinating Culture under Chemostat Growth Conditions, Master thesis, Oregon State University.

Berggren, D.R. V., I.P. Marshall, M.A. Azizian, A.M. Spormann. 2013. Effects of Sulfate Reduction on the Bacterial Community and Kinetic Parameters of a Dechlorinating Culture under Chemostat Growth Conditions. Environmental Science and Technology. 47(4) 1879-1886.

Boyd, E, J Spear, and J Peters. 2009. "[FeFe]-Hydrogenase Genetic Diversity Provides Insight Into Molecular Adaptation in a Saline Microbial Mat Community." *Applied and Environmental Microbiology* (May 8). doi:10.1128/AEM.00582-09.

Breznak, J. A., 1994. Acetogenesis from carbon dioxide in termite guts, p. 303–330. In H. L. Drake (ed.), Acetogenesis. Chapman & Hall, Inc., New York, N.Y.

Caro-Quintero, Alejandro, and Konstantinos T Konstantinidis. 2012. "Bacterial Species May Exist, Metagenomics Reveal." *Environmental Microbiology* 14 (2) (February): 347–355. doi:10.1111/j.1462-2920.2011.02668.x.

Christiansen, NINA, and Birgitte Ahring. 1996. "Desulfitobacterium Hafniense Sp. Nov., an Anaerobic, Reductively Dechlorinating Bacterium." *International Journal of Systematic and Evolutionary Microbiology* 46 (2) (April 1): 442. doi:10.1099/00207713-46-2-442.

Clapp, L., Semment, M., Novak, P., and Hozalski, R., 2004. Model for In Situ Perchloroethene Dechlorination via Membrane-Delivered Hydrogen. J. Environ. Engg., 130: 1367-1381.

Clement, P.T., Gautam, T.R., Lee, L.L., Truex, M.J., Davis G.B., 2004. Modeling of DNAPL-dissolution, rate-limited sorption and biodegradation reactions in groundwater systems, Bioremediation., 8:47–64.

Cord-Ruwisch, R., H.-J. Seitz, Conrad, R., 1988. The capacity of hydrogenotrophic anaerobic bacteria to compete for traces of H2depends on the redox potential of the terminal electron acceptor. Arch. Microbiol., 149: 350–357.

Cord-Ruwisch, R, DR Lovley, and B Schink. 1998. "Growth of Geobacter Sulfurreducens with Acetate in Syntrophic Cooperation with Hydrogen-Oxidizing Anaerobic Partners." *Applied and Environmental Microbiology* 64 (6) (June): 2232–2236.

Cupples, Alison M, Alfred M Spormann, and Perry L McCarty. 2003. "Growth of a Dehalococcoides-Like Microorganism on Vinyl Chloride and Cis-Dichloroethene as Electron Acceptors as Determined by Competitive PCR." *Applied and Environmental Microbiology* 69 (2) (February): 953–959.

Cupples, A., Spormann, A., McCarty, P.L., 2004. Vinyl chloride and cis-dichloroethene dechlorination kinetics and microorganism growth under substrate limiting conditions. Environ. Sci. Technol., 38:1102–1107.

Da Silva, M.L., Daprato, R.C., Gomez, D.E., Hughes, J.B., Ward, C.H., Alvarez, P.J., 2006. Comparison of bioaugmentation and biostimulation for the enhancement of dense nonaqueous phase liquid source zone bioremediation. Water. Environ. Res., 78:2456–65.

Deng, B., Campbell, T., and Burris, D., 1997. Hydrocarbon formation in metallic iron/water system. Environ. Sci. Technol., 31:1185-1190.

DeSantis, Todd Z, Eoin L Brodie, Jordan P Moberg, Ingrid X Zubieta, Yvette M Piceno, and Gary L Andersen. 2007. "High-Density Universal 16S rRNA Microarray Analysis Reveals Broader Diversity Than Typical Clone Library When Sampling the Environment." *Microbial Ecology* 53 (3) (April 1): 371–383. doi:10.1007/s00248-006-9134-9.

DiStefano, T.D., Gossett, J.M., Zinder, S.H., 1991. Reductive dechlorination of high concentrations of tetrachloroethene to ethene by an anaerobic enrichment culture in the absence of methanogenesis. Appl. Environ. Microbiol., 57: 2287.

Dugat-Bony, E, M Missaoui, E Peyretaillade, C Biderre-Petit, O Bouzid, C Gouinaud, D Hill, and P Peyret. 2011. "HiSpOD: Probe Design for Functional DNA Microarrays." *Bioinformatics* 27 (5) (February 20): 641–648. doi:10.1093/bioinformatics/btq712.

Edgar, R C. 2004. "MUSCLE: Multiple Sequence Alignment with High Accuracy and High Throughput." *Nucleic Acids Research* 32 (5) (March 8): 1792–1797. doi:10.1093/nar/gkh340.

Ellis, D., Lutz, E., Odom, J., Buchanan, R., Bartlett, C., Lee, M., Harkness, M., Deweerd, K., 2000. Bioaugmentation for accelerated in situ anaerobic bioremediation. Environ. Sci. Technol., 34: 2254-2260.

EPA. 1993. Evaluation of the likelihood of DNAPL presence at NPL sites, national results; EPA 540-R-93-073; U.S. Environmental Protection Agency, Office of Solid Waste and Emergency Response: Washington, D.C.

Fennell, D., Gossett, J., 1998. Modeling the Production of and Competition for H_2 in a Dechlorinating Culture. Environ. Sci. Technol., 32: 2450-2460.

Finneran, Kevin T, Heather M Forbush, Catherine V Gaw VanPraagh, and Derek R Lovley. 2002. "Desulfitobacterium Metallireducens Sp. Nov., an Anaerobic Bacterium That Couples Growth to the Reduction of Metals and Humic Acids as Well as Chlorinated Compounds." *International Journal of Systematic and Evolutionary Microbiology* 52 (Pt 6) (November 1): 1929–1935.

Flynn, S.J., Loffler, F.E., Tiedge, J.M., 2000. Microbial community changes associated with a shift from reductive dechlorination of PCE to reductive dechlorination of cis-DCE and VC. Environ. Sci. Technol., 34:1056–1061.

Futamata, Hiroyuki, Shinichi Kaiya, Mariko Sugawara, and Akira Hiraishi. 2009. "Phylogenetic and Transcriptional Analyses of a Tetrachloroethene-Dechlorinating 'Dehalococcoides' Enrichment Culture TUT2264 and Its Reductive-Dehalogenase Genes." *Microbes and Environments* 24 (4): 330–337.

Gao, Haichun, Zamin K Yang, Terry J Gentry, Liyou Wu, Christopher W Schadt, and Jizhong Zhou. 2007. "Microarray-Based Analysis of Microbial Community RNAs by Whole-Community RNA Amplification." *Applied and Environmental Microbiology* 73 (2): 563–571. doi:10.1128/AEM.01771-06.

Gattiker, Alexandre, Elisabeth Gasteiger, and Amos Bairoch. 2002. "ScanProsite: a Reference Implementation of a PROSITE Scanning Tool." *Applied Bioinformatics* 1 (2): 107–108.

Gossett, J., 1987. Measurement of Henry's law constants for C_1 and C_2 chlorinated hydrocarbons. Environ. Sci. Technol., 21: 202-20.

Guindon, Stéphane, and Olivier Gascuel. 2003. "A Simple, Fast, and Accurate Algorithm to Estimate Large Phylogenies by Maximum Likelihood." *Systematic Biology* 52 (5) (October 1): 696–704.

Häggblom, M., Bossert, I., 2003. Halogenated organic compounds - a global perspective. In Dehalogenation: microbial processes and environmental applications; Häggblom, M. M., Bossert, I. D., Eds.; Kluwer Academic Publishers: Boston / Dordrecht / London, 1-29.

Haston, Z.C., McCarty, P.L., 1999. Chlorinated ethene half-velocity coefficients (Ks) for reductive dehalogenation. Environ Sci Technol., 3:223–226.

He, J., Ritalahti, K., Yang, K., Koenigsberg, S., Loffler, F., 2003. Detoxification of vinyl chloride to ethene coupled to growth of an anaerobic bacterium. Nature., 424: 62-65.

Heimann, A., Jakobsen, R., 2006. Experimental evidence for a lack of thermodynamic control on H2concentrations during anaerobic degradation of chlorinated ethenes. Environ. Sci. Technol., 40: 3501-3507.

Heimann, A.C., Friis, A.K., Jakobsen, R., 2005. Effects of sulfate on anaerobic chloroethene degradation by an enriched culture under transient and steady-state hydrogen supply. Water Res., 39:3579–86.

Hendrickson, Edwin R, Jo Ann Payne, Roslyn M Young, Mark G Starr, Michael P Perry, Stephen Fahnestock, David E Ellis, and Richard C Ebersole. 2002. "Molecular Analysis of Dehalococcoides 16S Ribosomal DNA From Chloroethene-Contaminated Sites Throughout North America and Europe." *Applied and Environmental Microbiology* 68 (2) (February): 485–495.

Heraty, L., Fuller, M., Huang, L., Abrajano, T., Sturchio, N., 1999. Isotopic fractionation of carbon and chlorine by microbial degradation of dichloromethane. Organic Geoch., 30: 793-799.

Hoehler, T., Alperin, M., Albert, D., Martens, C., 2001. Apparent minimum free energy requirements for methanogenic Archaea and sulfate-reducing bacteria in an anoxic marine sediment. FEMS Microbiol. Ecol., 38: 33-41.

Hoelen, T.P., Reinhard, M., 2004. Complete biological dehalogenation of chlorinated ethylenes in sulfate containing groundwater. Biodegradation:15:395–403.

Hoff, Katharina J. 2009. "The Effect of Sequencing Errors on Metagenomic Gene Prediction." *BMC Genomics* 10: 520. doi:10.1186/1471-2164-10-520.

Holliger, C., Hahn, D., Harmsen, H., Ludwig, W., Schumacher, W., Tindall, B., Vazquez, F., Weiss, N., Zehnder, A.J., 1998. *Dehalobacter* restrictus gen.nov. andsp.nov., a strictly anaerobic bacterium that reductively dechlorinates tetra- and trichloroethene in an anaerobic respiration. Arch. Microbiol., 169: 313-321.

Holliger, C., Schraa, G., Stams, A., Zehnder, A., 1993. A highly purified enrichment culture couples the reductive dechlorination of tetrachloroethene to growth. Appl. Environ. Microbiol., 59: 2991-2997.

Holliger, C., Schumacher, W., 1994. Reductive dehalogenation as a respiratory process. Anton. Leeuw. Int. J. G., 66: 239-246.

Holliger, C., Wohlfarth, G., Diekert, G., 1999. Reductive dechlorination in the energy metabolism of anaerobic bacteria. FEMS Microbiol. Rev., 22: 383-398.

Huang, L., Sturchio, N., Abrajano Jr, T., Heraty, L.; Holt, B., 1999. Carbon and chlorine isotope fractionation of chlorinated aliphatic hydrocarbons by evaporation. Organic Geochemistry, 30: 777-785.

Krajmalnik-Brown, Rosa, Tina Hölscher, Ivy N Thomson, F Michael Saunders, Kirsti M Ritalahti, and Frank E Löffler. 2004. "Genetic Identification of a Putative Vinyl Chloride Reductase in Dehalococcoides Sp. Strain BAV1." *Applied and Environmental Microbiology* 70 (10) (October): 6347–6351. doi:10.1128/AEM.70.10.6347-6351.2004.

Lane, D J, B Pace, G J Olsen, D A Stahl, M L Sogin, and N R Pace. 1985. "Rapid Determination of 16S Ribosomal RNA Sequences for Phylogenetic Analyses." *Proceedings of the National Academy of Sciences of the United States of America* 82 (20) (October): 6955–6959.

Lee, I., Bae, J., Yang, Y., McCarty, P., 2004. Simulated and experimental evaluation of factors affecting the rate and extent of reductive dehalogenation of chloroethenes with glucose, J. Cont. Hydrol., 74: 313-331.

Leloup, Julie, Henrik Fossing, Katharina Kohls, Lars Holmkvist, Christian Borowski, and Bo Barker

Jørgensen. 2009. “Sulfate-Reducing Bacteria in Marine Sediment (Aarhus Bay, Denmark): Abundance and Diversity Related to Geochemical Zonation.” *Environmental Microbiology* 11 (5) (May): 1278–1291. doi:10.1111/j.1462-2920.2008.01855.x.

Li, Weizhong, and Adam Godzik. 2006. “Cd-Hit: a Fast Program for Clustering and Comparing Large Sets of Protein or Nucleotide Sequences.” *Bioinformatics* 22 (13) (July 1): 1658–1659. doi:10.1093/bioinformatics/btl158.

Loffler, F.E., Edwards, E.A., 2006. Harnessing microbial activities for environmental cleanup. Curr. Opin. Biotechnol.,17:274–84.

Löffler, F.E., Edwards, E.A., 2006. Harnessing microbial activities for environmental cleanup. Curr. Opin. Biotechnol., 17:274-284.

Löffler, F.E., Tiedje, J., Sanford. R., 1999. Fraction of electrons consumed in electron acceptor reduction and H_2 thresholds as indicators of halorespiratory physiology. Appl. Environ. Microbiol., 65:4049–4056.

Lovley, D., Klug, M., 1983. Methanogenesis from methanol and methylamines and acetogenesis from H2and carbondioxide in the sediments of a eutrophic lake. Appl. Environ. Microbiol. 45 : 1310–1315.

Luijten, M.L., Roelofsen, W., Langenhoff, A., Schraa, G., Stams, A.J., 2004. Brief Report: Hydrogen threshold concentrations in pure cultures of halorespiring bacteria and at a site polluted with chlorinated ethenes. Environ. Microbiol., 6:646–650.

Magnuson, Jon K., Margaret F Romine, David R. Burris, and Mark T. Kingsley. 2000. “Trichloroethene Reductive Dehalogenase From Dehalococcoides Ethenogenes: Sequence of tceA and Substrate Range Characterization.” *Applied and Environmental Microbiology* 66 (12) (December): 5141–5147. doi:10.1128/AEM.66.12.5141-5147.2000.

Major, D., McMaster, M., Cox, E., Edwards, E., Dworatzek, S., Hendrickson, E., Starr, M., Payne, J., Buonamici, L., 2002. Field demonstration of successful bioaugmentation to achieve dechlorination of tetrachloroethene to ethene. Environ. Sci. Technol., 36: 5106-5116.

Marshall, Ian PG, Dusty RV Berggren, Mohammad F Azizian, Luke C Burow, Lewis Semprini, and Alfred M Spormann. 2012. “The Hydrogenase Chip: a Tiling Oligonucleotide DNA Microarray Technique for Characterizing Hydrogen-Producing and -Consuming Microbes in Microbial Communities.” *The ISME Journal* 6: 814–826. doi:10.1038/ismej.2011.136.

Maymo´-Gatell, X., Chien, Y.-T., Gossett, J., Zinder, S., 1997. Isolation of a bacterium that reductively dechlorinates tetrachloroethene to ethene. Science, 276:1568–1571.

McCarty, P., 1997. Breathing with chlorinated solvents. Science., 276:1521–2.

McCarty, P.L., 1993. In situ bioremediation of chlorinated solvents. Curr. Opin. Biotechnol., 4:323-330.

McInerney, M J, and M P Bryant. 1981. “Anaerobic Degradation of Lactate by Syntrophic Associations of Methanosarcina Barkeri and Desulfovibrio Species and Effect of H2 on Acetate Degradation.” *Applied and Environmental Microbiology* 41 (2) (February 1): 346–354.

McMurdie, Paul J, Sebastian F Behrens, Jochen A Müller, Jonathan Göke, Kirsti M Ritalahti, Ryan Wagner, Eugene Goltsman, et al. 2009. “Localized Plasticity in the Streamlined Genomes of Vinyl Chloride Respiring Dehalococcoides.” *PLoS Genetics* 5 (11) (November): e1000714. doi:10.1371/journal.pgen.1000714.

Miles, Zachary D, Reid M McCarty, Gabriella Molnar, and Vahe Bandarian. 2011. “Discovery of Epoxyqueuosine (oQ) Reductase Reveals Parallels Between Halorespiration and tRNA Modification.” *Proceedings of the National Academy of Sciences* 108 (18) (May 3): 7368–7372.

doi:10.1073/pnas.1018636108.
Muyzer, G, E C de Waal, and A G Uitterlinden. 1993. “Profiling of Complex Microbial Populations by Denaturing Gradient Gel Electrophoresis Analysis of Polymerase Chain Reaction-Amplified Genes Coding for 16S rRNA.” *Applied and Environmental Microbiology* 59 (3) (March 1): 695–700.
Müller, Jochen A, Bettina M Rosner, Gregory Von Abendroth, Galit Meshulam-Simon, Perry L McCarty, and Alfred M Spormann. 2004. “Molecular Identification of the Catabolic Vinyl Chloride Reductase From Dehalococcoides Sp. Strain vs and Its Environmental Distribution.” *Applied and Environmental Microbiology* 70 (8) (August 1): 4880–4888. doi:10.1128/AEM.70.8.4880-4888.2004.
Newell, C., Hass, P., Hughes, J., Khan, T., 2000. In Results From Two Direct H2Delivery Field Tests for Enhanced Dechlorination; Battelle Remediation of Chlorinated and Recalcitrant Compounds Conference, Monterey, CA.
Nielsen, J., Villadsen, J., Liden, G., 2003. Bioreaction Engineering Principles, 2nd ed.; Kluwer Academic/Plenum: New York.
Rahm, Brian G, and Ruth E Richardson. 2008. “Correlation of Respiratory Gene Expression Levels and Pseudo-Steady-State PCE Respiration Rates in Dehalococcoides Ethenogenes.” *Environmental Science and Technology* 42 (2) (January 15): 416–421.
Rosner, B.M., McCarty, P.L., Spormann, A.M., 1997. In vitro studies on reductive vinyl chloride dehalogenation by an anaerobicmixed culture. Appl. Environ. Microbiol., 63: 4139–4144.
Sabalowsky, A.R., Semprini, L., 2010. Trichloroethene and cis-1,2-dichloroethene concentration-dependent toxicity model simulates anaerobic dehalogenation at high concentrations: I. batch-fed reactors. Biotech. Bioeng., 107: 529–539.
Sabalowsky, A.R., Semprini, L., 2010. Trichloroethene and cis-1,2-dichloroethene concentration-dependent toxicity model simulates anaerobic dehalogenation at high concentrations. II: Continuous flow and attached growth reactors. Biotech. Bioeng., 107: 403–592.
Sanford, R A, J R Cole, F E Löffler, and J M Tiedje. 1996. “Characterization of Desulfitobacterium Chlororespirans Sp. Nov., Which Grows by Coupling the Oxidation of Lactate to the Reductive Dechlorination of 3-Chloro-4-Hydroxybenzoate.” *Applied and Environmental Microbiology* 62 (10) (October): 3800–3808.
Schink, B., 1997. Energetics of syntrophic cooperation in methanogenic biodegradation. Microbiol. Mol. Biol. Rev., 61:262–280.
Scholz-Muramatsu, H., Neumann, A., Mebmer, M., Moore, E., Diekert, G., 1995. Isolation and Characterization of Dehalospirillum Multivorans Gen. Nov., Sp. Nov., A Tetrachloroethene-Utilizing, Strictly Anaerobic Bacterium. Arch. Microbiol., 163:48-56.
Smatlak C., Gossett, J., Zinder, S., 1996. Comparative kinetics of H_2 utilization for reductive dechlorination of tetrachloroethene and methanogenesis in an anaerobic enrichment culture. Environ. Sci. Technol., 30:2850–2858.
Smyth, Gordon K, and Terry Speed. 2003. “Normalization of cDNA Microarray Data.” *Methods* 31 (4) (December 1): 265–273.
Sung, Y., Ritalahti, K., Sanford, R.; Urbance, J.; Flynn, S., Tiedje, J., Loffler, F., 2003. Characterization of two tetrachloroethene-reducing, acetate-oxidizing anaerobic bacteria and their description as Desulfuromonas michiganensis sp nov. Appl. Environ. Microbiol., 69: 2964-2974.
Suyama, Akiko, Masaki Yamashita, Sadazo Yoshino, and Kensuke Furukawa. 2002. “Molecular Characterization of the PceA Reductive Dehalogenase of Desulfitobacterium Sp. Strain Y51.” *Journal of Bacteriology* 184 (13) (July): 3419–3425.

Sung, Y., Ritalaliti, K., Apkarian, K., Ramos-Hernandez, R., Sanford, N., Mesbah, R., Loffler, F., 2006. Geobacter lovleyi sp nov strain SZ, a novel metal-reducing and tetrachloroethene-dechlorinating bacterium. Appl. Environ. Microbiol., 72: 2775-2782.

Taş, Neslihan, Miriam H A van Eekert, Willem M de Vos, and Hauke Smidt. 2010. "The Little Bacteria That Can - Diversity, Genomics and Ecophysiology of 'Dehalococcoides' Spp. in Contaminated Environments." *Microbial Biotechnology* 3 (4) (July): 389–402. doi:10.1111/j.1751-7915.2009.00147.x.

Thauer, R., Jungermann, K., Decker, K., 1977. Energy conservation in chemotrophic anaerobic bacteria. Bacteriol. Rev., 41: 100-180.

Utkin, I, C Woese, and J Wiegel. 1994. "Isolation and Characterization of Desulfitobacterium Dehalogenans Gen. Nov., Sp. Nov., an Anaerobic Bacterium Which Reductively Dechlorinates Chlorophenolic Compounds." *International Journal of Systematic Bacteriology* 44 (4) (October): 612–619.

Vignais, Paulette M, and Bernard Billoud. 2007. "Occurrence, Classification, and Biological Function of Hydrogenases: an Overview." *Chemical Reviews* 107 (10) (October 1): 4206–4272. doi:10.1021/cr050196r.

Villemur, Richard, Martin Lanthier, Réjean Beaudet, and François Lépine. 2006. "The Desulfitobacterium Genus." *FEMS Microbiology Reviews* 30 (5) (September): 706–733. doi:10.1111/j.1574-6976.2006.00029.x.

Vogel, T.; Criddle, C.; McCarty, P., 1987. Transformations of halogenated aliphatic compounds. Environ. Sci. Technol., 21: 722-736.

Wang, D., Roddick, F., Anderson, B., 1999. Remediation of trichloroethylene contamination using zero-valent iron under anaerobic conditions. In: Johnston, C. D. (ed.) Proceedings of the 1999 Contaminated Site Remediation Conference "Challenges Posed by Urban and Industrial Contaminants 21-25 March 1999. Fremantle, WA, pp 665-670.

Wang, Qiong, George M Garrity, James M Tiedje, and James R Cole. 2007. "Naive Bayesian Classifier for Rapid Assignment of rRNA Sequences Into the New Bacterial Taxonomy.." *Applied and Environmental Microbiology* 73 (16) (August): 5261–5267. doi:10.1128/AEM.00062-07.

WHO Guidelines for drinking-water quality. 1993, Volume 1: Recommendations; 3rd ed.; WHO: Geneva.

Wiedemeier, T., Rifai, H., Newell, C., Wilson, J., 1999. Natural attenuation of fuels and chlorinated solvents in the subsurface; John Wiley & Sons: New York.

Xing, Defeng, Nanqi Ren, and Bruce E Rittmann. 2008. "Genetic Diversity of Hydrogen-Producing Bacteria in an Acidophilic Ethanol-H2-Coproducing System, Analyzed Using the [Fe]-Hydrogenase Gene." *Applied and Environmental Microbiology* 74 (4) (February 1): 1232–1239. doi:10.1128/AEM.01946-07.

Yang, Y., McCarty, P., 1998. Competition for H_2 within a chlorinated solvent dehalogenating anaerobic mixed culture. Environ. Sci. Technol., 32: 3591-3597.

Yang, Y., McCarty, P.L., 2002. Comparison between donor substrates for biologically enhanced tetrachloroethene DNAPL dissolution. Environ Sci Technol., 36:3400–4.

Yu, S., 2003. Kinetics and modeling investigations of the anaerobic reductive dechlorination of chlorinated ethylenes using single and binary mixed cultures and silicon-based organic compounds as slow release substrates. Ph.D. thesis, Oregon State University, Corvallis.

Yu, S., Dolan, M.E., Semprini, L., 2005. Kinetics and inhibition of reductive dechlorination of chlorinated ethylenes by two different mixed cultures. Environ. Sci. Technol., 39:195–205.

Yu, S., Semprini, L., 2004. Kinetics and Modeling of Reductive Dechlorination at High PCE and TCE Concentrations, Biotechnol. Bioengg., 88: 451-464.

APPENDICES

Appendix A: EV culture preparation

The EV culture has been grown in a basal growth medium. A basal growth medium stock was prepared as previously described using reagent grade salts (Yang and McCarty, 1998; Yu et al., 2005). The basal medium for each reactor was augmented with additional Na_2S (anhydrous) to a final concentration of 0.45 mM. Na_2CO_3 (0-220 mg anhydrous) per 250 mL batch of reactor feed was supplied as needed for additional pH buffering capacity to counteract acidification from dechlorination. The basal growth media contained the following constituents per liter of Milli-Q water: 1.0 g of K_2HPO_4, 3 g of Na_2CO_3, 20 mL of minerals solution (40 g of NaCl, 50 g of NH4Cl, 5 g of KCl, 5 g of KH_2PO_4, 5 g of $MgCl_2.6H_2O$, and 2g of $CaCl_2.2H_2O$ L-1), 5 mL of trace metal solution (1 g of $FeCl_2.4H_2O$, 1 g of $MnC_{l2}.4H_2O$, 0.2 g of $CoCl_2.6H_2O$, 0.12 g of H_3BO_3, 0.02 g of $ZnCl_2$, 0.02 g of $CuC_{l2}.2H_2O$, 0.02 g of NiCl2.6H_2O, 0.02 g of $Na_2MoO_4.2H_2O$, 0.02 g of Na_2SeO_4, 0.02 g of $Na_2WO_4.2H_2O$, 0.04 g of $Al_2(SO_4)_3.18H_2O$, and 10 mL of 1 N HCl L-1), 1 mL of filter-sterilized vitamin stock solution (0.02 g of biotin, 0.02 g of folic acid, 0.1 g of pyridoxine, 0.05 g of riboflavin, 0.05 g of thiamine, 0.05 g of nicotinic acid, 0.05 g of pantothenic acid, 0.05 g of p-aminobenzoic acid (PABA), 0.05 g of cyanocobalamine, and 0.05 g of thioctic acid L-1), and 5 mg of Na_2S as a sulfur source and reductant (Yang and McCarty 1998).

Appendix B

B.1 Articles in peer-reviewed journals:

1) Berggren, D.R. V., I.P. Marshall, M.A. Azizian, A.M. Spormann. 2013. Effects of Sulfate Reduction on the Bacterial Community and Kinetic Parameters of a Dechlorinating Culture under Chemostat Growth Conditions. Environmental Science and Technology. 47(4) 1879-1886.

2) Marshall, Ian P.G., Mohammad F. Azizian Ph.D, Lewis Semprini, Alfred M. Spormann (submitted). Dynamics of reductively dechlorinating bacterial chemostat communities under stable and perturbed conditions

3) Marshall IP, Berggren DR, Azizian MF, Burow LC, Semprini L, Spormann AM. 2012. The Hydrogenase Chip: a tiling oligonucleotide DNA microarray technique for characterizing hydrogen-producing and -consuming microbes in microbial communities. ISME J. 2012 Apr;6(4):814-26.

4) Lohner S.T., AM Spormann. 2012. Identification of a Reductive Tetrachloroethene Dehalogenase in *Shewanella sediminis*, Phil Trans. R. Soc. B submitted.

5) Azizian MF, Marshall IP, Behrens S, Spormann AM, Semprini L. 2010. Comparison of lactate, formate, and propionate as hydrogen donors for the reductive dehalogenation of trichloroethene in a continuous-flow column.
J Contam Hydrol. 2010 Apr 1;113(1-4):77-92.

6) Behrens S, Azizian MF, McMurdie PJ, Sabalowsky A, Dolan ME, Semprini L, Spormann AM. 2008. Monitoring abundance and expression of "Dehalococcoides" species chloroethene-reductive dehalogenases in a tetrachloroethene-dechlorinating flow column. Appl Environ Microbiol. 2008 Sep;74(18):5695-703.

7) Azizian MF, Behrens S, Sabalowsky A, Dolan ME, Spormann AM, Semprini L. 2008. Continuous-flow column study of reductive dehalogenation of PCE upon bioaugmentation with the Evanite enrichment culture. J Contam Hydrol. 2008 Aug 20;100(1-2):11-21.

B.2 Technical reports:

Ian P. G. Marshall. PhD Thesis. 2012. A Tiling DNA Microarray Approach for the Functional Analyses in Microbial Ecosystems. Stanford University

Dusty Berggren. MS Thesis. 2011. Kinetic and Molecular Effects of Sulfate Reduction on a Dechlorinating Culture under Chemostat Growth Conditions. (Oregon State University)

B.3 Conference or symposium proceedings:

Semprini, L., M. Azizian, S. F. Behrens, I. P. G. Marshall, and A. M. Spormann, "Transition Studies of Reductive Dehalogenation in a Chemostat Using Formate as an Electron Donor," SERDP-ESTCP Partners in Environmental Technology Technical Symposium and Workshop, December 2-4, Washington D.C. 2008

Semprini, L., M. Azizian, I. Marshall and A.M. Spormann. Comparison of lactate, formate, and propionate as substrates for TCE reductive dehalogenation in a continuous-flow column. SERDP-ESTCP Partners in Environmental Technology Technical Symposium and Workshop, Washington D.C., Dec. 1-3, 2009

Azizian,M.F., D. Berggren, I. P. G. Marshall, A. M. Spormann, and L. Semprini. PCE Dehalogenation and Sulfate Reduction in Chemostats under Lactate Fermenting Conditions. SERDP-ESTCP Partners in Environmental Technology Technical Symposium and Workshop, Washington. D.C. Nov. 30-Dec. 2, 2010

M. Azizian, I. Marshall, S. Brehens, A. Spormann, and L. Semprini. 2011. Evaluation in a continuous-flow column of the different fermenting substrates for the reductive dehalogenation of trichloroethene. GQ10-Groundwater Quality Management in a Changing Worl. Proc. 7th International Groundwater Quality Conference, Zurich Switzerland 13-18 June 2010. IAHS Publ 342 (2011) 209-212.

Semprini, L., D. R.V. Berggren, M. F. Azizian, I. P.G. Marshall, Alfred M. Spormann. PCE Dehalogenating Chemostat Response to Sulfate Reduction and Sulfide Accumulation: Shifts in the Dehalogenation Rates and Community Structure. SERDP-ESTCP Partners in Environmental Technology Technical Symposium and Workshop, Washington D.C., Nov 29-Dec 1, 2011.

Appendix C: Protocols/User guides

Supplemental Materials
Materials and Methods

Chemical Analysis Methods: Headspace methods were used to determine the concentrations of CAH, ethene, and H_2 in aqueous samples obtained from the chemostats as described by Azizian et al. (2008). The headspace sample was created by adding 1 ml of liquid sample to a 2 mL glass vial and vortexing. Gas samples from batch reactors were extracted directly from the reactor headspace. A 100 µL gastight syringe (Hamilton, Leno, NV) was used to extract the 100µL samples headspace samples were injected to the gas chromatograph (GC). CAHs and ethene were measured with an HP-6890 GC equipped with a photoionization flame ionization detector and a 30m-0.53mmGS-Q column (J&W Scientific, Folsom, CA), with helium as the carrier gas (15 mL/min). The GC oven was initially set at 150°C for 2 min, heated at 45°C/min to 220°C, and held at 220°C for 1.44 min. Aqueous concentrations were calculated using published Henry's constants [82]. A Dionex-500 HPLC chromatograph equipped with UV/VIS detector and an Alltech Prevail Organic acid column was used to measure lactate, propionate, and acetate concentrations. Liquid samples (0.25 mL) from the chemostate were centrifuged for 2 minutes at 14,000 RPM, and diluted ten times with ultrapure water for analysis.

Total protein concentrations were measured using the Thermo Scientific Pierce BCA Protein Assay kit according to manufactures instructions except cell samples were washed twice prior to analysis to remove the resazurin indicator and sulfide precipitates found to influence colometric analysis. 2 mL of culture was extracted and centrifuged at 14,000 RPM for 5 minutes. Supernatant was decanted from the cell pellet using a pipette, and the sample was re-suspended in 1 mL of DI water via vortexing. The spinning process was repeated, and the final cell pellet was re-suspended in 50 µL of deionized water for analysis.

DNA Extraction: DNA extraction was performed as previously described[1].

Dehalococcoides hupL clone libraries: Primers HupL_F (5'- ATGCAGAAGATAGTAATTGAYC-3') and HupL_R (5'- GCCAATCTTRAGTTCCATMR-3') designed during a previous study for amplification of a 1246bp fragment of the *hupL* gene from *Dehalococcoides* sp. Primers were used at a concentration of 0.5µM each to PCR-amplify *hupL* in 50µL reactions with 25µL 2X DreamTaq Green Master Mix, cycled with an initial 95ºC denaturation step for 3min, followed by 45 cycles with 30s at 95ºC, 30s at 55ºC, 30s at 72ºC, then a final 72ºC extension step of 10min. PCR products were cloned using the TOPO TA cloning kit (Invitrogen) with the pCR2.1-TOPO cloning vector, then Sanger-sequenced using the M13F primer (5'- GTAAAACGACGGCCAGT-3) (Beckman-Coulter Genomics, Danvers, MA). Clones were assigned to clusters by aligning sequences with *hupL* nucleotide sequences from sequenced *Dehalococcoides* genomes using the MUSCLE algorithm [2] and the PHYML tree-building algorithm [3] implemented in the Geneious software package (Biomatters, Auckland, New Zealand).

Quantitative PCR Measurement of Changes in Phylotype Abundance: All quantitative PCR (qPCR) methods used were based on those previously described [4]. All plasmids were linearized prior to use using the PciI restriction enzyme for 3-5 hours. Standard plasmids used were pCR2.1-TOPO vectors (Invitrogen) containing 1.4kb fragments of bacterial 16S rRNA obtained as part of community analysis of the reductive dechlorinating soil column inoculated with the Point Mugu culture [5]. Bacterial 16S rRNA genes were quantified using the primers Eub341F (5'-CCTACGGGAGGCAGCAG-3') and Eub534R (5'-ATTACCGCGGCTGCTGGC-3') [6]. *Dehalococcoides* 16S rRNA genes were quantified using primers Dehalo505F (5'-GGCGTAAAGTGAGCGTAG-3') and Dehalo686R (5'-GACAACCTAGAAAACCGC-3') [4]. Primers for measurement of *Desulfitobacterium* 16S rRNA gene abundance were Dsb406F (5'- GTACGACGAAGGCCTTCGGGT-3') and Dsb619R (5'-CCCAGGGTTGAGCCCTAGGT-3').

VC Monod Experiments

Method: VC Monod experiments were performed with cells harvested from each chemostat on three occasions. The experimental method varied slightly between tests to accommodate changes in chemostat performance. Four purged batch reactors were prepared for each multi-equilibrium experiment. Reactors acclimated to the batch environment with PCE and H_2 for at least seven hours (except the first test with PM-2L), then were purged and augmented with H_2 (~15,000 nM, aqueous) and gaseous VC (2-900 μM). The multi-equilibration method of Yu and Semprini 2005 was used; however, each bottle was started at a different VC concentration and cycled through the range of analysis in subsequent equilibrations to demonstrate that growth and/or up regulation of VC reductases over the 2 to 3 day experiment was not skewing the results.

VC, ethene, and H_2 concentrations were monitored over time. H_2 was maintained at non-limiting concentrations (>7000 nM) throughout the experiment. VC dechlorination rates were determined through linear regression of 3-6 data points showing the total mass of ethene generated over time as the GC-FID is more sensitive to ethene. Twelve to twenty-four rates were measured between the four reactors within a three day period.

The Monod parameters (k_mX and K_s) for VC transformation were determined from non-linear regression of the rate vs. liquid VC concentration data from each individual reactor. The least-squared error between experimental data and the Monod model (Eq. S1) was found through fitting k_mX and K_s using Microsoft Excel Solver (2007).

Eq. S1

$$\frac{dM_{VC}}{dt} = \frac{(k_{m,VC}X)C_{L,VC}V_L}{K_{s,VC} + C_{L,VC}}$$

The total mass of VC is represented by M_{VC}, the liquid concentration of VC as $C_{L,VC}$, and the liquid volume as V_L.

Results: Multi-equilibrium VC Monod tests were conducted with cells harvested from the chemostats on days 2L-417, 2L-1039, and 2L-1187 for PM-2L The PM-2L VC Monod tests were

performed on days 417, 1039, and 1187, The test on day 1187 was unsuccessful due to the culture's inability to sustain VC reduction at an appreciable, consistent rate.

Monod curve data produced for the PM-2L harvested cells is shown in Figure S1, and the average value for Monod parameters determined though fitting the Monod curve (Eq. S1) are presented in Table S1. The standard deviations in the parameter values from each individual analysis is also presented. The standard deviations represented 19 to 35% of the X k_{max} estimate and 50 to 60% of the K_s estimate,

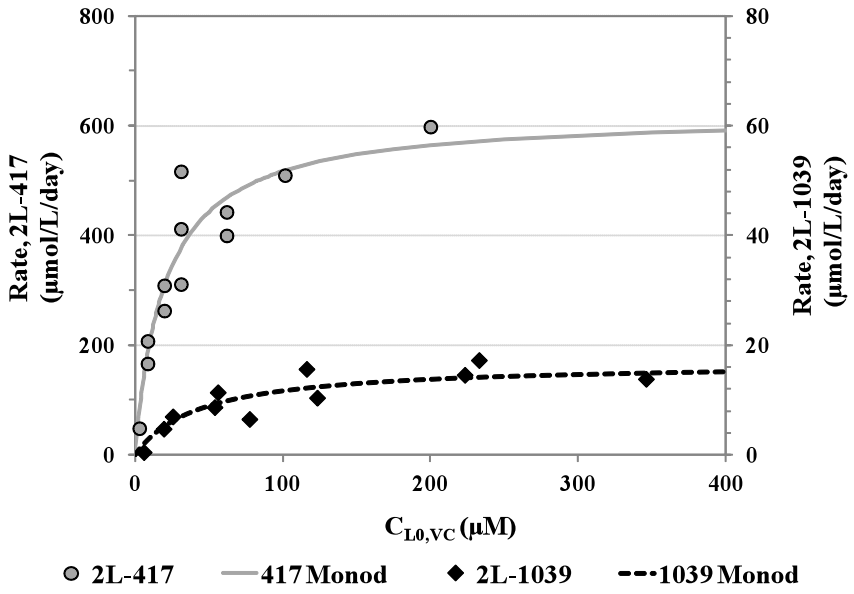

Figure S1: VC Monod curves with culture harvested from the PM-2L chemostat. Note the difference in scales between 2L-417 and 2L-1039.

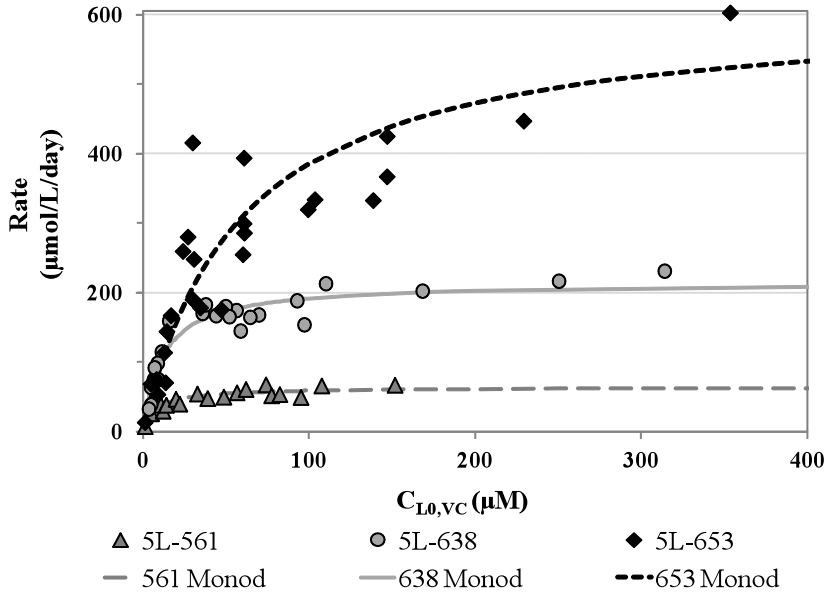

Figure S2: VC Monod curves with culture harvested from the PM-5L chemostat during Stage 5-III.

Table S1: VC Monod parameters with standard deviations for the chemostat cultures.

Batch ID	k_mX (μmol/L/day)	K_s (μM)	Chemostat VC Concentration (μM)	$k_mX/(K_s+VC)$ (1/day)
2L-417	622± 84	20.3 ± 10.4	549	-
2L-1039	16.7 ± 3.1	43.9 ± 27.5	507	-
2L-1187	Not Feasible	Not Feasible	733	-

Clearly, the k_mX of the PM-2L chemostat greatly decreased while the K_s remained in the same order of magnitude. This decline in VC dechlorination rate well resembles what was observed in the PM-2L chemostat, with the 2L-1039 k_mX falling between the modeled 2L-1012 and 2L-1089 k_mX values.

.

The $K_{s,VC}$ found though these tests was significantly lower than the $K_{s,VC}$ of 602 μM found by Yu when the culture was maintained under batch growth conditions {Yu 2005}, suggesting that the culture had undergone a shift to microbial consortia more capable of metabolic VC dechlorination under chemostat conditions. The K_s from the 5L-638 VC Monod test was selected for modeling all PCE-to-ethene batch data as Monod parameters could be directly compared with the modeling results of the PCE-to-ethene batch data carried out with the same culture. Applicability of this K_s and Yu's K_s values for the other CAHs will be verified later in the Supplemental Materials.

Model Development

The basic Monod equation with competitive inhibition (Eq. 5.1 in the text) had to be modified to appropriately account for the conditions within the batch reactors and be suited for Excel spreadsheet modeling. Two-phase (liquid and gas) reactor systems were employed for this study; therefore, it was necessary to account for partitioning of the substrates and inhibitors in the model. Equilibrium partitioning was assumed given the batch reactors here rapidly shaken at 200 rpm a shaker table, allowing use of Henry's constant (H_{cc}) to describe partitioning between the liquid (V_L) and gas (V_G) phases (Eq. 5.3).

Eq. S2

$$C_{L,z} = \frac{M_z}{V_L + V_G H_{CC,z}}$$

Substituting Equation S2 into Equation 5.1 yielded a Monod-style equation based on total reactor mass. This relationship was used to numerically model CAH transformations from PCE to ethene in Microsoft Excel 2007 given defined physical and kinetic parameters and the total initial mass of each substrate in the reactor. Euler's method was employed to step through reaction time, resulting in the following set of equations:

Eq. S3

$$M_{PCE,t+\Delta t} = M_{PCE,t} - \frac{(k_{m,PCE}X)M_{PCE,t}V_L}{K_{cor,PCE} + M_{PCE,t}}\Delta t$$

Eq. S4

$$M_{TCE,t+\Delta t} = M_{TCE,t} + (M_{PCE,t} - M_{PCE,t+\Delta t}) - \frac{(k_{m,TCE}X)M_{TCE,t}V_L}{K_{cor,TCE}\left(1 + \frac{M_{PCE,t}}{K_{cor,PCE}}\right) + M_{TCE,t}}\Delta t$$

Eq. S5

$$M_{DCE,t+\Delta t} = M_{DCE,t} + \left(\frac{(k_{m,TCE}X)M_{TCE,t}V_L}{K_{cor,TCE}\left(1 + \frac{M_{PCE,t}}{K_{cor,PCE}}\right) + M_{TCE,t}} - \frac{(k_{m,DCE}X)M_{DCE,t}V_L}{K_{cor,DCE}\left(1 + \frac{M_{TCE,t}}{K_{cor,TCE}}\right) + M_{DCE,t}}\right)\Delta t$$

Eq. S6

$$M_{VC,t+\Delta t} = M_{VC,t} + \left(\frac{(k_{m,DCE}X)M_{DCE,t}V_L}{K_{cor,DCE}\left(1 + \frac{M_{TCE,t}}{K_{cor,TCE}}\right) + M_{DCE,t}} - \frac{(k_{m,VC}X)M_{VC,t}V_L}{K_{cor,VC}\left(1 + \frac{M_{TCE,t}}{K_{cor,TCE}} + \frac{M_{DCE,t}}{K_{cor,DCE}}\right) + M_{VC,t}}\right)\Delta t$$

Eq. S7

$$M_{ETH,t+\Delta t} = M_{ETH,t} + \left(\frac{(k_{m,VC} X) M_{VC,t} V_L}{K_{cor,VC}\left(1 + \frac{M_{TCE,t}}{K_{cor,TCE}} + \frac{M_{DCE,t}}{K_{cor,DCE}}\right) + M_{VC,t}} \right) \Delta t$$

Where

Eq. S8

$$K_{cor,z} = K_{s,z}\left(V_L + V_G H_{CC,z}\right)$$

The biomass term (X) can represent the concentration of biomass, protein, or cells carrying out the reaction of interest. As the relative proportions of *Dehalococcoides* strains with different metabolic characteristics were assumed to vary within the chemostat over time, the combined k_mX was determined for comparison purposes to highlight changes in the overall dechlorination abilities of the culture.

Equations for biomass growth and decay were not included in this model as their contributions were considered negligible over the time-scale of the kinetic tests. This assumption was tested in a preliminary analysis using published growth and decay constants representative of *Dehalococcoides* species [32]. If all biomass was assumed to be dehalogenators, the net change in biomass concentration would be less than 10% of the total biomass over the length of a PCE-to-ethene experiment. This assumption made k_mX a constant for each data set.

Euler's method, a low-order version of the Taylor series expansion, facilitated use of Excel's Solver function to simultaneously determine the set of Monod parameters (k_mX and K_s) that yield the least-squared error between PCE to ethene rate test data and the model. Constant time steps of 5 minutes were used, and initial conditions for the model were set to match experimental conditions. The initial mass of PCE was set at the average total mass of CAHs and ethene measured during the batch experiments to ameliorate errors in initial PCE measurements due to dissolution time and adsorption to reactor surfaces.

A Newtonian search method was used by Solver to find the Monod parameters for each CAH with a convergence setting of 10^{-4}. This method sequentially perturbed each decision variable (Monod parameters) during an iteration, updated all cells referencing it, then approximated the new Jacobian matrix using finite differences [83]. When the target cell (the sum of squared errors) converged, the Solver routine ended and reported the best-fit parameters. As discussed in the text, a standard set of K_s parameters generally representing the culture was fixed for modeling

purposes, and the k_mX parameters were varied. This ensured unique results for comparison of kinetics over time.

Model Validation: To verify the accuracy of the masses output by the lower-order, constant time step Euler's method model, the dechlorination equations were input to COMSOL 4.1, which used second- to fifth-order Backward Differentiation Formulae (BDF) to determine the time steps when numerically integrating the set of equations. Both models were run using a gas-phase volume of 106 mL, liquid volume of 50 mL, initial PCE mass of 17 μmol, and an initial mass of 0 μmol for all other CAHs. Kinetic parameters were chosen to generally represent the culture in its current state. The standard set of K_s parameters (3.9, 2.8, 1.9, and 11.8 μM for PCE, TCE, cis-DCE, and VC, respectively) and k_mX values of 369, 741, 244, and 220 μM/day for PCE, TCE, cis-DCE, and VC from initial modeling attempts were used.

Over 7200 data points from the model using Euler's method with five-minute time steps were compared to the COMSOL model output, yielding a total standard error of estimate less than 0.16% of the initial CAH mass. These outputs were essentially the same, confirming the accuracy of the Euler-based model.

Batch Reactor Modeling and Verification of Appropriate Parameters

The model described in the previous section was applied to all PCE-to-ethene batch rate tests. A 'standard' set of K_s parameters was established, and consisted of the values determined by Yu et al. {Yu 2005} for PCE (3.9 μM), TCE (2.8 μM), and cis-DCE (1.9 μM), and the K_s of 11.8 μM for VC given the VC Monod results above. This section shows the concentration profiles from each PCE-to-ethene batch rate test with the associated model results, and determines whether the standard set of K_s parameters provided valid k_mX estimates.

Batch Modeling Results with Standard K_s Set

Concentration profiles for PCE-to-ethene batch tests are shown in Figures S3 and S4 for the PM-2L and PM-5L chemostats, respectively. Modeling results (general representation of the data and k_mX values) are discussed in the text.

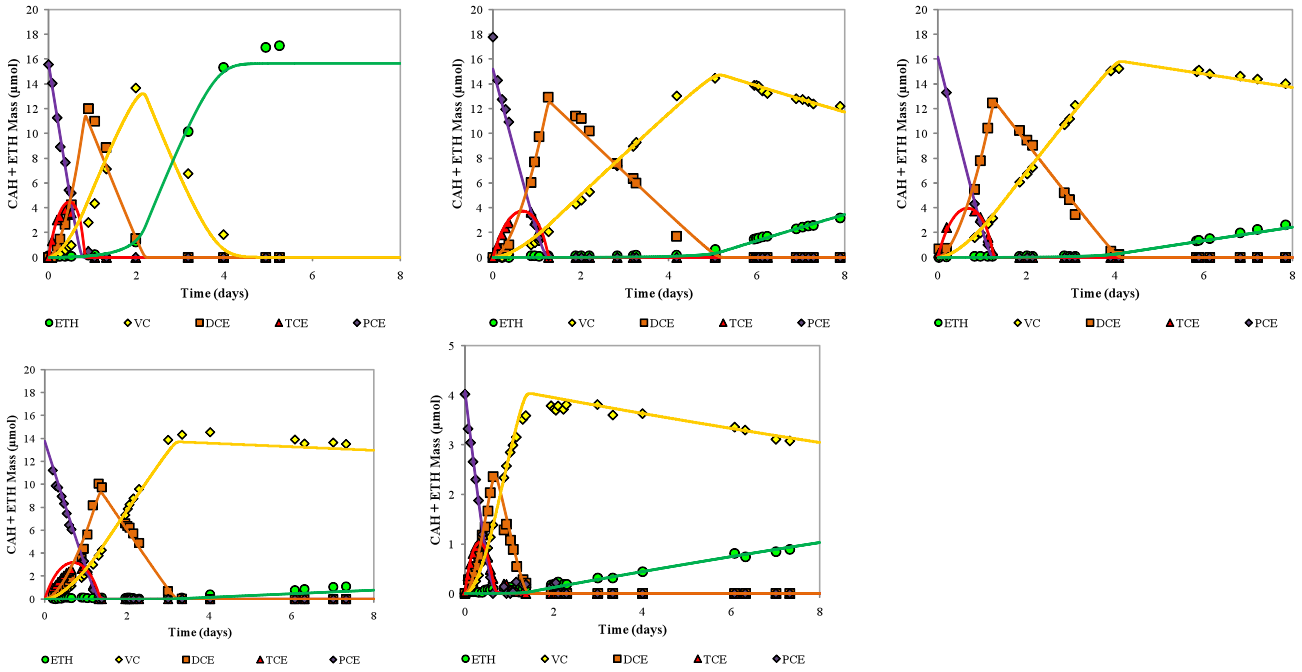

Figure S3: Rate data (symbols) and associated the model fits (lines) using the standard K_s parameter set for the the a) 2L-781 b) 2L-1012, c) 2L-1089, d) 2L-1172 high and e) 2L-1172 low concentration PCE-to-ethene rate experiments. Only one replicate is shown.

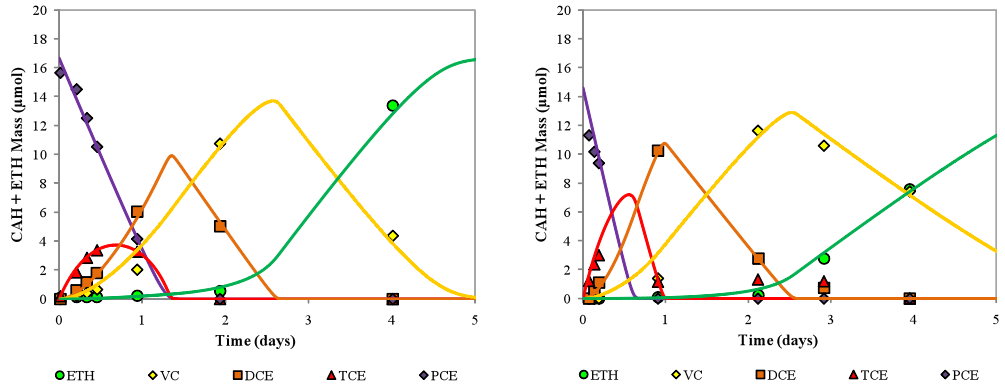

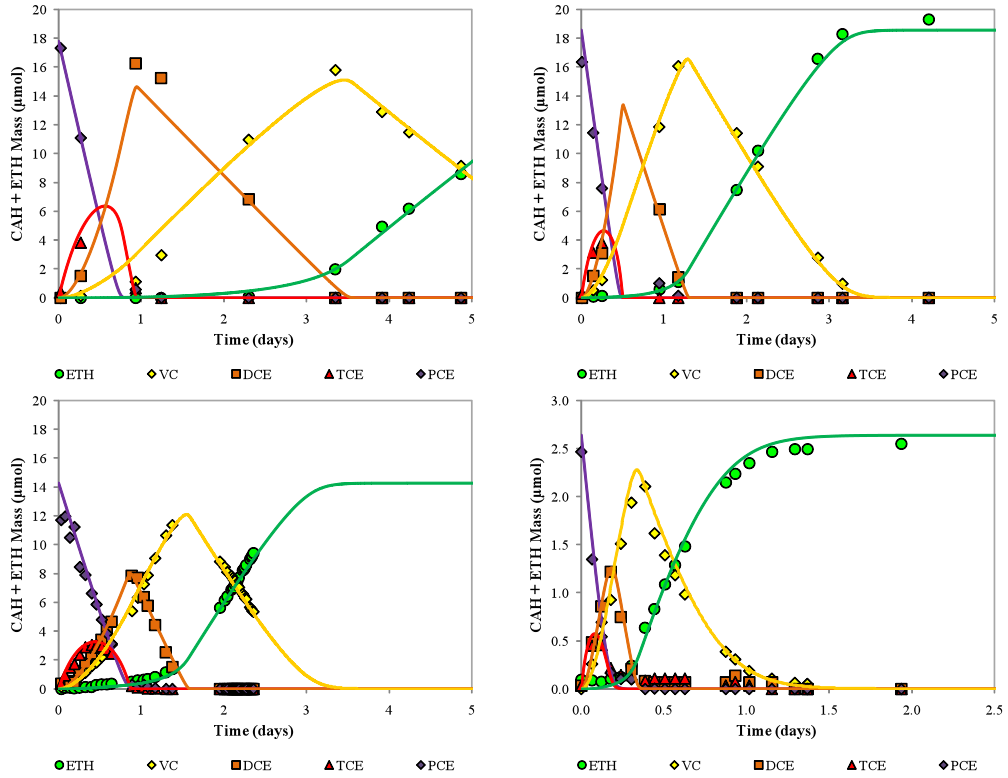

Figure S4: Rate data (symbols) and associated the model fits (lines) using the standard K_s parameter set for the a) 5L-273 b) 5L-343, c) 5L-535, d) 5L-589, e) 5L-638 high concentration, and f) 5L-638 low concentration PCE-to-ethene rate experiments. Only one replicate is shown.

Verification of k_mX and K_s parameters: The applicability of the standard K_s parameter set to the PM culture was verified by two lines of evidence: approximately equal k_mX outputs when the model is applied to data from high- and low-concentration PCE-to-ethene rate tests performed with culture harvested from the chemostat on the same day, and model k_mX output equal to or slightly higher than experimentally-measured maximum dechlorination rates at high CAH concentrations. These two points demonstrate that the model results are broadly applicable (assuming no Haldane or other inhibition is present in the system), and that they have physical significance.

Comparison of model results from a high- and low-concentration rate test: To demonstrate the effect of an unsuitable K_s, the data from both the high- and low-concentration 5L-638 tests were modeled using the standard set of K_s parameters (Table S2), and the standard K_s set with Yu's published $K_{s,VC}$ of 602 µM substituted for the standard $K_{s,VC}$ {Yu 2005}. Model-derived k_mX parameters are presented in Table S2.

Table S2: Comparison of k_mX parameters experimentally measured and those derived using different $K_{s,VC}$ parameters in the Multi-fit Monod Model for 5L-638 data.

CAH	Standard K_s Set	Standard ($K_{s,VC}$= 11.8 µM)		Yu's Published ($K_{s,VC}$= 602 µM)	
		Low-conc. k_mX (µmol/L/day)	High-conc. k_mX (µmol/L/day)	Low-conc. k_mX (µmol/L/day)	High-conc. k_mX (µmol/L/day)

PCE	3.9	347	369	345	368
TCE	2.8	693	739	691	730
cis-DCE	1.9	227	244	223	241
VC	11.8	194	220	5974	2286
SEE	-	3.7%	3.6%	3.9%	3.8%

Both modeling scenarios fit the data well, with similar standard error of estimates (SEE). Yu's $K_{s,VC}$, however, produced a VC curve that slightly overshot the experimental VC concentration peak and grossly overestimated the inhibition of TCE and *cis*-DCE on VC dechlorination as evidenced by the suppressed ethene generation curve (not shown).

High- and low-concentration k_mX outputs compared well for each CAH, except for VC when Yu's published $K_{s,VC}$ was employed. The k_mX for the low- concentration data with Yu's $K_{s,VC}$ is over 2.5 times that of the high-concentration data set, while similar k_mX values were found when the standard $K_{s,VC}$ was used. This demonstrates the suitability of all CAH parameters in the standard K_s set for modeling the PM-5L culture.

A high-and low-concentration test was also performed with culture extracted from the PM-2L chemostat on 2L-1172. Modeling yielded the parameters in Table S3. Both data sets yielded parameters of similar magnitude for all CAHs, indicating that the standard set of K_s parameters employed for modeling provide a reasonable fit to the data. The estimated k_mX parameters for PCE and TCE, however, did show some deviation from one another, suggesting that the microbial community performing these two dechlorination steps likely shifted over time and a different K_s value would better represent these reactions.

Table S3: Comparison of k_mX parameters determined for the 2L-1172 high- and low-concentration rate tests.

CAH	Low-conc. k_mX (µmol/L/day)	High-conc. k_mX (µmol/L/day)
PCE	152	246
TCE	273	476
cis-DCE	77	107
VC	4	5

Low-concentration tests were not performed in conjunction with the other data sets; therefore analysis must be based solely on the correlation of the k_mX parameters determined by the model and the pseudo-k_mX derived from the experimentally-measured maximum rates of reduction.

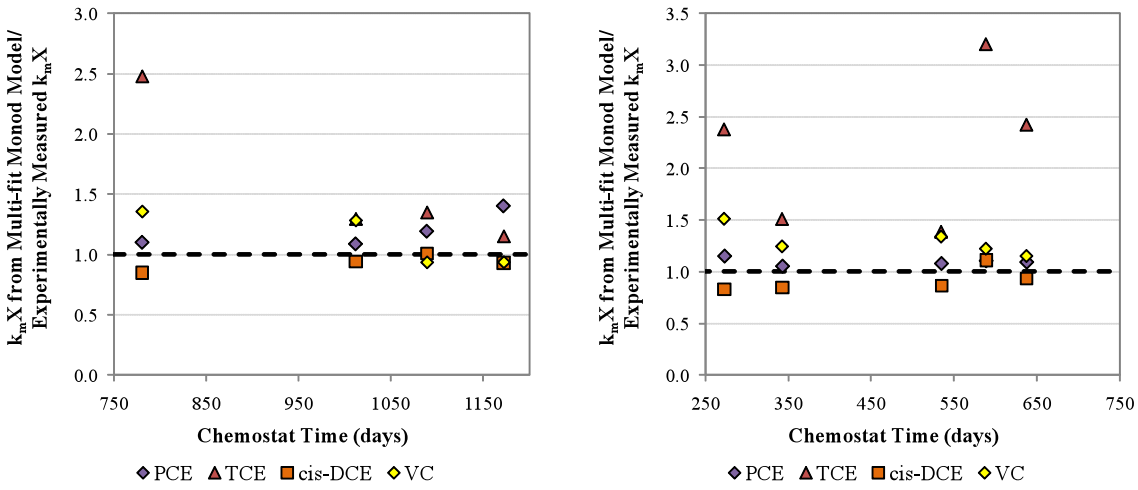

Figure S5: Comparison of k_mX values derived from the model and from experimentally-measured maximum rate for all high-concentration PM-2L (left) and PM-5L (right) experiments.

Sensitivity of Parameter Output to Location of Data Points: PCE-to-ethene batch tests performed to track changes in the kinetics of the PM-5L chemostat culture were not monitored as intensively as the 5L-638 tests, and thus CAH reduction trends were not as well characterized. A limited-data analysis was performed with the high-concentration data sets from the "Intensive" 5L-638 test to determine the range of error in k_mX values derived for the "Limited" data sets (5L-273, 5L-343, 5L-535, and 5L-589). The number of data points from the Intensive 5L-638 test was first reduced in a way that mimicked each Limited test, with each retained point falling in approximately the same stage of transformation as the test to which it was being compared. After the 5L-638 limited-data set was created, the model was applied, yielding a new best-fit k_mX. These new values were then compared to the parameters found using the full 5L-638 data set.

The percent difference between the full- and limited- data model results averaged around 3.5%, with all values falling below 10% except the k_mX estimate for TCE in the 5L-535 analysis (23%). The low magnitude percent differences suggest that all Limited data sets were sufficiently characterized for accurate analysis with the model except for the early stages of 5L-535. This larger error is believed to be due to the lack of data spanning the initial 24 hours of the experiment (Figure S3c), leaving the PCE and TCE reduction trends relatively uncharacterized.

Long-Term Batch Incubations to Enrich for Different Populations

Introduction

Two sets of long-term incubations were performed using culture from the PM-5L chemostat to elucidate the potential causes of the kinetic and molecular changes observed in the PM-2L chemostat following sulfate addition. Having had a shared history, the microbial community in the PM-5L control chemostat was assumed to well represent the state of the PM-2L chemostat culture prior to the addition of sulfate. Changes observed in the PM-5L culture in the long-term batch

incubations could then be compared with changes in the continuous PM-2L chemostat to help elucidate the influencing factors for decreased dechlorination rates in the PM-2L chemostat.

Batch reactors were maintained as either single- or dual-electron acceptor reactors, receiving periodic injections of the initial electron acceptor(s) and donor over the incubation period. Four types of batch incubations were prepared as detailed in the methods section: "S" reactors received sequential additions of sodium sulfate, "P" reactors received PCE, and "SP" reactors received both sulfate and PCE as a electron acceptors at each feeding, while "PAS" reactors received PCE at each feeding and an initial dose of abiotic sulfide. These reactors were constructed to determine whether:

- sulfate reduction would occur at the same rate in the presences and absence of CAH dechlorination
- efficient VC dechlorination would continue in the presence and/or absence of sulfate reduction
- the addition of abiotic sulfide to reactors only reducing CAHs would yield the same CAH dechlorination patterns as the reactor reducing both CAHs and sulfate
- molecular results could clarify trends seen in the kinetics of the single- and dual-electron acceptor reactors
- trends in both kinetics and the *Dehalococcoides* community structure of the SP and/or PAS batch reactors would resemble those seen in the PM-2L chemostat

Additionally, by carrying out these experiments at non-limiting electron donor concentrations, we may further suggest that the changes in the PM-2L chemostat performance following sulfate addition were not primarily due to competition for the electron donor.

1) Methods

Batch experiments were carried out in 125-mL Borosilicate glass reactors fitted with phenolic screw-on caps with gray chlorobutyl rubber septa (Wheaton Industries, Millville, NJ). Before use, these batch reactors were stored open in an anaerobic hood (90%N_2, 10% H_2) to ensure all oxygen was removed from the system. Reactors were tightly sealed and transferred out of the hood immediately before use. Fifty-mL of culture was anaerobically transferred from the chemostat under investigation into each batch reactor via the PEEK tubing. Each reactor was then purged with a furnace treated 75:25 Ar/CO_2 (or 75:25 N_2/CO_2) gas mixture (Airco, Inc. (Albany, OR)) for 15-20 minutes to remove any residual CAHs, ethene, or H_2 from the transfer. Reactors were amended as specified in the following paragraphs. The reactors then were incubated at 20°C and continuous shaking at 200 rpm to maintain gas/liquid equilibrium. PCE and transformation products, H_2, sulfate, sulfide, and organic acids (propionic and acetic) concentrations were tracked over time using the methods described in Section 2).

Culture was harvested from the PM-5L chemostat on days 5L-273 and 5L-535to initiate the Set 273 and Set 535 incubations. These harvest time points fell just prior to, and well into, the long-term steady-state of the PM-5L chemostat history where PCE dechlorination to ethene was 87%

and 98% complete, respectively. These incubations were prepared to enrich different populations in the culture (dehalogenating ["P"], sulfate reducing ["S"], sulfide-tolerant dehalogenators ["PAS"], and combination of sulfate and dehalogenating microbes ["SP"]), and to elucidate the cause of the changes observed in the performance of the PM-2L competitive chemostat. Batch incubations were prepared as summarized in Table S4 from the purged batch reactors described above.

Table S4: Initial augmentation of long-term batch incubation reactors.

Reactors	SO_4^{2-}	PCE	$S^=$	H_2
-	µmol	µmol[a]	mg/L	% atm.
P-273 & P-535	-	15 / 18	-	1.8
S-273	17	-	-	1.8
SP-273 & SP-535	17	15 / 18	-	1.8
PAS-535	-		7	1.8

[a]PCE masses are provided for the Set 273 and Set 535 reactors, respectively, separated by a forward slash.

Neat PCE (99%, Alfa Aesar), a 228 mM Na_2SO_4 solution in media, and a 300 mg/L Na_2S solution in media were used for amendments where appropriate. Sulfate and PCE were added to achieve an initial electron accepting equivalent ratio similar to that of the PM-2L influent assuming sulfate was reduced to sulfide and PCE was reduced to ethene. Hydrogen (82 µmols) was also injected to the headspace of every bottle, creating an initial H_2 liquid concentration around 15 µM.

Each incubation was carried out in duplicate. Hydrogen was added whenever aqueous concentrations neared 1000 nM, and bottles were restimulated to their initial PCE and sulfate levels after PCE and sulfate had been completely reduced to VC, ethene, and sulfide in all bottles. Acetate concentrations were measured at approximately every restimulation, and sulfide concentrations every third restimulation (for Set 535 only).

After 44-46 days (and eight to ten restimulations), all reactors were subjected to the same dual-electron acceptor composition as the SP bottles, i.e. 18 µmols of PCE and 17 µmols of sulfate were added to all reactors. The reactors were sacrificed for molecular analysis 1.2 days into the dual substrate experiment. The cells were transferred to a 50 mL polypropylene Falcon tubes, then centrifuged for 30 minutes at 9000 rpm and 4°C. Supernatant was decanted, and the pellet stored at -80°C. An initial cell sample was also collected from the chemostat in this same manner at the time the culture was harvested for the batch experiments.

Set 273 was composed of duplicate P, S, and SP reactors (denoted P-273, S-273, and SP-273, respectively). The P and SP incubations were replicated in Set 535 (P-535 and SP-535, respectively), and an additional reactor, PAS (PAS-535), was also prepared for Set 535. No liquid or gas was added to the reactors during the incubation beside these substrates. Only the liquid and headspace gas necessary for sampling was removed, therefore, VC, ethene, and sulfide accumulated within the reactor. Details of the electron acceptor mass per feeding and total mass added over the 45-47 day lifetime of the reactors are recorded in Table A1.

Both PCE and sulfate require 8 eeq/mol to be completely reduced. Sulfate and PCE were added in a nearly 1-to-1 molar ratio in the Set 273 reactors, providing equal opportunity to accept electrons assuming sulfate was reduced to sulfide and PCE was reduced to ethene. In the Set 535 reactors,

the sulfate-to- PCE ratio was reduced to around 55% to clarify the role of competition between these two electron acceptors when incubated with non-limiting H_2.

The temporal chloroethene composition of the reactors recorded over the experimental period was used to determine the change in reaction rates over time. For each PCE-to-ethene dechlorination cycle, the Multi-fit Monod model was applied to estimate a k_mX for each step of CAH reduction assuming the standard set of K_s values generally represented the culture. DNA and RNA was extracted from cell pellets obtained from each reactor at the end of experimentation. An initial cell sample from the chemostat was also analyzed. The DNA and RNA extraction and analysis was performed by Ian P.G. Marshall. A combination of results from application of the H2ase Chip DNA reductase gene microarray, a clone library, and qPCR are presented. These methods elucidated the population shifts in key dechlorinating and sulfate-reducing populations in each culture, the relative distribution of *Dehalococcoides* strain relatives present, and their dechlorinating activity.

2) Chemical Trends

Trends in the chemical composition of each batch reactor over its lifetime will be highlighted in the following section. As replicate reactors produced nearly identical results, only one replicate is shown in the figures.

i. Sulfate-Only Reactors

Reactors receiving only sulfate as an electron acceptor (S-273) showed slow sulfate reduction rates during the first four days of incubation. Essentially complete sulfate reduction was observed within nine days as illustrated in Figure P.1a. Thereafter, sulfate reduction rates were rapid, averaging 15 μmol/day. H_2 utilization was minimal during the first nine days (Figure P.1b); however, uptake rates increased thereafter due to both active sulfate reduction and homoacetogenesis. Homoacetogenic activity was indicated by the gradual increase of acetate in the reactor from 4.2 mM on day 9 to 8.8 mM at the end of the 45 day experimental period (Figure P.1b). This was also demonstrated in the cumulative electron balance for the reactor presented in Figure P.2. During the dual-substrate experiment, initiated on day 44, sulfate reduction carried on at the same rate as previous injections, and no PCE reduction products were observed (data not shown). The mass of PCE itself decreased from around 16 μmol to 8 μmol at a rate of 6.0 μmol/day, which is near that observed in abiotic controls (4.3 μmol/day, data not shown). This decline in observed PCE mass is primarily attributed to adsorption of PCE to the septa and other components of the reactor.

ii. PCE-Only Reactors

PCE-only reactors (P-273 and P-535) yielded the chemical trends displayed in Figures P.3 and P.4, respectively. In P-273, each PCE injection was dechlorinated to ethene, with VC reduction only occurring when higher chlorinated ethenes were reduced to low concentrations (Figure P.3a). Ethene accumulated in the reactors. The maximum TCE, cis-DCE, and VC concentrations were 50, 95, and 70 to 95 μM, respectively, during each feeding cycle. H_2 utilization increased within the first ten days of the incubation, likely due to rising homoacetogenic activity indicated by an increase in acetate concentration from 4.2 mM to around 8.5 mM over the 45 day experimental period (Figure P.3b). No sulfate reduction was observed in the 1.2 days of the dual-substrate experiment initiated on day 44 (data not shown). Dechlorination rates were not affected by the presence of sulfate (Figure P.3a).

The P-535 experiment was designed to replicate the P-273 experiment, with injections of PCE scheduled to occur on the same experimental day as those in the previous experiment. Due to an oversight in experimental design, each PCE injection contained an additional 3 μmol of PCE compared to the P-273 experiment. This resulted in a longer dechlorination cycle compared to P-273 and less VC reduction time in the absence of the more-chlorinated ethenes. Initially, PCE was completely dechlorinated to ethene (Figure P.4a). After the fourth PCE injection, accumulation of VC was evident. Ethene production then decreased from an average rate of 5.4 to 1.9 μmol/day. The maximum TCE and cis-DCE mass observed during each feeding cycle was near 50 and 240 μmols, respectively. Acetogenesis activity proceeded more rapidly in P-535 than P-273, resulting in very rapid H_2 utilization (Figure P.4b). The acetate concentration remained steady around 3.1 mM for the first 12 days, then rapidly increased to a final concentration of 26 mM. The increase in homoacetogenic activity between Set-273 and Set-535 is highlighted in the electron balance for the reactor presented in Figure P.5, where the green bars represent the cumulative amount of electrons directed toward acetate formation. The percentage of electrons used for acetate formation in P-273 remained low compared to the approximate 50% of electrons captured in acetate in P-535. It is not known why homoacetogenic activity was stimulated in the Set-535 reactors. No sulfate reduction was observed in the 1.2 days of the dual-substrate experiment (data not shown). CAH dechlorination did not appear to be affected by the presence of sulfate.

iii. Sulfate and PCE Reactors

The dual substrate reactors (SP-273 and SP-535) showed co-current sulfate and CAH reduction. Both sets had very similar outcomes as illustrated in Figures P.6 through P.9. Initially, PCE was readily dechlorinated to ethene in both SP-273 and SP-535 (Figures 6a and 8a). VC accumulation became apparent after the third complete PCE reduction cycle in both SP-273 and SP-535. The accumulation of VC followed complete reduction of the initial sulfate addition (around 10 days), and ethene accumulation slowed thereafter. After four cycles of PCE and sulfate addition, TCE and cis-DCE dechlorination rates increased relative to PCE and VC dechlorination rates. By day 30, TCE and cis-DCE no longer accumulated to measurable concentrations, while VC and ethene continued to accumulate. A final mass of VC around 87 μmols (517μM) and ethene around 56 μmols (51 μM) was measured at the end of SP-273, and 35 μmols (237 μM) and 5 μmols (6 μM) at the end of SP-535 for VC and ethene, respectively. This lower final mass in SP-535 is due to the reactor headspace purge on day 31.

Negligible sulfate reduction was observed for the first 4 to 9 days of incubation, but complete reduction of the first sulfate addition was attained within 12 days (Figures P.6b and P.8b). Sulfate reduction rates were then rapid, exhibiting a range similar to that of the sulfate-only S-273 reactors (Figure P.1a). Dissolved sulfide concentrations were not measured in the original Set 273 experiments; however, the SP-535 reactors showed an increase to 4.2 mg/L sulfide by day 12, and reached a maximum of 9.1 mg/L on day 31 (Figure P.8b). Sulfide was partially stripped from the system as hydrogen sulfide when the headspace was purged on day 31 of the Set 535 experiment, but recovered to nearly 8 mg/L before the end of experimentation.

Acetate patterns differed between the two sets. In SP-273, the acetate concentration gradually increased to a maximum of 6 mM near day 25, then appeared to decrease again to its initial level, suggesting that the sulfate reducers may have developed the ability to preferentially use acetate (Figure P.7). The acetate concentration in SP-535 reactors remained steady for the first 19 days, then rapidly began to increase to a final concentration near 23 mM (Figure P.9). This was accompanied by significantly more rapid H_2 utilization rates compared to the SP-273 reactor. Like that for the PCE-only reactors, the electron balance shows significant homoacetogenic activity in SP-535 relative to SP-273 (Figure P.10). No oxidation of acetate is believed to occur in this reactor. Acetogenesis was delayed in SP-535 relative to the P-535 and PAS-535 reactors (Figure P.4b and P.11b), but once initiated, the acetate production rates were all similar.

iv. Sulfide and PCE Reactors

During sulfate reduction, sulfide is produced. Literature has cited sulfide as a potential inhibitor of cis-DCE and VC dechlorination. Therefore, the PAS-535 reactor was constructed to differentiate the effect of the sulfate reduction process itself from the potentially inhibitory effects of the sulfide product. The chemical composition of this PCE-dechlorinating reactor containing abiotic sulfide is shown in Figures P.11 and P.12. The target dissolved sulfide concentration was equivalent to the sulfide produced from one addition of sulfate. Approximately 7 mg/L of sulfide was measured initially, and the concentration steadily declined to around 0.9 mg/L over the course of the experiment (Figure P.12). Only a small portion of sulfide was stripped out of the system in the purging process. CAH reduction was almost identical to that in the SP-535 reactors (Figure P.8a), with the only notable difference being a lack of VC reduction during the initial injection cycle just after sulfide was added (Figure P.12). The reactor headspace was also purged with N_2/CO_2 (75:25) gas on day 31, removing around 75 µmol VC and 40 µmol ethene. At the end of experimentation, the reactor contained 107 µmols (733µM) VC and 43µmols (48 µM) ethene. Like other Set 535 reactors, the acetate concentration remained steady at 3.1 mM for the first 12 days, then rapidly increased to 26 mM (Figure P.11b). The electron balance (Figure P.13) was very similar to other Set- 535 reactors. Similar to the P-273 and P-535 reactors (Figures P.2c and P.3c, respectively), no sulfate reduction was evident during the final 1.2 day dual-substrate phase, while dechlorination proceeded in a manner similar to previous feeding cycles.

3) Reduction Rates

The rates of chloroethene reduction and sulfate reduction were compared between the single- and dual-electron acceptor reactors to determine how the dechlorination affected sulfate reduction and vice versa. The effect of dechlorination of sulfate reduction was analyzed first.

Linear regression analysis was used to determine the rate of sulfate reduction for each sequential addition of sulfate in the S-273 sulfate-only and the SP-273 dual electron acceptor reactors. Average rates of sulfate reduction for the duplicate reactors were then calculated. The ratio between the average sulfate reduction rates of S-273 and SP-273 reactors is presented in Figure P.14. With the value of the rate-ratio centered around unity, the sulfate reduction rates did not differ significantly between the sulfate-only reactors and those reducing both sulfate and CAHs in the Set 273 experiments. Active dechlorination therefore did not appear to affect sulfate reduction.

To compare the trends of CAH reduction in the P and SP reactors, the Multi-fit Monod model was used. The masses of each CAH present at the beginning of a PCE-reduction cycle were entered as the initial conditions. The standard set of K_s values were used. As in previous chapters, growth was considered insignificant over one reduction cycle; however, there were changes in biomass concentration over the lifetime of the reactors. For this reason, k_mX values were compared between reactors instead of normalizing to an undefined total protein concentration.

An example of the Multi-fit Monod Model output for the initial, fourth, and ninth PCE dechlorination cycle of the P-273 and SP-273 experiments are displayed in Figures P.15 and P.16. The model was capable of fitting the data from each step very well, producing approximate k_mX parameters associated with the standard set of K_s values for each CAH. The k_mX parameters output for each PCE dechlorination cycle were used to determine whether sulfate reduction affected any step of CAH reduction, by plotting the ratio of the parameters generated for the P and SP reactors. For the Set 273 data (Figure P.17), the ratio of k_mX values for PCE, TCE, and cis-DCE were around unity, while that of VC increased dramatically with time. This trend was also observed with the Set 535 data in Figure P.18. These trends indicate that the rates of PCE, TCE, and cis-DCE dechlorination are not significantly affected by sulfate reduction, while VC dechlorination rates decreased dramatically with each sequential dechlorination cycle in the reactors reducing both sulfate and CAHs relative to those just reducing CAHs.

To determine whether this effect on VC reduction was primarily attributed to sulfate reduction itself or to the sulfide product, abiotic sulfide was added to a reactor only reducing CAHs. As discussed in the previous section and presented in Figures P.8 and P.11, the SP-535 and PAS-535 reactors showed similar patterns of CAH reduction. This was further demonstrated through this

rate analysis, where the ratio of PAS-535 k_mX output values to that of the SP-535 were around unity for all CAHs (Figure P.19), including VC. These results indicate that sulfide accumulation was the likely factor causing the decline in VC reduction efficiency in this culture. As a single, low dose of abiotic sulfide was added to the PAS-535 reactor at the beginning of the experiment, the gradual decrease in VC reduction is not likely due to increasing sulfide concentrations with time (as occurred in the SP-535 reactor). It is more likely attributed to a gradual shift in the dechlorinating population due to the presence of sulfide, as will be shown in the molecular analysis of the reactors. Dechlorinators that are more sulfide-tolerant, or that grow better in the geochemical environment created with sulfide presence, but are not capable of efficient VC dechlorination, were likely enriched.

4) Molecular Analysis

Molecular analyses of the cell pellets collected at the end of the incubations were used to elucidate the factors involved in the differing kinetic trends of the single- and dual-electron acceptor reactors. An initial analysis with the H2ase chip revealed that the dechlorinating population was composed of *Dehalococcoides* and *Desulfitobacterium,* while *Desulfovibrio* were responsible for sulfate reduction. qPCR was used to quantify the relative concentrations of the dechlorinating species for the culture associated with the Set 273 incubations.

The distributions based on gene copy numbers are shown in Figure P.20. The total concentration of dechlorinating species increased in the PCE-dechlorinating P-273 reactor and decreased in the CAH-free S-273 reactor relative to the chemostat sample collected at the time of reactor preparation (5L-273). This is consistent with the increased rates of CAH reduction in the P-273 reactor (Figure P.1) and the low, possibly negligible CAH reduction observed in the S-273 reactors during the 1.2 day dual-substrate incubation (data not shown). The reactor containing both electron acceptors (SP-273) had a concentration of dechlorinating species in between that of the P-273 and S-273 reactors, indicating that sulfate reduction did, in some manner, impact the growth of dechlorinating microbial population. This further corroborates the slowing of VC dechlorination rates in the SP-273 reactor relative to the P-273 reactor (Figure P.17).

In every case, the concentration of *Dehalococcoides* was higher than that of *Desulfitobacterium*. *Desulfitobacterium* sp. generally dechlorinate PCE and TCE to cis-DCE. Many *Dehalococcoides* strains are metabolically capable of carrying out a greater extent of the PCE dechlorination series.

To determine what *Dehalococcoides* strain relatives were present in the PM-5L culture, further analysis with the H2ase chip and clone libraries were performed. Figure P.21 shows an approximate distribution of the *Dehalococcoides* population based on the bright probe intensity of related hupL gene indicators on the H2ase chip. A relative to strain-195, which has been shown to only co-metabolically reduce VC, was present in every sample. Interestingly, during the incubation period, the P-273 and the S-273 reactors did not undergo a shift from their original distribution of *Dehalococcoides* strain relatives. However, a strain-195 relative was favored in the SP-273 reactors.

CBDB1/GT and BAV1 are known to have very similar hupL sequences, potentially leading to cross-hybridization on the microarray. The nearly equal proportions of CBDB1/GT and BAV1 suggest

that cross-hybridization did occur; therefore, these two categories may represent the same strain relative. Further information is necessary to distinguish between these three strain relatives.

Clone library analysis of the Set 535 culture supported results obtained in the Set 273 experiment. As shown in Figure P.22, P-535 reactors remained fairly close to the initial chemostat *Dehalococcoides* community composition (5L-535), while SP-535 underwent a significant shift to a 195-like strain. Interestingly, a shift of similar magnitude was determined for the PAS-535 reactor.

This shift in the *Dehalococcoides* species relative distribution was also observed in the clone library analysis of the dual-substrate PM-2L chemostat culture at various time points before and after the addition of sulfate displayed in Figure P.23. Rates of VC reduction in short-term, sulfate- and sulfide-free batch experiments using culture harvested directly from the PM-2L chemostat at various time points gradually slowed following the addition of sulfate to the chemostat on day 2L-731, similar to the effect observed in the SP-273, SP-535, and PAS-535 batch reactors. However, sulfate was actively reduced for over nearly 200 days before a major change in both *Dehalococcoides* community structure and CAH dechlorination efficiency was observed. This change coincided with a significant increase in the extent of sulfate reduction within the chemostat. These results indicate that sulfide triggers a slow shift in the *Dehalococcoides* community to one more enriched in a 195-like strain regardless of H_2 abundance or active sulfate reduction.

Kinetic data and molecular results were compared to further explain the effect of sulfide on the deteriorating capacity for VC reduction. Kinetic data showed a gradual decrease in rates of VC reduction in both SP-535 and PAS-535 reactors, suggesting that sulfide was not toxic to the reduction process itself, but created an environment that favored the relative growth of a strain-195 relative. Strain-195 co-metabolically reduces VC, and therefore, more slowly carries out the reduction process. This relative may have similar metabolic capabilities. The selection pressure associated with sulfide may be the elevated sulfide concentration alone, or may be attributed to the sequestration of trace metals necessary for growth of the VC-reducing strains through precipitation with sulfide. Further experimental work is required to illuminate the key selection pressure for these *Dehalococcoides* strains.

Table A1: Actual substrate additions over the incubation period (45-47 days) for each reactor.

Exp. Reactors	Restimulation Levels			Total Augmentations			Total Approx. Mass Added		
	SO_4^{2-}	PCE	H_2	SO_4^{2-}	PCE	H_2	SO_4^{2-}	PCE	H_2
-	µmol	µmol	% atm.	-	-	-	µmol	µmol	µmol
P-273	-	15	1.8	1	11	26	16	165	2130
S-273	17	-	1.8	10	1	26	170	16	2130
SP-273	17	15	1.8	9	10	24	156	150	1890
P-535	-	18	1.8	1	9	53	10	165	6110
SP-535	10	18	1.8	8	9	52	84	165	5945
PAS-535	-	18	1.8	1	9	54	10	165	6230

Exp. Reactors	Remnants					
	SO4 remaining	ETH Remaining	VC Remaining	cDCE Remaining	TCE remaining	PCE Remaining
-	µmol	µmol	µmol	µmol	µmol	µmol
P-273	16	154	11	0.0	0.0	0.0
S-273	0.0	0.8	0.0	0.0	0.3	5.4
SP-273	0.0	56	88	0.0	0.2	6.4
P-535	10	80	69	0.2	0.3	9.3
SP-535	0.0	43	105	0.0	0.2	9.8
PAS-535	10	43	107	0.4	0.6	10.5

Table A2: Actual electron balances over the incubation period (45-47 days) for each reactor.

Reactor	Electrons to SO_4	Electrons to CAHs	Electrons to acetate	Unaccounted
-	%	%	%	%
P-273	0%	31%	23%	46%
S-273	32%	0%	15%	53%
SP-273	33%	26%	-8%	49%
P-535	0%	9%	56%	36%
SP-535	6%	8%	53%	34%
PAS-535	0%	8%	49%	43%

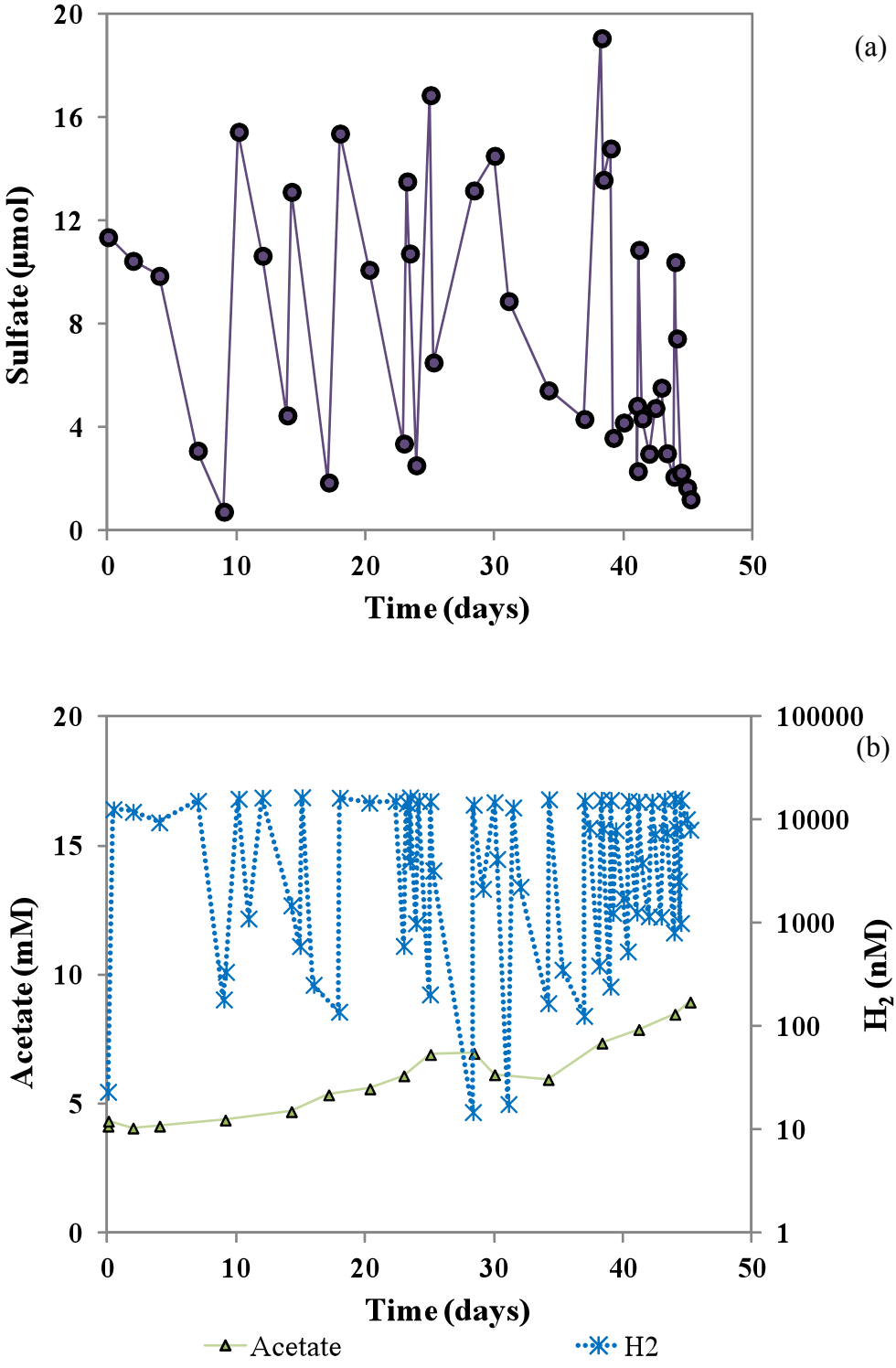

Figure P.1: Time course of S-273 experiments.

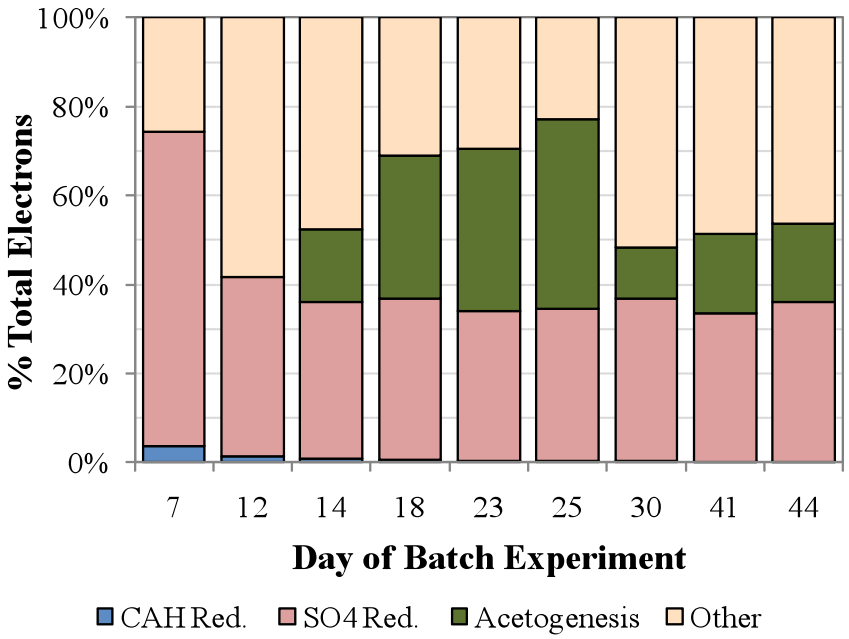

Figure P.2: Cumulative electron balance for the S-273 reactor.

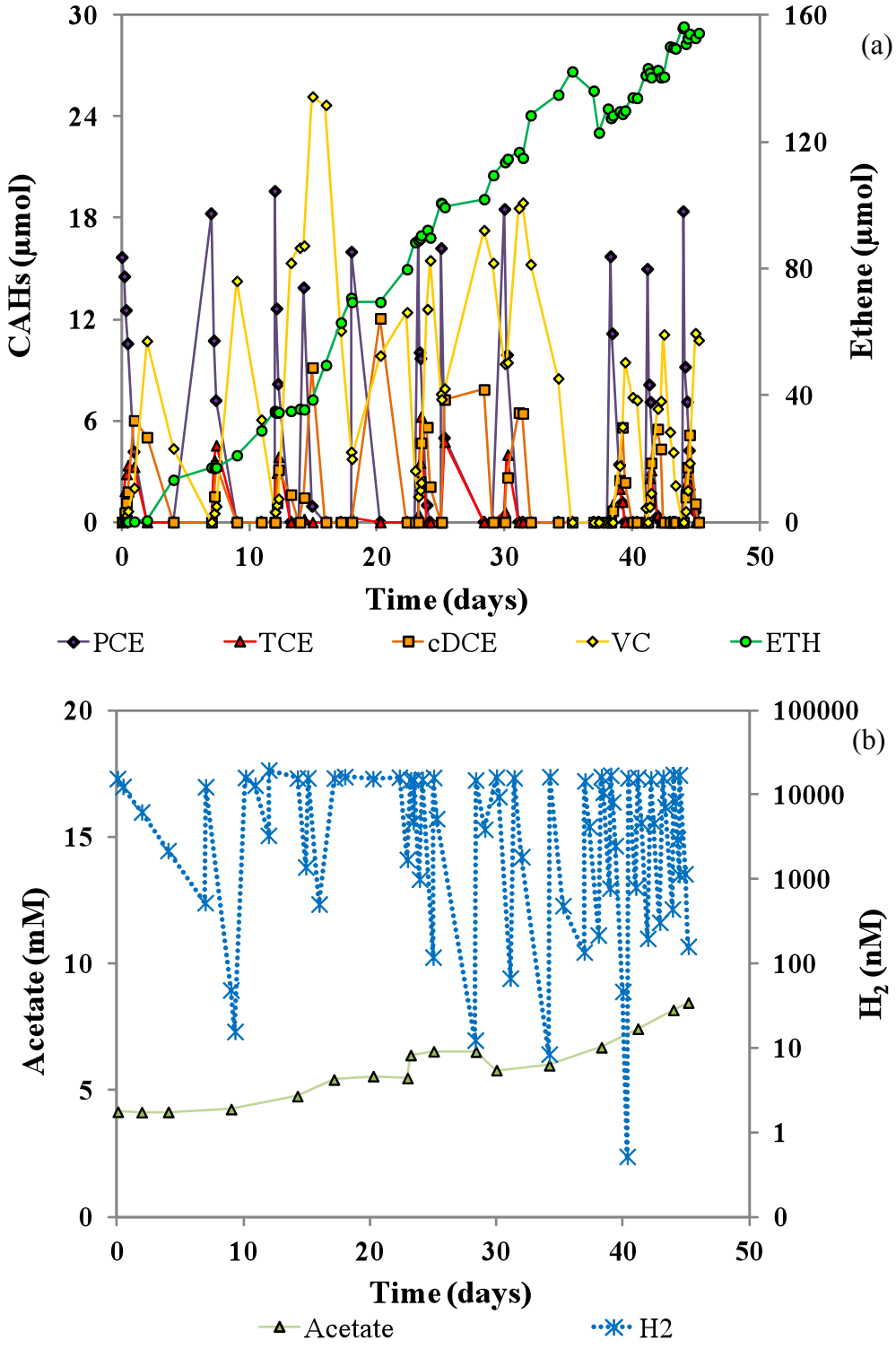

Figure P.3: Time course of P-273 experiment.

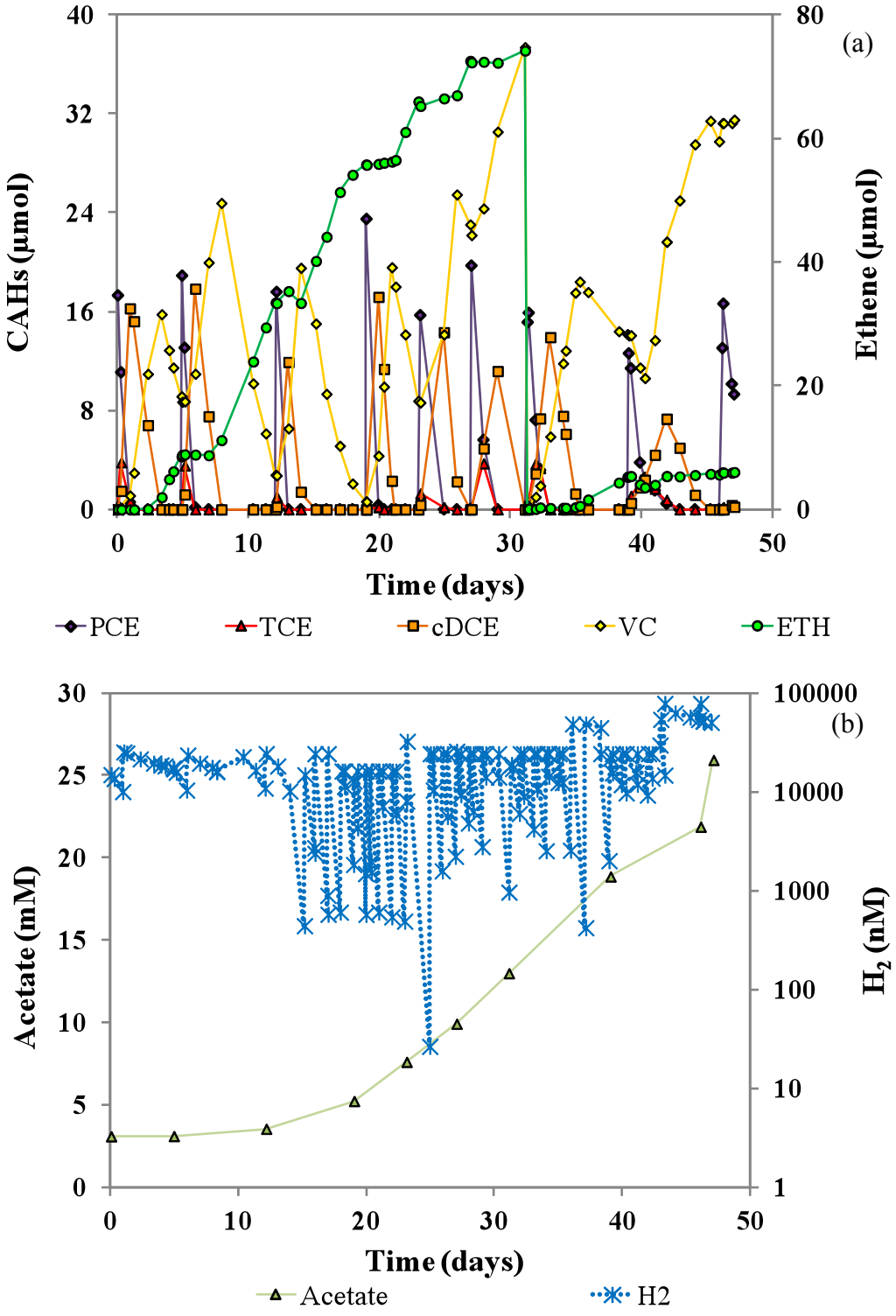

Figure P.4: Time course of P-535 experiments.

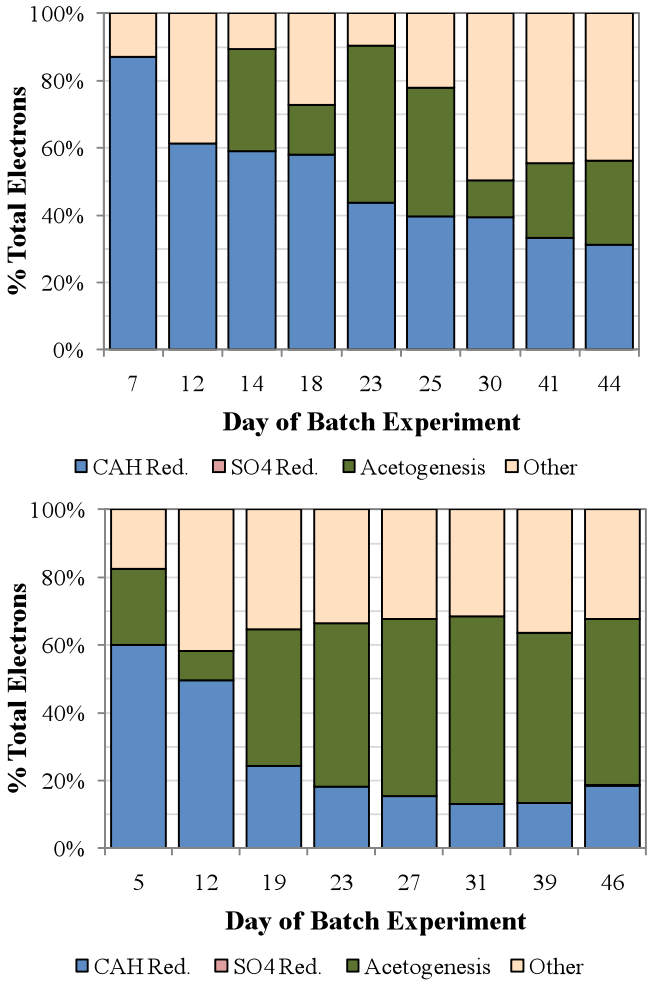

Figure P.5: Electron balances for the P-273 (left) and P-535 (right) reactors

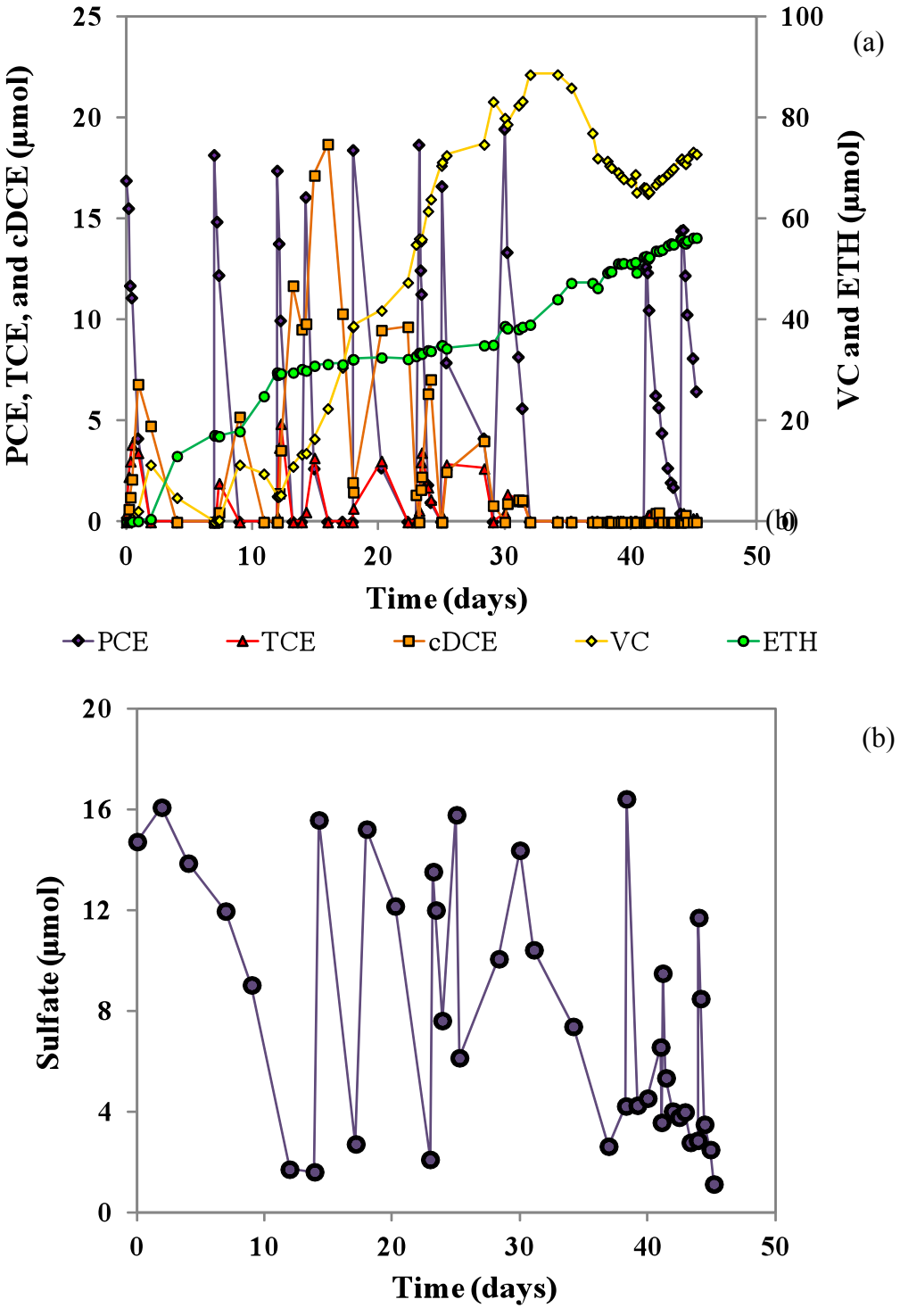

Figure P.6: Time course of SP-273 experiments.

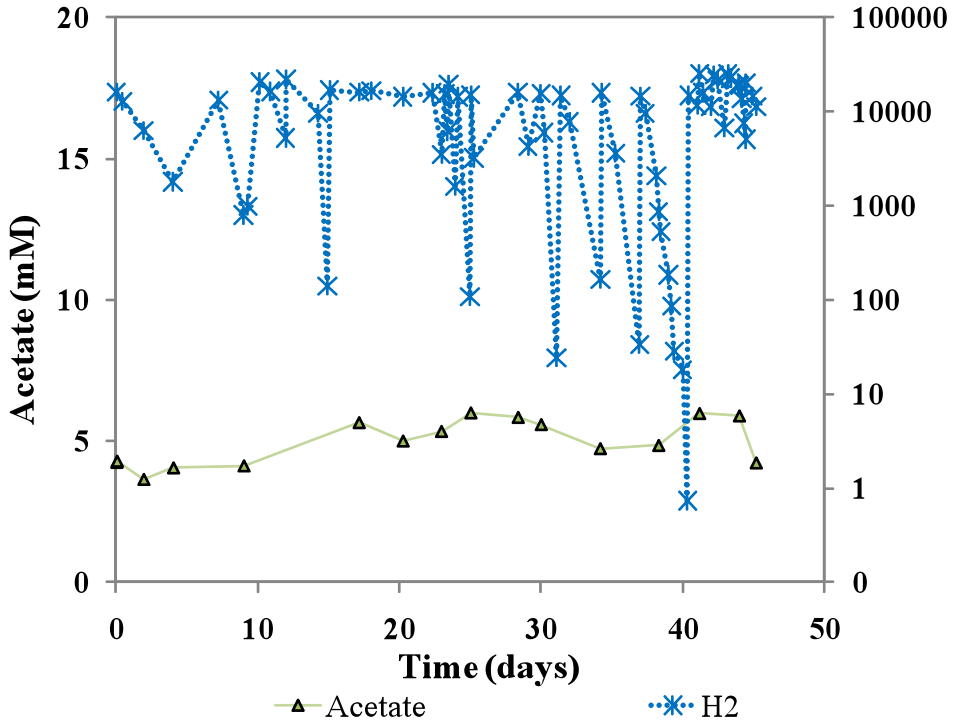

Figure P.7: Time course of SP-273 experiments.

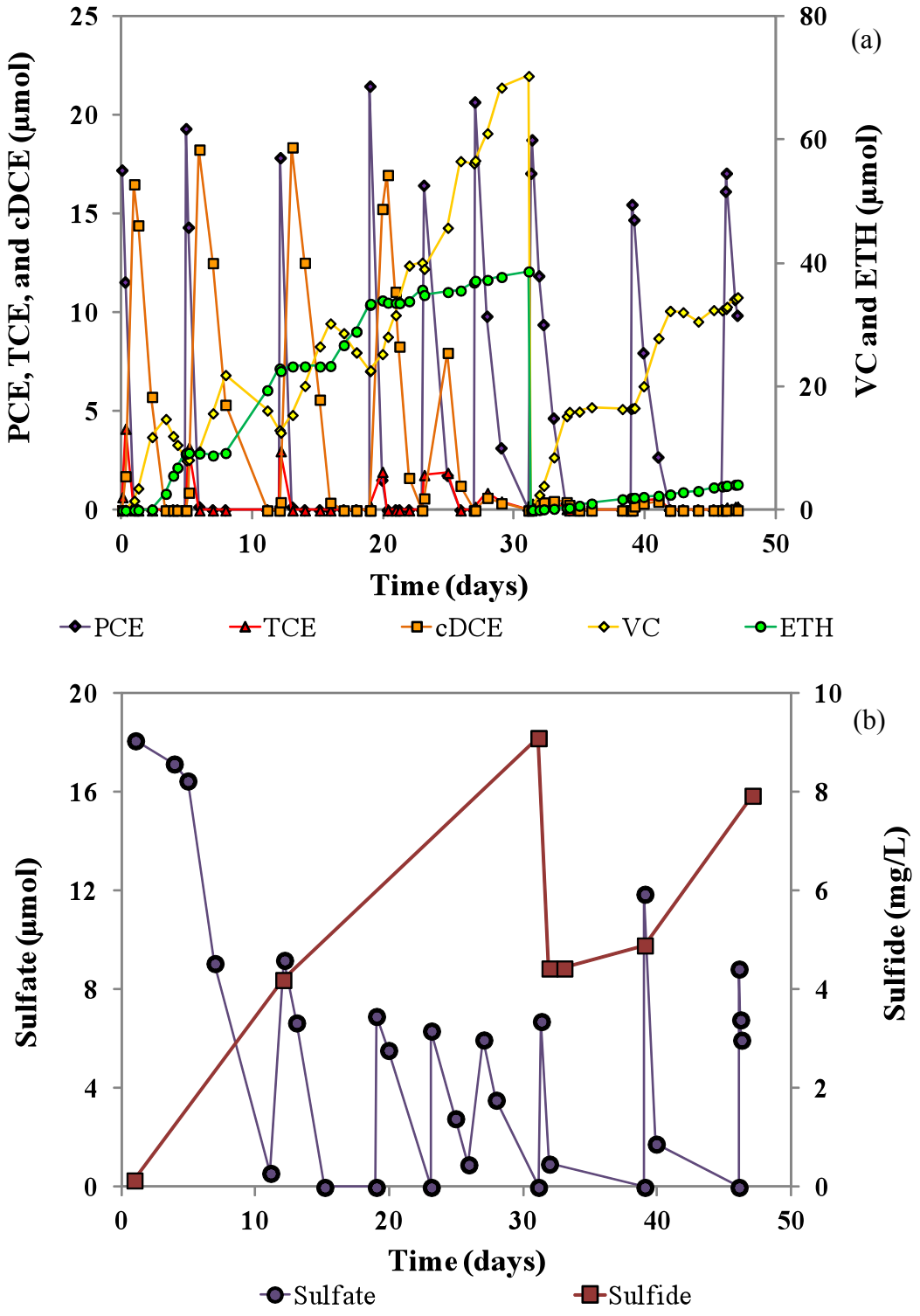

Figure P.8: Time course of SP-535 experiments.

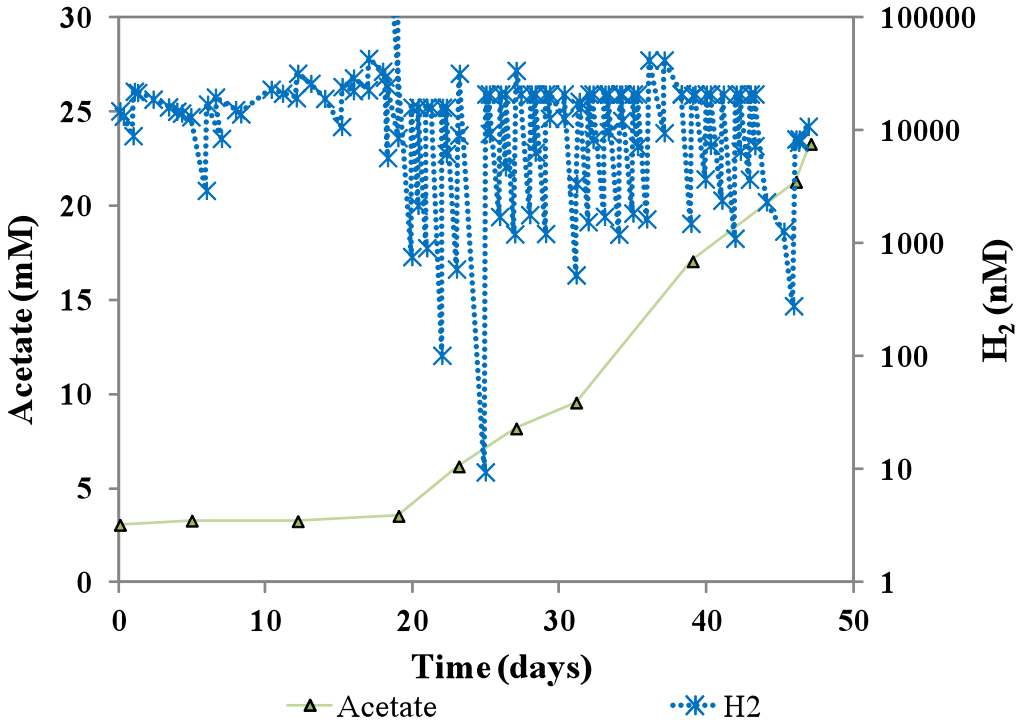

Figure P.9: Time course of SP-535 experiment.

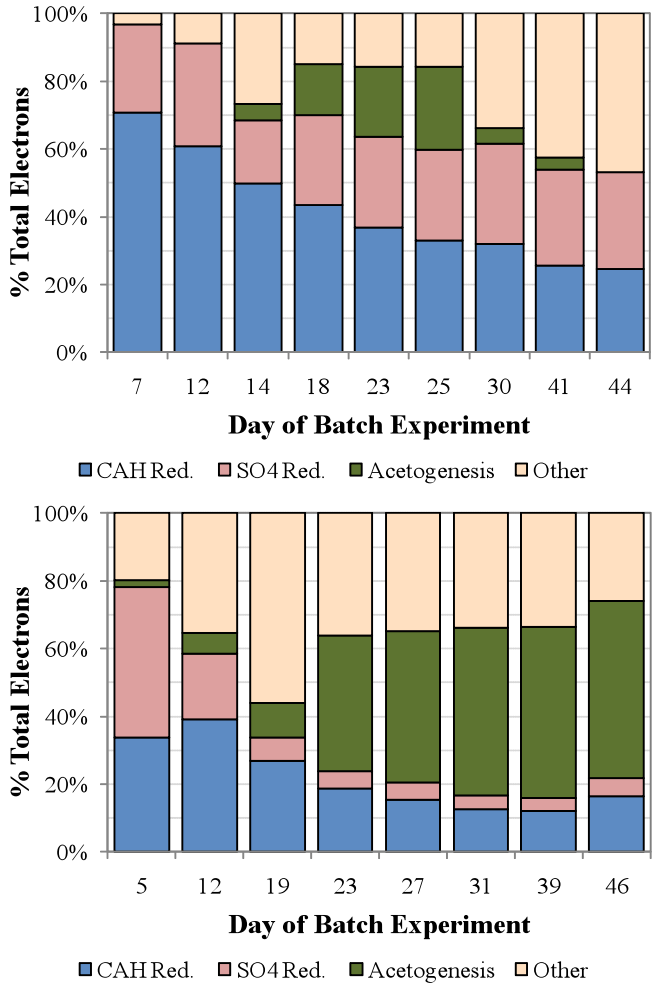

Figure P.10: Electron balance for the SP-273(left) andSP-535 (right) reactors

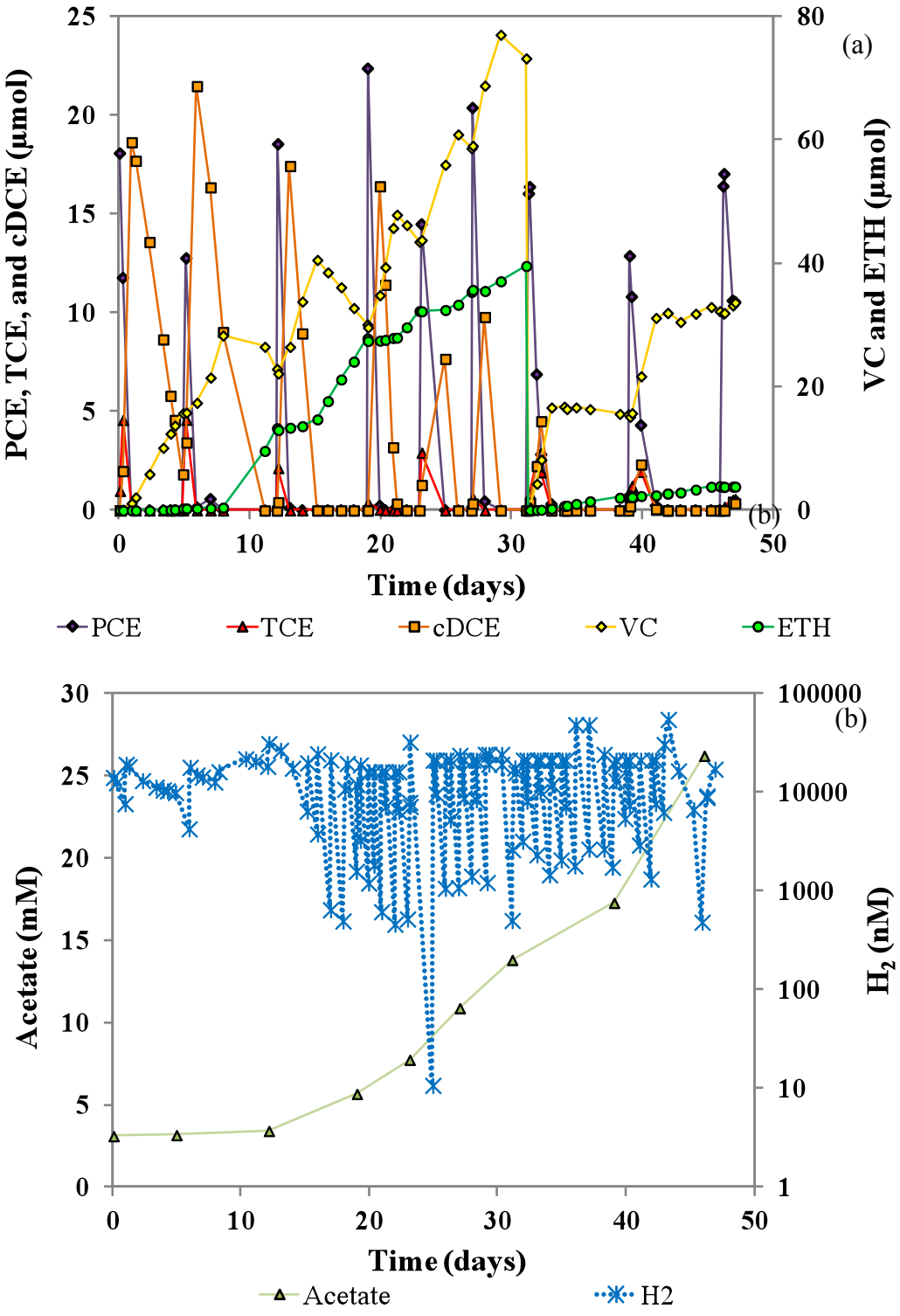

Figure P.11: Time course of PAS-535 experiments.

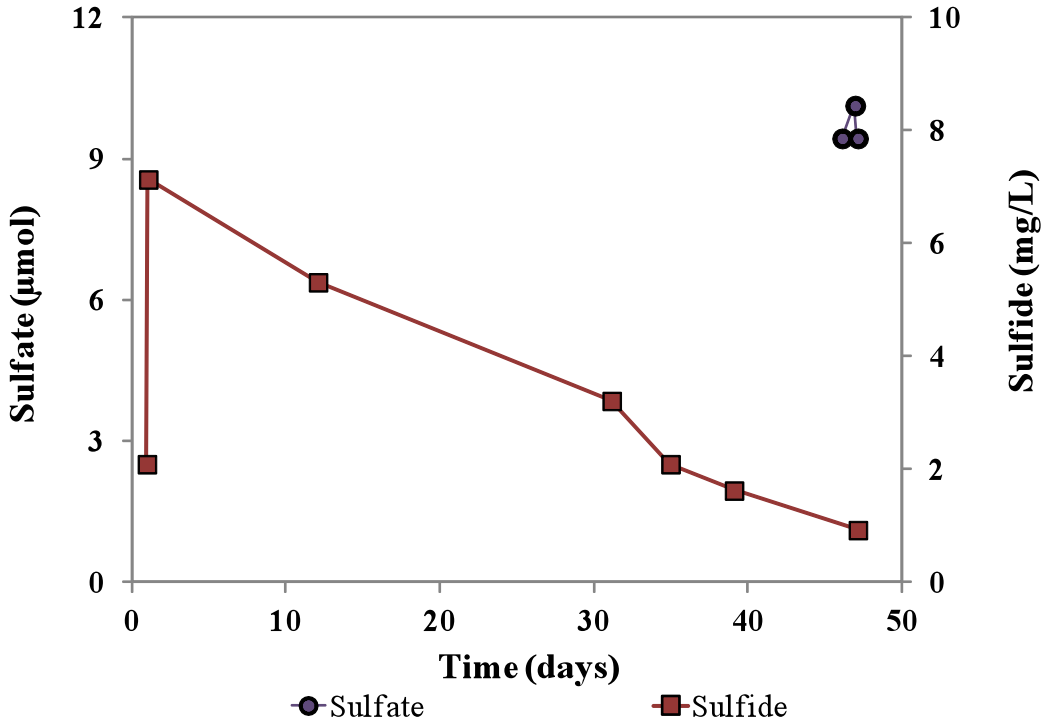

Figure P.12: Time course of PAS-535 experiments.

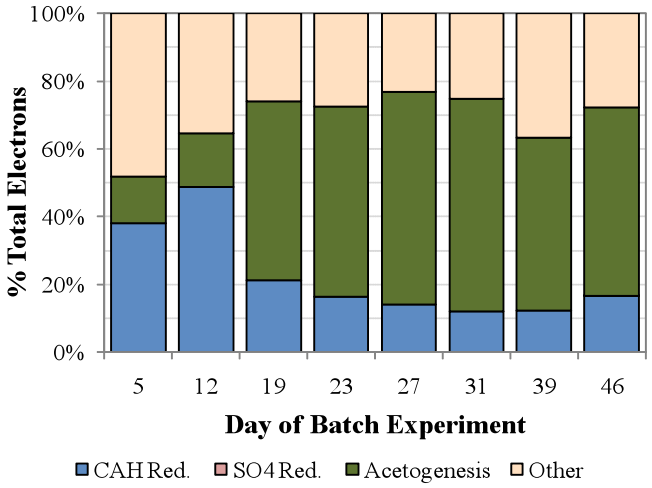

Figure P.13: Electron balance for the PAS-535 reactors

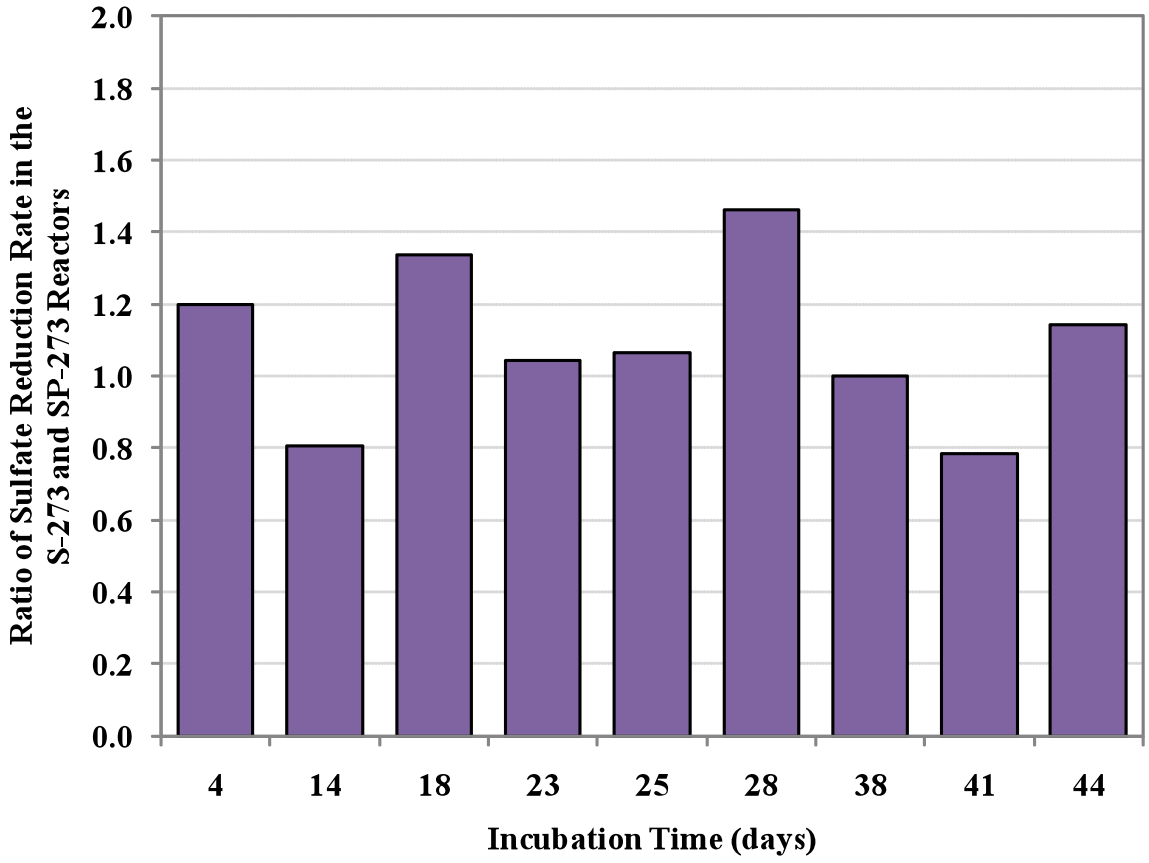

Figure P.14: Ratio of sulfate reduction rates between the S-273 and SP-273 reactors.

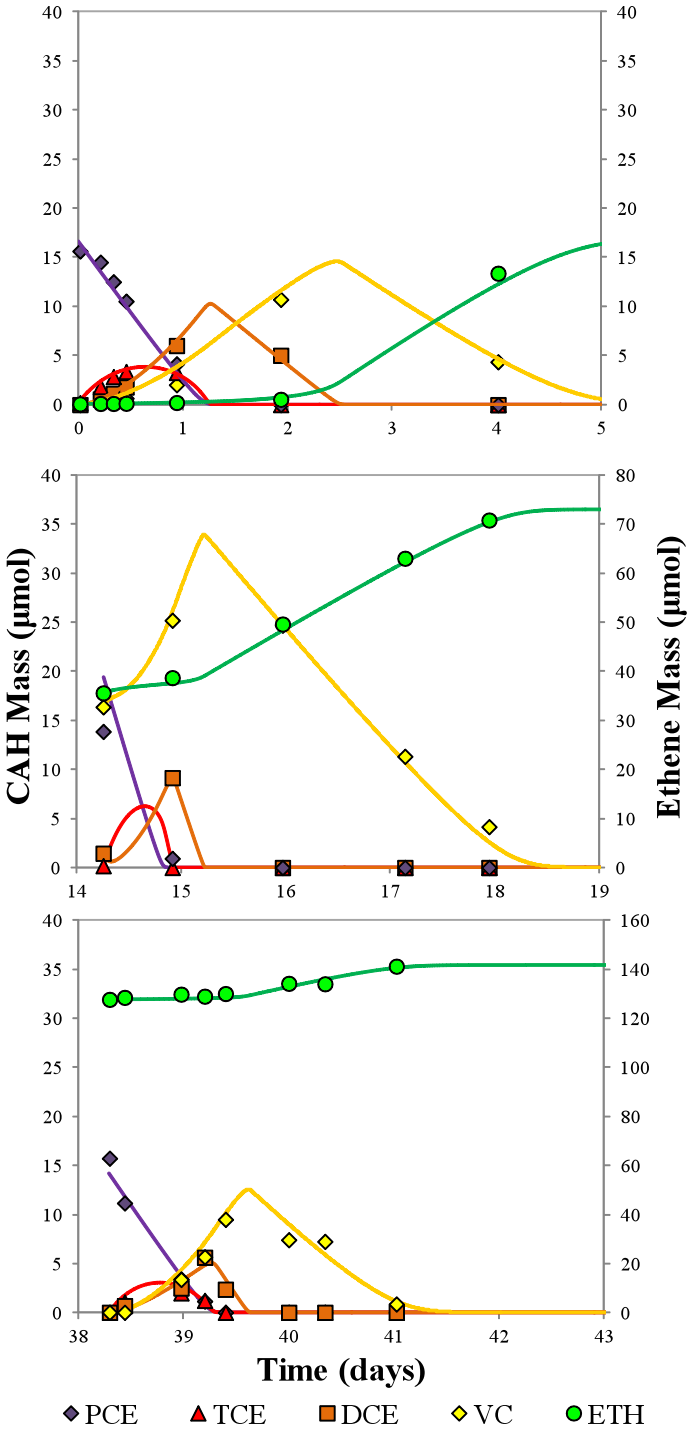

Figure P.15: Model fits over the first five days of the (a) initial, (b) fourth, and (c) ninth PCE dechlorination cycles of the P-273 reactor. Note that the range of the ethene Mass scale (right) doubles with each successive model fit to capture ethene accumulation in the reactor.

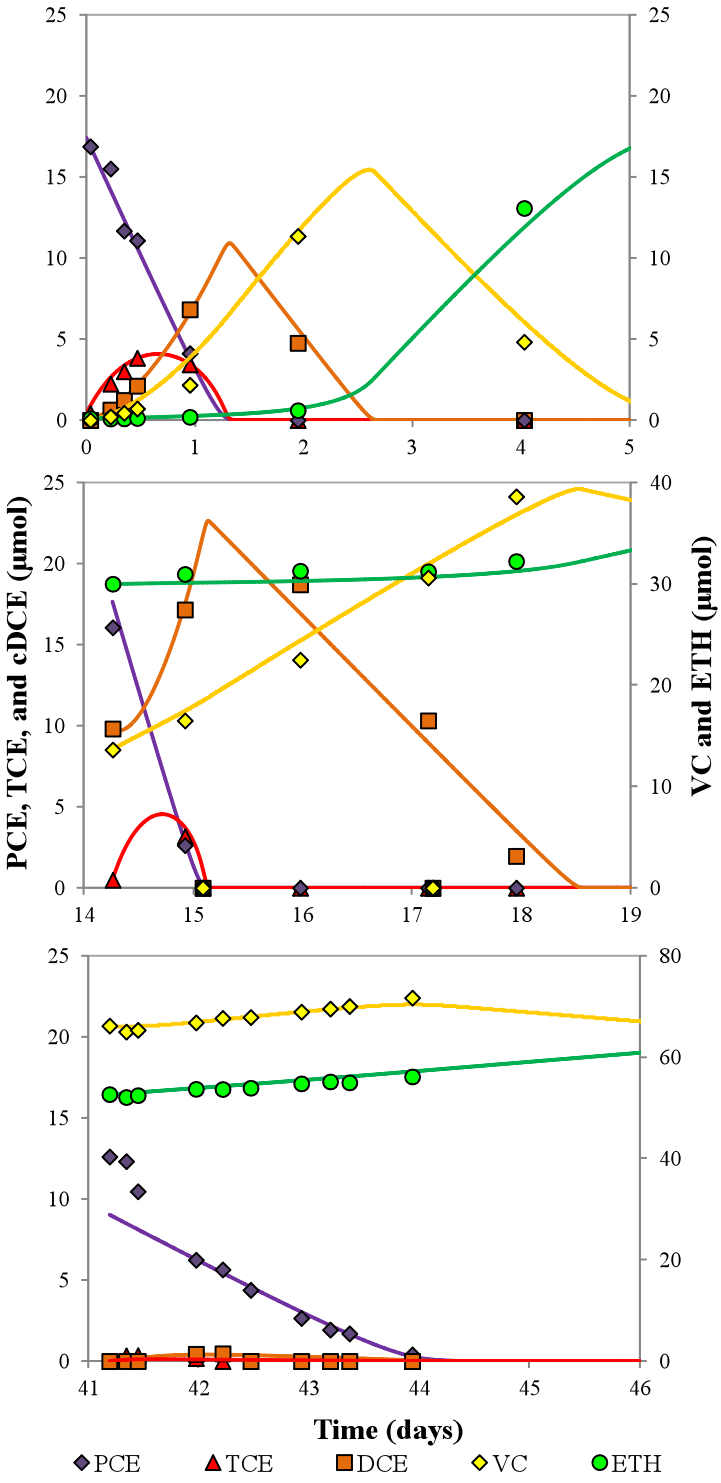

Figure P.16: Model fits over the first five days of the (a) initial, (b) fourth, and (c) ninth PCE dechlorination cycles of the SP-273 reactor. Note that the range of the VC and ETH scale (right) doubles with each successive model fit to capture accumulation of these two compounds in the reactor.

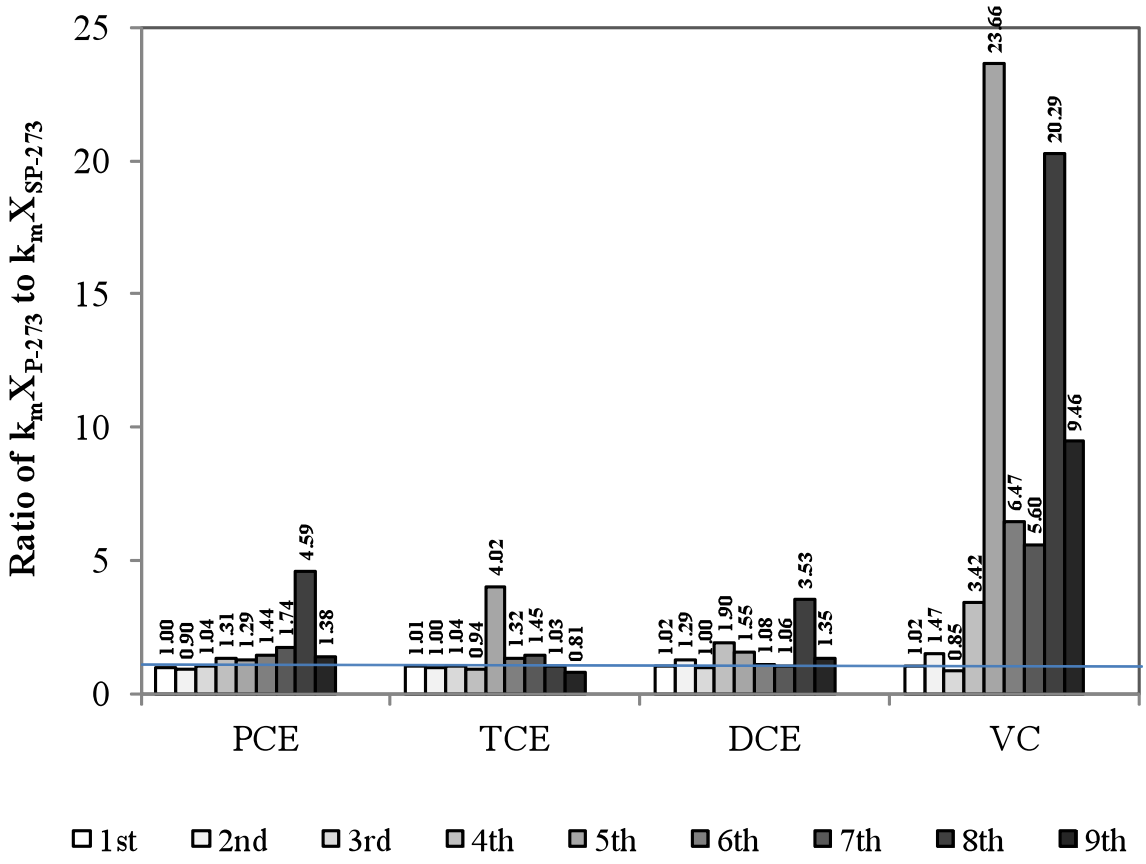

Figure P.17: Ratio of the k_mX parameters estimated by the Multi-fit Monod model for the P-273 and SP-273reactors. Each bar represents a feeding cycle. Bars greater than unity (horizontal line at 1) indicate a relative reduction in dechlorination rate in the dual substrate SP-273 reactor relative to the PCE-only P-273 reactor.

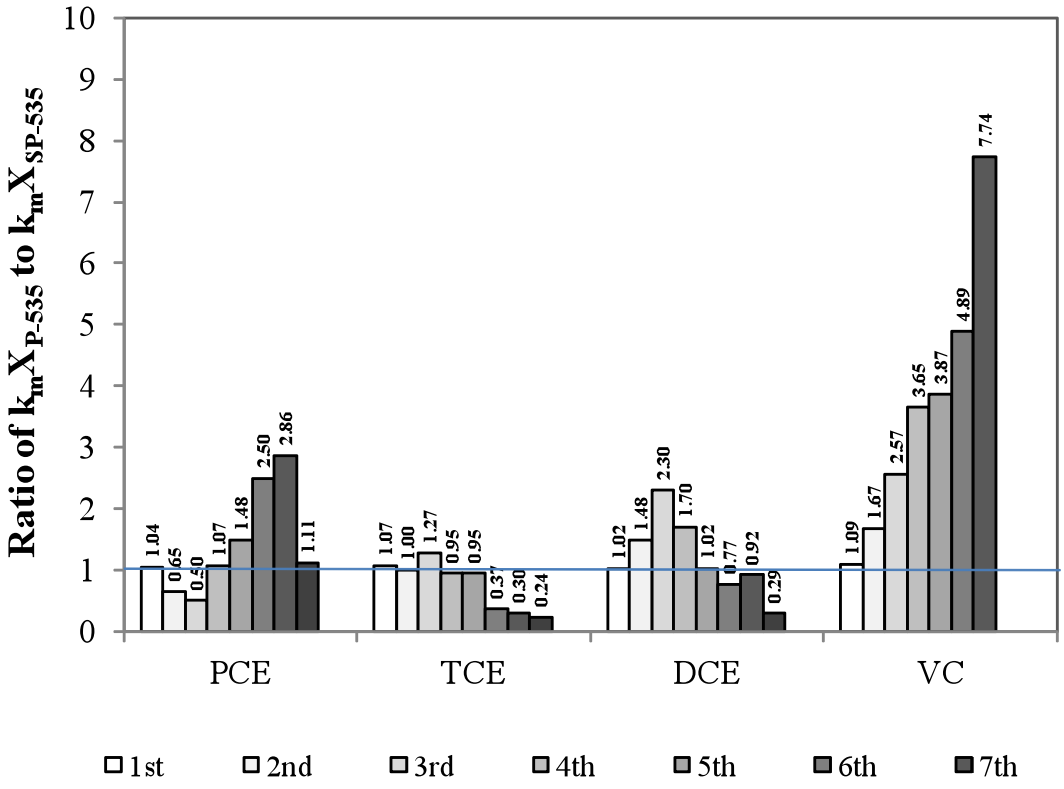

Figure P.18: Ratio of the k_mX parameters estimated by the Multi-fit Monod model for the P-535and SP-535 reactors. Each bar represents a feeding cycle. Bars greater than unity (horizontal line at 1) indicate a relative reduction in declorination rate in the dual substrate SP-535 reactor relative to the PCE-only P-535 reactor.

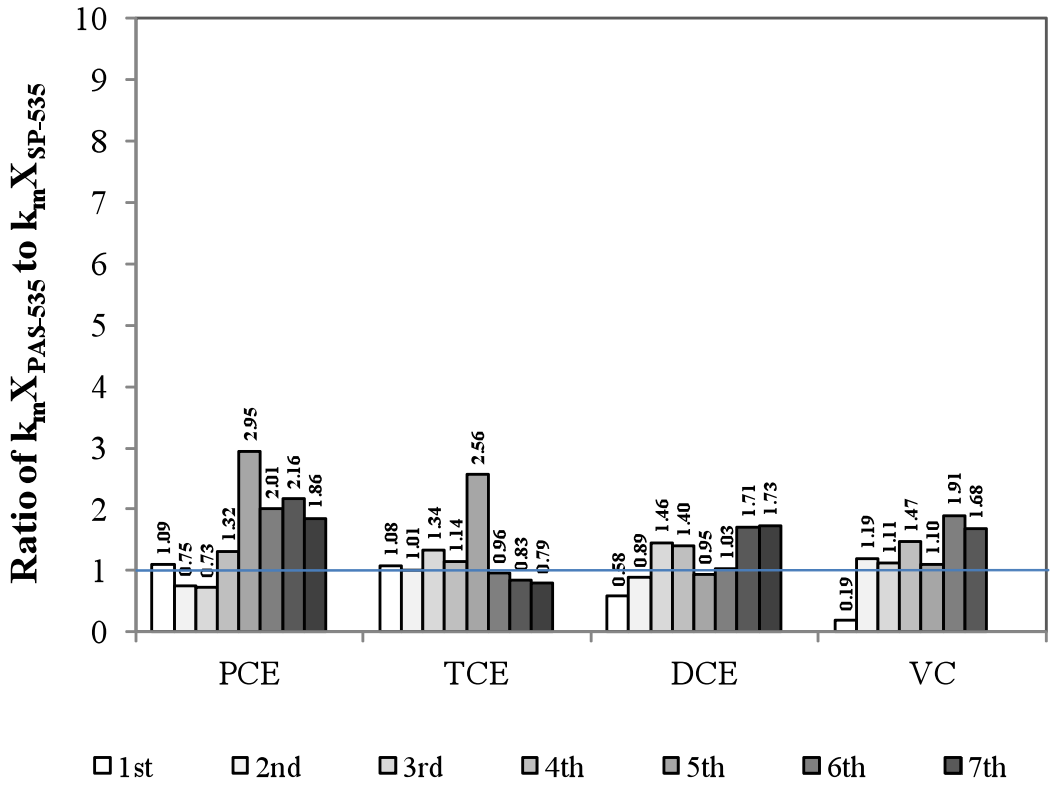

Figure P.19: Ratio of the k_mX parameters estimated by the Multi-fit Monod model for the PAS-535and SP-535 reactors. Each bar represents a feeding cycle. Bars near unity (horizontal line at 1) indicate a similar reduction rates between the PAS-535 and SP-535 reactors.

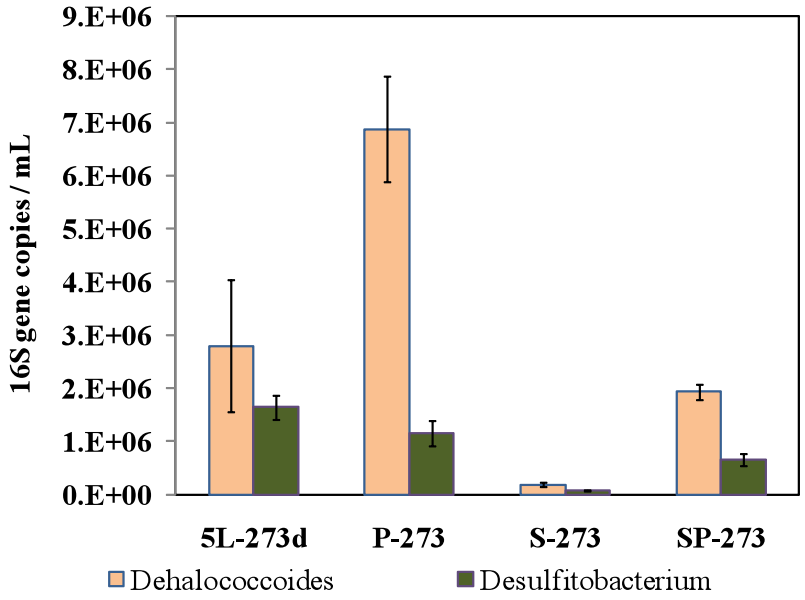

Figure P.20: Quantification of *Dehalococcoides* and *Desulfitobacterium* dechlorinating species in the Set 273 reactors determined through qPCR. Sample 5L-273 represents the sample harvested from the chemostat at the beginning of the Set 273 incubation test.

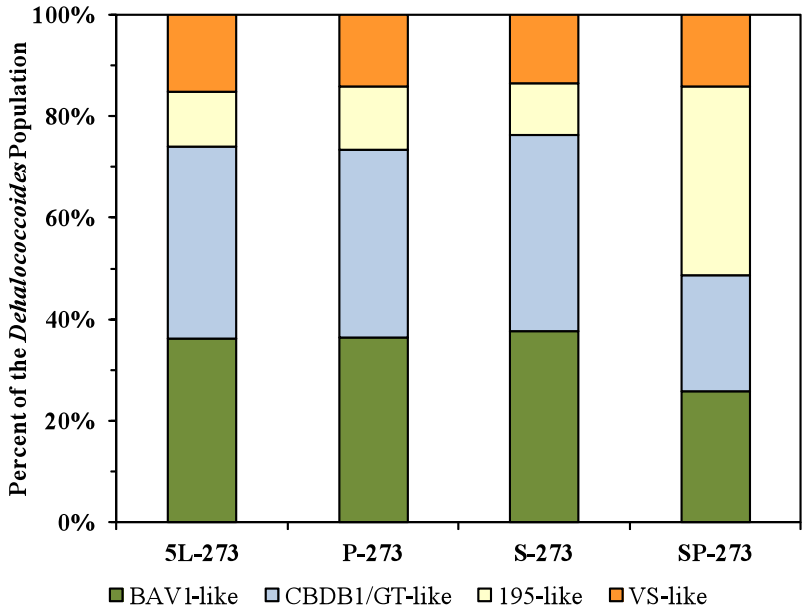

Figure P.21: Set 273 *Dehalococcoides* strain-type hupL distribution after a 45 day incubation as determined through H2ase Chip analysis. Sample 5L-273 represents the sample harvested from the chemostat at the beginning of the Set 273 incubation

test. Each bar represents the total *Dehalococoides* population. Note that, as shown in Figure P.12, the concentration of *Dehalococcoides* changed in each reactor over the incubation. Therefore, having equal percentages in this figure does not translate to equal strain-relative concentrations in the reactor.

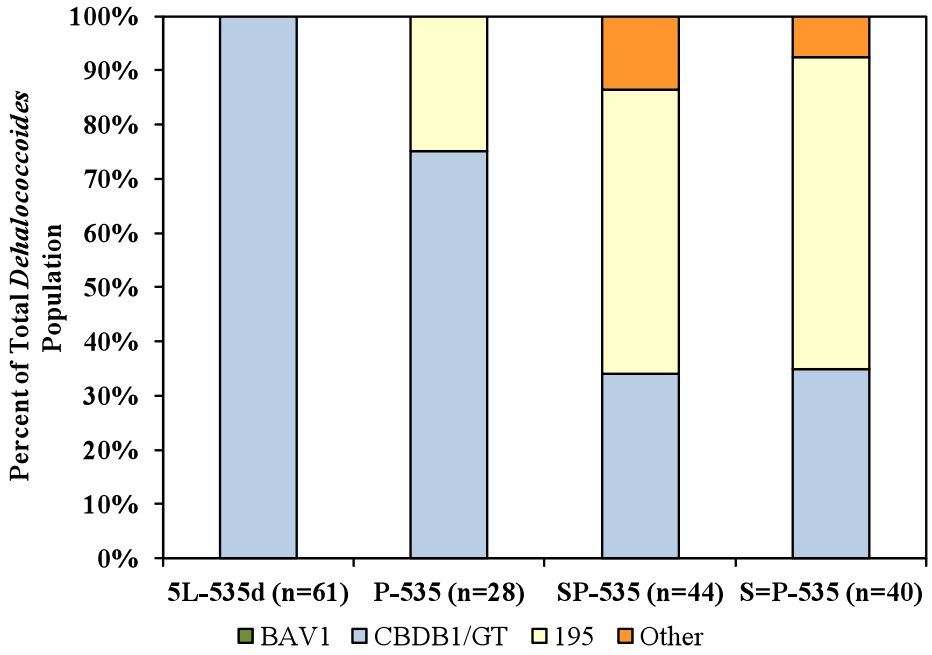

Figure P.22: Set 535 *Dehalococcoides* strain-type hupL distribution after 47 days of incubation as determined through Dhc hupL clone libraries. Each bar represents the total *Dehalococoides* population. Sample 5L-535 represents the sample harvested from the chemostat at the beginning of the Set 535 incubation test. The number of clones analyzed for the distribution is indicated by the "n=##" beside each sample ID. Note that the concentration of *Dehalococcoides* likely changed during the incubations. Therefore, having equal percentages in this figure does not translate to equal strain-relative concentrations in the reactor.

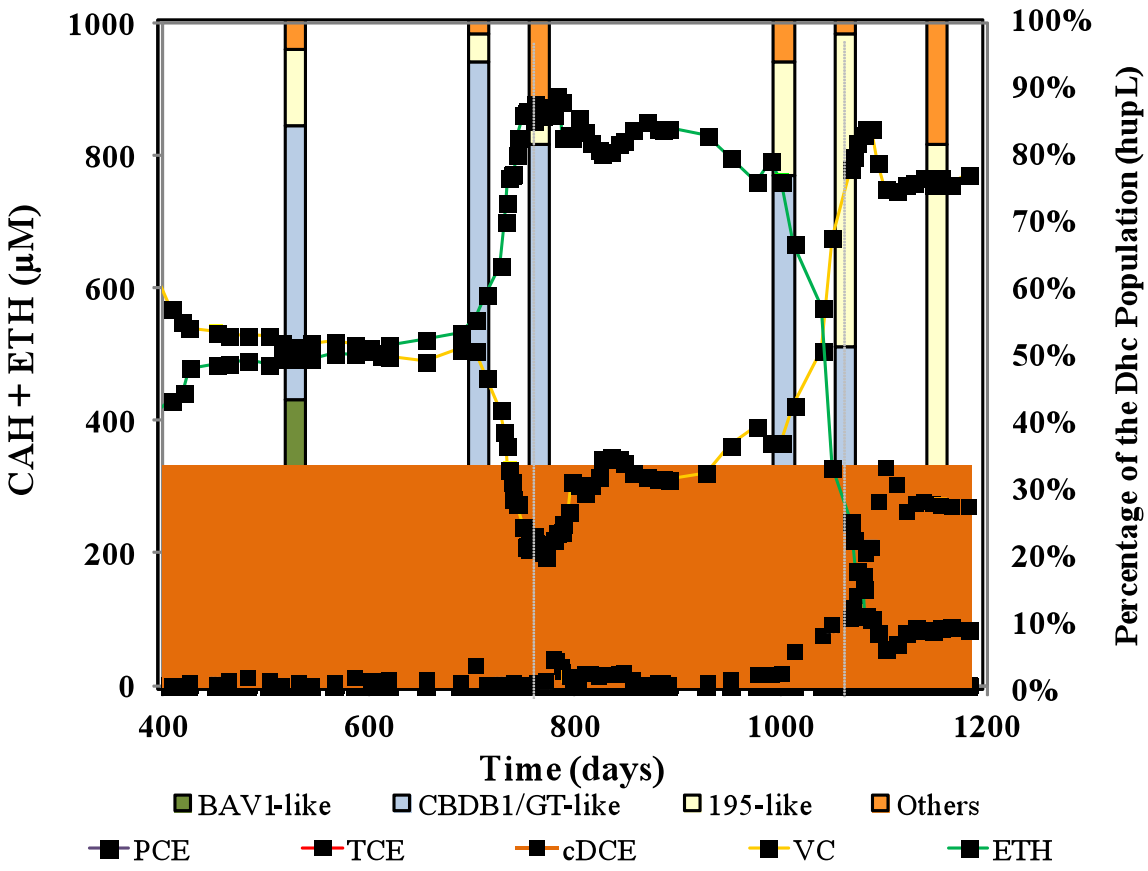

Figure P.23: *Dehalococcoides* strain-type hupL distribution (vertical bars) from culture samples harvested from the PM-2L chemostat at various time points. Chemostat dechlorination performance is indicated by the chemical profile of PCE and dechlorination products.

List of Tables, Appendix C

List of Figures, Appendix C